AD-A112 474 GENERAL DYNAMICS CORP · FORT WORTH TX FORT WORTH DIV F/G 11/4
A COMPARISON OF THE DELAMINATION AND ENVIRONMENTAL RESISTANCE O--ETC(U)
SEP 81 D J WILKINS N00019-80-C-0415
UNCLASSIFIED NAV-GD-0037 NL

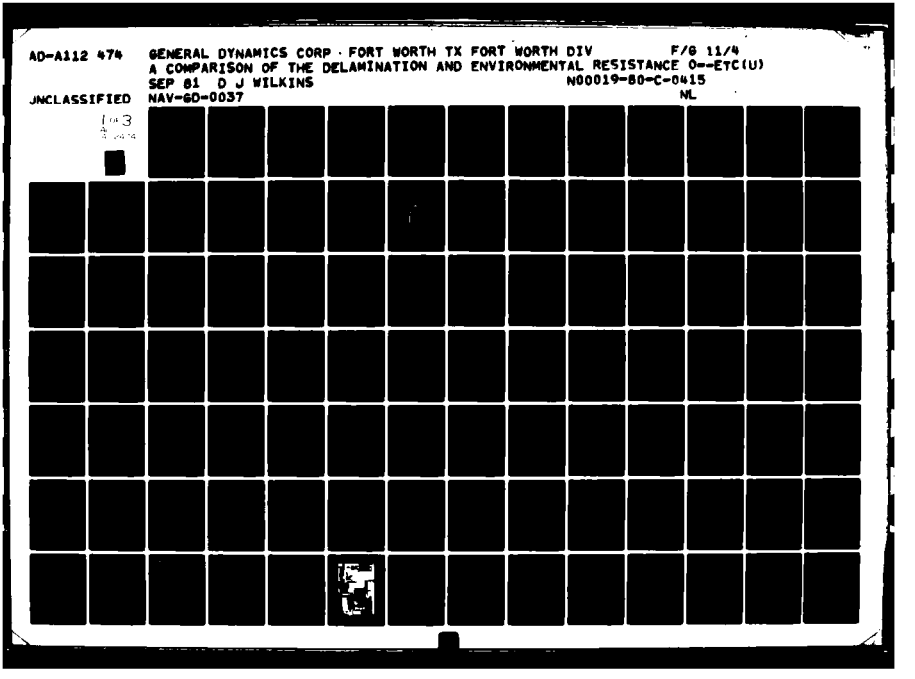

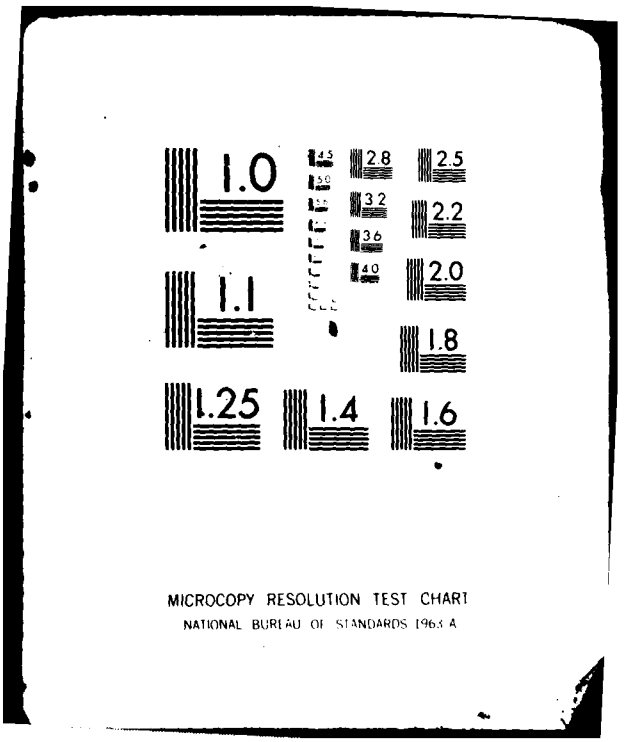
1.0
1.1
1.25
1.4
1.6
1.8
2.0
2.2
2.5
2.8
3.2
3.6
4.0
MICROCOPY RESOLUTION TEST CHART
NATIONAL BUREAU OF STANDARDS 1963 A

(12)

NAV-GD-0037

AD A112474

A COMPARISON OF THE DELAMINATION AND ENVIRONMENTAL RESISTANCE OF A GRAPHITE-EPOXY AND A GRAPHITE-BISMALEIMIDE

Dick J. Wilkins
General Dynamics
P. O. Box 748
Fort Worth, Texas 76101

15 September 1981

Final Report for Period 1 October 1980 – 1 August 1981

APPROVED FOR PUBLIC RELEASE; DISTRIBUTION UNLIMITED

Prepared for

NAVAL AIR SYSTEMS COMMAND
Washington, D.C. 20361

UNCLASSIFIED

SECURITY CLASSIFICATION OF THIS PAGE (When Data Entered)

REPORT DOCUMENTATION PAGE	READ INSTRUCTIONS BEFORE COMPLETING FORM
1. REPORT NUMBER: NAV-GD-0037	2. GOVT ACCESSION NO.: AD-A112474
	3. RECIPIENT'S CATALOG NUMBER:
4. TITLE (and Subtitle): A COMPARISON OF THE DELAMINATION AND ENVIRONMENTAL RESISTANCE OF A GRAPHITE-EPOXY AND A GRAPHITE-BISMALEIMIDE	5. TYPE OF REPORT & PERIOD COVERED: Final Report, 1 Oct. 1980 - 1 Aug. 1981
	6. PERFORMING ORG. REPORT NUMBER:
7. AUTHOR(s): Dick J. Wilkins	8. CONTRACT OR GRANT NUMBER(s): N00019-80-C-0415
9. PERFORMING ORGANIZATION NAME AND ADDRESS: GENERAL DYNAMICS, Fort Worth, Texas 76101	10. PROGRAM ELEMENT, PROJECT, TASK AREA & WORK UNIT NUMBERS: 62241N, WF-41-422
11. CONTROLLING OFFICE NAME AND ADDRESS: Department of the Navy, Naval Air Systems Command (AIR-320B), Washington, D.C. 20361	12. REPORT DATE: 15 September 1981
	13. NUMBER OF PAGES: 205
14. MONITORING AGENCY NAME & ADDRESS (if different from Controlling Office)	15. SECURITY CLASS. (of this report): Unclassified
	15a. DECLASSIFICATION/DOWNGRADING SCHEDULE

16. DISTRIBUTION STATEMENT (of this Report)

Approved for Public Release; Distribution Unlimited

17. DISTRIBUTION STATEMENT (of the abstract entered in Block 20, if different from Report)

18. SUPPLEMENTARY NOTES

19. KEY WORDS (Continue on reverse side if necessary and identify by block number)

Composite Materials, Environments, Moisture, Heat, Thermal Expansion, Test Methods, Mechanical Properties, Fracture (Mechanics), Fatigue (Mechanics), Crack Propagation

20. ABSTRACT (Continue on reverse side if necessary and identify by block number)

The objectives of this program were to compare the delamination and environmental resistance of a graphite-epoxy system (AS1/3501-6) and a graphite-bismaleimide system (T300-6K/V378A). An experimental program was conducted to determine critical values of strain-energy release rate for Mode I (peel) and Mode II (forward shear) delamination. Static delamination fracture and constant amplitude fatigue delamination growth rate data were obtained from

(Continued)

DD FORM 1 JAN 73 1473 EDITION OF 1 NOV 65 IS OBSOLETE

UNCLASSIFIED

SECURITY CLASSIFICATION OF THIS PAGE (When Data Entered)

dry specimens at -65°F, 75°F, 300°F, and 350°F, and on moisture-conditioned specimens at -65°F and 75°F. Additional testing was performed to characterize the thermal spike resistance, glass transition temperature, and the flexure, interlaminar and in-plane shear, and compression properties.

Two major differences were found between the systems. The graphite-bismaleimide retains its structural properties to a temperature of about 100°F above the limit temperature of the graphite-epoxy. On the other hand, the Mode II toughness of the graphite-epoxy is about 50% higher than that of the graphite-bismaleimide at all environmental conditions tested.

PREFACE

This report was prepared by the Fort Worth Division of General Dynamics for the Naval Air Systems Command under Contract N00019-80-C-0415, "Delamination Failure Criteria for Composite Structures." The contract was administered by Dr. Daniel R. Mulville, Composites Technology Administrator, Naval Air Systems Command.

The Composite Structures Engineering Group at General Dynamics was responsible for the work. The program manager and principal investigator was Dr. Dick J. Wilkins. Other General Dynamics personnel that made major contributions were:

E. L. McKague (Materials Engineering) - Environmental Test Planning/Coordination

W. S. Margolis (Metallurgy Lab) - Fracture Testing

R. O. Nay (Metallurgy Lab) - Fracture Testing

J. D. Reynolds (Chemistry Lab) - Environmental Testing

J. E. Fruit (Chemistry Lab) - Specimen Preparation

G. E. Law (Composite Structures Engineering) - Data Analysis and Final Report

TABLE OF CONTENTS

Section	Title	Page
	LIST OF ILLUSTRATIONS	vii
	LIST OF TABLES	xiii
I	INTRODUCTION	1
II	MATERIALS	2
III	DELAMINATION RESISTANCE	3
	3.1 Specimen Preparation	4
	3.2 Test Procedures	7
	3.2.1 Mode I	8
	3.2.2 Mode II	9
	3.3 Test Results	10
	3.3.1 Mode I	10
	3.3.2 Mode II	17
IV	ENVIRONMENTAL RESISTANCE	35
	4.1 Resin Content, Gel Time, and Tack	35
	4.2 Thermal Spike Resistance	38
	4.3 Dry and Wet Glass Transition Temperatures	40
	4.4 Flexure and Interlaminar Shear	47
	4.5 In-Plane Shear	50
	4.6 Compression	58
V	CONCLUSIONS	61
VI	RECOMMENDATIONS	64
	REFERENCES	66
	APPENDIX A Material Data	67
	APPENDIX B Mode I Static Testing	75
	B.1 Double Cantilever Beam Equations	77
	B.2 Sample Data Reduction	79
	B.3 Epoxy Mode I Static Data	83
	B.4 Bismaleimide Mode I Static Data	95

TABLE OF CONTENTS (Continued)

Section	Title	Page
	APPENDIX C Mode I Fatigue Testing	107
	C.1 Epoxy Mode I Fatigue Data	108
	C.2 Bismaleimide Mode I Fatigue Data	118
	APPENDIX D Mode II Static Testing	129
	D.1 Equations for the Mode II Specimen	129
	D.2 Sample Data Reduction	137
	D.3 Epoxy Mode II Static Data	140
	D.4 Bismaleimide Mode II Static Data	149
	APPENDIX E Mode II Fatigue Testing	167
	E.1 Epoxy Mode II Fatigue Data	168
	E.2 Bismaleimide Mode II Fatigue Data	175
	APPENDIX F Photomicrographs	183
	Distribution List	201

LIST OF ILLUSTRATIONS

Illustration	Title	Page
1.	Mode I Coupon	5
2.	Mode II Coupon	6
3.	Epoxy Mode I Toughness Versus Temperature	13
4.	Epoxy Mode I Dry Static/Fatigue Correlation	15
5.	Epoxy Mode I Wet Static/Fatigue Correlation	16
6.	Bismaleimide Mode I Toughness Versus Temperature	19
7.	Bismaleimide Mode I Dry Static/Fatigue Correlation	21
8.	Bismaleimide Mode I Wet Static/Fatigue Correlation	22
9.	Epoxy Mode II Toughness Versus Temperature	25
10.	Epoxy Mode II Dry Static/Fatigue Correlation	27
11.	Epoxy Mode II Wet Static/Fatigue Correlation	28
12.	Bismaleimide Mode II Toughness Versus Temperature	30
13.	Bismaleimide Mode II Dry Static/Fatigue Correlation	33
14.	Bismaleimide Mode II Wet Static/Fatigue Correlation	34
15.	Moisture Absorptivity Due to the Effect of Ten Thermal Spikes after Soaking at 180°F/75% R.H.	39
16.	Thermal Expansion of Dry 15-Ply AS1/3501-6 (200 gm. Load)	41
17.	Coefficient of Thermal Expansion for Dry AS1/3501-6	42
18.	Thermal Expansion of Wet AS1/3501-6 (100 gm. Load)	43
19.	Coefficient of Thermal Expansion for Wet AS1/3501-6	44
20.	Thermal Expansion of Dry T300-6K/V378A (100 gm. Load)	45
21.	Coefficient of Thermal Expansion for Dry T300-6K/V378A	46
22.	Thermal Expansion of Wet T300-6K/V378A (100 gm. Load)	48
23.	Coefficient of Thermal Expansion for Wet T300-6K/V378A	49

LIST OF ILLUSTRATIONS (Continued)

Illustration	Title	Page
24.	Stress-Strain Response of Wet $(\pm 45)_{2S}$ AS1/3501-6	52
25.	Stress-Strain Response of Wet $(\pm 45)_{2S}$ T300-6K/V378A	53
26.	Wet Shear Strength of T300-6K/V378A and AS1/3501-6 Saturated at 75% R.H.	56
27.	Wet Initial Shear Modulus of T300-6K/V378A and AS1/3501-6 Saturated at 75% R.H.	57
28.	Miniature Sandwich Beam	59
B-1	Custom Load Frame for Mode I Static and Fatigue Fracture Testing	76
B-2	Double Cantilever Beam	78
B-3	Sample Load-Deflection Curves for a Mode I Static Test	80
B-4	Sample Mode I Data in Graphical Form	81
B-5	Test E1CDS of Specimen E1-4-3	84
B-6	Test E1CDS of Specimen E1-4-9	85
B-7	Test E1CWS of Specimen E1-5-8	86
B-8	Test E1RDS of Specimen E1-4-1	87
B-9	Test E1RDS of Specimen E1-4-2	88
B-10	Test E1RWS of Specimen E1-5-9	89
B-11	Test E1RWS of Specimen E1-5-3	90
B-12	Test E1EDS of Specimen E1-2-4	91
B-13	Test E1EDS of Specimen E1-3-2	92
B-14	Test E1PDS of Specimen E1-2-8	93
B-15	Test E1PDS of Specimen E1-3-1	94
B-16	Test P1CDS of Specimen P1-4-1	96
B-17	Test P1CDS of Specimen P1-4-5	97

LIST OF ILLUSTRATIONS (Continued)

Illustration	Title	Page
B-18	Test P1CWS of Specimen P1-1-3	98
B-19	Test P1RDS of Specimen P1-4-2	99
B-20	Test P1RDS of Specimen P1-4-9	100
B-21	Test P1RWS of Specimen P1-1-2	101
B-22	Test P1EDS of Specimen P1-3-5	102
B-23	Test P1EDS of Specimen P1-2-10	103
B-24	Test P1PDS of Specimen P1-3-8	104
B-25	Test P1PDS of Specimen P1-2-3	105
C-1	Test E1CDF of Specimen E1-4-6	109
C-2	Test E1CDF of Specimen E1-1-4	110
C-3	Test E1CWF of Specimen E1-5-7	111
C-4	Test E1RDF of Specimen E1-4-4	112
C-5	Test E1RWF of Specimen E1-5-2	113
C-6	Test E1RWF of Specimen E1-5-4	114
C-7	Test E1EDF of Specimen E1-2-1	115
C-8	Test E1EDF of Specimen E1-2-6	116
C-9	Test E1PDF of Specimen E1-2-1	117
C-10	Test P1CDF of Specimen P1-5-2	119
C-11	Test P1CWF of Specimen P1-1-8	120
C-12	Test P1RDF of Specimen P1-4-4	121
C-13	Test P1RDF of Specimen P1-4-7	122
C-14	Test P1RDF of Specimen P1-5-4	123
C-15	Test P1RWF of Specimen P1-1-1	124
C-16	Test P1RWF of Specimen P1-1-9	125
C-17	Test P1EDF of Specimen P1-5-7	126

LIST OF ILLUSTRATIONS (Continued)

Illustration	Title	Page
C-18	Test P1PDF of Specimen P1-2-4	127
D-1	Custom Load Frame for Mode II Static and Fatigue Fracture Testing	130
D-2	Strength of Materials Model of CLS Specimen	131
D-3	Finite Element Model of CLS Specimen	133
D-4	Finite Element Mesh in Crack Tip Region Illustrating Modified Crack Closure Technique	134
D-5	Plot of Strain Energy Release Rate Versus Crack Length for CLS Specimen	136
D-6	Sample Load-Deflection Curves for a Mode II Static Test	138
D-7	Sample Computer Plots for Mode II Static Delamination Test	139
D-8	Test E2CDS of Specimen E2-3-5	141
D-9	Test E2CDS of Specimen E2-4-7	142
D-10	Test E2CWS of Specimen E2-1-8	143
D-11	Test E2RDS of Specimen E2-2-5	144
D-12	Test E2RDS of Specimen E2-2-6	145
D-13	Test E2RWS of Specimen E2-1-1	146
D-14	Test E2EDS of Specimen E2-5-10	147
D-15	Test E2PDS of Specimen E2-4-9	148
D-16	Test P2CDS of Specimen P2-1-6	150
D-17	Test P2CDS of Specimen P2-1-8	151
D-18	Test P2CWS of Specimen P2-5-3	152
D-19	Test P2RDS of Specimen P2-1-1	153
D-20	Test P2RDS of Specimen P2-1-2	154
D-21	Test P2RDS of Specimen P2-2-5	155
D-22	Test P2RDS of Specimen P2-6-1	156

LIST OF ILLUSTRATIONS (Continued)

Illustration	Title	Page
D-23	Test P2RDS of Specimen P2-7-1	157
D-24	Test P2RWS of Specimen P2-5-2	158
D-25	Test P2RWS of Specimen P2-5-5	159
D-26	Test P2RWS of Specimen P2-6-2	160
D-27	Test P2RWS of Specimen P2-7-2	161
D-28	Test P2EDS of Specimen P2-2-2	162
D-29	Test P2EDS of Specimen P2-2-9	163
D-30	Test P2PDS of Specimen P2-2-7	164
D-31	Test P2PDS of Specimen P2-2-6	165
E-1	Test E2CDF of Specimens E2-4-1 (◈) and E2-4-3 (⊡)	169
E-2	Test E2CWF of Specimen E2-1-3	170
E-3	Test E2RDF of Specimen E2-2-7	171
E-4	Test E2RWF of Specimens E2-1-2 (◈) and E2-1-5 (⊡)	172
E-5	Test E2EDF of Specimen E2-4-8	173
E-6	Test E2PDF of Specimen E2-5-7	174
E-7	Test P2CDF of Specimens P2-3-3 (▲) and P2-3-1 (⊡)	176
E-8	Test P2CWF of Specimen P2-5-1	177
E-9	Test P2RDF of Specimens P2-1-10 (◈) and P2-1-3 (⊡)	178
E-10	Test P2RWF of Specimens P2-5-7 (⊡) and P2-5-8 (◈)	179
E-11	Test P2EDF of Specimen P2-3-7	180
E-12	Test P2EDF of Specimen P2-3-8	181
E-13	Test P2PDF of Specimen P2-2-1	182
F-1	Photomicrographs of Glass Transition Panels	184
F-2	Photomicrographs of Thermal Spike Panels	185
F-3	Photomicrographs of Miniwich Panels	186

LIST OF ILLUSTRATIONS (Continued)

Illustration	Title	Page
F-4	Photomicrographs of #1 Flex Panels	187
F-5	Photomicrographs of #2 Flex Panels	188
F-6	Photomicrographs of #1 $\pm$45 Panels	189
F-7	Photomicrographs of #2 $\pm$45 Panels	190
F-8	Photomicrographs of #1 Mode I Panels	191
F-9	Photomicrographs of #2 Mode I Panels	192
F-10	Photomicrographs of #3 Mode I Panels	193
F-11	Photomicrographs of #4 Mode I Panels	194
F-12	Photomicrographs of #5 Mode I Panels	195
F-13	Photomicrographs of #1 Mode II Panels	196
F-14	Photomicrographs of #2 Mode II Panels	197
F-15	Photomicrographs of #3 Mode II Panels	198
F-16	Photomicrographs of #4 Mode II Panels	199
F-17	Photomicrographs of #5 Mode II Panels	200

LIST OF TABLES

Table	Title	Page
1.	Epoxy Mode I Static Data Summary	11
2.	Epoxy Mode I Fatigue Data Summary	14
3.	Bismaleimide Mode I Static Data Summary	18
4.	Bismaleimide Mode I Fatigue Data Summary	20
5.	Epoxy Mode II Static Data Summary	24
6.	Epoxy Mode II Fatigue Data Summary	26
7.	Bismaleimide Mode II Static Data Summary	29
8.	Bismaleimide Mode II Fatigue Data Summary	32
9.	Resin Content and Specific Gravity of Test Panels	36
10.	Comparison of T300-6K/V378A Polyimide and AS1/3501-6 Epoxy Gel Times	37
11.	Glass Transition Temperatures and Coefficients of Linear Thermal Expansion	47
12.	Dry Flex and Shear Properties of AS1/3501-6 and T300-6K/V378A	51
13.	$(\pm 45°)_{2S}$ Tensile Data on Wet T300-6K/V378A	54
14.	$(\pm 45°)_{2S}$ Tensile Data on Wet AS1/3501-6	55
15.	Compression Miniature Sandwich Beam Results (0/$\pm$45/90)	60

I INTRODUCTION

It is now widely recognized that the maximum aircraft structural use temperature for 350°F-curing graphite-epoxy systems is about 250°F. This limit is a result of the depression of the epoxies' glass transition temperature (T_g) after absorption of atmospheric moisture. The aircraft industry would much prefer to replace aluminum with a lighter and stiffer material whose thermal limit is compatible with that of aluminum (about 300°F). Therefore, General Dynamics screened a number of candidate higher temperature materials. The results of the screening (Reference 1) identified a bismaleimide resin (U.S. Polymeric's V378A) that met the requirements.

At the same time, it is becoming apparent that the delamination failure mode has the potential for being the major life-limiting failure process for laminated composites (Reference 2). General Dynamics has developed new test methods for characterizing the delamination process.

Thus, in the interest of providing better performance for future Navy aircraft, this study was conceived to directly compare the standard Navy graphite-epoxy system (Hercules' AS1 fiber and 3501-6 resin) with the new U.S. Polymeric resin (V378A), reinforced with Union Carbide's Thornel 300 fiber in the 6000-ends-per-tow version (T300-6K).

II MATERIALS

The graphite-epoxy (G/E) material used in this program was AS1/3501-6, a product of Hercules, Incorporated, Magna, Utah. Sixteen pounds of 12-inch wide unidirectional tape were purchased according to specification MMS 549, Revision A, Type I. The vendor certification sheet is included in Appendix A. Cure procedures were provided by the Naval Air Systems Command (NASC).

The graphite-bismaleimide (G/P) material was T300-6K/V378A, a product of U.S. Polymeric, Santa Ana, California. This modified bismaleimide resin belongs to the general class of resins commonly known as addition polyimides. Its fabrication procedures and properties are so different from those of the condensation polyimides (Larc-160, PMR-15) that although the symbol "P" is used here to denote the polyimide material, the word bismaleimide will be consistently used in this report. Approximately fifteen pounds were purchased in the form of 6-inch-wide unidirectional tape, according to the preliminary specification for this material. Both the specification and vendor certification data are included in Appendix A.

III DELAMINATION RESISTANCE

Methods for characterizing interlaminar toughness in terms of strain-energy release rate were developed earlier by General Dynamics and were reported in Reference 2. The test specimens and procedures previously developed were used directly or adapted for use in the present study.

Here, critical Mode I and Mode II values of strain-energy release rate, G_{IC} and G_{IIC}, were obtained for dry specimens at -65° F, 75° F, 300° F, and 350° F. For wet specimens, (equilibrated at 180° F in 75% relative humidity), tests were conducted only at -65° F and 75° F to avoid complications of specimen drying at high test temperatures. Delamination growth rates under constant amplitude fatigue (R = 0.1) were also measured at each of the six environmental combinations.

In order to more readily identify the various specimen types and test conditions, an identification code was developed. A five-digit alphanumeric symbol is used to identify each test type as follows:

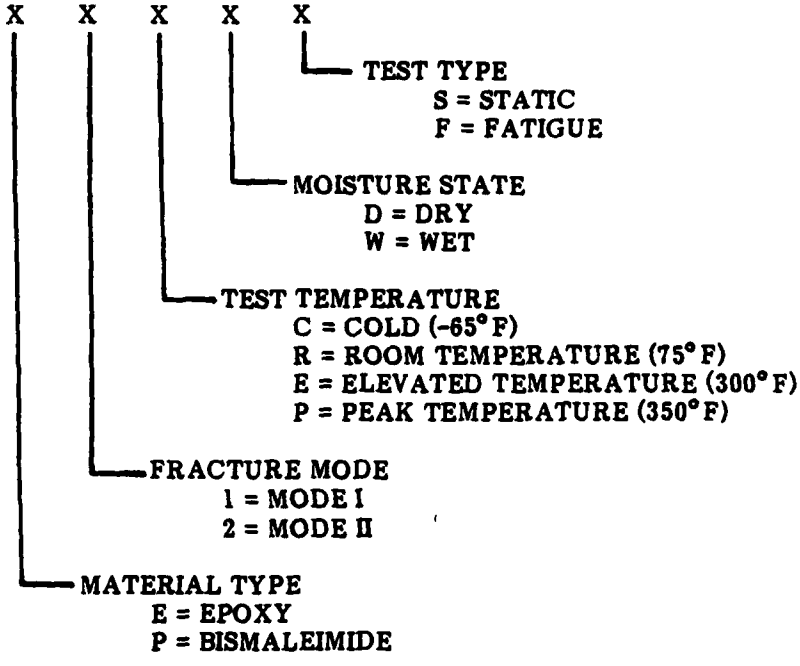

For example, E1CDS identifies an epoxy, Mode I, cold, dry specimen tested statically.

3.1 Specimen Preparation

The Mode I specimens were fabricated according to the drawing shown in Figure 1. Only the unidirectional version (denoted as -1) was used in this study. Five panels of ten specimens each were fabricated from each material. Each specimen was 10 inches long by 1 inch wide allowing crack growth measurements over a crack length of a = 2.5 to 7.0 inches.

The Mode II specimens (Figure 2) were modified from those used in the Reference 2 study. In that study, delaminations at both 0/0 and 0/90, ply interfaces were studied. It was found that all the necessary data could be obtained at the 0/0 interface, so the Mode II coupon was re-designed for this program. Again, five panels of ten specimens each

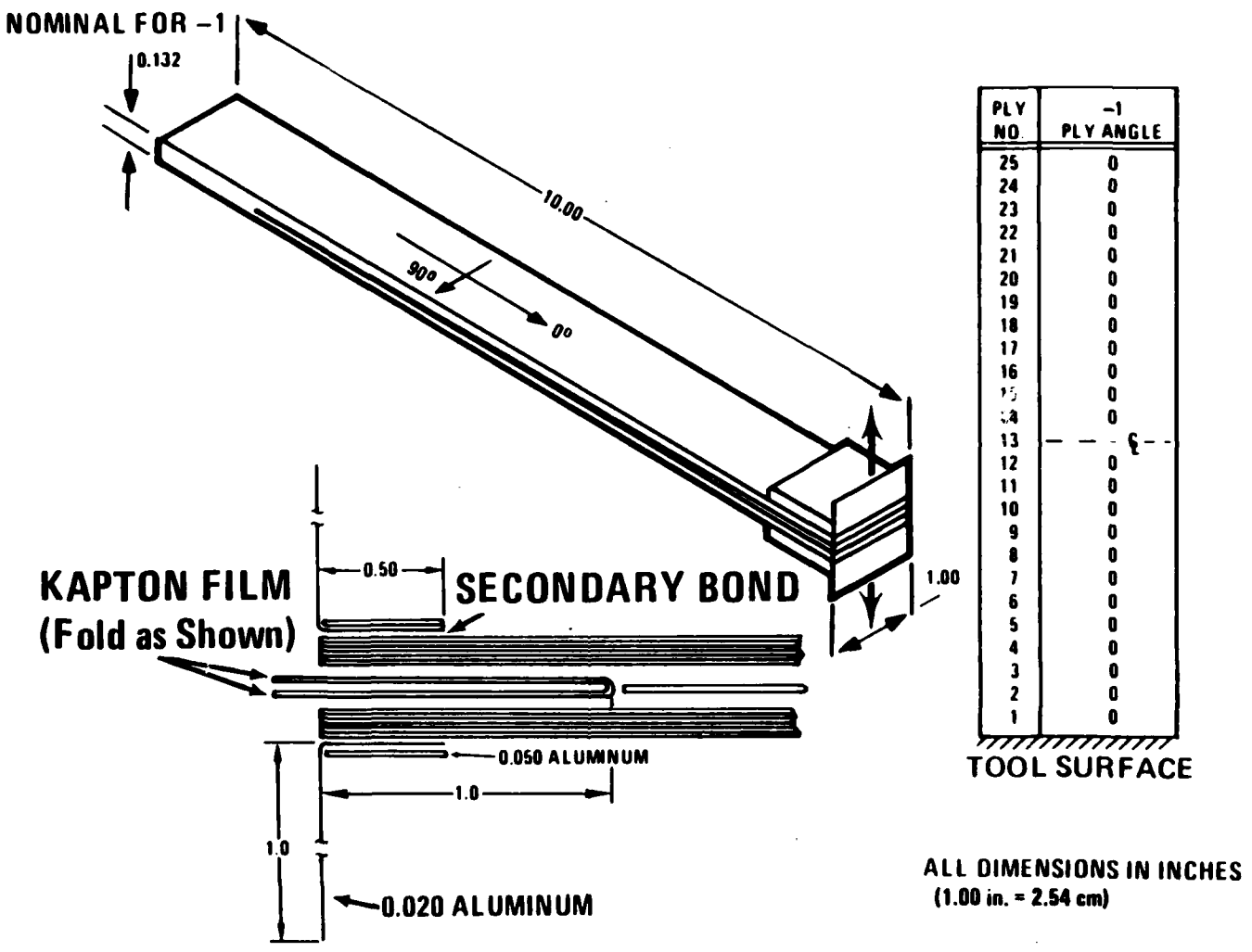

Figure 1. Mode I Coupon

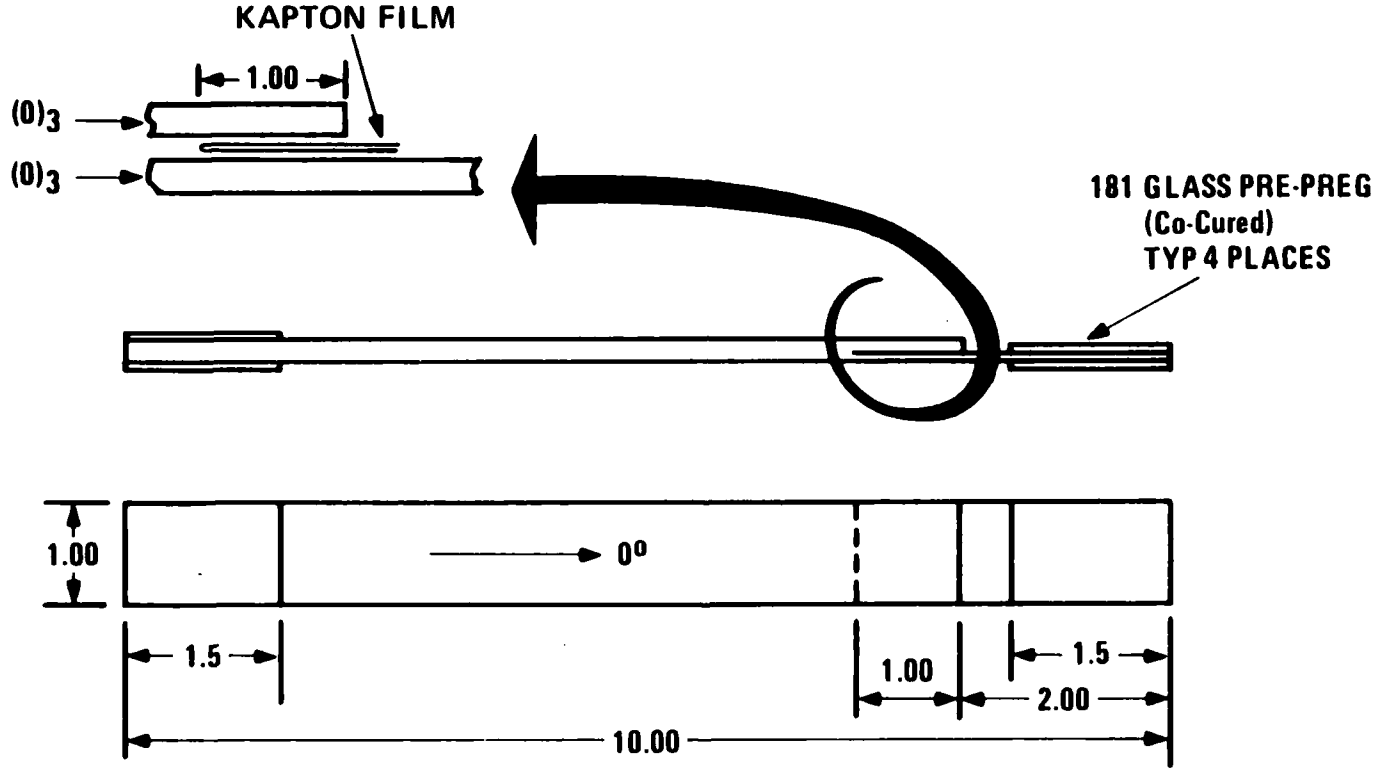

NOTE: ALL DIMENSIONS IN INCHES

Figure 2. Mode II Coupon

were fabricated from each material. The ten-inch overall length of the specimens allowed crack growth mesurements to be made over crack lengths from a = 2.0 to 7.0 inches.

A code was developed for identifying each of the specimens:

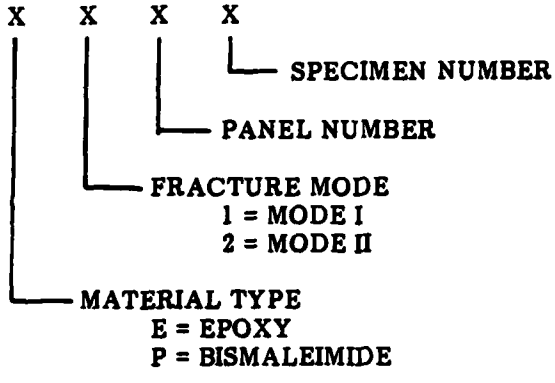

For example, E1-2-3 is an epoxy, Mode I specimen cut from panel number 2, and it is specimen number 3 from that panel.

3.2 Test Procedures

The aim of the tests was to measure the critical strain-energy release rate, G_c, and the subcritical growth associated with a particular value of G. For the geometry of these specimens (Reference 3),

$$G = P^2 (dC/da)/2w, \quad (1)$$

where P is the applied load, C is the compliance, a is the crack length, and w is the specimen width.

3.2.1 Mode I

Critical G values for the Mode I coupon were obtained in a custom displacement-controlled test machine. The edges of the specimens were painted with a white coating (typewriter correction fluid) marked at 0.5-in increments to aid in crack observation.

The first load application was made to break the Kapton film and create a natural crack for the first set of measurements. Several tests were performed on each specimen. The displacement was applied to initiate crack growth and was increased until the crack propagated slowly to the next mark on the specimen edge. The displacement was then returned to zero, and the process repeated. Visual crack length observations were made with an X20 microscope. Load was continuously plotted as a function of crosshead displacement. An example of the data reduction is given in Appendix B.

Constant-amplitude (R = 0.1) fatigue tests were performed in the same custom displacement-controlled test frames. The applied load was servo-controlled by position feedback. An automated test procedure was used to perform compliance measurements, compare them to the compliance/crack-length relationship developed in static tests, and calculate the instantaneous crack length. A methodology was developed to begin cycling at G values near the critical value to obtain cracking rates in the range of 10^{-4} to 10^{-3} in/cycle. As the crack extended, the G corresponding to the fixed displacement diminished, allowing slower cracking rates to be obtained. Cycle counts were selected to give accurately measurable crack growth increments of about 0.02 to 0.05 in. for each test point. The data reduction is explained further in Appendix C.

3.2.2 Mode II

Both static and fatigue tests of the Mode II coupon were performed in custom made fixtures, which were commanded by a Varian computer. A position feedback arrangement was used for control. This setup allowed for a fine incremental control of the crack extension. The feedback measuring device was a Hewlett-Packard 7DCT-500 linear-differential transformer. It was mounted on the hydraulic ram and was referenced to the test frame.

In static tests, curves of axial load and axial displacement were recorded on an X-Y plotter. Load was measured from a custom-made load cell. The load cell used 4-arm strain gage bridges to measure the load. The displacement was measured from a voltage take-off of the same device used for feedback control. The crack length was measured from adjacent scales and viewed through a 20X microscopes. An example of the data reduction is presented in Appendix D.

The development of the test frames revealed a necessity for a rigid end condition. When this condition is maintained a linear load-displacement curve is obtained. The requirements were to minimize grip slippage and out-of-plane rotation of the gripping area during loading. Separable serrated grips were designed which met these requirements.

Procedures similar to those for the Mode I coupons (see Appendix C) were used for the Mode II constant-amplitude (R = 0.1) fatigue tests, except that visual crack measurements were used throughout.

3.3 Test Results

Because of the large volume of data generated in this task, the results are only discussed in summary form here. The data obtained from each test are compiled for reference in the appendices. Rather than repeat the phrase "strain-energy release rate," the word "toughness" may be used instead.

3.3.1 Mode I

A summary of the static Mode I toughness of AS1/3501-6 is presented in Table 1. For each coupon tested, Table 1 lists the specimen thickness, and both the initial and final crack lengths used in the test. Table 1 also contains the experimentally determined constants A_1 and A_2 where the compliance

$$C = A_1 a^3,$$

the load required to initiate crack growth

$$P = A_2/a,$$

and a is the crack length. Finally, the value of G_{IC} is listed, where

$$G_{IC} = 3A_1 A_2^2/2w,$$

and w is the specimen width. Appendix B contains a detailed description of the above relations along with the data reduction plots for each test coupon. As noted in Table 1,

TABLE 1. EPOXY MODE I STATIC DATA SUMMARY

Experiment Code	Specimen Code	Thickness (in)	Initial Crack Length (in)	Final Crack Length (in)	A_1 $(lb\text{-}in^2)^{-1}$	A_2 (in lb)	G_{IC} (in lb/in^2)
E1CDS	E1-4-3	0.151	2.5	6.0	0.00169	16.75	0.71
	E1-4-9	0.146	2.5	6.2	0.00176	16.20	0.69
E1CWS	E1-5-8	0.146	3.0	6.5	0.00172	16.17	0.68
E1RDS	E1-4-1	0.140	3.0	6.5	0.00181	16.52	0.74
	E1-4-2	0.147	3.0	6.5	0.00168	17.28	0.75
E1RWS	E1-5-9	0.136	2.5	5.5	0.00180	20.88	1.18
	E1-5-3	0.157	4.0	6.5	0.00135	19.11	0.74
E1EDS	E1-2-4	0.148	3.0	6.0	0.00147	24.08	1.28
	E1-3-2	0.151	3.0	6.5	0.00146	22.97	1.16
E1PDS	E1-2-8	0.144	3.5	6.5	0.00134	24.31	1.19
	E1-3-1	0.151	3.5	6.6	0.00119	28.49	1.45

NOTE: All specimens had a rough crack surface with some fiber pull-out. The elevated and peak temperature test coupons were exceptionally rough.

some of the data are questionable because of the roughness of the fracture surface. Some of the panels exhibited excessive "nesting" of the fibers in the layers adjacent to the crack surface. (End views of the cut ends of each of the panels are documented later in Appendix F). This nesting of fibers is expected to produce higher values of toughness than would be exhibited in typical structural laminates in which a nearly planar layer of resin separates the plies.

Critical values of Mode I toughness for graphite-epoxy are plotted in Figure 3 as a function of temperature. The vertical bar indicates the range of individual data points. The toughness tends to increase with temperature, and does not appear to be significantly affected by moisture. The values for AS1/3501-6 are about 50% higher than comparable values for T300/5208 (Reference 2). However, some of this difference is clouded by the roughness of the fracture surfaces.

The Mode I fatigue results for the AS1/3501-6 system are summarized in Table 2, and compiled in Appendix C. For each coupon tested, Table 2 contains the specimen thickness, the initial and final crack length of the test, and the minimum and maximum loads applied during the test expressed in terms of the strain-energy release rate. Also listed are the experimentally determined parameters B and n of the incremental crack growth/strain-energy release rate relation

$$da/dN = BG^n.$$

The extrapolated value of G at a crack growth rate of 0.01 inches per cycle is included for a comparison with the static G_c values. In an attempt to correlate the fatigue and static data, the G-intercepts of the da/dN versus G curves at a crack growth rate of 10^{-2} inches/cycle are compared to the static G_c data in Figures 4 and 5 for the dry and wet test data respectively. Taking account of data scatter and surface roughness, the previous trends are more or less confirmed.

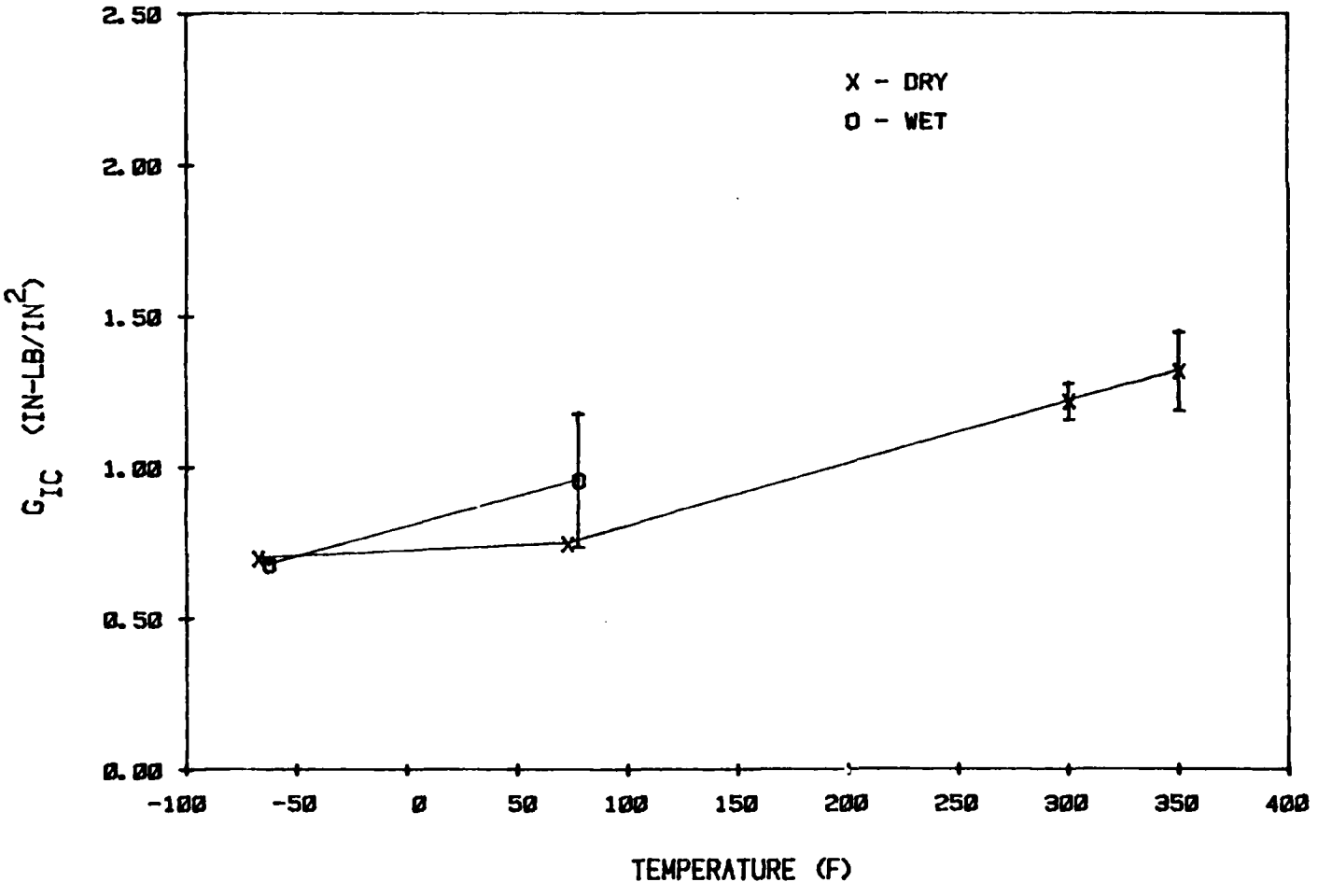

Figure 3. Epoxy Mode I Toughness Versus Temperature

TABLE 2. EPOXY MODE I FATIGUE DATA SUMMARY

Experiment Code	Specimen Code	Thickness (in)	Initial Crack Length (in)	Final Crack Length (in)	G_{min} (in.lb/in^2)	G_{max} (in.lb/in^2)	B	n	G_I at da/dN=10^{-2} (in.lb/in^2)
E1CDF	E1-4-6	0.151	4.9	5.2	0.19	0.20	5.61×10^{3}	57.0	0.79
	E1-1-4	0.149	3.7	4.0	0.40	0.50	1.05×10^{2}	18.1	0.60
E1CWF	E1-5-7	0.148	3.0	3.4	0.35	0.49	7.81×10^{4}	18.1	0.50
E1RDF	E1-4-4	0.149	2.5	2.6	0.66	0.80	0.23	28.8	0.90
E1RWF	E1-5-2	0.149	3.4	3.9	0.72	1.2	2.60×10^{-4}	18.2	1.22
	E1-5-4	0.132	4.0	5.2	0.48	1.0	2.05×10^{-4}	7.5	1.68
E1EDF	E1-2-1*	0.142	5.2	6.3	0.62	1.22	1.65×10^{-2}	11.0	0.96
	E1-2-6	0.146	4.2	4.7	0.64	0.83	9.12×10^{-2}	25.0	0.92
E1PDF	E1-2-1*	0.142	4.6	5.1	0.62	0.91	4.57×10^{-3}	12.6	1.06

NOTE: All specimens had a rough crack surface with some fiber pull-out.

* This specimen was tested twice, the second time at a lower temperature.

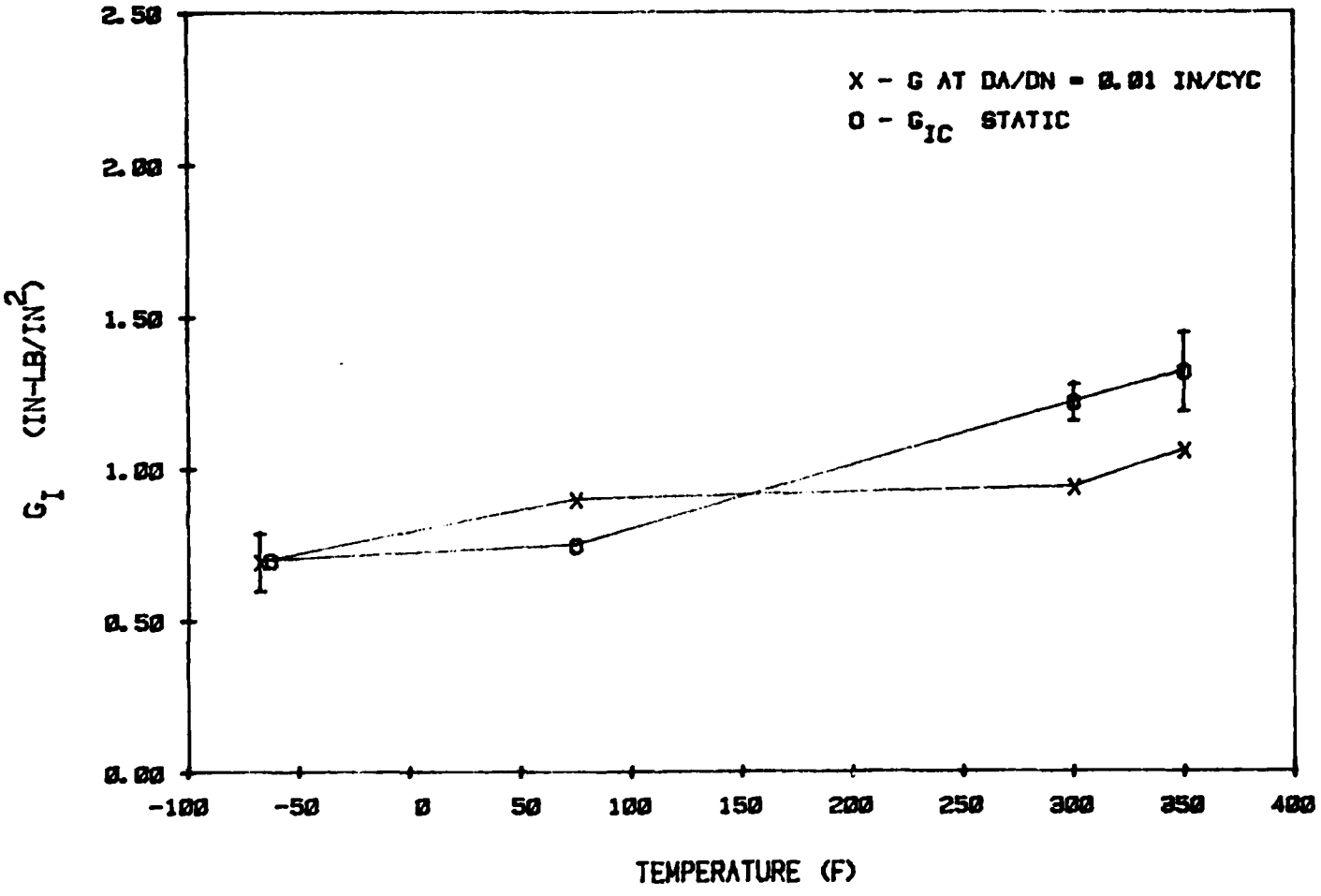

Figure 4. Epoxy Mode I Dry Static/Fatigue Correlation

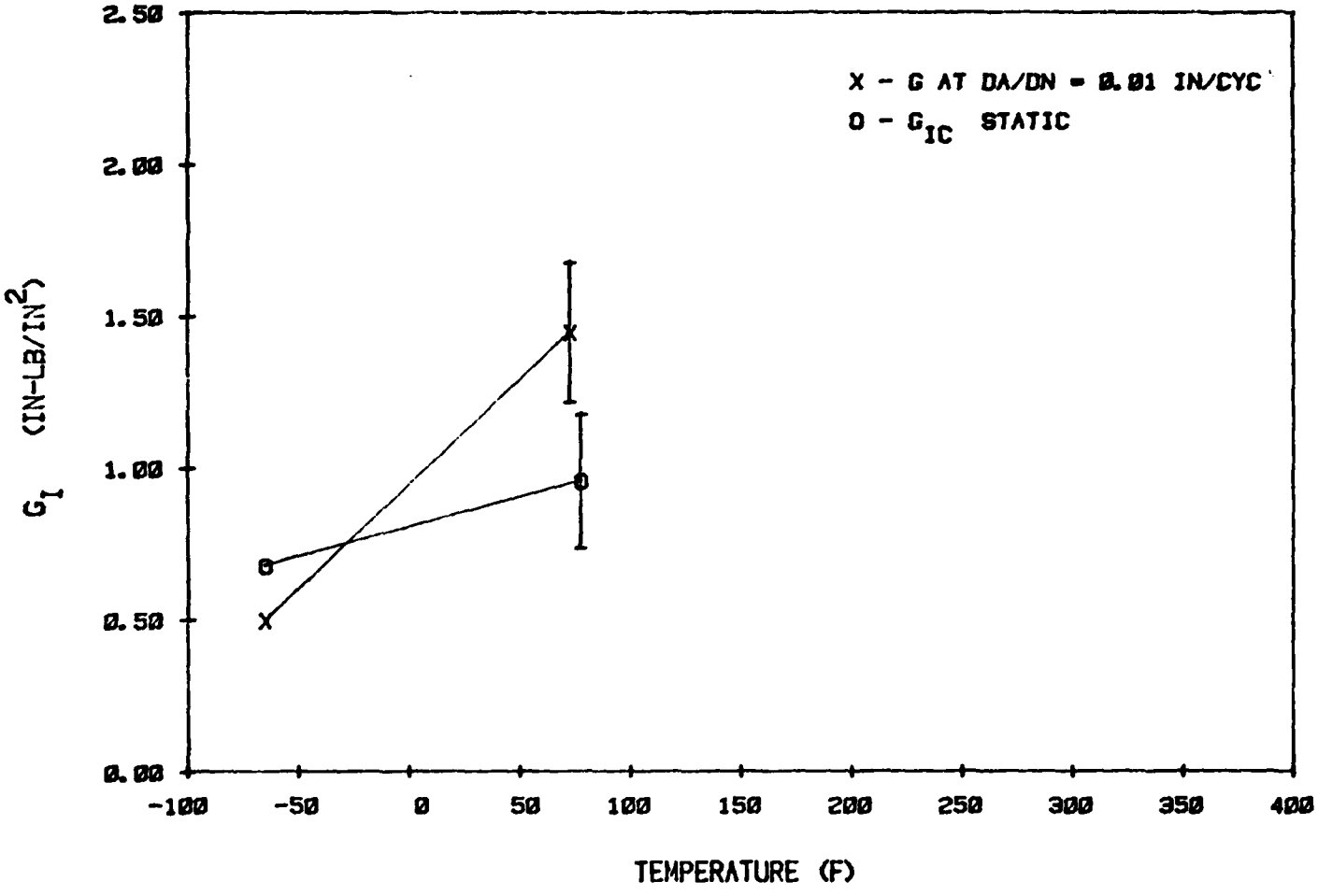

Figure 5. Epoxy Mode I Wet Static/Fatigue Correlation

The graphite-epoxy Mode I fatigue data exhibit the high crack growth rates observed previously (Reference 2). The empirical constants B and n are not being viewed as material constants in the same sense as the critical G values. The constants B and n are subject to scatter, number of data points, spread of the data in terms of crack growth rate, and possibly other variables such as stress ratio and test cyclic frequency. The phrase "high growth rate" is used here for values of n above 15. As expected, the B constants are approximately inversely proportional to the critical G values. In other words, the crack growth curves shift up or down as the toughness changes.

The graphite-bismaleimide Mode I toughness data is summarized in Table 3. Individual specimen data plots are gathered in Appendix B. Again, there is considerable scatter in the data due to the roughness of the fracture surface. As shown in Figure 6, the behavior is remarkably similar to that shown in Figure 3 for graphite-epoxy.

The fatigue data for the graphite-bismaleimide Mode I specimens are summarized in Table 4 and the individual data are preserved in Appendix C. Extrapolated G values from the fatigue tests can be compared to the static toughness as shown in Figures 7 and 8 for the dry and wet conditions respectively. The static trends are again largely supported by the fatigue results, and high delamination growth rates were observed.

3.3.2 Mode II

Because no careful characterization of environmental effects on Mode II toughness or growth rate has been performed before the present study, these results are expected to provide new information on the interlaminar shear failure behavior of laminates. Unlike the Mode I tests, the crack surface roughness in these tests was quite uniform throughout the test section, and little fiber pullout was observed.

TABLE 3. BISMALEIMIDE MODE I STATIC DATA SUMMARY

Experiment Code	Specimen Code	Thickness (in)	Initial Crack Length (in)	Final Crack Length (in)	A_1 $(lb\text{-}in^2)^{-1}$	A_2 (in lb)	G_{IC} (in lb/in^2)
P1CDS	P1-4-1	0.142	4.0	5.5	0.00142	19.37	0.80
	P1-4-5	0.141	3.0	5.5	0.00157	17.70	0.74
P1CWS	P1-1-3	0.140	2.5	6.5	0.00153	17.12	0.67
P1RDS	P1-4-2	0.142	3.0	5.5	0.00147	19.91	0.87
	P1-4-9	0.143	3.0	5.5	0.00146	19.47	0.83
P1RWS	P1-1-2	0.142	3.5	6.5	0.00124	21.56	0.87
P1EDS	P1-3-5	0.141	3.0	7.0	0.00125	21.10	0.83
	P1-2-10	0.144	3.0	6.5	0.00139	19.70	0.81
P1PDS	P1-3-8	0.141	3.0	6.0	0.00125	26.39	1.3
	P1-2-3	0.145	3.5	6.5	0.00122	22.87	0.96

NOTE: All specimens had a rough crack surface with some fiber pull-out. The elevated and peak temperature test coupons were exceptionally rough.

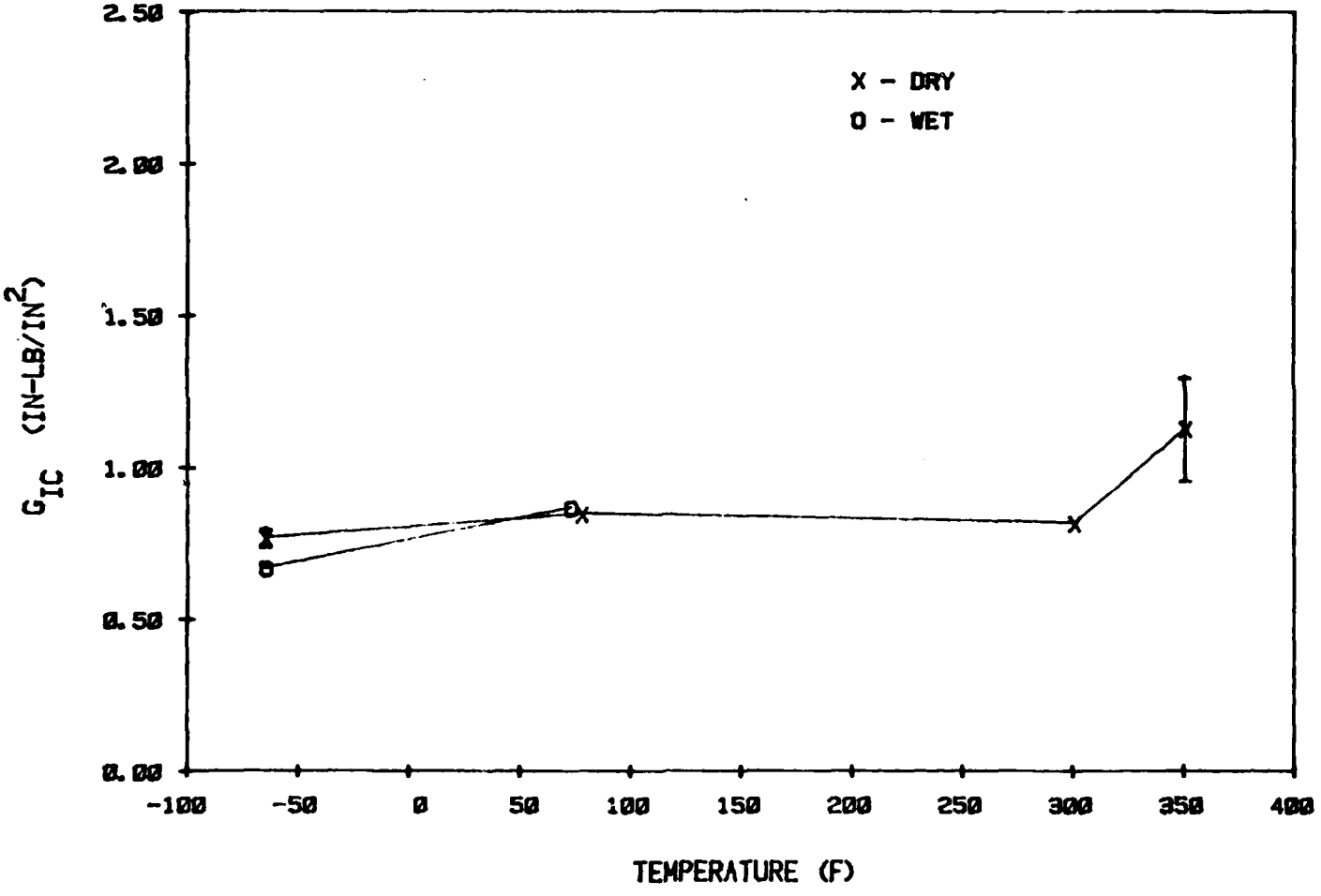

Figure 6. Bismaleimide Mode I Toughness Versus Temperature

TABLE 4. BISMALEIMIDE MODE I FATIGUE SUMMARY

Experiment Code	Specimen Code	Thickness (in)	Initial Crack Length (in)	Final Crack Length (in)	G_{min} (in.lb/in.^{2})	G_{max} (in.lb/in^2)	B	n	G_I at da/dN=10^{-2} (in.lb/in.^{2})
P1CDF	P1-5-2	0.139	3.3	3.4	0.50	0.52	2.10×10^{5}	190	0.51
P1CWF	P1-1-8	0.140	3.5	3.9	0.37	0.48	7.63×10^{7}	31.0	0.48
P1RDF	P1-4-4	0.143	5.2	5.6	0.54	0.75	0.22	19.6	0.85
	P1-4-7	0.143	2.6	4.4	0.67	1.05	1.97×10^{-2}	34.5	0.98
	P1-5-4	0.139	3.0	4.6	0.76	1.0	8.48×10^{-3}	31.1	1.01
P1RWF	P1-1-1	0.139	4.1	5.8	0.20	0.47	2.36×10^{3}	12.9	0.38
	P1-1-9	0.139	4.3	5.9	0.31	0.38	9.40×10^{15}	43.4	0.38
P1EDF	P1-5-7	0.139	5.1	5.2	0.55	0.67	5.23×10^{-2}	17.8	0.91
P1PDF	P1-2-4	0.140	3.0	3.2	0.87	1.15	5.19×10^{-5}	18.6	1.33

NOTE: All specimens had a rough crack surface with fiber pull-out.

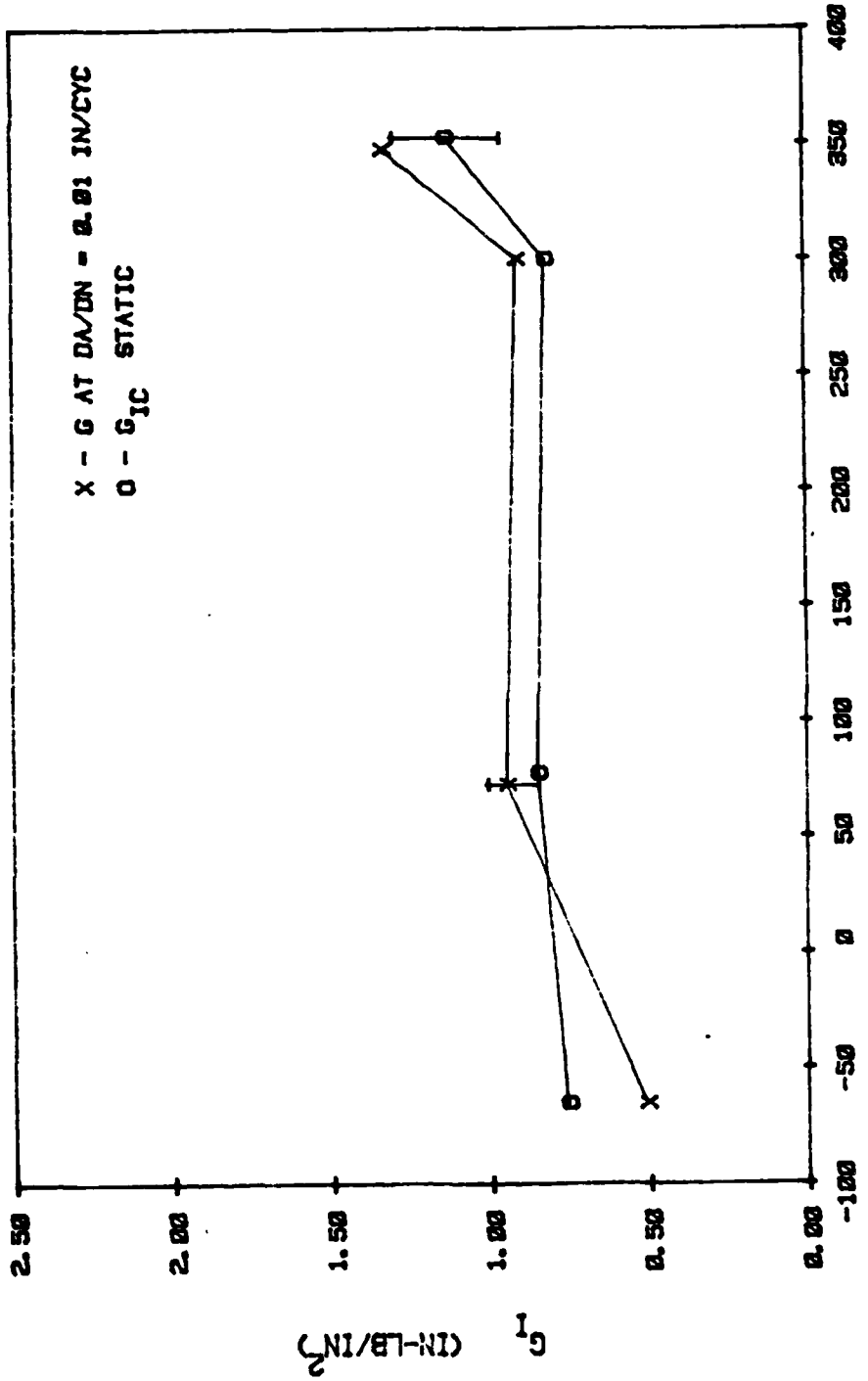

Figure 7. Bismaleimide Mode I Dry Static/Fatigue Correlation

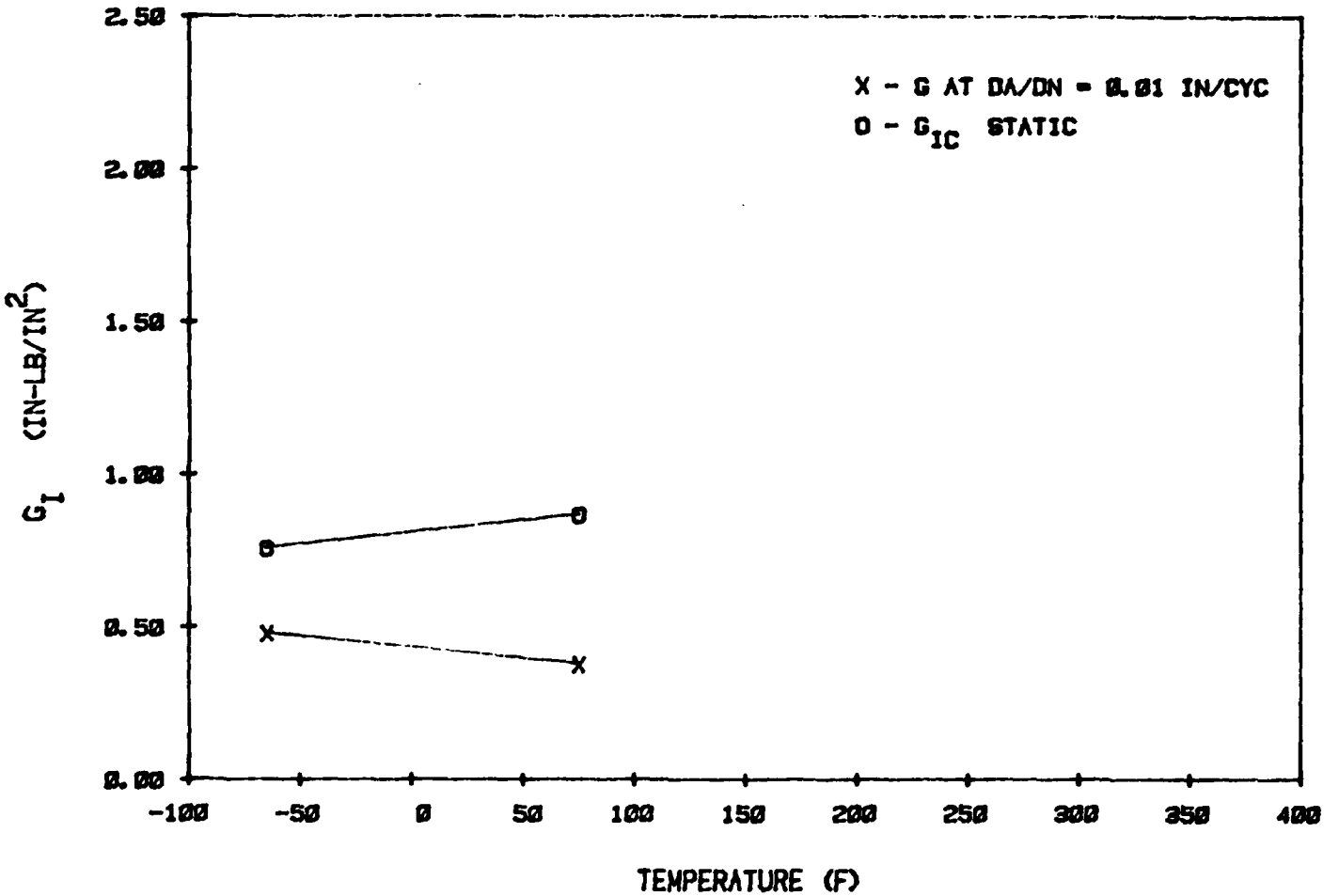

Figure 8. Bismaleimide Mode I Wet Static/Fatigue Correlation

The Mode II coupon used in the present experiments does not exhibit a pure Mode II crack growth. Rather, there is a mix of Mode I and Mode II components. The detailed analysis of this Mode II coupon, which is documented in Appendix D, indicates that both the Mode I and Mode II components of the strain-energy release rate are independent of the crack length. And, at a load near the measured critical load, the Mode I component is 23.5% of G_{TOT} and the Mode II component is 76.5% of G_{TOT}.

The graphite-epoxy Mode II static data are summarized in Table 5 from the original data plots presented in Appendix D. Looking at the toughness as a function of temperature in Figure 9, the trend is much different from the Mode I trend (Figure 3). At room temperature G_{IIC} is about twice as large as G_{IC}. But the Mode II toughness decreases significantly at elevated temperature, and becomes about equal to the Mode I toughness. Moisture seems to greatly improve the toughness at -65°F, without changing the room temperature value very much.

The graphite-epoxy Mode II fatigue data are summarized in Table 6. The growth plots are gathered in Appendix E. When appropriate G values from the fatigue tests are compared to the static data (Figures 10 and 11), a consistent data set is again observed. Growth rates in Mode II fatigue are much lower than those for Mode I. This trend was also observed in Reference 2.

The graphite-bismaleimide Mode II static toughness data are summarized in Table 7 from the data plots compiled in Appendix D. Again, toughness decreases with temperature as shown in Figure 12. Moisture improves the Mode II toughness somewhat at cold temperature, but seems to degrade it at room temperature. These trends are again quite similar to the observed behavior of graphite-epoxy, except that the observed toughness of the graphite-bismaleimide is about 2/3 of that measured for the graphite-epoxy.

TABLE 5. EPOXY MODE II STATIC DATA SUMMARY

Experiment Code	Specimen Code	t_a (in)	t_f (in)	Initial Crack Length (in)	Final Crack Length (in)	Compliance Slope C_1* (lb^{-1})	Compliance Intercept C_o* (in/lb)	P_c (lb)	G_{TOT} ($in.lb/in^2$)	G_{IIc}** ($in.lb/in^2$)
E2CDS	E2-3-5	0.0160	0.0175	3.5	5.0	2.0×10^{-6}	1.81×10^{-5}	1355	1.88	1.44
	E2-4-7	0.0155	0.0165	2.5	3.0	2.2×10^{-6}	1.60×10^{-5}	1515	2.56	1.96
E2CWS	E2-1-8	0.0160	0.0160	2.7	2.8	2.0×10^{-6}	1.24×10^{-5}	1710	2.98	2.28
E2RDS	E2-2-5	0.0151	0.0155	2.9	5.8	1.4×10^{-6}	1.86×10^{-5}	1730	2.13	1.61
	E2-2-6	0.0147	0.0163	2.5	3.2	2.0×10^{-6}	1.74×10^{-5}	1620	2.65	2.07
E2RWS	E2-1-1	0.0150	0.0160	2.5	5.2	1.7×10^{-6}	0.98×10^{-5}	1605	2.17	1.68
E2EDS	E2-5-10	0.0150	0.0142	2.1	4.4	1.2×10^{-6}	1.24×10^{-5}	1640	1.73	1.32
E2PDS	E2-4-9	0.0165	0.0170	3.1	5.5	1.3×10^{-6}	1.15×10^{-5}	1420	1.30	0.99

* Compliance $C = C_1 a + C_o$

** $G_{IIc} = (0.765)\, G_{TOT}$

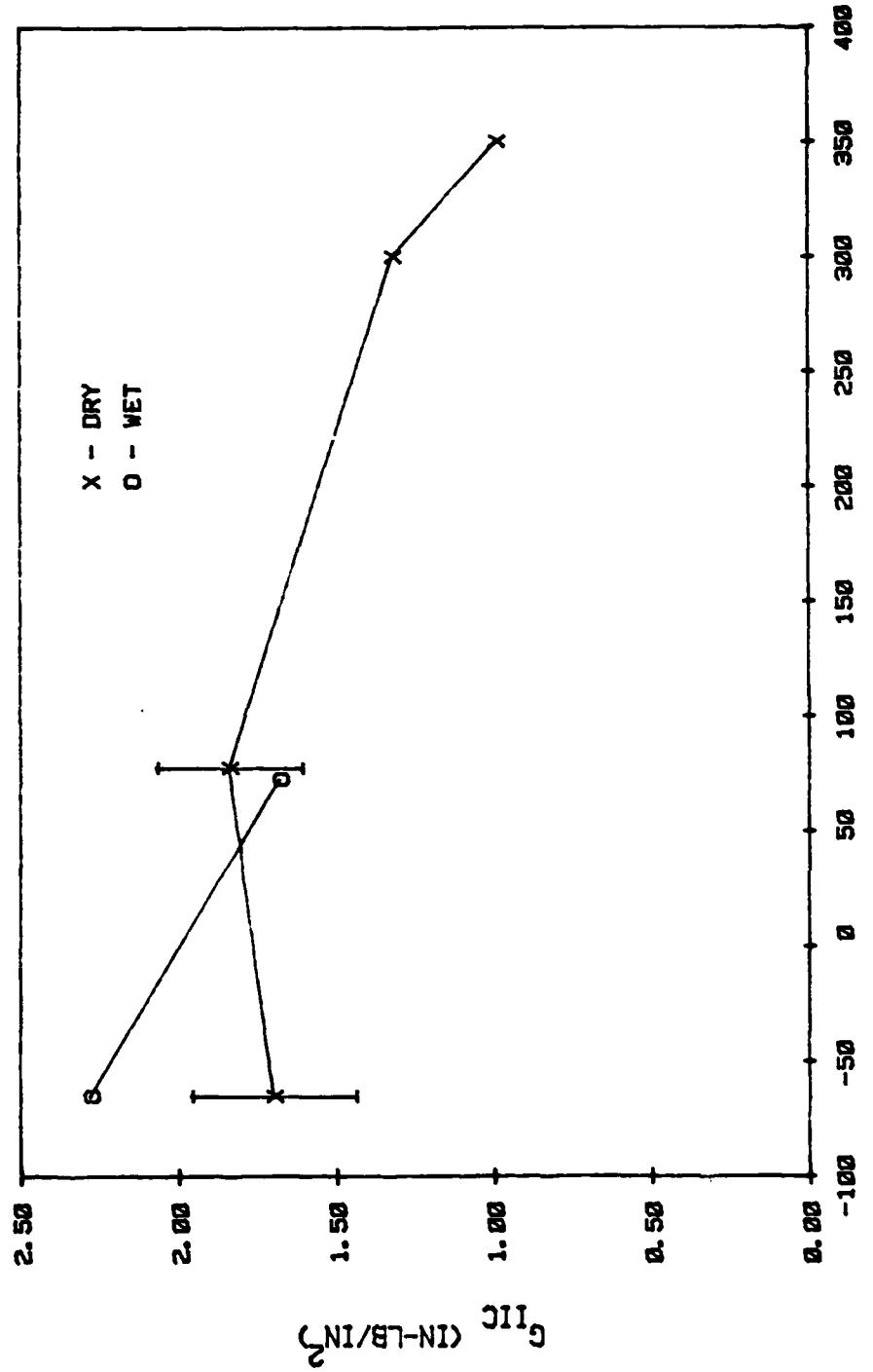

Figure 9. Epoxy Mode II Toughness Versus Temperature

TABLE 6. EPOXY MODE II FATIGUE DATA SUMMARY

Experiment Code	Specimen Code	t_s (in)	t_f (in)	Initial Crack Length (in)	Final Crack Length (in)	G_{min} (in.lb/in.^{2})	G_{max} (in.lb/in^2)	B	n	G_I at da/dN=10^{-2} (in.lb/in.^{2})
E2CDF	E2-4-1	0.0155	0.0170	2.4	3.1	1.79	2.08	*4.11×10^{-7}	11.9	1.79
	E2-4-3	0.0160	0.0165	2.9	3.5	1.28	2.08			
E2CWF	E2-1-3	0.0160	0.0155	2.5	3.1	1.45	1.98	2.37×10^{-7}	12.1	1.64
E2RDF	E2-2-7	0.0150	0.0157	2.9	5.3	0.70	1.58	7.65×10^{-5}	7.67	1.45
E2RWF	E2-1-5	0.0155	0.0150	2.5	4.8	0.68	1.65	*3.14×10^{-3}	8.8	1.49
	E2-1-2	0.0140	0.0190	2.5	4.6	1.02	1.65			
E2EDF	E2-4-8	0.0165	0.0160	2.9	4.3	0.83	1.32	1.72×10^{-4}	7.2	1.35
E2PDF	E2-5-7	0.0142	0.0158	3.5	4.2	1.03	1.36	1.39×10^{-4}	10.8	1.13

* Combined data in both specimens.

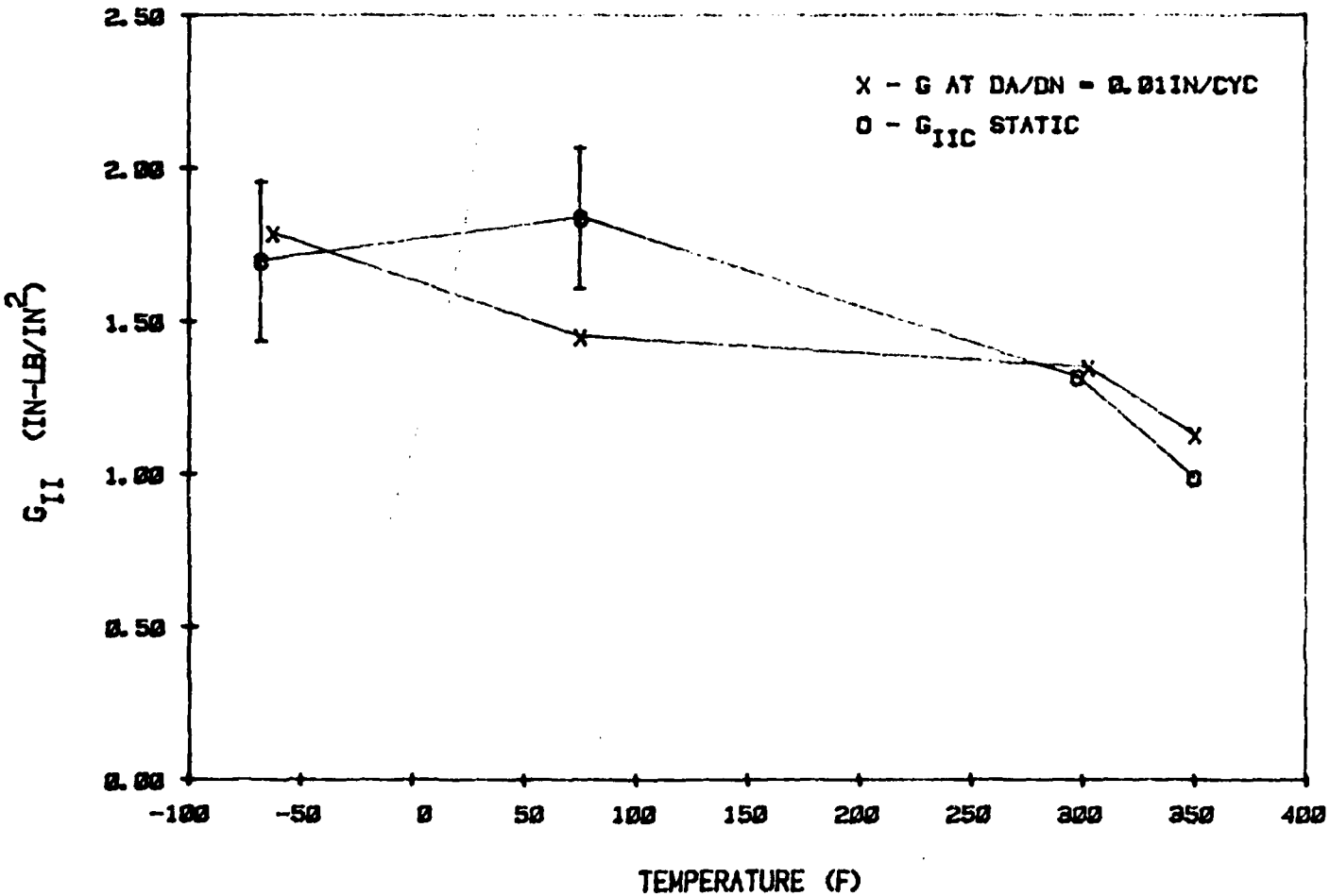

Figure 10. Epoxy Mode II Dry Static/Fatigue Correlation

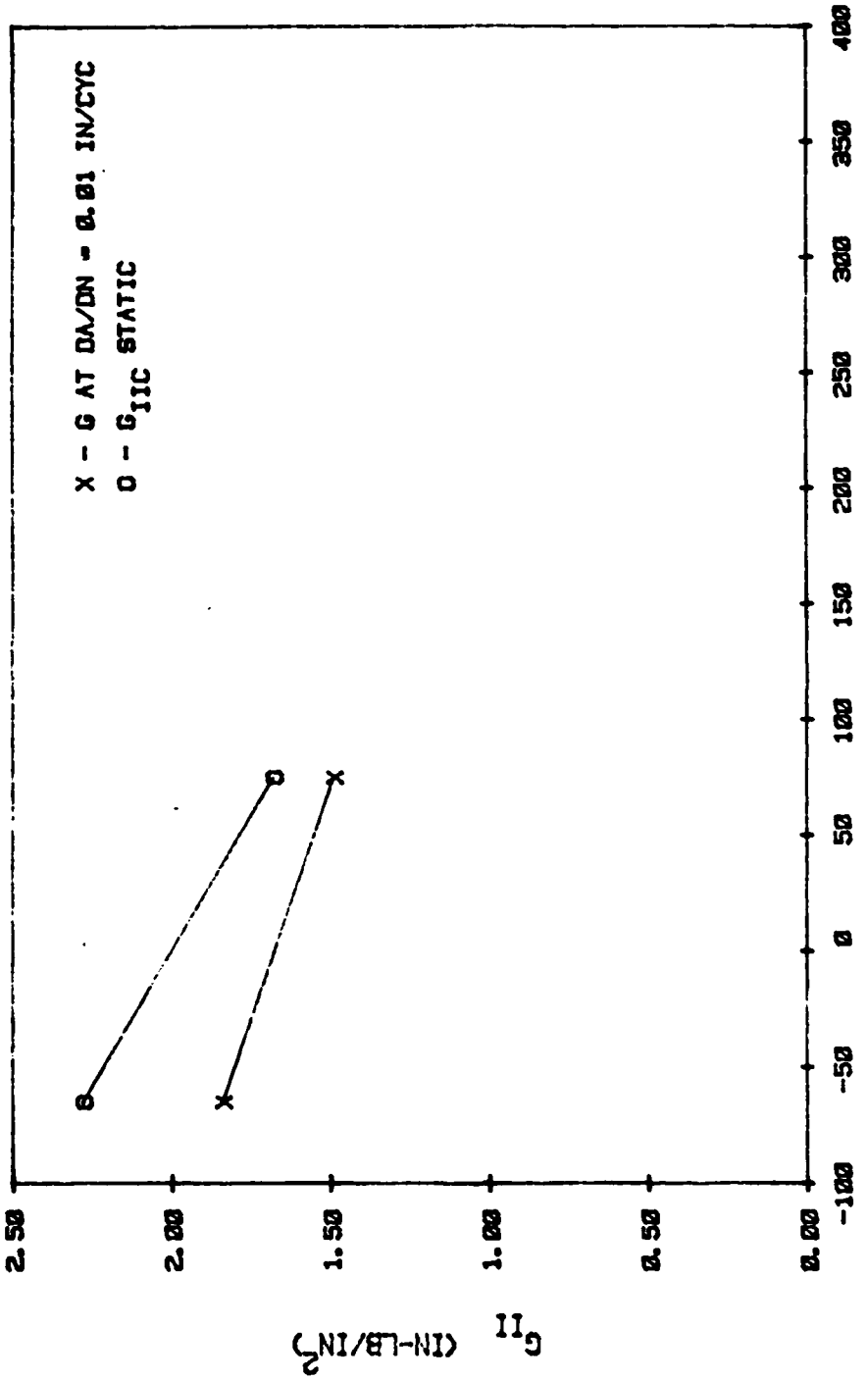

Figure 11. Epoxy Mode II Wet Static/Fatigue Correlation

TABLE 7. BISMALEIMIDE MODE II STATIC DATA SUMMARY

Experiment Code	Specimen Code	t_s (in)	t_f (in)	Initial Crack Length (in)	Final Crack Length (in)	Compliance Slope C_1* (lb^{-1})	Compliance Intercept C_o* (in/lb)	P_c (lb)	G_{TOT} (in.lb/in^2)	G_{IIc}** (in.lb/in^2)
P2CDS	P2-1-6	0.0180	0.0175	2.6	3.1	2.07×10^{-6}	1.24×10^{-5}	1240	1.60	1.22
	P2-1-8	0.0179	0.0175	2.7	5.2	1.69×10^{-6}	1.70×10^{-5}	1300	1.44	1.10
P2CWS	P2-5-3	0.0168	0.0180	2.3	3.2	1.65×10^{-6}	1.65×10^{-5}	1490	1.82	1.39
P2RDS	P2-1-1	0.0179	0.0210	2.5	5.5	1.65×10^{-6}	2.82×10^{-6}	1395	1.61	1.23
	P2-1-2	0.0180	0.0210	3.0	5.8	1.61×10^{-6}	2.44×10^{-6}	1300	1.36	1.04
	P2-2-5	0.0170	0.0210	3.0	4.6	1.47×10^{-6}	2.48×10^{-6}	1340	1.33	1.02
	P2-6-1 $	0.0149	0.0152	2.6	4.0	2.07×10^{-6}	1.33×10^{-5}	1200	1.50	1.15
	P2-7-1 $$	0.0146	0.0154	2.4	5.2	1.53×10^{-6}	1.59×10^{-5}	1110	0.96	0.73
P2RWS	P2-5-2	0.0175	0.0175	2.0	6.0	1.50×10^{-6}	1.65×10^{-5}	1200	1.07	0.82
	P2-5-5	0.0190	0.0190	2.6	5.8	1.78×10^{-6}	1.11×10^{-5}	1150	1.17	0.90
	P2-6-2 $	0.0154	0.0149	2.2	6.8	1.67×10^{-6}	1.46×10^{-5}	1190	1.18	0.90
	P2-7-2 $$	0.0153	0.0156	2.5	5.2	1.72×10^{-6}	1.59×10^{-5}	1105	1.05	0.80
P2EDS	P2-2-2	0.0180	0.0183	3.2	5.9	1.17×10^{-6}	1.10×10^{-5}	1210	0.87	0.67
	P2-2-9	0.0147	0.0204	2.6	6.6	1.49×10^{-6}	1.21×10^{-5}	1190	1.03	0.79
P2PDS	P2-2-7	0.0171	0.0172	3.0	6.3	1.89×10^{-6}	0.93×10^{-5}	1110	1.16	0.89
	P2-2-6	0.0184	0.0166	3.4	6.9	1.44×10^{-6}	1.33×10^{-5}	1200	1.05	0.80

* Compliance $C = C_1 a + C_o$

** $G_{IIc} = (0.765)\, G_{TOT}$

$ 309 fiber finish (rather than 314 fiber finish), post cured at 550° F.

$$ 309 fiber finish (rather than 314 fiber finish), post cured at 475° F.

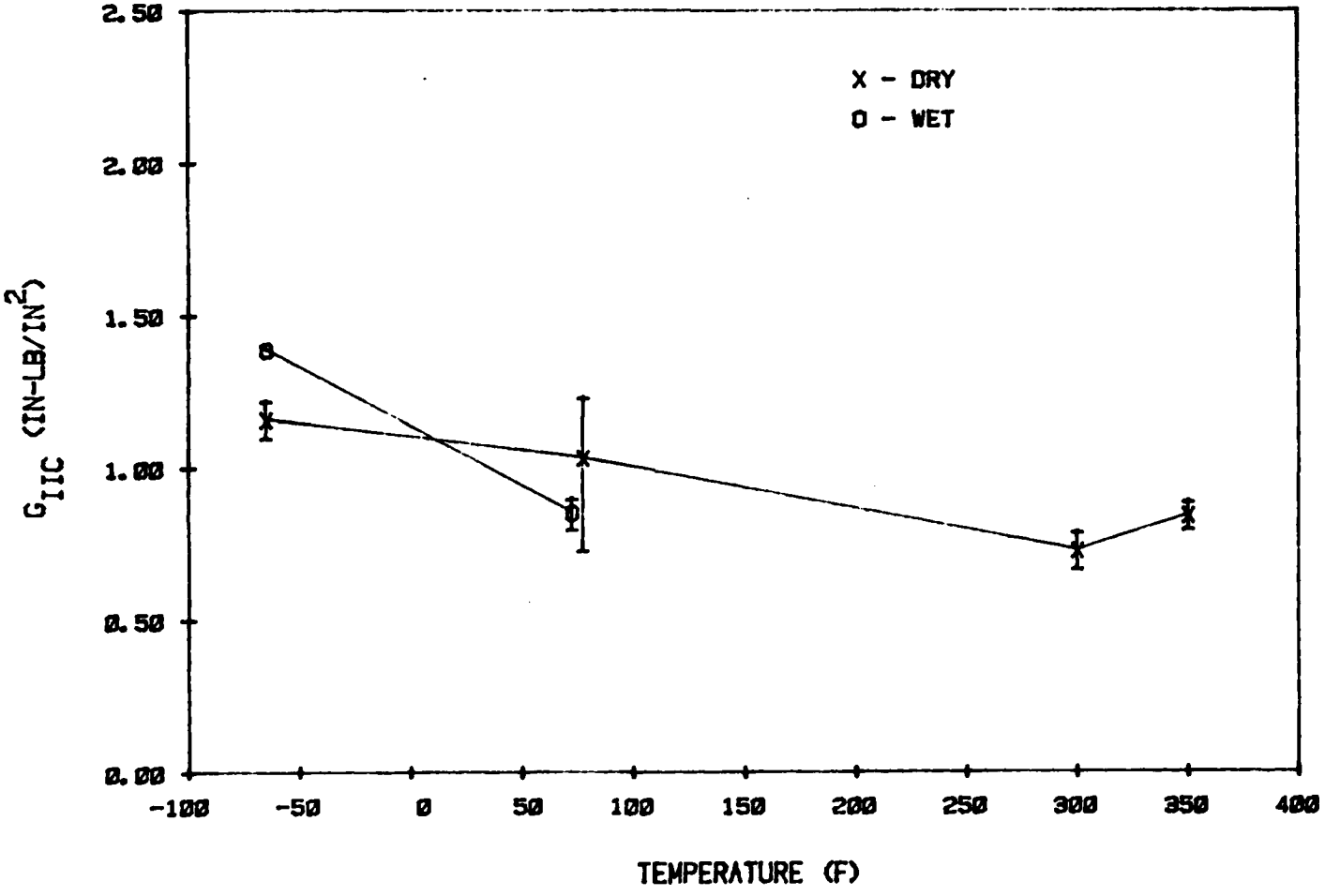

Figure 12. Bismaleimide Mode II Toughness Versus Temperature

The graphite-bismaleimide Mode II fatigue data are displayed in Table 8. Data plots can be found in Appendix E. The fatigue data are correlated to the static data for the dry and wet conditions in Figures 13 and 14 respectively, where they confirm the observed trends.

TABLE 8. BISMALEIMIDE MODE II FATIGUE DATA SUMMARY

Experiment Code	Specimen Code	t_o (in)	t_f (in)	Initial Crack Length (in)	Final Crack Length (in)	G_{min} (in.lb/in.^{2})	G_{max} (in.lb/in^2)	B	n	G_I at da/dN=10^{-2} (in.lb/in.^{2})
P2CDF	P2-3-1	0.0175	0.0180	2.1	2.9	0.85	1.22	*2.75×10^{-4}	13.7	0.99
	P2-3-3	0.0175	0.0175	2.1	3.3	0.54	1.12			
P2CWF	P2-5-1	0.0136	0.0179	3.2	4.6	0.83	1.20	1.41×10^{-4}	14.0	1.04
P2RDF	P2-1-3	0.0184	0.0211	2.9	4.9	0.55	1.20	*5.40×10^{-4}	9.8	1.03
	P2-1-10	0.0175	0.0178	2.6	4.0	0.77	1.20			
P2RWF	P2-5-6	0.0150	0.0178	2.1	4.3	0.69	1.20	*1.35×10^{-3}	13.4	0.89
	P2-5-7	0.0160	0.0168	2.1	4.6	0.75	1.26			
P2EDF	P2-3-7	0.0170	0.0185	2.8	4.5	0.49	0.74	3.94×10^{-2}	8.3	0.65
	P2-3-8	0.0175	0.0175	2.7	4.4	0.65	0.84	2.79×10^{-1}	13.6	0.60
P2PDF	P2-2-1	0.0180	0.0170	3.2	4.9	0.61	1.36	7.08×10^{-4}	8.7	1.04

* Combined data for both specimens.

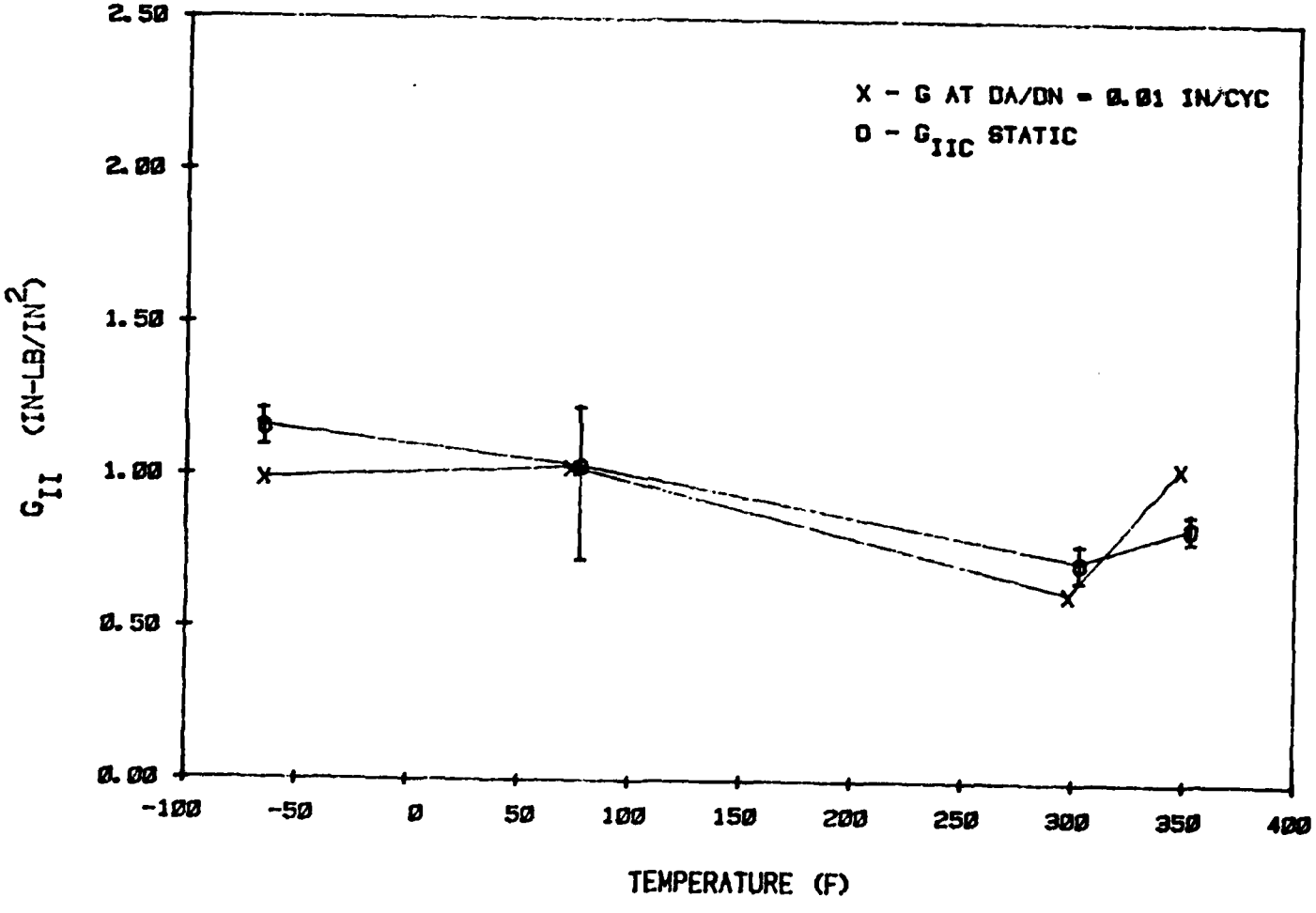

Figure 13. Bismaleimide Mode II Dry Static/Fatigue Correlation

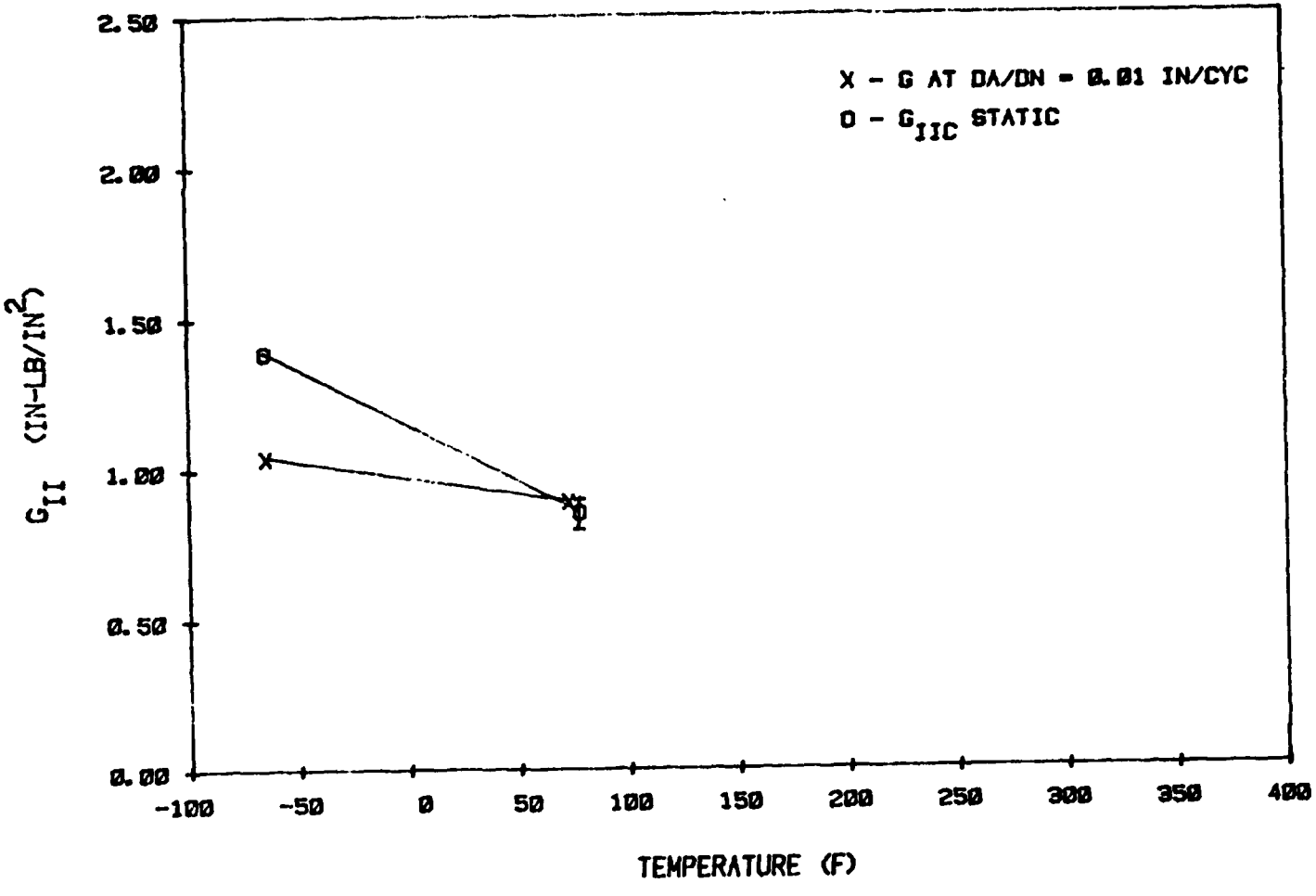

Figure 14. Bismaleimide Mode II Wet Static/Fatigue Correlation

IV ENVIRONMENTAL RESISTANCE

The two systems were submitted to various tests to screen wet and dry properties. These included the resin content, gel time, tack, thermal spike resistance, glass transition temperature, flexure, interlaminar shear, in-plane shear, and compression.

4.1 Resin Content, Gel Time, and Tack

Resin content of the prepreg material and of all test panels was measured by solvent extraction. Specimens of cured laminate were cut and weighed. The resin was then extracted from the fibers by an acid digestion method using hot sulfuric acid and hydrogen peroxide with a distilled water rinse. The clean fibers were reweighed and the resin solids content calculated. This information is tabulated in Table 9.

Gel time was measured isothermally using a Fisher-Johns Melting Point Apparatus as a temperature source. A small sample of resin was scraped from fresh prepreg and placed between two glass microscope slide cover slips. This sandwich was placed on the preheated Fisher-Johns stage and probed periodically until a cessation of flow indicated gellation time at temperature. A seven to ten power binocular microscope aided visual observations and improved repeatibility of results. The prepreg gel time is presented in Table 10.

To test the self-adhesion tack, samples of both prepreg materials were left at 80°F in their sealed shipping bags for 8 hours, followed by 4 hours outside of the shipping bags while in roll form, plus one hour at room temperature outside of any bag while in ply

TABLE 9 RESIN CONTENT AND SPECIFIC GRAVITY OF TEST PANELS

MATERIAL SYSTEM	BATCH NO/ROLL	PANEL TYPE		RESIN CONTENT (%)	SPECIFIC GRAVITY
T300-6K/V378A	4902/3	Pre Preg		30.63	-
AS-1/3501-6	1734/36B	Pre Preg		42.04	-
AS-1/3501-6	1734/36B	Tg		26.28	1.54
		Spike		27.50	1.61
		Miniwich		27.89	-
		Flex #1		33.08	1.60
		Flex #2		31.06	1.62
		+45 #1		27.67	1.61
		∓45 #2		27.30	1.63
		Mode	1-1	31.48	1.60
			1-2	30.46	1.62
			1-3	32.45	1.60
			1-4	31.98	1.60
			1-5	30.99	1.60
		Mode	2-1	25.86	1.67
			2-2	25.67	1.61
			2-3	26.08	1.65
			2-4	26.50	1.62
			2-5	25.55	1.64
T300-6K/V378A	4902/3	Tg		30.93	1.58
		Spike		28.81	1.57
		Miniwich		30.55	1.51
		Flex #1		30.45	1.56
		Flex #2		31.00	1.57
		+45 #1		29.48	1.55
		∓45 #2		30.85	1.52
		Mode	1-1	31.17	1.56
			1-2	32.05	1.56
			1-3	32.04	1.58
			1-4	31.77	1.55
			1-5	29.92	1.56
		Mode	2-1	29.35	1.58
			2-2	29.45	1.59
			2-3	28.35	1.58
			2-4	29.01	1.58
			2-5	29.53	1.58

TABLE 10 COMPARISON OF T300-6K/V378A POLYIMIDE AND AS1/3501-6 EPOXY GEL TIMES (MINUTES)

	300°F	275°F	250°F	225°F	200°F	175°F
T300-6K/V378A B 4902/3	-	10	17	32	57	90
AS1/3501-6 B 1734/36B*	43	85	170	-	-	-

*The epoxy was run at only the higher temperatures due to the length of gel time below 250°F.

form. Two 3-inch by 6-inch plies of unidirectional material were laid at 90° to each other, forming a "cross". The plies were pressed together, using hand pressure, at 65°F. These samples were then suspended from the end of one ply (hanging vertically) for five minutes at 75°F. Both materials satisfactorily passed this test for self-adhesion tack by sticking together for the required five minutes.

4.2 Thermal Spike Resistance

Test specimens 1.5 in. x 1 in. x $[0/\pm45/0]_S$ were prepared from both material systems. These specimens were conditioned seven days at 180°F/75% relative humidity, spiked twice weekly at seven temperature increments from 210°F to 375°F for a total of ten spikes, and then re-equilibrated for two weeks at 180°F/75% RH. Thermal spikes were applied by subjecting each group of specimens to a one-minute immersion in an oil bath maintained at the desired spike temperature. Specimens were then double rinsed in methyl ethyl ketone and returned to 180°F/75% RH. An instrumented specimen with a thermocouple imbedded at its geometric center was used to determine that all specimens reached temperature equilibrium in less than 10 seconds. The moisture content after this test cycle was normalized to unspiked control specimens soaked at 180°F/75% RH and the data are plotted in Figure 15. The normalizing produces some zero baseline scatter, but the thermal spike resistance comparison of the two materials is dramatic. The AS1/3501-6 specimens exhibited the accelerated moisture absorptivity characteristic of the thermal spike effect at spike temperatures above 250°F. The T300-6K/V378A material's absorptivity was not affected until spike temperatures exceeded 350°F.

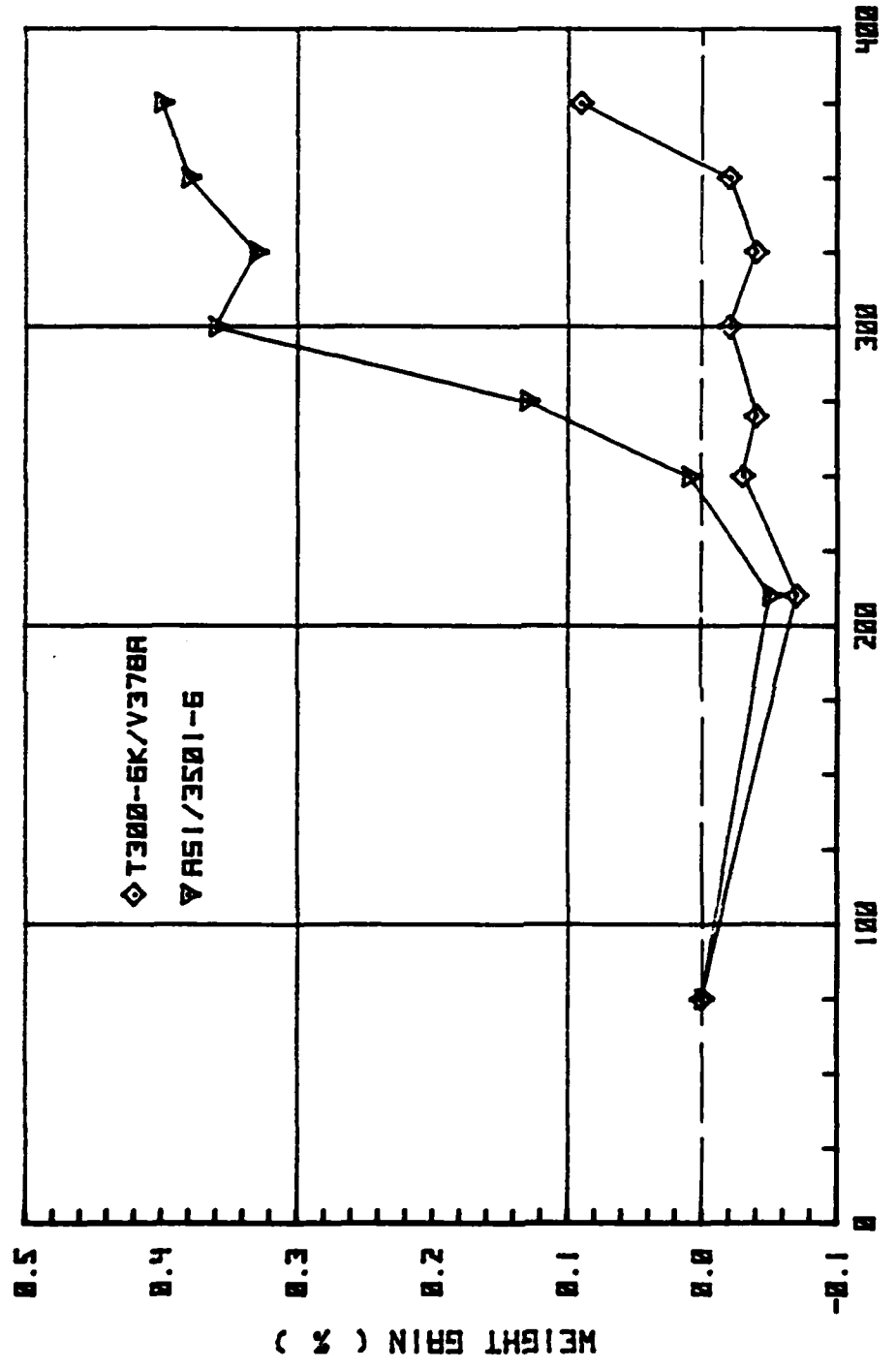

Figure 15. Moisture Absorptivity Due to the Effect of Ten Thermal Spikes after Soaking at 180°F/75% R.H.

4.3 Dry and Wet Glass Transition Temperature

Dry and wet glass transition temperatures (T_g) and coefficients of linear thermal expansion (CTE) were determined for both material systems. Data were obtained on a Perkin-Elmer TMS-1 Thermomechanical Analyzer (TMA) using the Loaded Column Expansion (LCE) method described by McKague, Reynolds, and Halkias in Reference 3.

LCE consists of loading a 0.5 in. tall x 0.25 in. wide x $[90]_{15}$ thick lamina specimen to approximately 60 psi in the TMA expansion apparatus. The specimen is cooled to -80°F, then heated to 700°F at a rate of 36°F/minute. Specimen dilation and temperature are recorded every 10°F, and a plot of thermal expansion versus temperature is computer printed. A second plot of instantaneous CTE versus temperature is then prepared to emphasize subtle inflection points.

The dry AS1/3501-6 exhibited an upward change in expansion rate typical of T_g at 450°F (Figures 16 and 17). Specimens were further dried and the test was performed a second time, again confirming the 440 to 450°F dry T_g.

Duplicate wet AS1/3501-6 specimens equilibrated at 75% relative humidity showed dramatic thermal expansion rate changes at 210°F to 250°F (Figures 18 and 19). This temperature correlates with the wet T_g of 230°F suggested by thermal spike data in Figure 15.

Dry T300-6K/V378A has a gradual expansion rate change (Figure 20) best observed in the instantaneous CTE plot (Figure 21). T_g values of 560 to 580°F are consistent in this material.

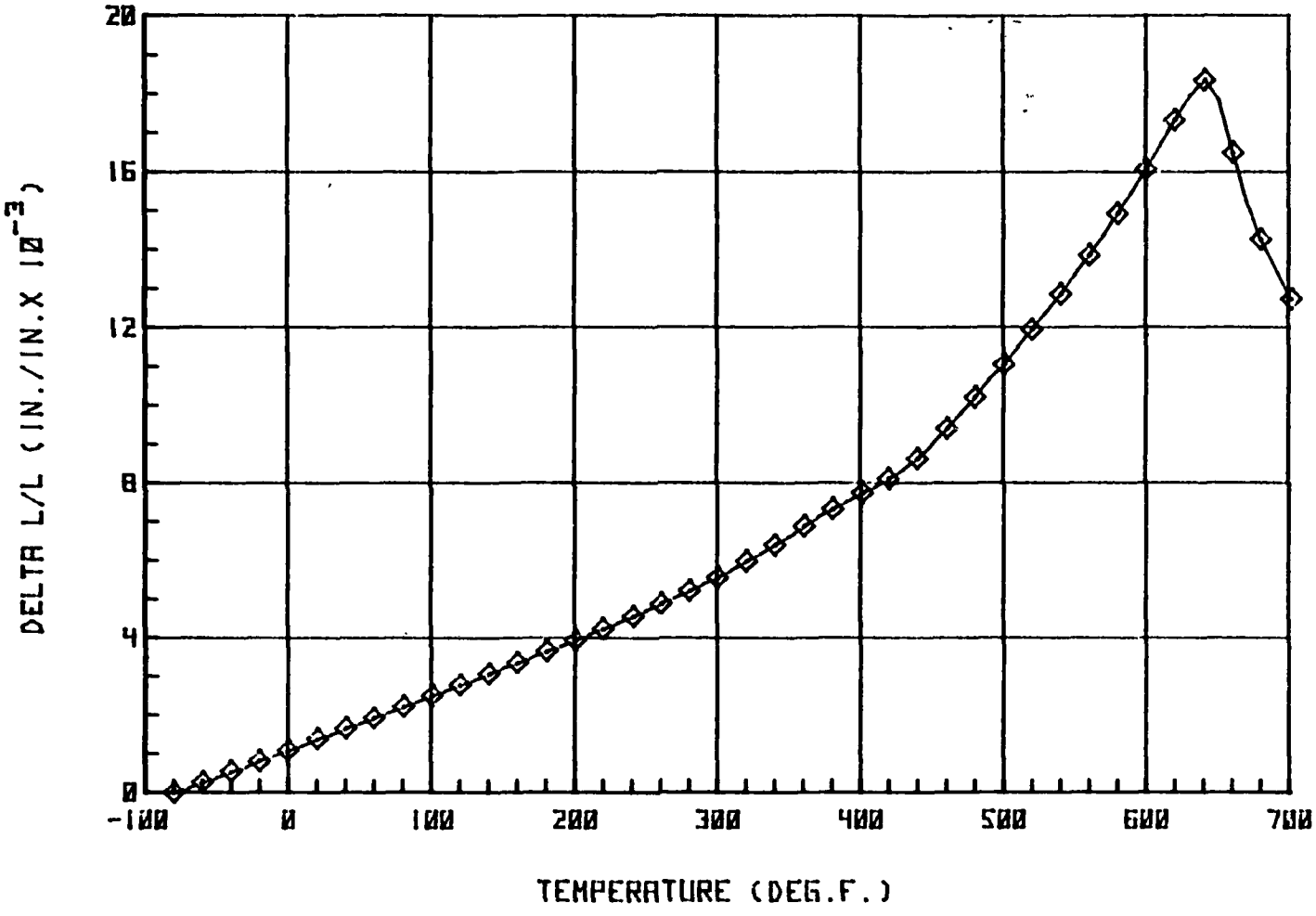

Figure 16. Thermal Expansion of Dry 15-Ply AS1/3501-6 (200 gm. Load)

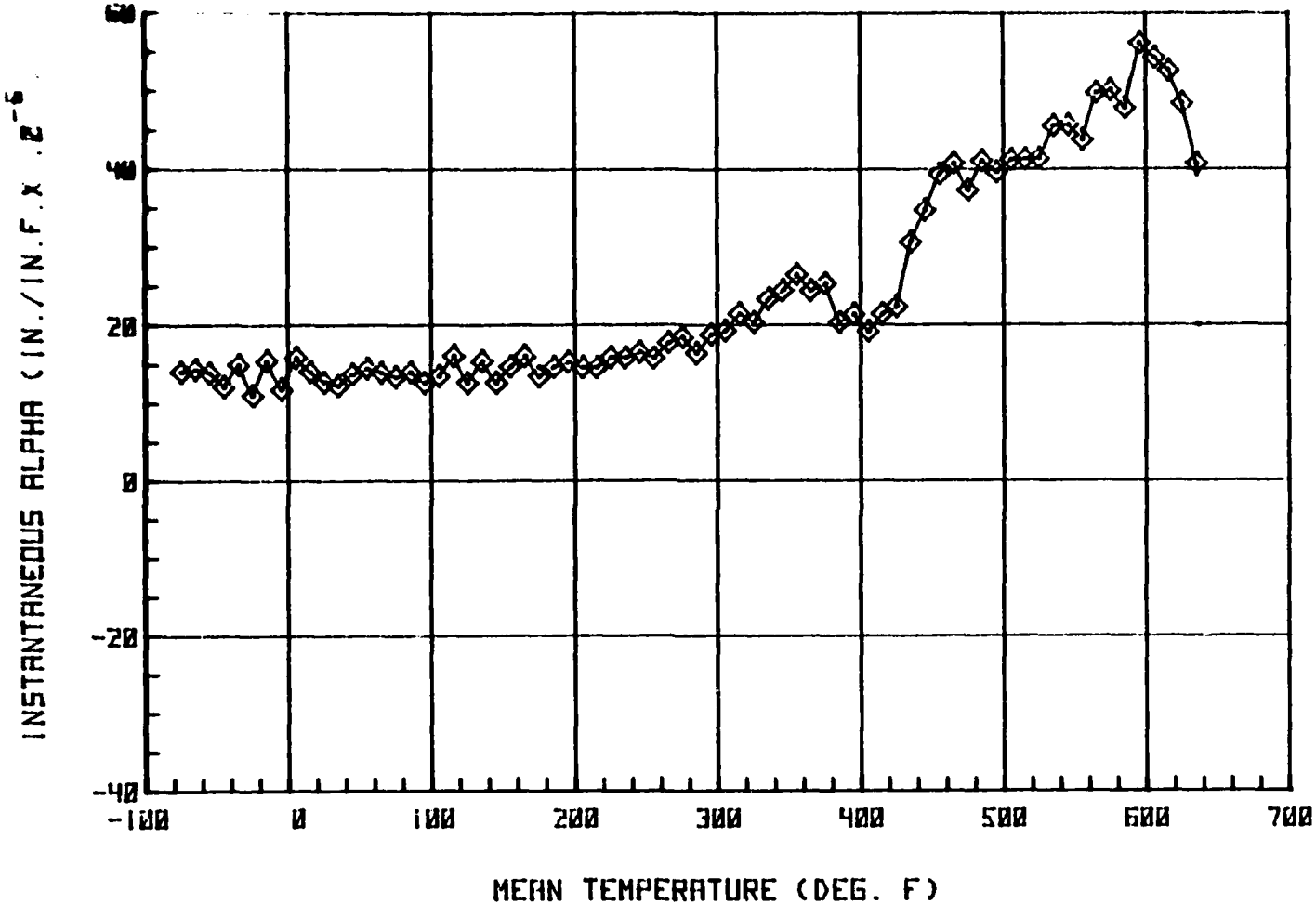

Figure 17. Coefficient of Thermal Expansion for Dry AS1/3501-6

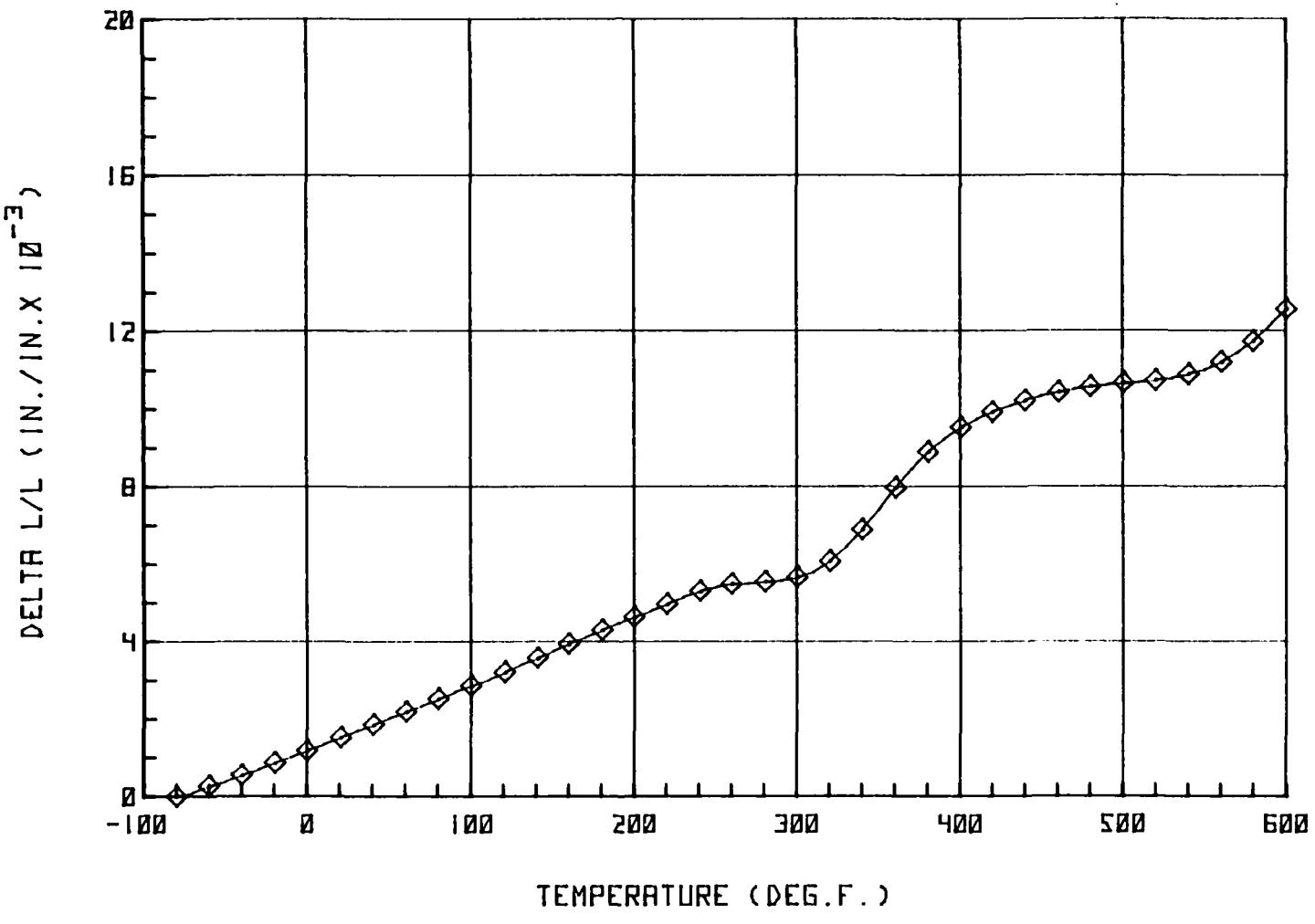

Figure 18. Thermal Expansion of Wet AS1/3501-6 (100 gm. Load)

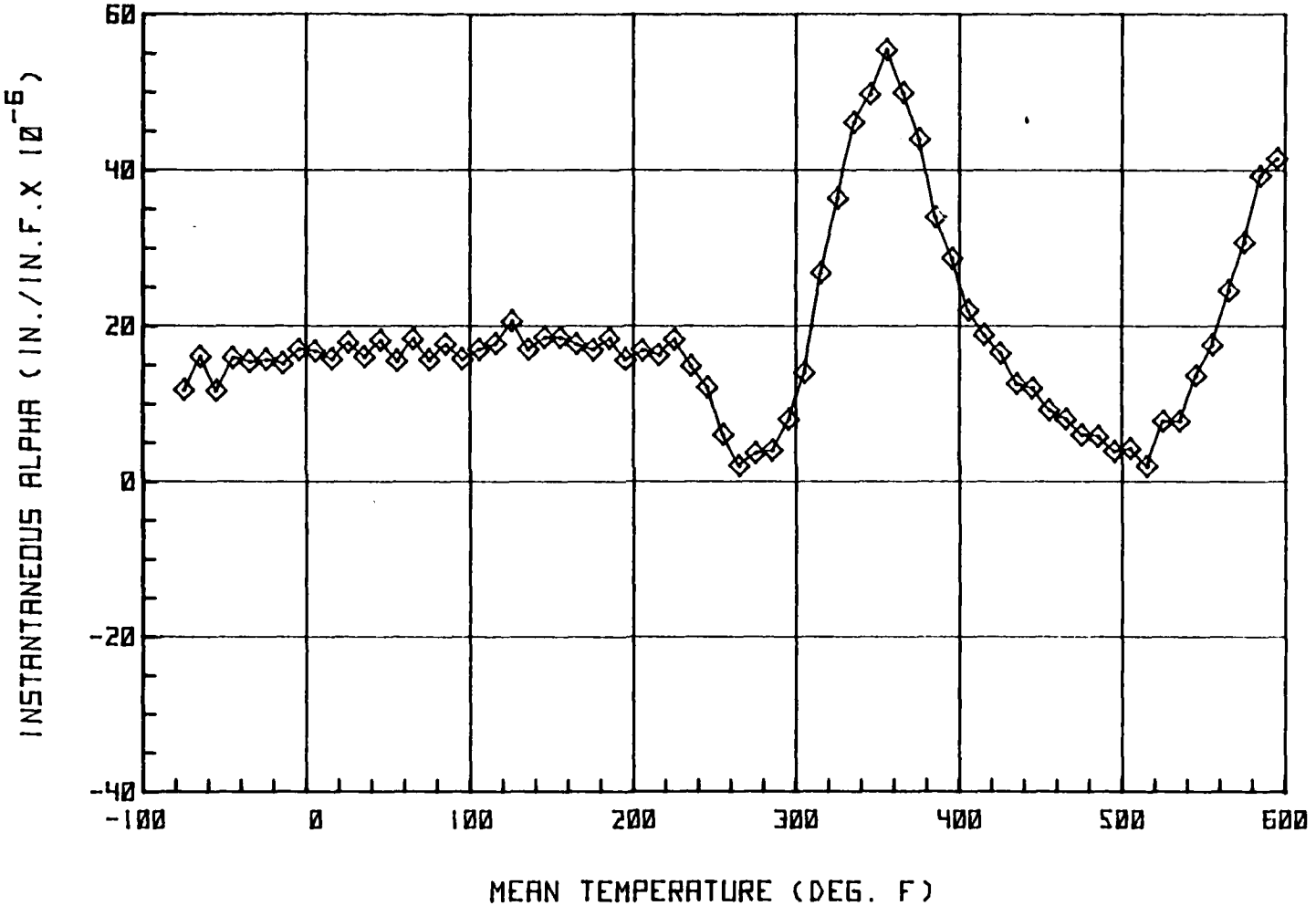

Figure 19. Coefficient of Thermal Expansion for Wet AS1/3501-6

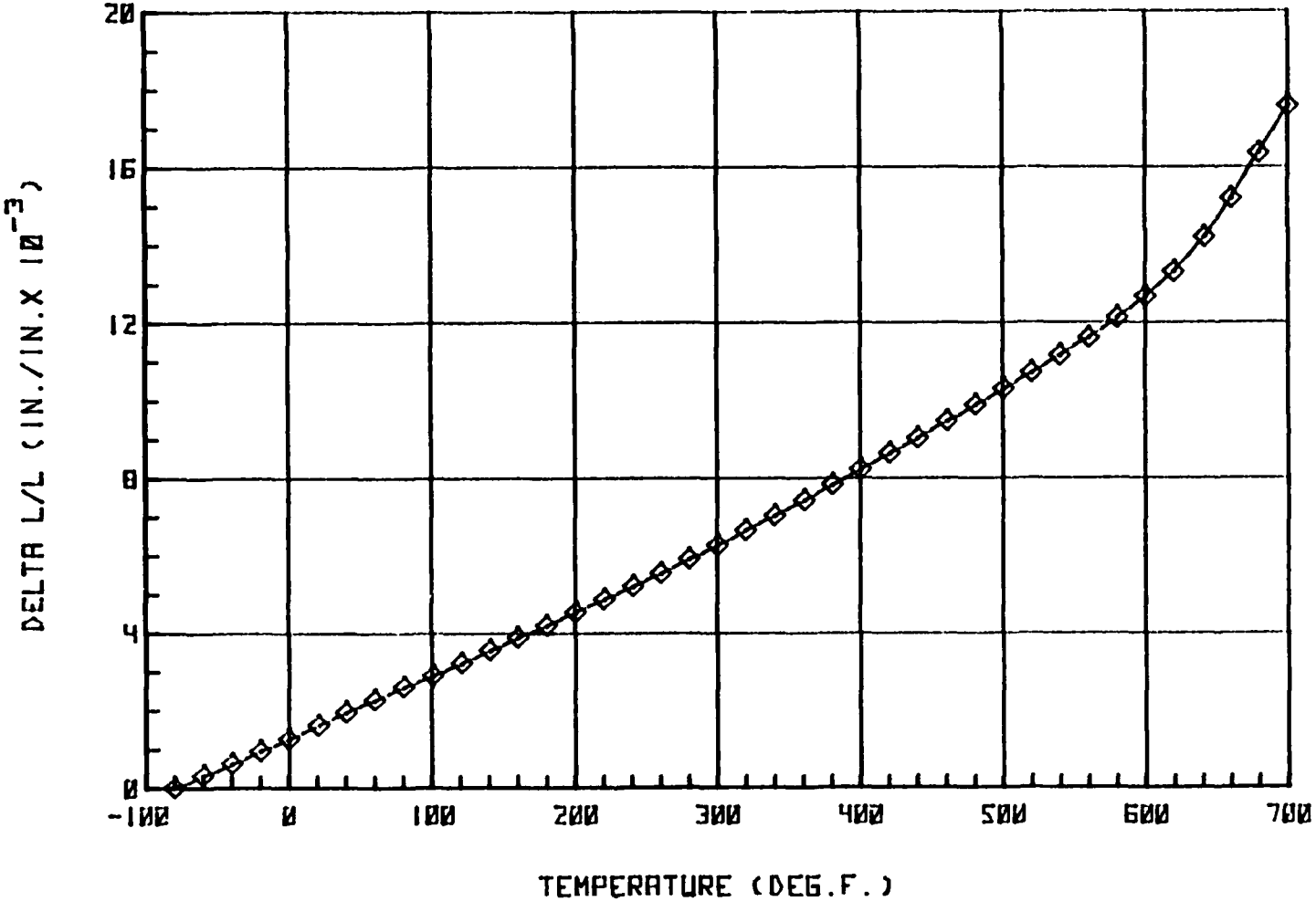

Figure 20. Thermal Expansion of Dry T300-6K/V378A (100 gm. Load)

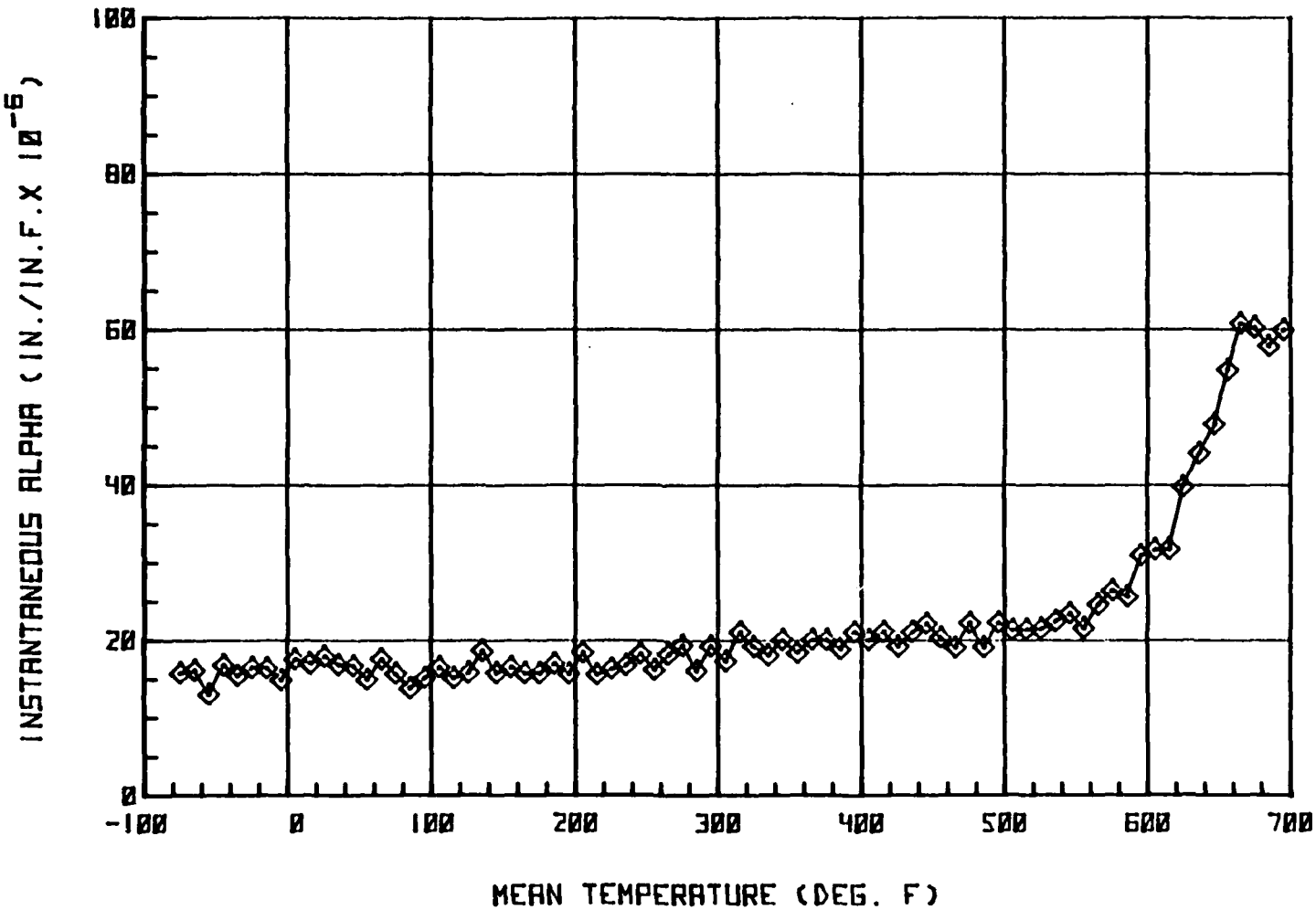

Figure 21. Coefficient of Thermal Expansion for Dry T300-6K/V378A

TMA LCE has been found to be unsuitable for wet T_g determination of T300-6K/V378A. Moisture diffuses through the material approximately ten times faster than epoxy systems, thus drying the specimen before the wet T_g is reached. A test run was performed to illustrate this point (Figures 22 and 23). The plot shows the material beginning to lose moisture and shrink around 200°F. The shrinkage continues until the moisture is removed around 500°F, and the specimen then exhibits the normal 570°F dry T_g.

The best available wet T_g value for the material is the 360°F obtained from thermal spike data. Glass transition temperature and thermal expansion data are summarized in Table 11.

TABLE 11 GLASS TRANSITION TEMPERATURES AND COEFFICIENTS OF LINEAR THERMAL EXPANSION

MATERIAL SYSTEM	EXPOSURE CONDITION	T_g (°F)	CTE from -80° to T_g (in/in °F x 10^{-5})
AS1/3501-6	Dry	450	1.71
AS1/3501-6	Dry (Redried)	450	1.71
AS1/3501-6	Wet (75% RH)	230	1.68
T300-6K/V378A	Dry	570	1.81
T300-6K/V378A	Wet (75% RH)	360	1.67

4.4 Flexure and Shear Properties

Twenty coupons of both materials were tested dry at -65°F, 75°F and 350°F in the 90° and 0° flexural configuration. Five short beam shear specimens from each material were also run at the same temperature values.

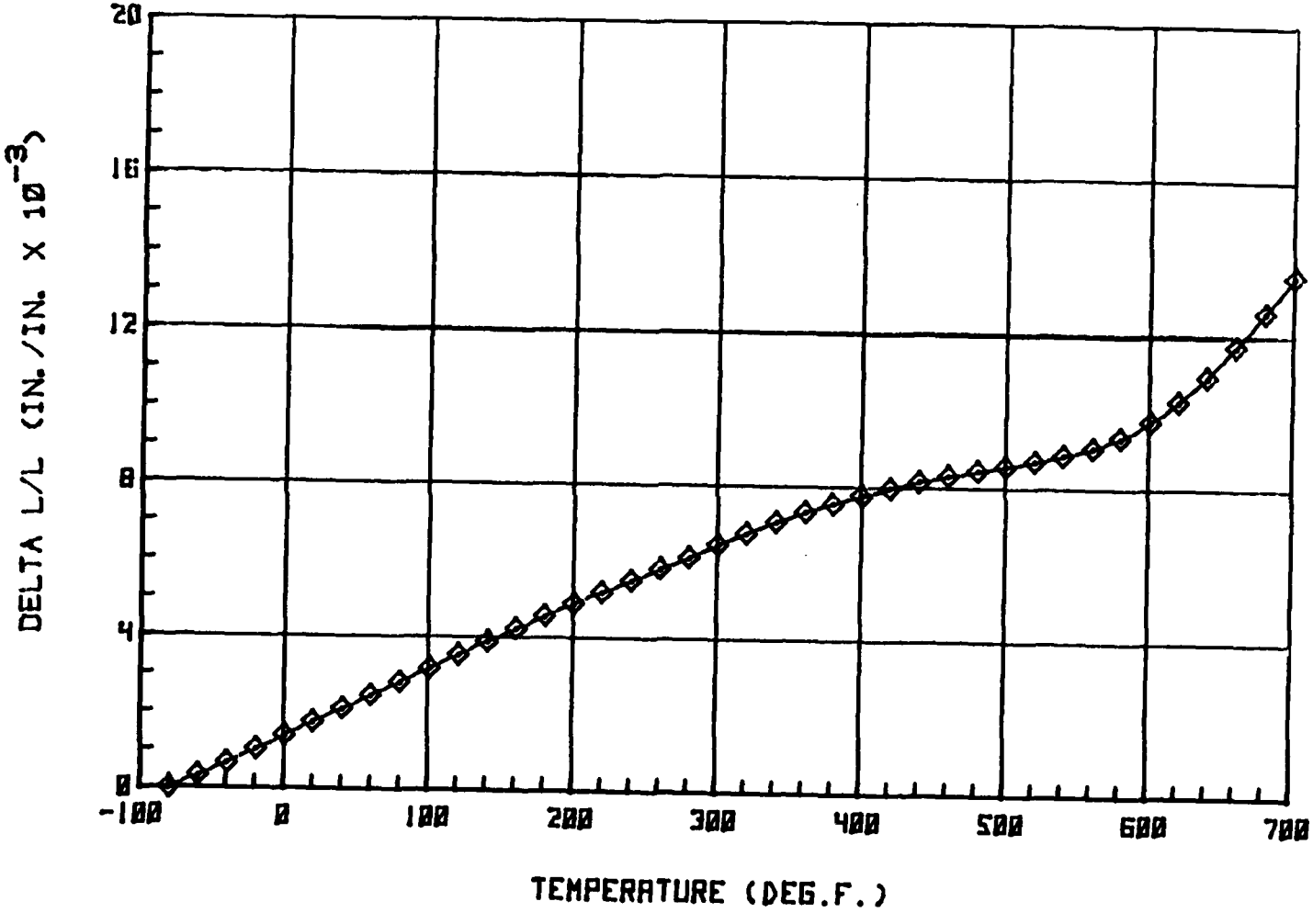

Figure 22. Thermal Expansion of Wet T300-6K/V378A (100 gm. Load)

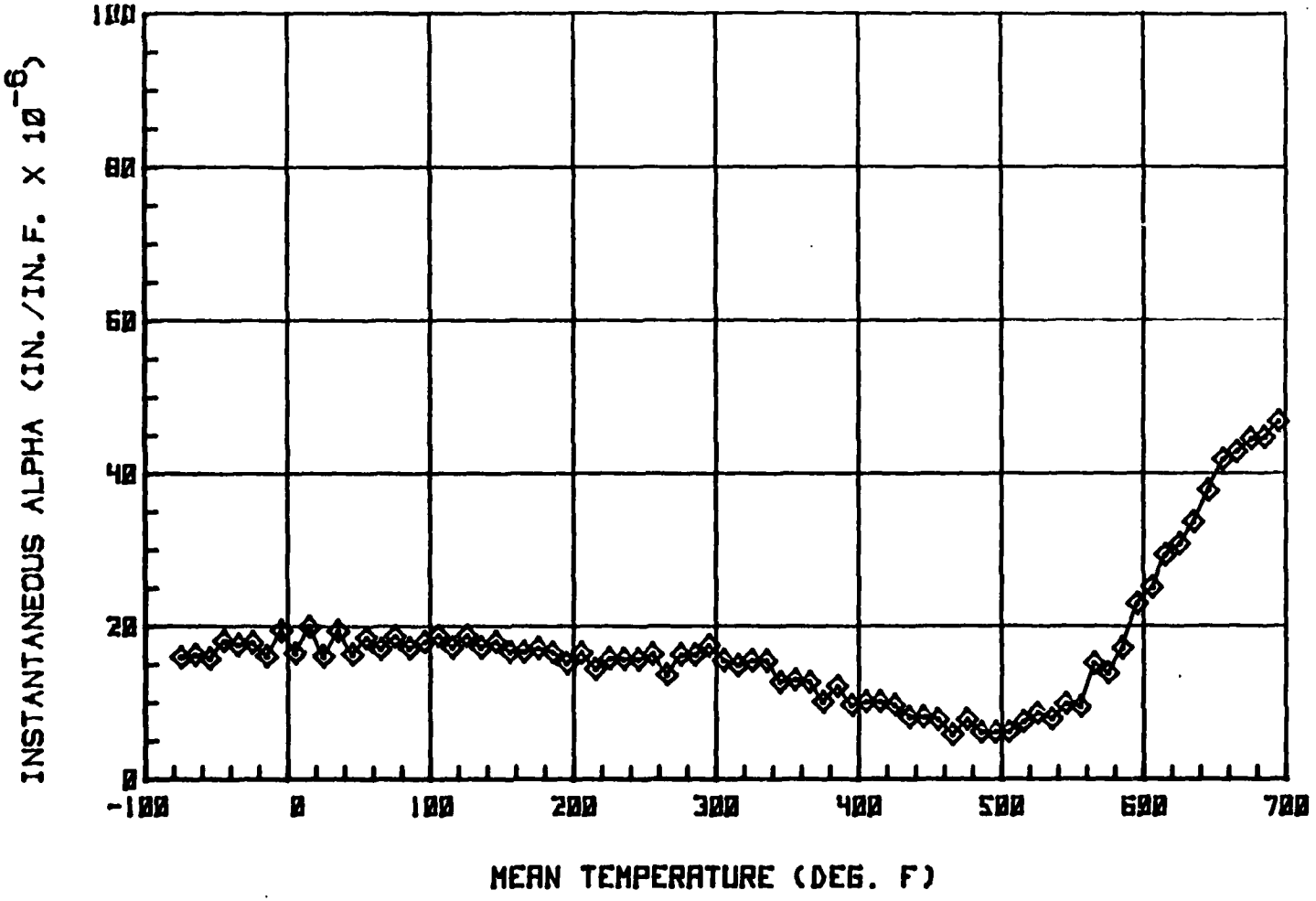

Figure 23. Coefficient of Thermal Expansion for Wet T300-6K/V378A

The dry flexure and shear properties of the two systems are very similar in terms of both mean value and statistical variability. The AS1/3501-6 data complies with the General Dynamics graphite/epoxy acceptance specification (FMS-2023), and the T300-6K/V378A values all meet the requirements set forth in preliminary specification FMS-3026 for the graphite-bismaleimide material. Test data for both materials are presented in Table 12.

4.5 In-Plane Shear

Testing of $[\pm 45]_{2S}$ tensile coupons equilibrated at 180°F/75% relative humidity was performed on both materials. The wet coupons were strain-gauged with one transverse and two longitudinal gauges, and were loaded at a rate of 0.2 inch/minute.

Hot-wet specimens were heated to 265°F, 300°F, and 350°F with electrically heated air guns. Two guns were mounted on either side of the specimen. Hot air diffusers directed air at the desired temperature to the test section of the specimen. This technique requires 45 seconds or less to bring the specimen to test temperature, and limits moisture desorption during testing.

Figures 24 and 25 show typical stress-strain curves of the wet AS1/3501-6 and T300-6K/V378A, respectively. (In comparing these data, it must be kept in mind that the graphite-epoxy is being tested above its glass transition temperature where poor structural performance can be anticipated.) Tables 13 and 14 present the test data obtained from the T300-6K/V378A and AS1/3501-6 respectively. Figure 26 is a plot of shear strength versus test temperature, and Figure 27 compares initial shear modulus to temperature for both materials. Comparison of the materials reveals slightly higher room

Table 12 Dry Flex and Shear Properties of AS1/3501-6 and T300-6K/V378A

MATERIAL PROPERTY	STATISTICAL PARAMETER	AS1/3501-6			T300-6K/V378A		
		-65°F	75°F	350°F	-65°F	75°F	350°F
0° Flex	$\bar{x}$	274.5	288.8	193.4	295.9	279.5	222.4
	σ	19.4	18.9	7.5	5.51	10.3	12.2
	c.v.	7.0	6.6	3.9	1.9	3.7	5.5
	n	20	20	20	20	20	20
90° Flex	$\bar{x}$	16.6	15.0	11.2	14.9	14.4	8.0
	σ	1.07	1.42	1.17	1.92	1.37	0.70
	c.v.	6.4	9.5	10.5	12.9	9.5	8.8
	n	20	20	20	20	20	20
Short Beam Shear	$\bar{x}$	23.2	19.0	10.2	19.3	16.3	12.0
	σ	0.74	0.25	0.09	0.81	0.65	0.39
	c.v.	3.2	1.3	0.9	4.2	4.0	3.2
	n	5	5	5	5	5	5

$\bar{x}$ = Mean Value (KSI)
σ = Standard Deviation (KSI)
c.v. = Coefficient of Variation (%)
n = Number of Specimens Tested

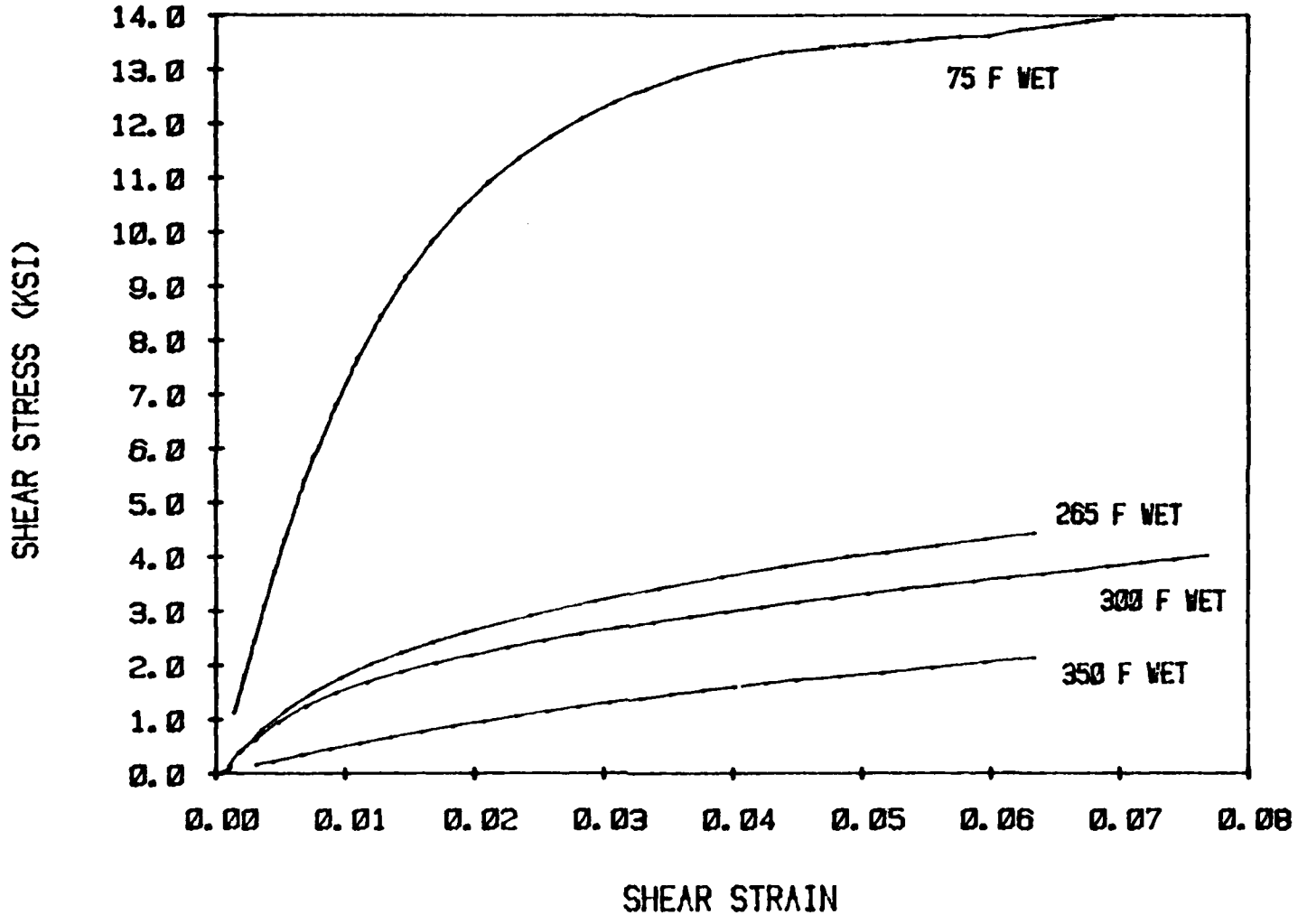

Figure 24. Stress-Strain Response of Wet $(\pm 45)_{2S}$ AS1/3501-6

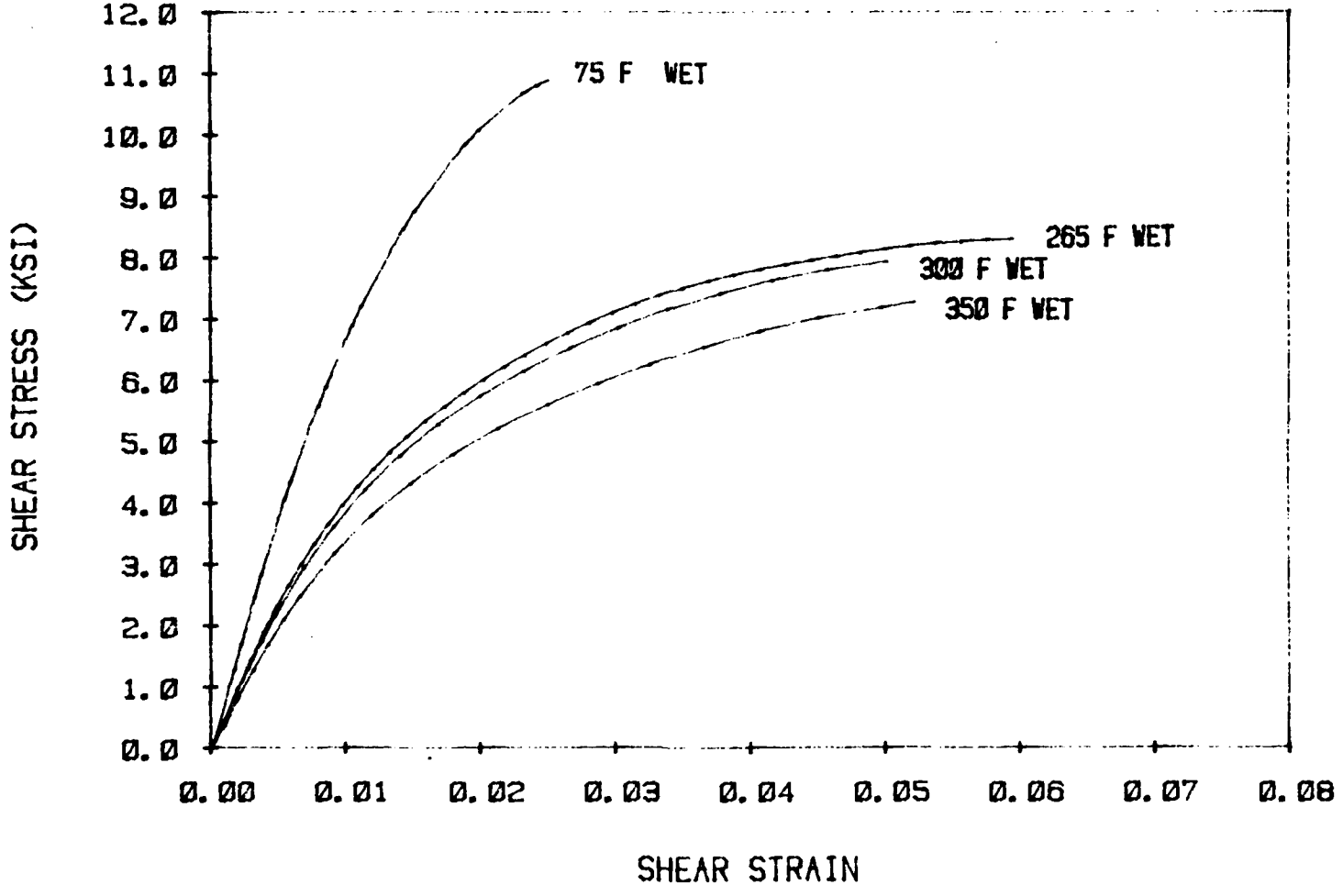

Figure 25. Stress-Strain Response of Wet $(\pm 45)_{2S}$ T300-6K/V378A

Table 13 $(\pm 45^{o})_{2S}$ Tensile Data on Wet T300-6K/V378A

CONDITION	TAU12 (KSI)	GAM12 (%)	G12 (MSI)	NUXY	$\sigma_{XY\ ULT}$ (KSI)	ϵ_{ULT} (%)	E_{XY} (MSI)
75F/75%RH	10.64	2.38	.743	.876	21.27	1.29	2.79
	10.88	2.51	.756	.872	21.76	1.36	2.83
	11.06	2.52	.726	.844	22.12	1.38	2.68
	10.96	2.37	.771	.848	21.92	1.28	2.85
Avg.	10.89	2.45	.749	.860	21.77	1.33	2.79
265F/75%RH	8.22	5.31	.518	1.010	16.45	2.81	2.07
	8.10	5.73	.483	0.986	16.20	3.12	1.93
	8.30	5.94	.491	1.091	16.59	2.80	2.05
	8.37	6.22	.521	1.022	16.74	2.97	2.11
Avg.	8.25	5.80	.503	1.027	16.50	2.93	2.04
300F/75%RH	8.27	6.93	.472	1.010	16.53	3.68	1.90
	8.30	6.94	.459	1.005	16.60	3.67	1.84
	8.43	7.00	.467	1.060	16.86	3.60	1.92
	8.38	6.61	.468	1.011	16.76	3.44	1.88
Avg.	8.35	6.87	.467	1.022	16.69	3.60	1.89
350F/75%RH	7.91	6.00	.424	1.095	15.82	3.12	1.76
	7.78	8.38	.386	1.230	15.56	4.00	1.72
	7.68	6.10	.417	1.148	15.36	3.03	1.79
	7.93	6.97	.402	1.146	15.86	3.44	1.72
Avg.	7.83	6.86	.407	1.155	15.65	3.40	1.75

Table 14 $(\pm 45^{o})_{2S}$ Tensile Data on Wet AS1/3501-6

CONDITION	TAU 12 (KSI)	GAM 12 (%)	G 12 (MSI)	NUXY	$\sigma_{XY\ ULT}$ (KSI)	ϵ_{ULT} (%)	E_{XY} (MSI)
75 F/75% RH	14.01	7.79	.819	.848	28.03	3.43	2.77
	13.52	12.9^	.822	.847	27.03	6.40	3.03
	13.41	11.63	.760	.943	26.81	5.72	2.84
AVG (3)	13.65	10.78	.800	.893	27.29	5.18	2.88
265 F/75% RH	4.70	6.93	.216	1.342	9.40	3.39	1.01
	5.09	8.06	.228	1.410	10.18	3.85	1.10
	5.14	7.51	.257	1.211	10.27	4.16	1.13
	4.40	6.67	.226	1.602	8.80	3.06	1.06
AVG (4)	4.83	7.29	.232	1.391	9.66	3.62	1.08
300 F/75% RH	3.50	4.42	.131	1.666	7.01	1.99	.699
	3.87	5.95	.146	1.549	7.74	3.07	.745
	3.62	6.35	.145	1.682	7.25	2.85	.778
AVG (3)	3.66	5.57	.141	1.632	7.33	2.64	.741
350 F/75%	1.63	4.41	.038	1.460	3.25	2.22	.286
	1.76	4.06	.046	1.546	3.52	1.59	.235
	2.95	4.80	.059	1.547	5.89	1.96	.301
	2.47	5.80	.064	1.408	4.95	2.41	.308
AVG (4)	2.20	4.77	.052	1.490	4.40	2.05	.283

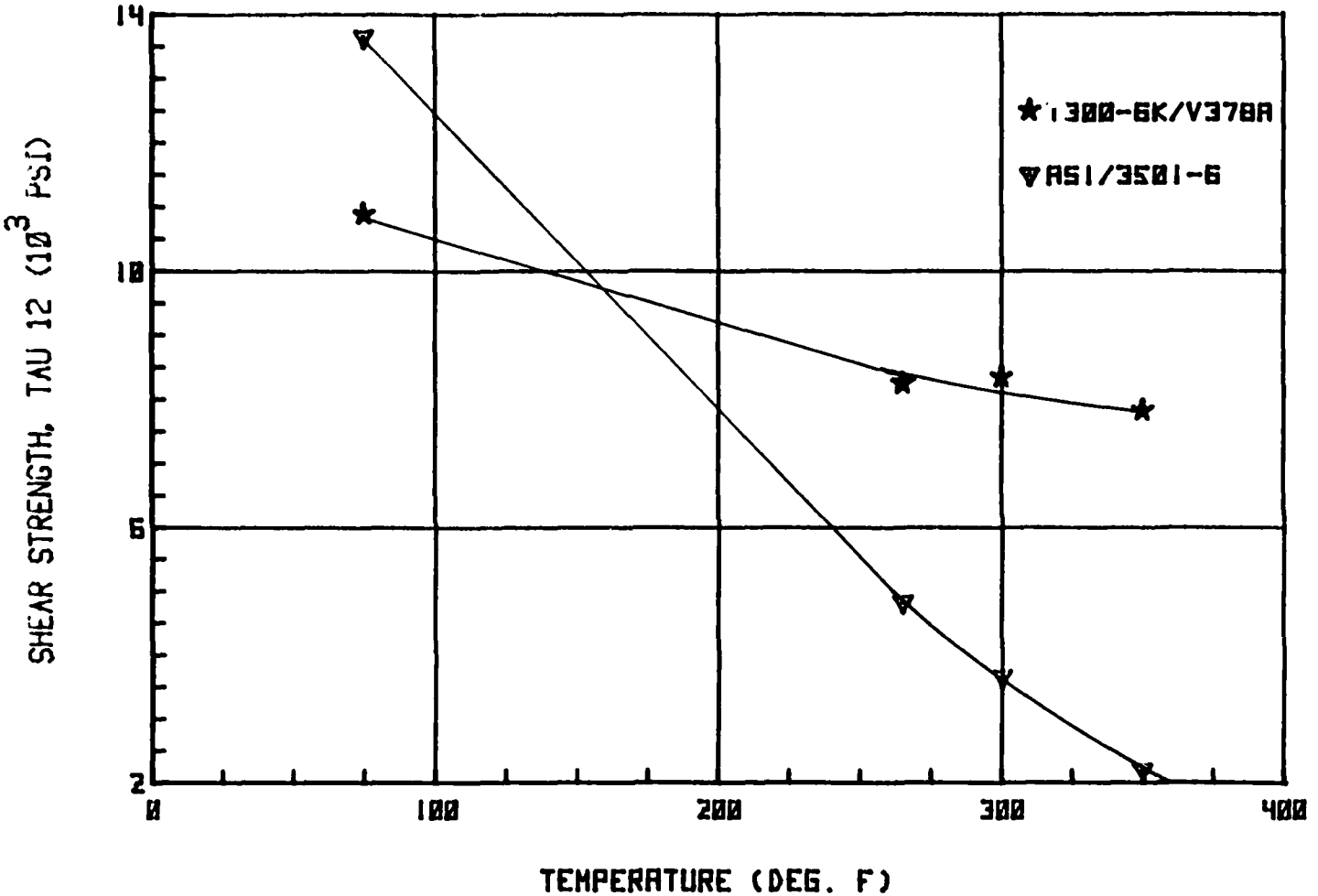

Figure 26. Wet Shear Strength of T300-6K/V378A and AS1/3501-6 Saturated at 75% R.H.

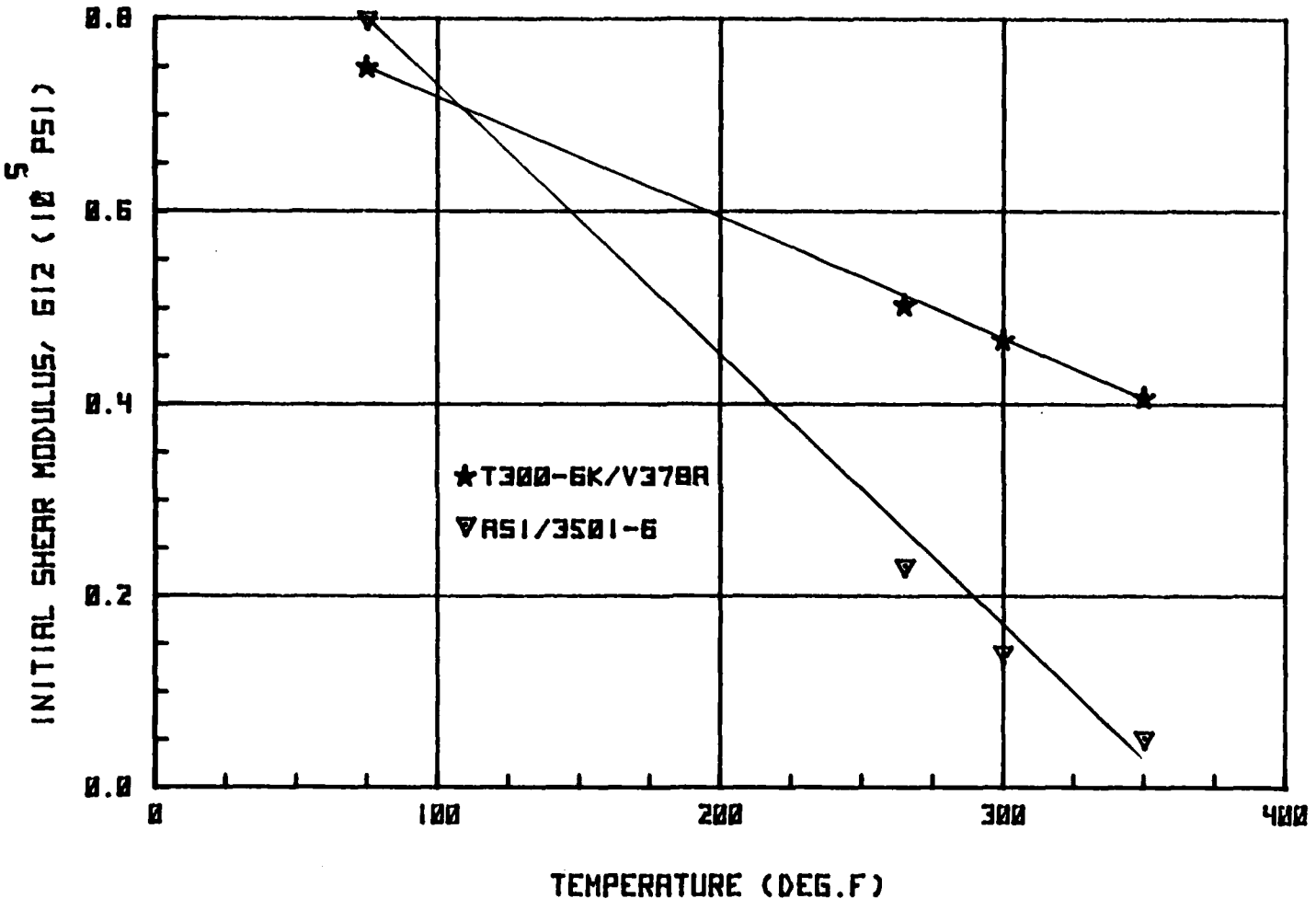

Figure 27. **Wet Initial Shear Modulus of T300-6K/V378A and AS1/3501-6 Saturated at 75% R.H.**

temperature values for the AS1/3501-6, but significantly improved properties in the T300-6K/V378A at all elevated temperature points.

4.6 Compression

Compression miniature sandwich beam (miniwich) specimens were fabricated from both material systems. Details of the specimens are shown in Figure 28, where the core referred to is 15 plies of 181 style glass cloth. These specimens have been developed over the past several years at General Dynamics to produce compression failure data at a much lower cost than the traditional honeycomb core sandwich beam test. Five miniwich beams of each material were moisture conditioned at 180°F/75% relative humidity and tested at 350°F, and five each were tested dry at room temperature. The T300-6K/V378A demonstrated higher values for ultimate stress, strain, and initial modulus in dry room temperature tests. The superiority of the graphite-bismaleimide system was dramatic at 350°F/75% relative humidity. Test values are listed in Table 15.

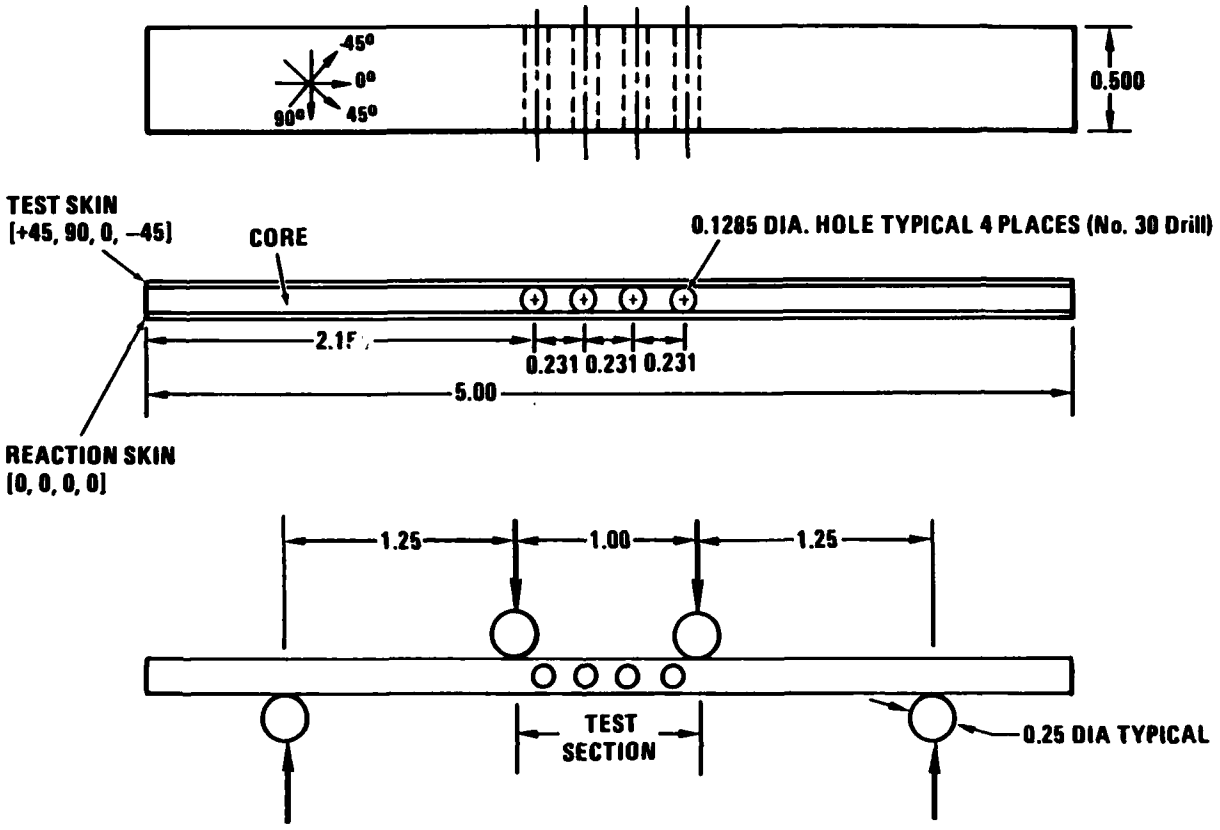

Figure 28. Miniature Sandwich Beam

Table 15 Compression Miniature Sandwich Beam Results (0/±45/90)

TEST CONDITION	MATERIAL SYSTEM	ULTIMATE STRESS (PSI)	ULTIMATE STRAIN (μIN/IN)	INITIAL MODULUS (PSI X 10^6)
75°F/Dry	T300-6K/V378A	95,690	13,190	7.85
		94,010	12,270	8.25
		110,000	14,250	8.14
		110,000	15,920	7.80
		92,150	13,040	7.73
	Average	100,370	13,730	7.95
75°F/Dry	AS-1/3501-6	77,520	11,580	7.39
		99,720	13,880	7.84
		64,050	8,730	7.61
		76,710	11,100	7.41
		94,520	13,790	7.58
	Average	82,500	11,820	7.57
350°F/75% RH	T300-6K/V378A	62,820	8,940	7.28
		66,490	8,680	8.12
		57,140	10,130	5.95
		70,570	11,610	6.51
		67,170	10,690	6.72
	Average	75,990	10,010	6.92
350°F/75% RH	AS-1/3501-6	18,870	3,010	7.25
		18,650	3,860	5.18
		17,190	3,480	4.97
		19,260	3,430	5.70
		16,940	2,960	5.74
	Average	18,180	3,350	5.77

V CONCLUSIONS

This program compared the delamination and environmental resistance of a graphite-epoxy (AS1/3501-6) and a graphite-bismaleimide (T300-6K/V378A) material system. In terms of overall program conclusions, Mode I toughness tests showed only minor differences between the two systems, but the Mode II toughness of the graphite-epoxy was significantly higher than that of the graphite-bismaleimide. As expected, the environmental resistance of the bismaleimide resin system was clearly superior to that of the epoxy resin system. These conclusions are supported by the following individual task conclusions.

- At a given environmental condition, both systems produced the same Mode I toughness. The Mode I fracture tests showed that the toughness of both materials increased with temperature and was relatively unaffected by moisture. Under fatigue loading, each system exhibited a high Mode I delamination growth rate. However, the Mode I specimens for both materials suffered excessive fiber nesting in adjacent plies of like orientation. This nesting may have caused the test measurements to overestimate the actual Mode I toughness.

- The Mode II tests were not significantly affected by the roughness of the fracture surfaces, and the tests showed differences in the materials not observed in the Mode I results. The observed Mode II toughness of AS1/3501-6 is about 50% higher than that of T300-6K/V378A. In contrast to the Mode I results, the Mode II toughness of both materials decreases with increasing temperature.

Further, this behavior was more noticeable in tests of moisture-conditioned specimens.

- Subcritical delamination growth tests were performed at each environmental condition. The growth rates in Mode II loading were markedly lower than those for Mode I. Although data scatter precluded a clear correlation, a general observation was that higher static toughness results in lower growth rates, and vice-versa. This trend applies to the entire data set, regardless of the type of loading.

- A comparison of the two materials on the basis of their resistance to thermal spikes after moisture conditioning showed that the bismaleimide can withstand spikes up to 350°F. On the other hand, the epoxy material began to show unacceptable performance after thermal spikes at about 250°F.

- The direct measurement of glass transition temperature (T_g) resulted in values for this graphite-epoxy system of 450°F and 230°F, in the dry and wet (75% RH) states, respectively. The dry T_g of the graphite-bismaleimide was 570°F, while the wet T_g was estimated at 360°F.

- As expected, the dry zero-degree flexure data were equivalent for both systems. Likewise, the dry ninety-degree flexure performance of the two materials was the same except at 350°F, where the epoxy strength was higher. The dry short beam shear data showed the epoxy to be somewhat stronger at cold and room temperatures, with the bismaleimide performing better at 350°F. No significant differences in statistical variability were observed in the twenty-specimen flexure test data sets.

- The in-plane shear behavior of the systems was measured at 75°F, 265°F. 300°F, and 350°F after moisture conditioning at 75% relative humidity. The initial shear moduli of the two systems were about equal at room temperature. The shear modulus of the T300-6K/V378A decreased linearly with temperature to about half its room temperature value at 350°F. Because all the elevated temperature points were above the T_g of the graphite-epoxy, its shear moduli at elevated temperature were only 10-20% of the room temperature values. Similarly, the shear strength of the bismaleimide system was affected much less by temperature than the epoxy system.

- The compression performance of each material was measured at both room temperature, dry and 350°F, wet test conditions. The bismaleimide performed better than the epoxy at room temperature, dry conditions and much better at hot, wet conditions.

To re-state the overall conclusions in a different way, the only clear disadvantage associated with using the T300-6K/V378A system in place of the AS1/3501-6 is a reduced resistance to Mode II delamination. But the significance of the Mode II toughness and the translation of this property to structural performance are not well understood, so the implication of this conclusion will depend on more detailed structural application studies.

The obvious advantage of using the bismaleimide system was demonstrated by the thermal spike tests, the glass transition temperature tests, the in-plane shear tests, and the compression tests. This advantage is an environmental resistance margin of about 100°F above that of AS1/3501-6.

VI RECOMMENDATIONS

The results of this program suggest several avenues of further development. Because the environmental resistance results were confirmed by several test methods, the environmental differences were clearly demonstrated. In the delamination area, however, some clarification is needed.

One of the main concerns is the moderate scatter in the toughness measurements and wide scatter in the delamination growth rate measurements. The test methods need to be carefully examined to isolate the sources of scatter in the areas of material variability, specimen design, specimen fabrication, test equipment, test procedure, and data reduction techniques. As was observed after the Mode I tests, for example, a method for minimizing fiber nesting is needed for the fabrication of Mode I coupons. After identifying and minimizing error sources, experiments can then be designed to measure the scatter in toughness and growth rates.

To begin the correlation of these delamination coupons to the performance of structural laminates, non-destructive inspection (NDI) and fractography procedures will have to be applied. Tested specimens should be examined by NDI, then broken apart to study their fracture surfaces. In this way, external inspections and performance measurements can be correlated with microscopically observable differences in the fracture surfaces.

The decrease in Mode II toughness as temperature increased strongly suggests that the Mode II toughness is influenced by the shear modulus of the resin, which behaved in a similar fashion. Additional Mode II tests in the hot, wet environmental condition (up to

212° F), will allow analyses to evaluate the connection between shear modulus and shear toughness.

The recommendations can be re-stated in terms of specific tasks:

- o Isolate error sources,
- o Minimize controllable variability,
- o Perform testing to evaluate statistical variability of toughness and growth rate,
- o Examine specimens by NDI,
- o Apply fractography to verify crack measurements and correlate fracture surface features to failure modes,
- o Extend fracture testing to hot, wet conditions.

REFERENCES

1. McKague, E. L., "V378A Polyimide Resin - A New Composite Matrix for the 80's," Presented at the ASTM Symposium on Composites for Extreme Environments, Bal Harbour, Fla., November, 1980 (to appear in ASTM STP 768).

2. Wilkins, D. J., Eisenmann, J. R., Camin, R. A., Margolis, W. S., and Benson, R. A., "Characterizing Delamination Growth in Graphite-Epoxy," Presented at the ASTM Symposium on Damage in Composite Materials, Bal Harbour, Fla., November, 1980 (to appear in ASTM STP 775).

3. McKague, E. L., Reynolds, J. D., and Halkias, J. E., "Moisture Absorbtion, Swelling, and Glass Transition Relationships for Epoxy Resin", Journal of Applied Polymer Science, Vol. 22, 1643-1654, (1978).

4. Paris, P. C. and Sih, G. C., in Fracture Toughness Testing, ASTM STP 381, 1970, pp. 30-83.

5. Rybicki, E. F. and Kanninen, M. F., "A Finite Element Calculation of Stress Intensity Factors by a Modified Crack Closure Integral," Engineering Fracture Mechanics, Vol. 9, 1977, pp. 931-938.

APPENDIX A

MATERIALS DATA

On the following pages are included the vendor certification for the Hercules AS1/3501-6, the GD requirements for T300-6K/V378A, and the U.S. Polymeric certification for the latter material.

HERCULES INCORPORATED
QUALITY ASSURANCE CERTIFICATION

December 1, 1980

CUSTOMER: General Dynamics/Fort Worth

PURCHASE ORDER NO: 961442

MATERIALS: Graphite Fiber/Epoxy Material,3501-6/AS1, 12" Prepreg tape.

SPECIFICATION: MMS 549, Rev. A, Type I

QUANTITY: 16.00 lbs.

LOT NO: 1734 Manufactured November 5, 1980

SPOOL NO: 36B

RESIN LOT NO: 126 Manufactured by Hercules Inc.

FIBER LOT NO: 174-1 Manufactured by Hercules Inc.

I. Fiber Properties

	Spec Req	(Lot Average)
Tensile Str.,ksi	410 minimum	470
Tensile Mod.,msi	32 - 36	34
Density,lb/in^3	0.0640-0.0660	0.0654

II. Prepreg Physical Properties

(48" test data) Spool No.	Resin Flow Spec Req 10 - 25, %	Volatiles Spec Req 1.5 % maximum Average/Individual	Tack Spec Req Table I
1	17	1.2/1.0,1.3,1.3	Conforms

III. Laminate Mechanical Properties

(48" test data)	Spec Req (min.ind)	Panel No. Spool 1	Average/Individual
0° Tensile Str.,RT,ksi*	200	11546	250/248,252,252
0° Tensile Mod.,RT,msi*	18.0	11546	20.8/20.2,21.2,20.8
0° Elongation,RT, in/in x 10^3	10.0	11546	13.2/15.2,12.4,12.0
Short Beam Shear,RT,ksi	15.0	11545	18.8/17.9,18.6,19.7
Short Beam Shear,250°F,ksi	9.0	11545	14.3/14.3,14.3,14.3
Short Beam Shear,250°F,ksi (24 hour H_2O boil)	7.5	11545	10.6/10.6,10.4,10.8

* Normalized to 0.0416 Panel Thickness.

IV. Panel Physical Properties

(48" test data)	Spec Req	
Spool No./Panel No.		1/11546
Ply Thickness,inches	0.0052 +/- 0.0003	0.0051

V. Individual Spool Physical Properties

Spec Req	Average/Individual 42 +/- 3	Average/Individual 145 - 155
Spool No.	Resin Content,%	Fiber Areal Wt.,gm/m^2
36B	44/43,44	148/146,149

J. A. Rasmussen, Representative
QUALITY ASSURANCE DEPARTMENT

JAR:ln

REQUIREMENTS FOR THORNEL 300-6K/V378A GRAPHITE/ POLYIMIDE PREPREG

The Thornel 300-6K/V378A graphite/polyimide prepreg shall meet the following general and specific requirements.

1. General Requirements. The T300-6K/V378A prepreg shall be provided in the form of unidirectional tape that is 6.0" wide on a net-width carrier of release coated paper. Each role shall be packaged in foil or equivalent vapor barrier material and must arrive at purchaser's plant without breakage, tearing, or unsealing of the vapor barrier package. Prepreg shall be kept at 0°F or below during shipment.

2. Property Requirements. The T300-6K/V378A prepreg shall satisfy the following specific requirements for the uncured and cured/postcured states.

2.1 Resin Content. The prepreg resin content shall be 28.5% ±1.5% by weight and shall be in this range at any point within a roll and from roll to roll.

2.2 Gel Time. Gel time at 212F under inert atmosphere shall be greater than 20 minutes after 7 days at room temperature, when observed during probing on a suitably modified Fisher-Johns Melt Point Apparatus.

2.3 Ply Thickness. The mean value and 14 out of 16 individual measurements of the nominal cured ply thickness shall be in the range of 0.0055 ±0.0004 inch when thickness of a (0/90)-class laminate is measured with a 4-place micrometer.

2.4 Glass Transition. The dry glass transition temperature of cured and postcured material shall be at least 550F when determined by thermomechanical analysis (TMA).

2.5 Mechanical properties of dry laminates having 28.5% ±1.5% cured resin content shall meet or exceed the following requirements.

Property	Test Temperature 75F	350F
0°Flex Strength, KSI	250	210
0°Flex Modulus, MSI	18.5	18.5
Short Beam Shear, KSI	13.0	10.0
90° Flex Strength, KSI	12.0	8.0

3. Data Requirements. The following information shall be provided for each batch of material within thirty days after batch shipment. This information shall be mailed directly to the attention of Lee McKague, Mail Zone 2860.

3.1 Viscosity Data. Rheometric data showing the viscosity and storage modulus of unsupported V378A resin vs. temperature shall be developed using a heating rate of 2°C per minute until start of gel. The resin samples shall be taken during the batch impregnation cycle so that they represent the resin heat history at the beginning and at the end of the impregnation cycle. Identity of the samples with respect to these cycle end points shall be preserved. Samples shall be stored and handled so that viscosity changes are minimized during preparations for testing. During test, use parallel plate oscillating technique (25 or 50 mm. plate, depending on experience):

- o Frequency about 5 rad/sec.
- o Strain about 15%

3.2 HPLC Data. A high-pressure liquid chromatogram trace shall be provided for each batch of resin. Samples shall represent the beginning and completion points of the impregnation cycle. Test procedures shall be identified.

3.3 DSC-II Data. Using a Perkin-Elmer DSC-II, develop thermograms from samples representing the beginning and completion points of the impregnation cycle of each batch of resin.

Thermograms from each area should be run at both of the following conditions:

(1) 25 to 205°C at a rate of 10°C/min.

(2) 25 to 177°C at a rate of 2°C/min plus a 4 hour hold at 177°C.

Sample identification and weight and all DSC-II run parameters will be recorded on each thermogram.

3.4 Batch-Constituent Lot Numbers. Lot number(s) shall be provided for the T300-6K fibers in each batch of prepreg. Lot numbers also shall be provided for each of the resin batch constituents, which shall be listed according to some reference identification plan. The prepreg batch number shall correspond to the resin batch number.

4. Samples. A resin film sample shall be provided with each batch of material, for use in testing. This sample shall be representative of the batch of resin used in the prepreg batch.

U.S. Polymeric
a division of HITCO

700 East Dyer Rd., Santa Ana, Calif. 92707 / 714-549-1101

TWX 910-595-1130

General Dynamics
P.O. Box 748
Ft. Worth, TX 76101

cc: R. Pointer

Date 1/6/81

U.S.P. Order No. 7843

This is to certify that the material furnished to you on our packing slip number 18456 against your P. O. # 959842 covering 15.1 lbs. of 6" T300/6K/V378A Unidirectional Tape Lot No. 2W 4902 Impregnation Date 12/10/80 Meets the requirements of the purchase order, except as noted.

ROLL NO.	RESIN SOLIDS%	Min:Sec GEL TIME	Min:Sec FIBER AREAL WT.	Cured PLY	Inch THICKNESS
3	29.4	26.2	150.0		0.0056
REQUIRED	27-30%	20:00 Min.	C&R		0.0051-0.0059

LOT IDENTIFICATION DATA

Prepreg Lot No. 2W 4902
Resin Mix No. WR 7119
Resin Mix Ingredient Numbers WR 7116
USP 22918, 22562, 23067, 23268
Fiber Lot 24098
Store @ 0°F Max.
Expiration date 2/10/81
Roll history Sheet Attached

Structural Test Data Attached

U. S. POLYMERIC

Quality Control Department
James B. Rock, Manager

mr

Form USP-144

TEST		RESULTS	REQUIRED
Resin Content, %	*	26.2	28.5 ± 1.5
0° Flex Strength, KSI @ RT		302.6	250
@ 350°F	*	227.2	80% of RT
0° Flex Modulus, MSI @ RT		19.3	18.5
@ 350°F		20.7	18.5
Short Beam Shear, KSI @ RT		15.7	13.0
@ 350°F		10.1	10.0
90° Flex Strength, KSI @ RT		17.3	12.0
@ 350°F		10.0	8.0

* Failing Results

APPENDIX B

MODE I STATIC TESTING

Critical values for the Mode I coupon were obtained in a custom displacement-controlled load frame shown in Figure B-1. Thin metal-foil connectors were used as "plastic hinges" between the double cantilever beam (DCB) specimen and the test fixture to minimize the applied moment on the coupon. The specimen's weight was supported as shown. The edges of the specimens were painted with a white coating (typewriter correction fluid) marked at 0.5-in. increments to aid in crack observation.

The first load application was made to break the Kapton film and create a natural crack for the first set of measurements. Then a displacement load was applied to initiate crack growth, and the displacement was increased until the crack propagated slowly to the next mark on the specimen's edge. The displacement was then returned to zero, and the process repeated. In this manner, several tests were performed on each specimen. Initial crosshead speeds were 0.02 in/min for the short cracks, and were increased to a maximum of 0.2 in/min near the end of the specimen. The load was plotted as function of crosshead displacement and visual observations of the crack length were made with a X20 microscope.

This section contains a sample data reduction for a Mode I static test including the development of the compliance as a function of crack length, the critical load as a function of crack length, and the strain-energy release rate equations for the DCB specimen. Also, the Mode I static data for both the epoxy and the bismaleimide material systems are included.

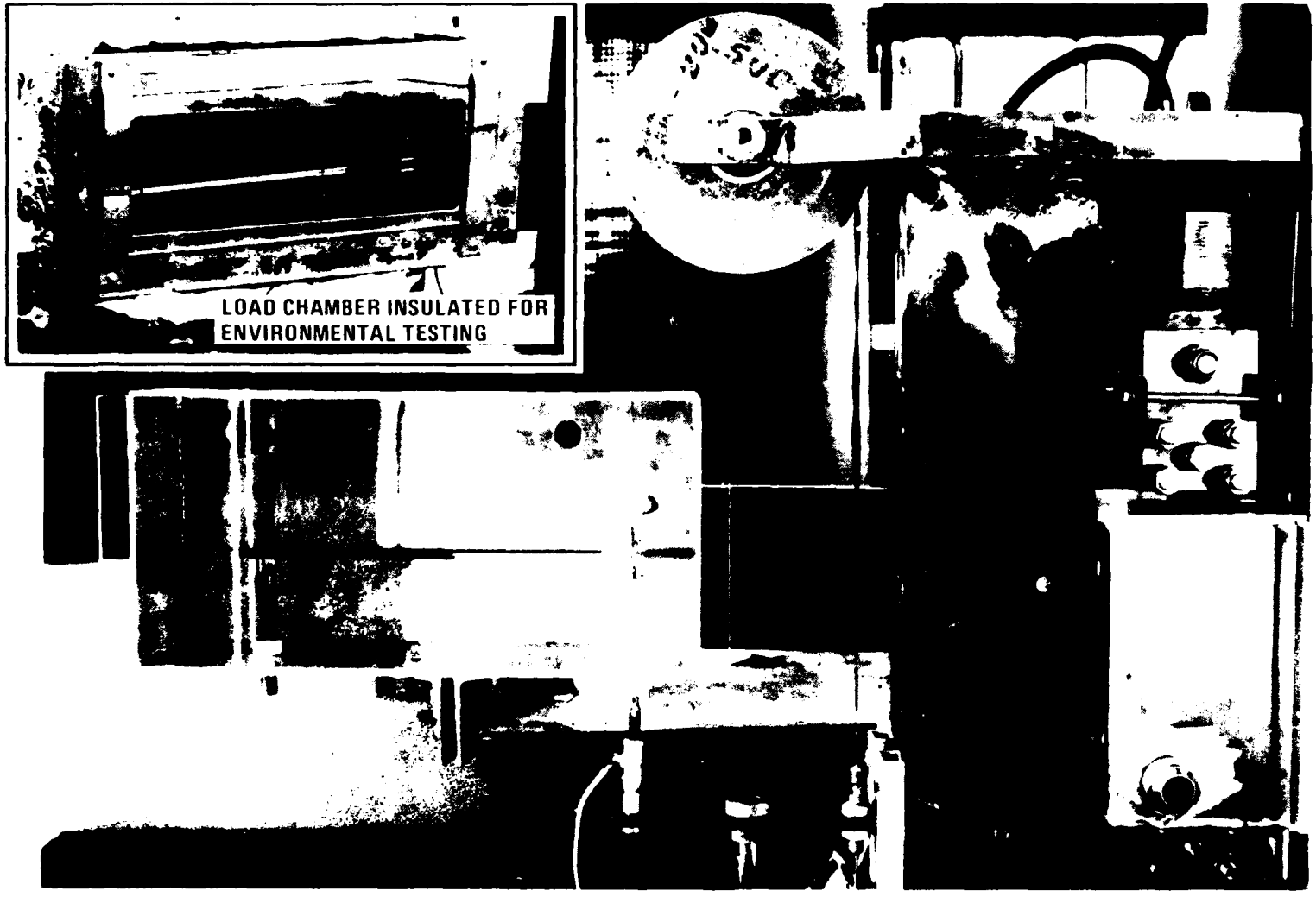

Figure B-1 Custom Load Frame for Mode I Static and Fatigue Fracture Testing

B.1 Double Cantilever Beam Equations

For a linear elastic double-cantilever beam, as shown in Figure B-2, the load-deflection relation is

$$\delta = 2\,Pa^3/3EI, \tag{B1}$$

where E is the extensional stiffness and I is the moment of inertia of the section. The compliance relation is

$$C = \delta/P = 2a^3/3EI. \tag{B2}$$

Since E and I are independent of the length a, the compliance may be rewritten as

$$C = A_1\,a^3, \tag{B3}$$

where the constant A_1 is 2/3EI.

The energy release rate for this beam section is described by (Ref. 4)

$$G = (P^2/2w)(dC/da) \tag{B4}$$

where w is the width of the beam using Equation (B3), G becomes

$$G = 3A_1P^2a^2/2w. \tag{B5}$$

The critical load P_c required to propagate a crack of length a is then

$$P_c = A_2a^{-1}, \tag{B6}$$

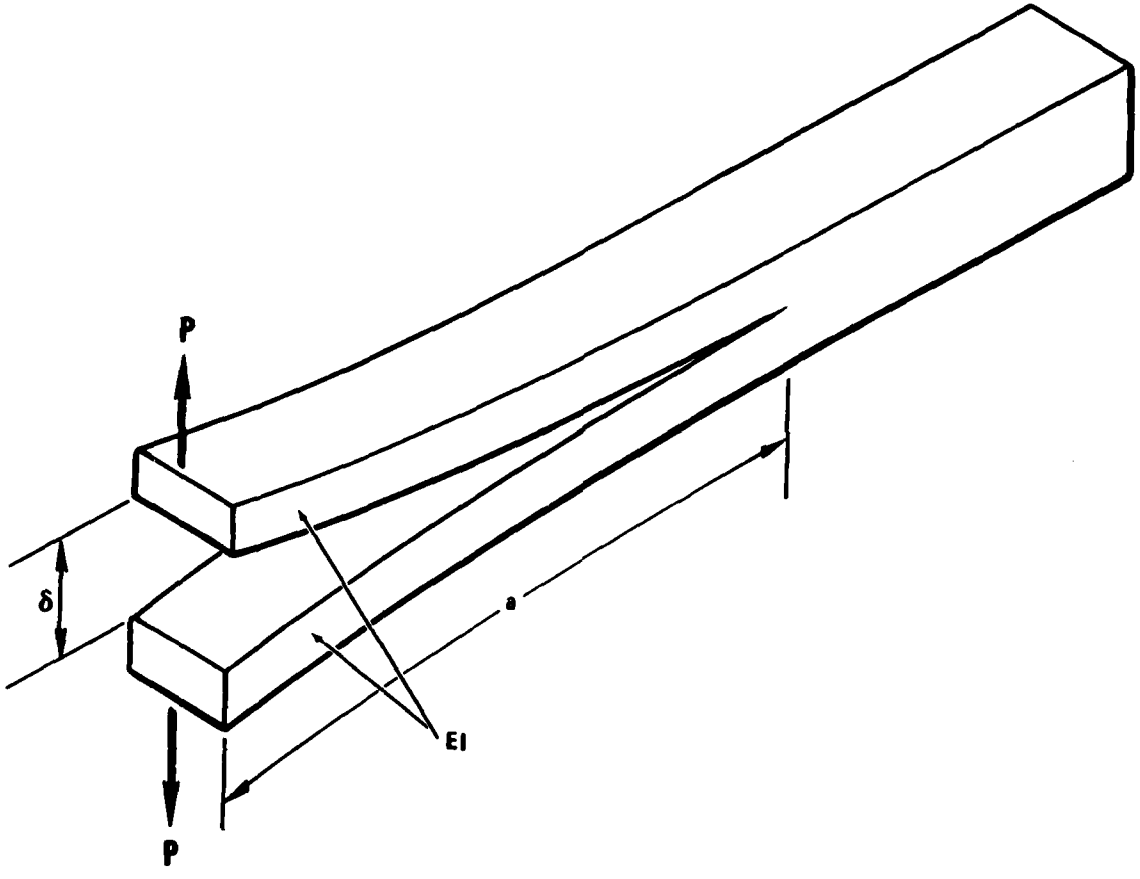

Figure B-2 Double Cantilever Beam

where

$$A_2 = (2wG_c/3A_1)^{1/2}. \tag{B7}$$

Experimentally, the C-a and P_c-a relations (as per Equations (B3) and (B6)) are measured giving the values of the constants A_1 and A_2. Thus, the critical energy release rate is calculated by substituting Equation (B6) into (B5) as

$$G_c = 3A_1A_2^2/2w. \tag{B8}$$

B.2 Sample Data Reduction

The load vs. crosshead displacement data for the P1-4-9 specimen (bismaleimide, Mode I, 75°F, dry) is shown in Figure B-3 for six (6) initial crack sizes. The initial curvature of these P-δ curves was caused by initial deformations in the grip areas. The following linear portion of the curve was used to obtain the compliance values. Finally, the critical load to initiate crack growth (P_c) was indicated by a sudden change in the P-curve. At this point in the experiment, the displacement was increased until the crack propagated slowly down the specimen to a previously marked point. The displacement was then returned to zero, and the process was repeated with a new initial crack length.

For the load-displacement curve shown in Figure B-3(a), with an initial crack length of 3.1 inches, P_c was 5.85 pounds and the compliance was 0.0489 in/lb. These values were compiled by computer for each crack length and are presented in a concise graphical form as shown in Figure B-4. Also shown are the results of a least squares regression of the compliance and the critical load as a function of crack length. In this case, A_1 is 0.00146 lb^{-1} in^{-2} and A_2 = 19.465 in/lb. G_c was then determined by Equation (B8).

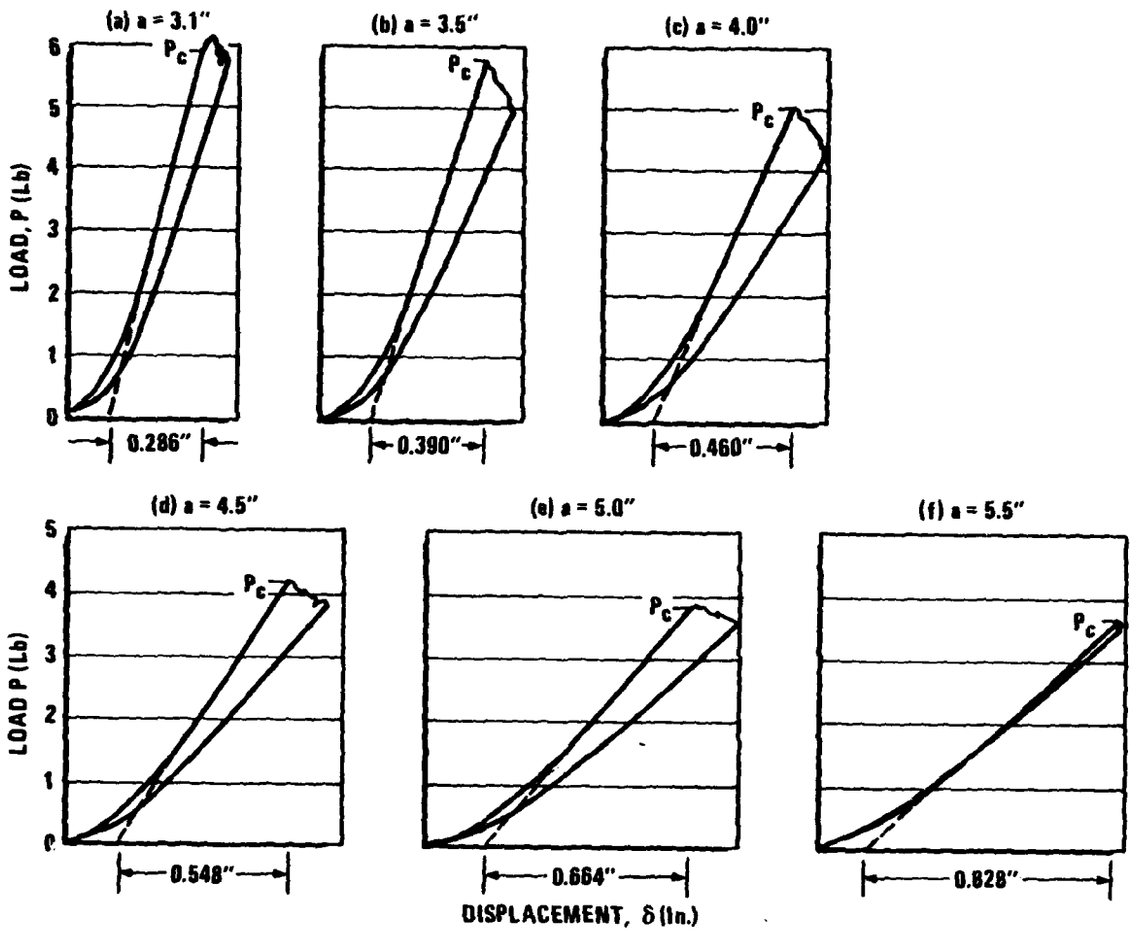

Figure B-3 Sample Load-Deflection Curves for a Mode I Static Test

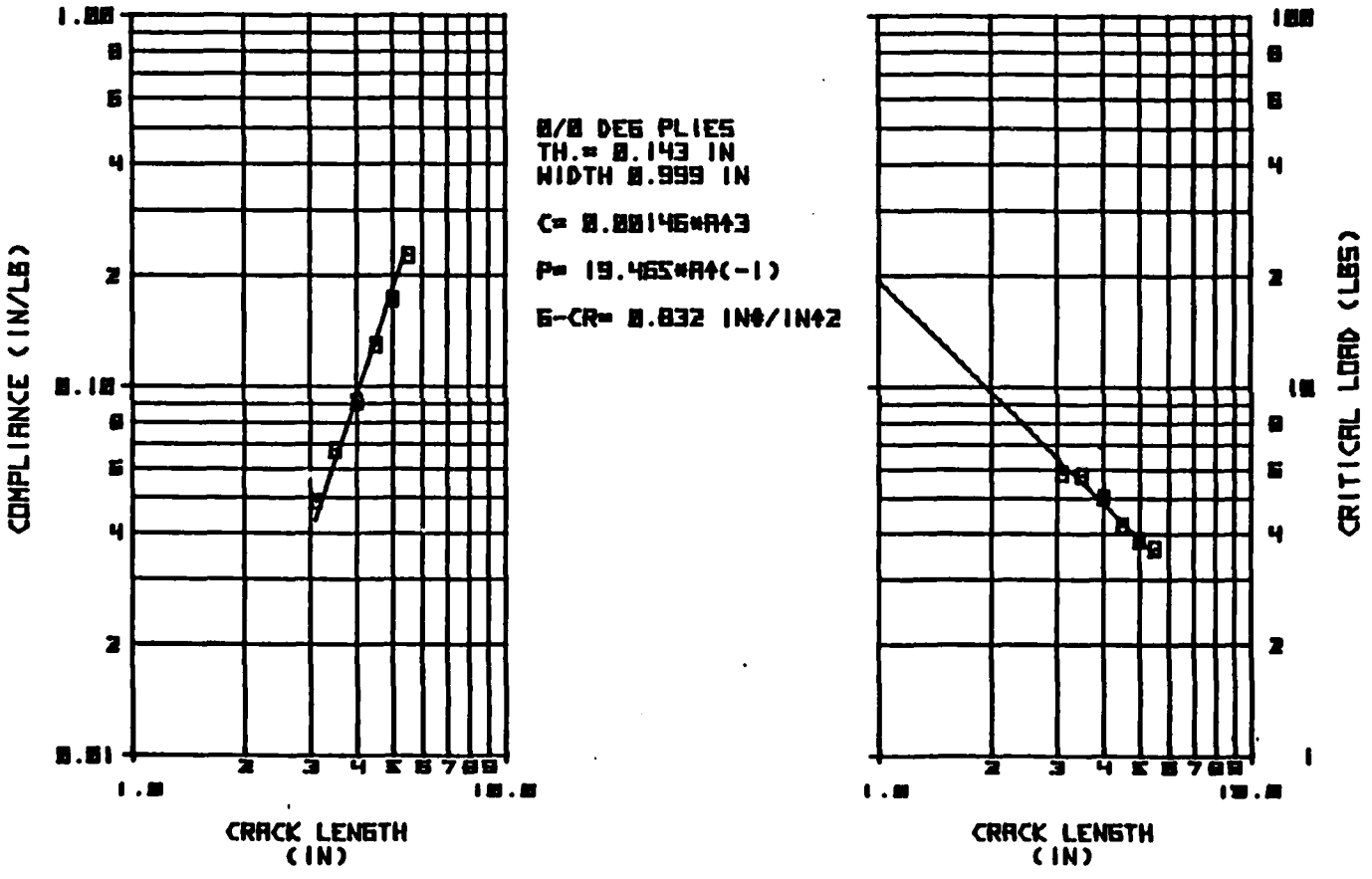

Figure B-4 Sample Mode I Data in Graphical Form

In some of the experiments the first data point was considered to be an erroneous value caused by grip slippage in the initial load. These points were censored as indicated by an "X" in the ensuing plots.

B.3 Epoxy Mode I Static Data

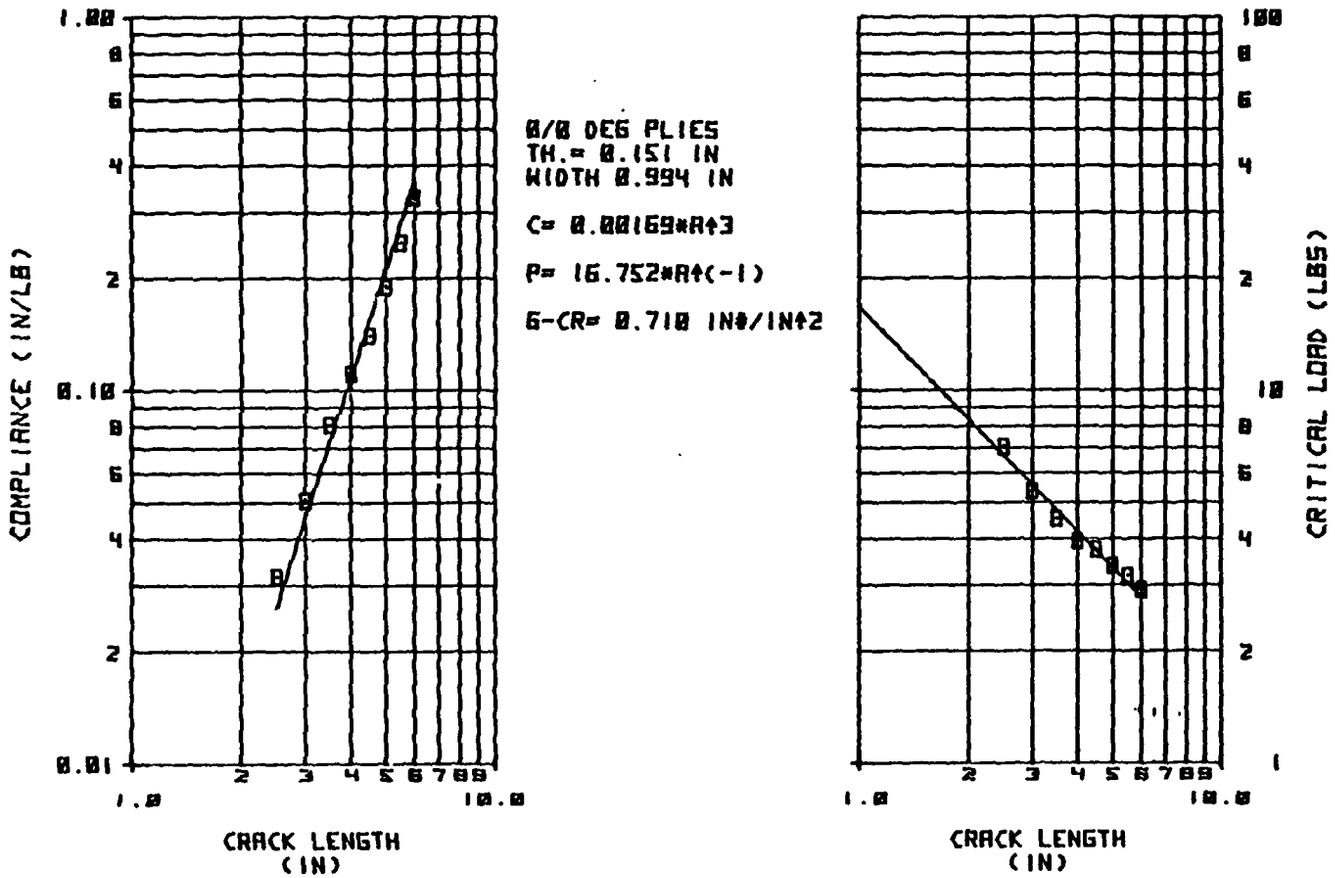

Figure B-5 Test EICDS of Specimen E1-4-3

AD-A112 474 GENERAL DYNAMICS CORP FORT WORTH TX FORT WORTH DIV F/G 11/4
A COMPARISON OF THE DELAMINATION AND ENVIRONMENTAL RESISTANCE O--ETC(U)
SEP 81 D J WILKINS N00019-80-C-0415
UNCLASSIFIED NAV-GD-0037 NL

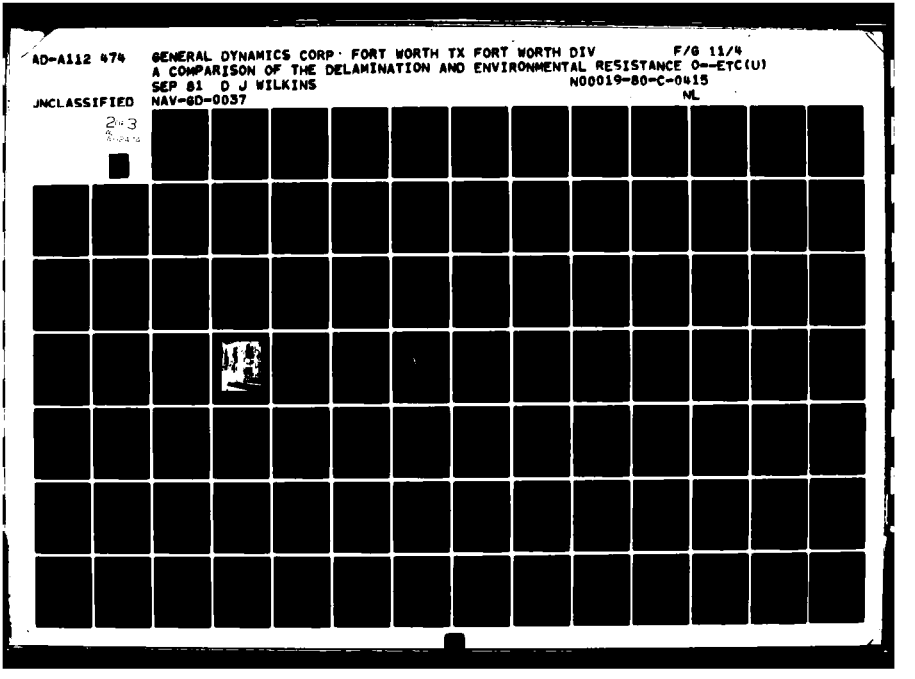

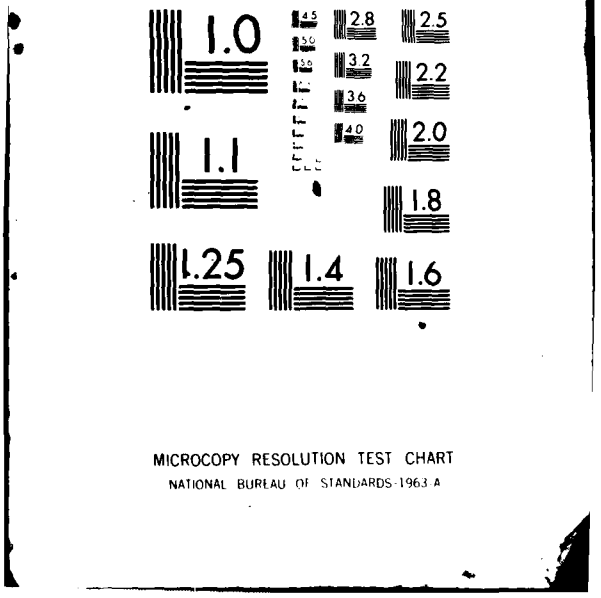
1.0
1.1
1.25
1.4
1.6
1.8
2.0
2.2
2.5
2.8
3.2
3.6
4.0
4.5
5.0
5.6
MICROCOPY RESOLUTION TEST CHART
NATIONAL BUREAU OF STANDARDS-1963-A

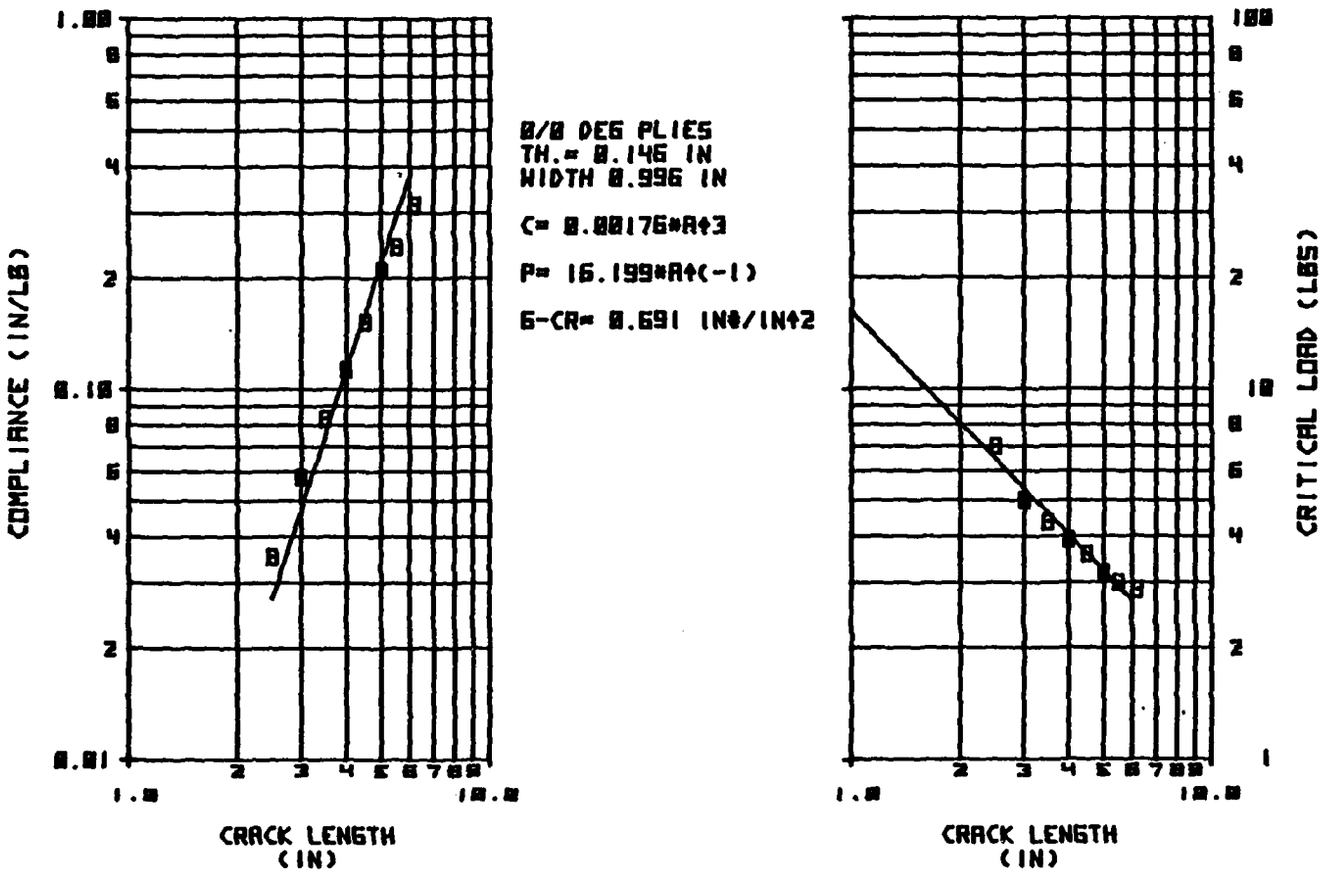

Figure B-6 Test E1CDS of Specimen E1-4-9

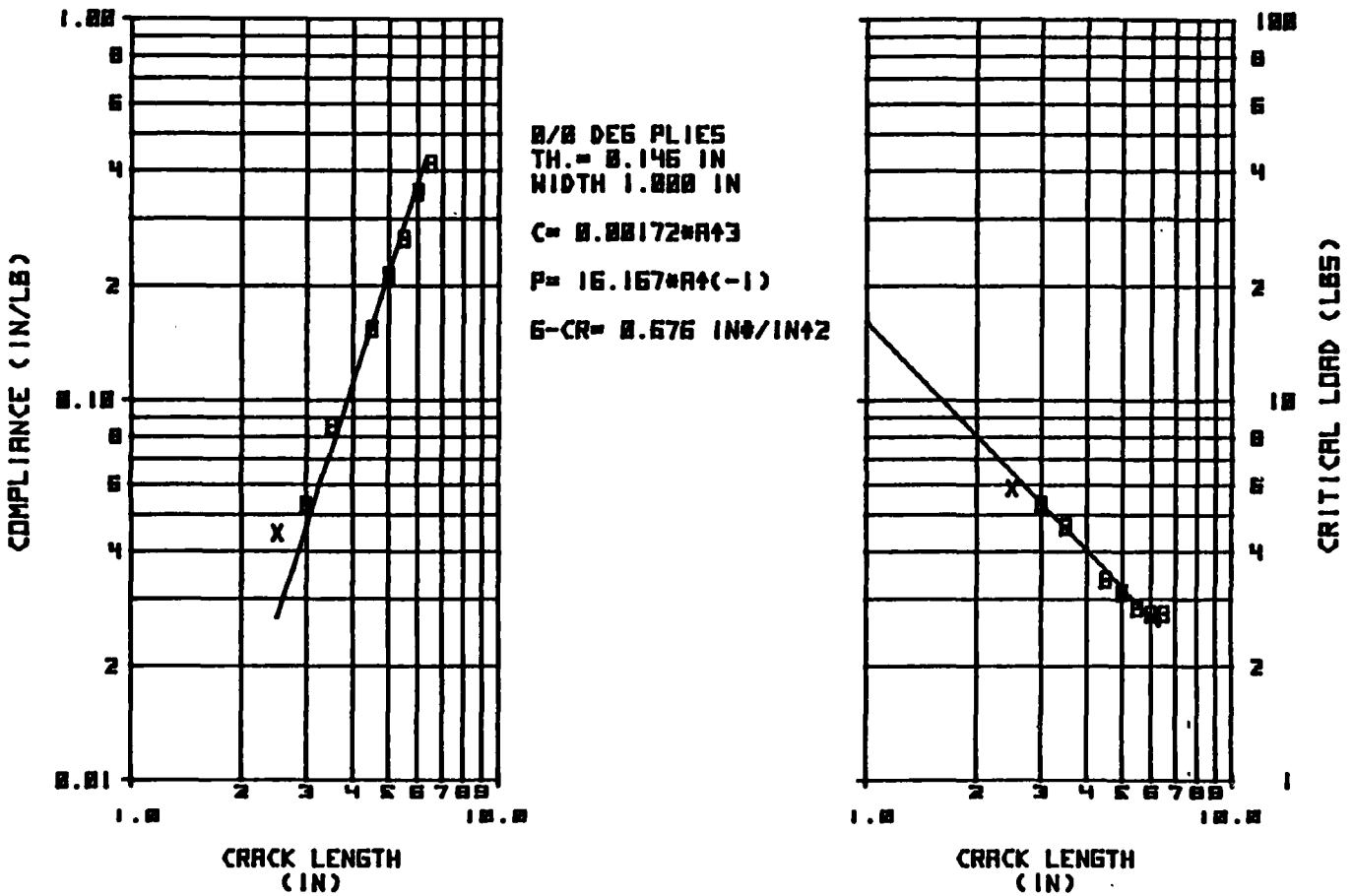

Figure B-7 Test E1CWS of Specimen E1-5-8

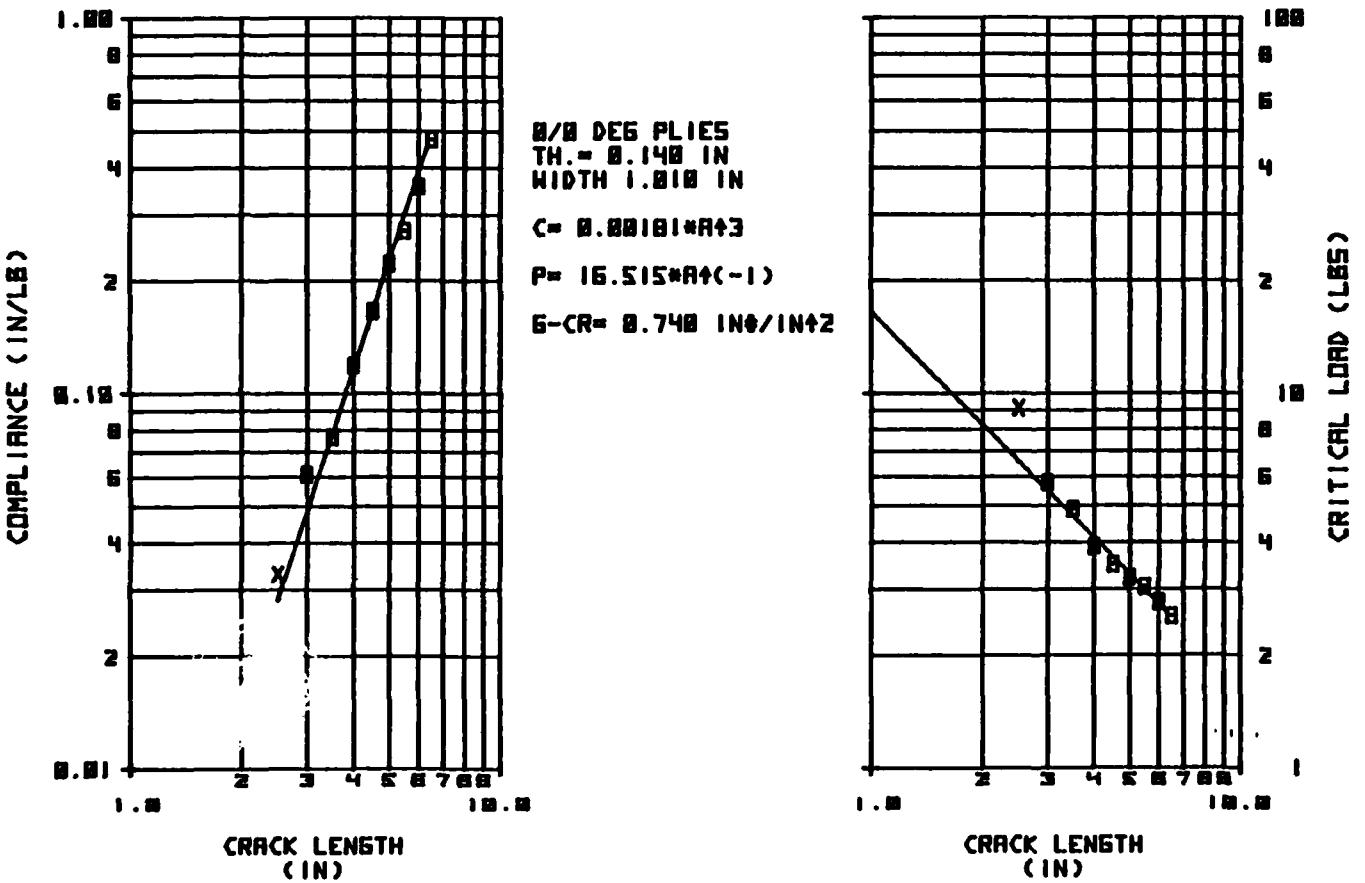

Figure B-8 Test EIRDS of Specimen E1-4-1

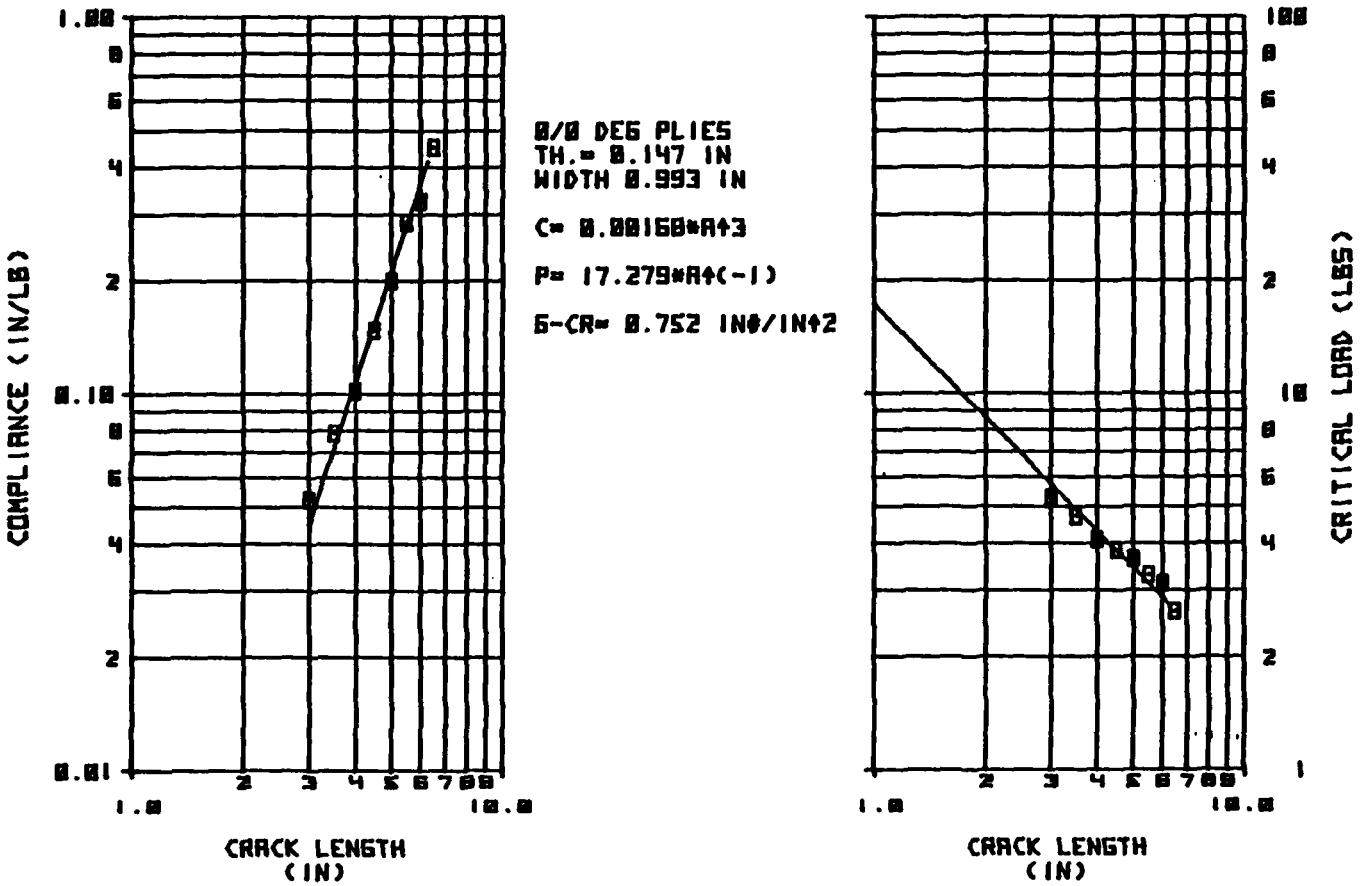

Figure B-9 Test EIRDS of Specimen E1-4-2

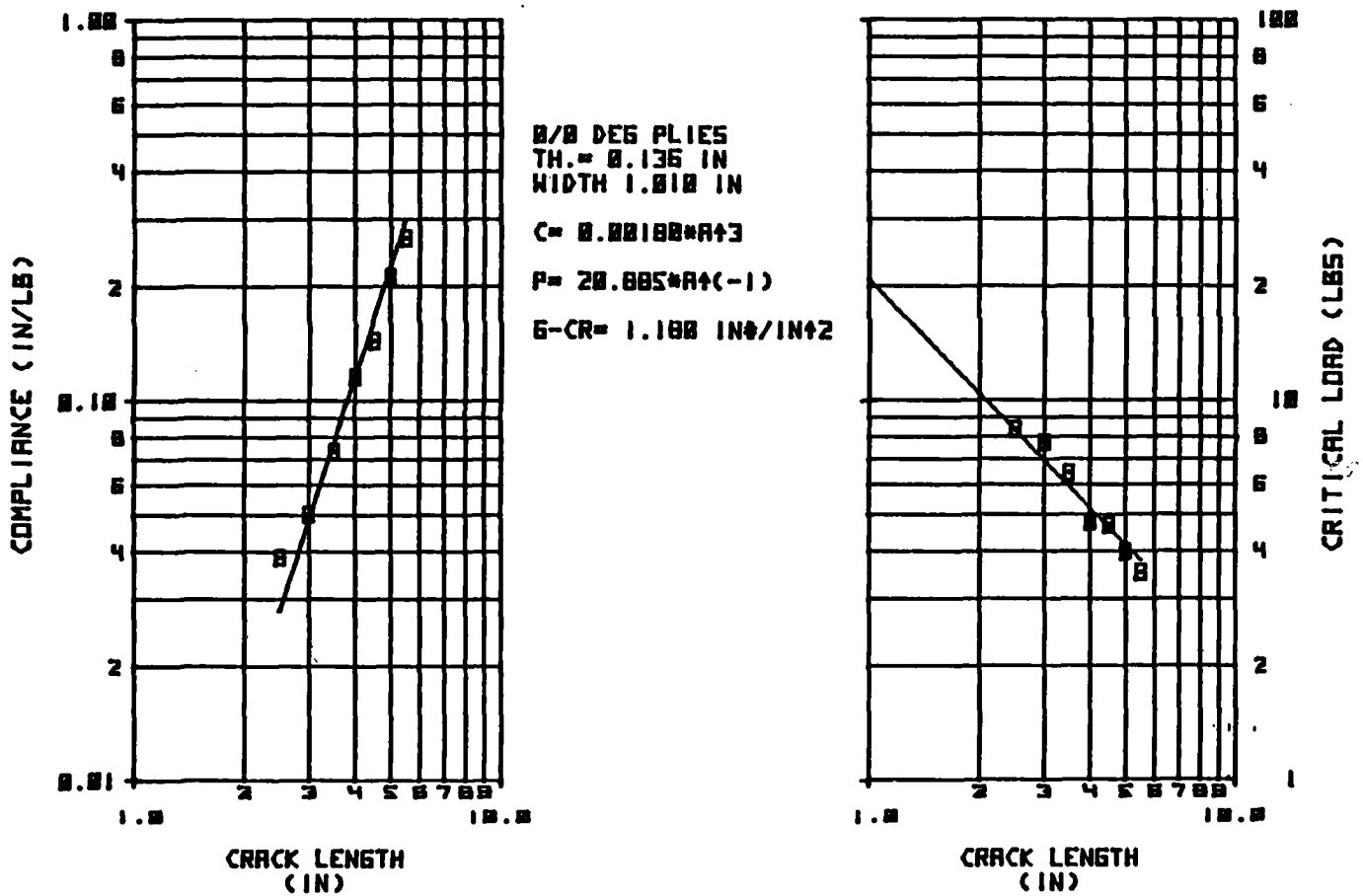

Figure B-10 Test E1RWS of Specimen E1-5-9

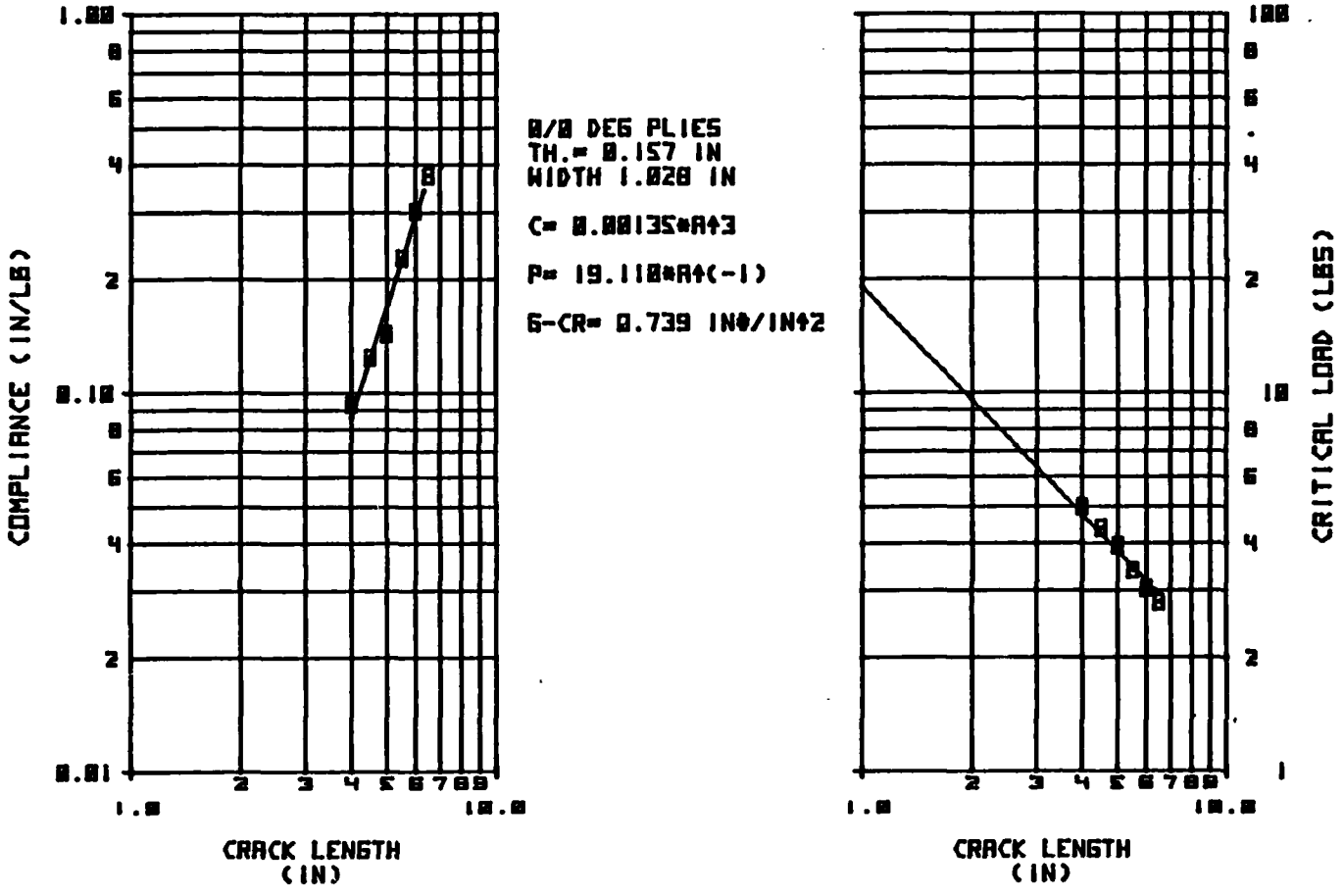

Figure B-11 Test E1RWS of Specimen E1-5-3

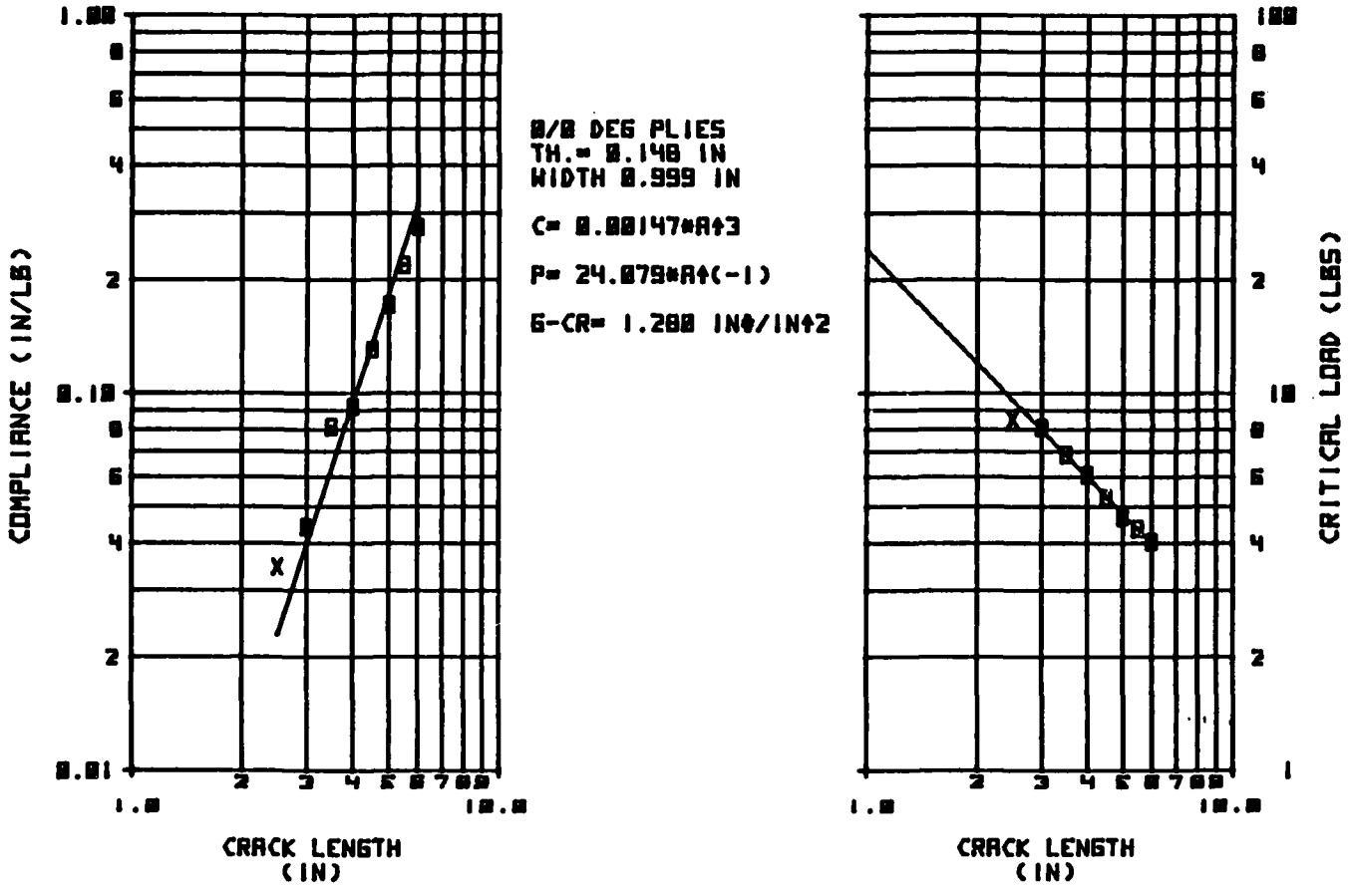

Figure B-12 Test E1EDS of Specimen E1-2-4

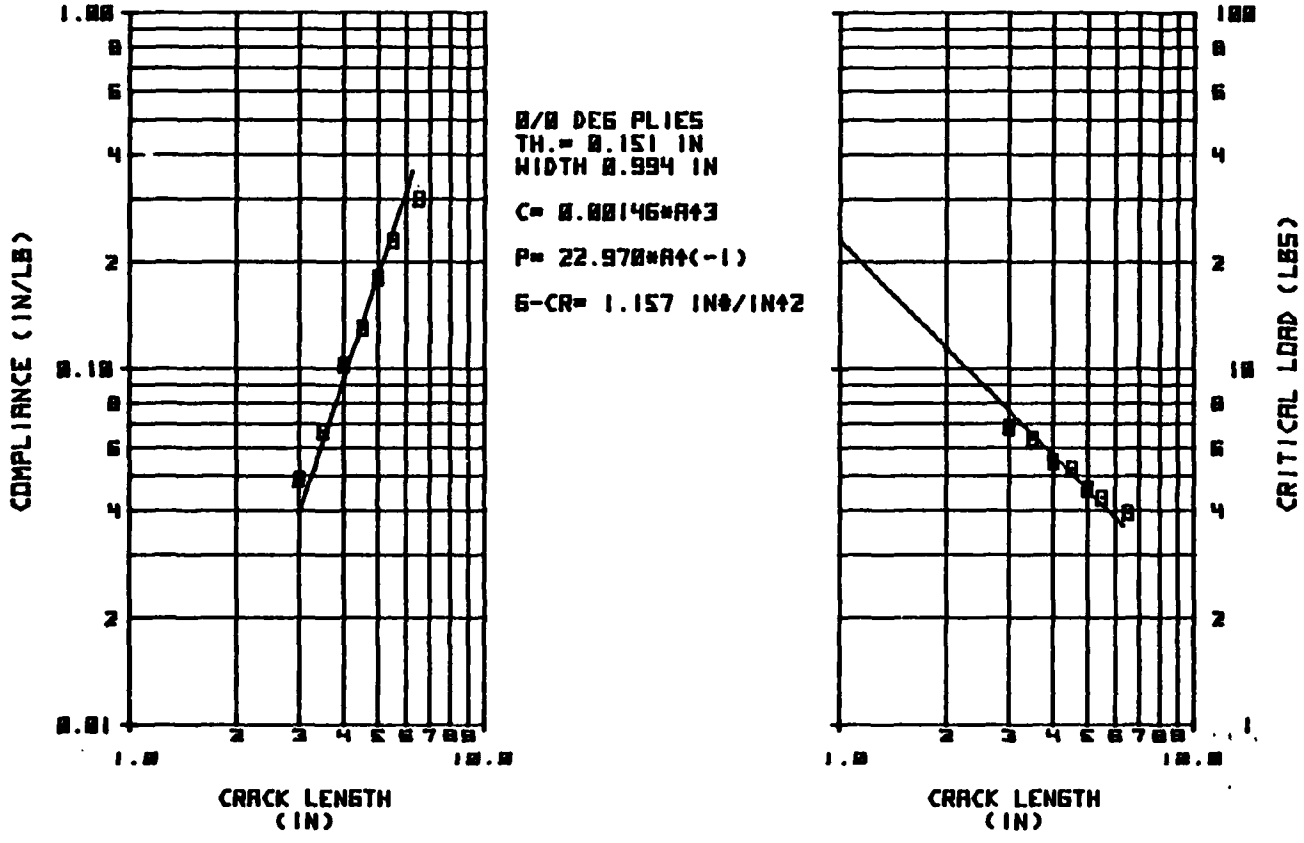

Figure B-13 Test EIEDS of Specimen E1-3-2

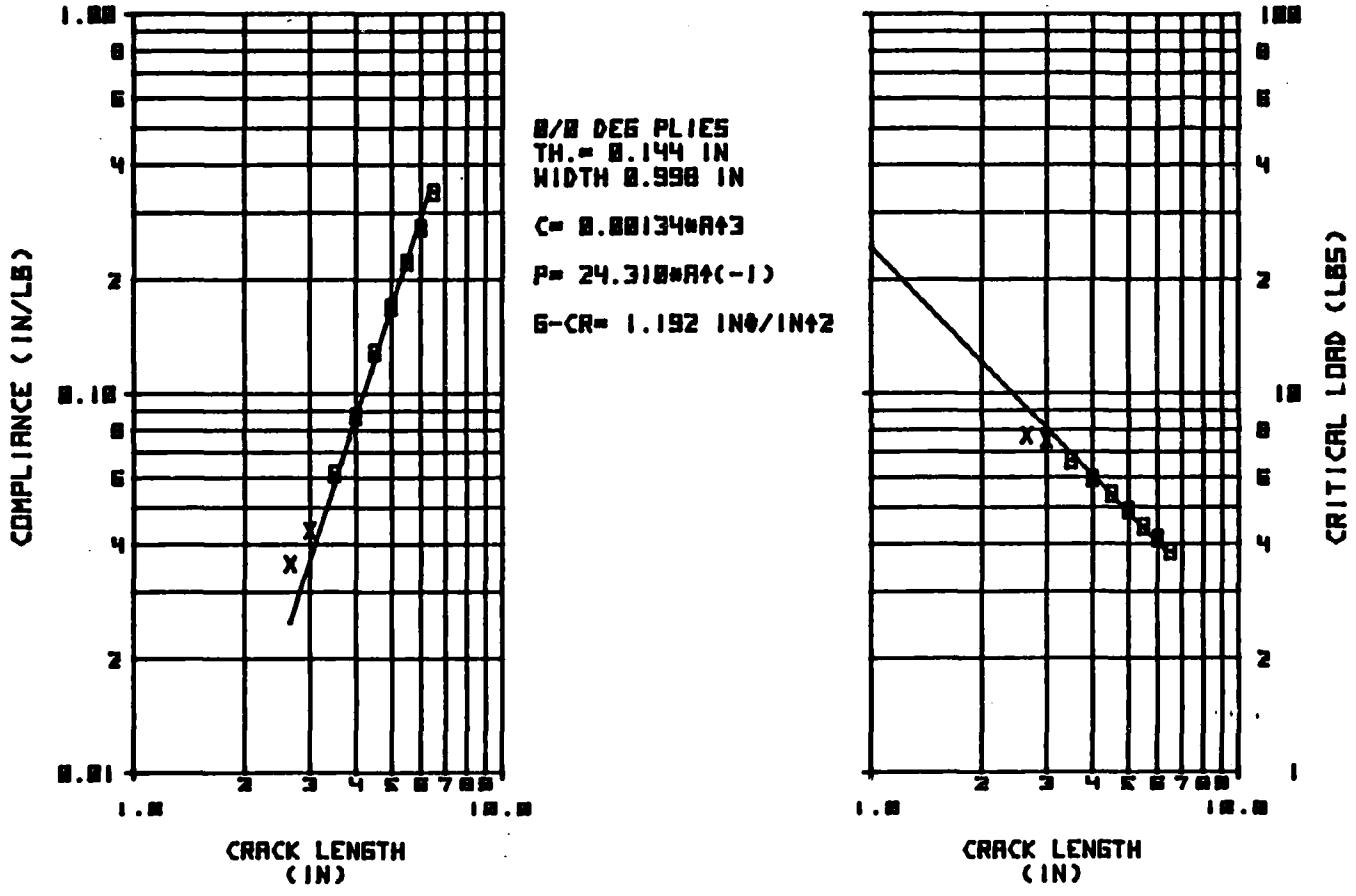

Figure B-14 Test E1PDS of Specimen E1-2-8

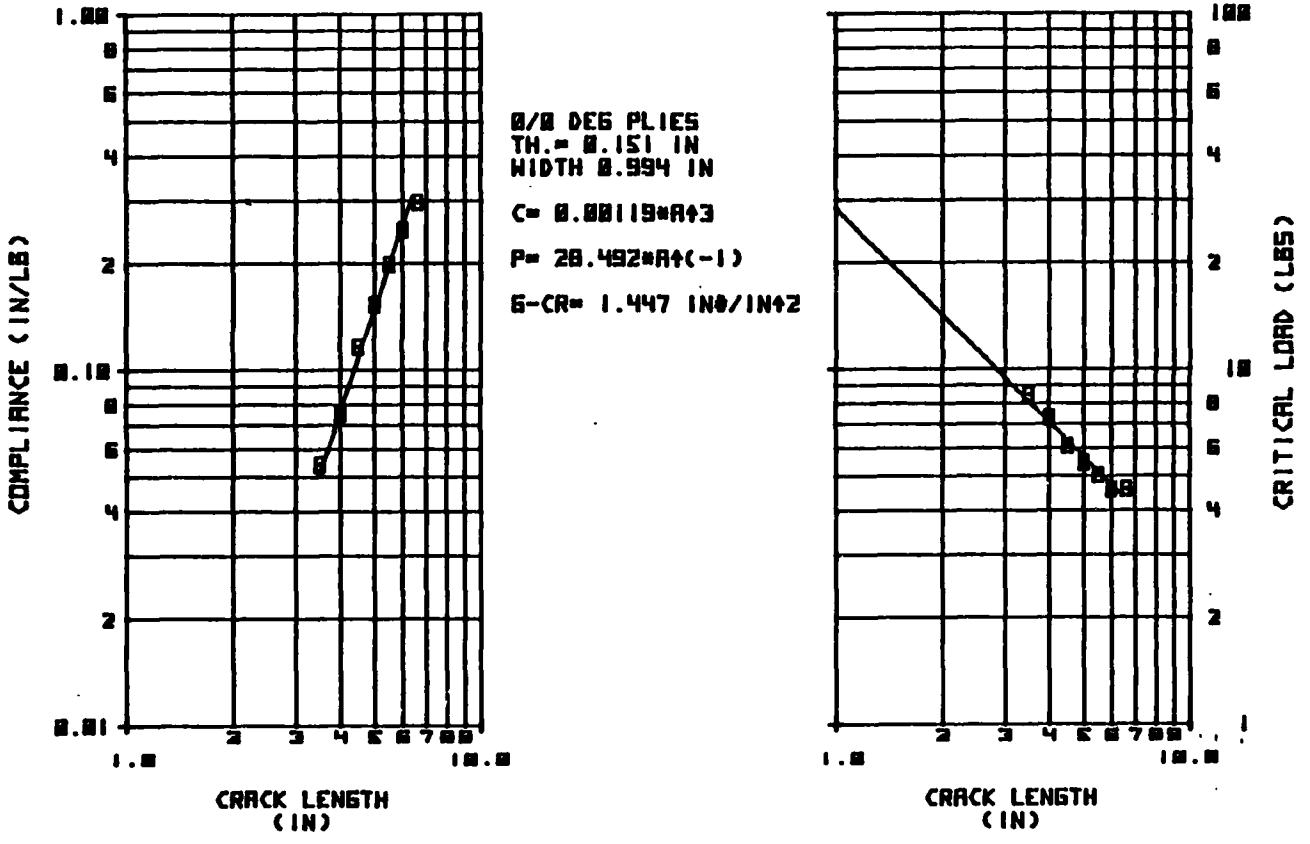

Figure B-15 Test E1PDS of Specimen E1-3-1

B.4 Bismaleimide Mode I Static Data

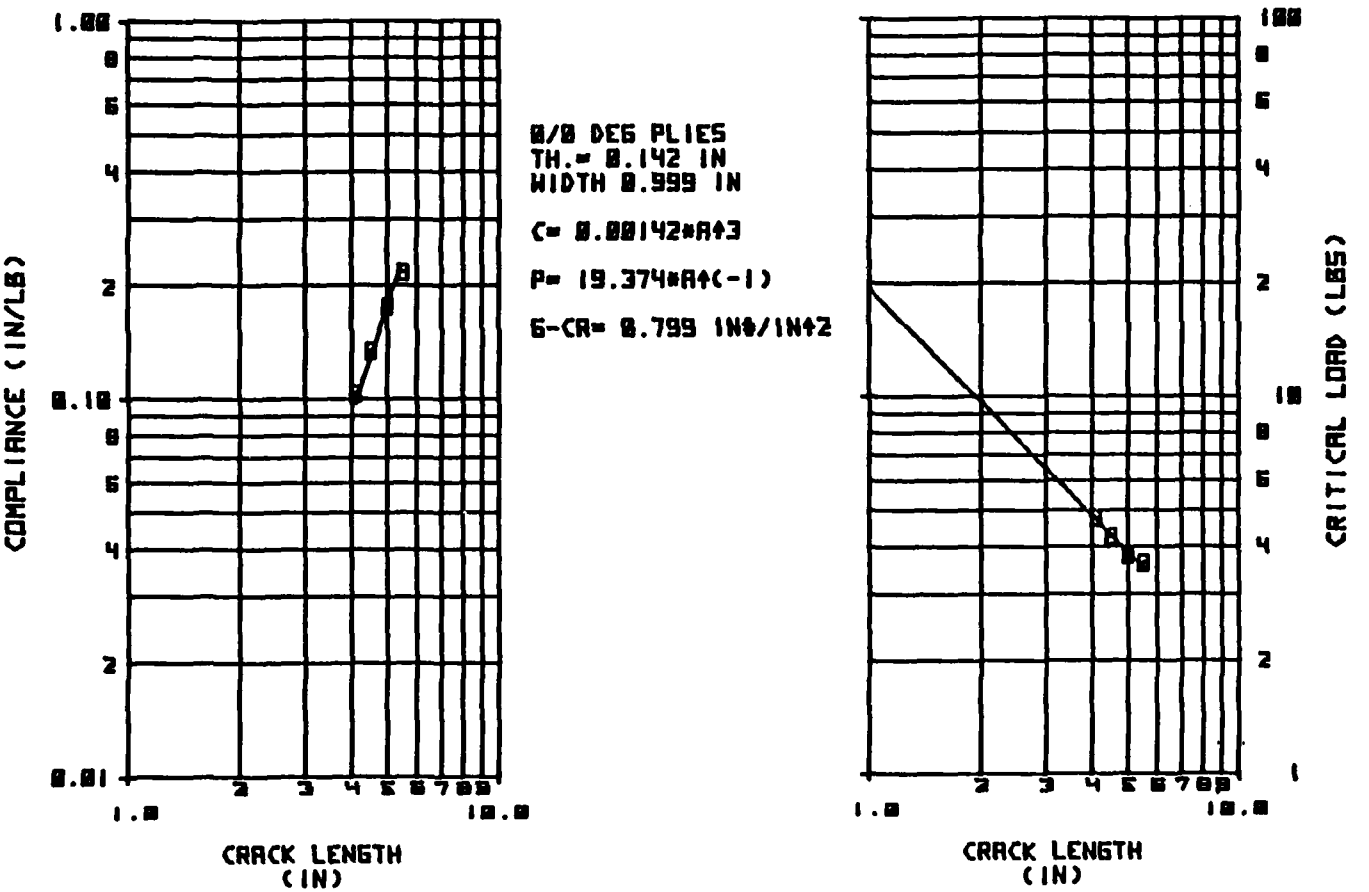

Figure B-16 Test P1CDS of Specimen P1-4-1

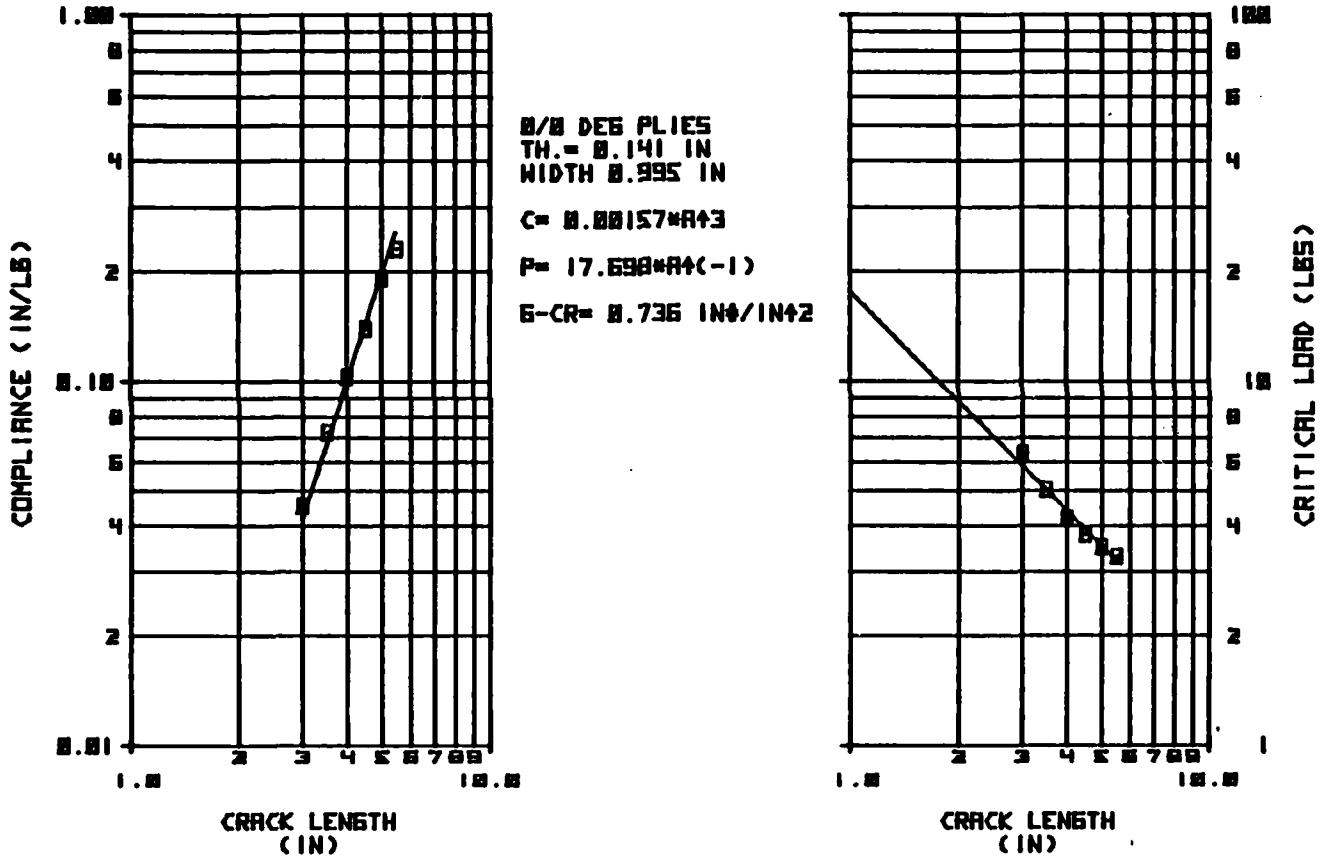

Figure B-17 Test P1CDS of Specimen P1-4-5

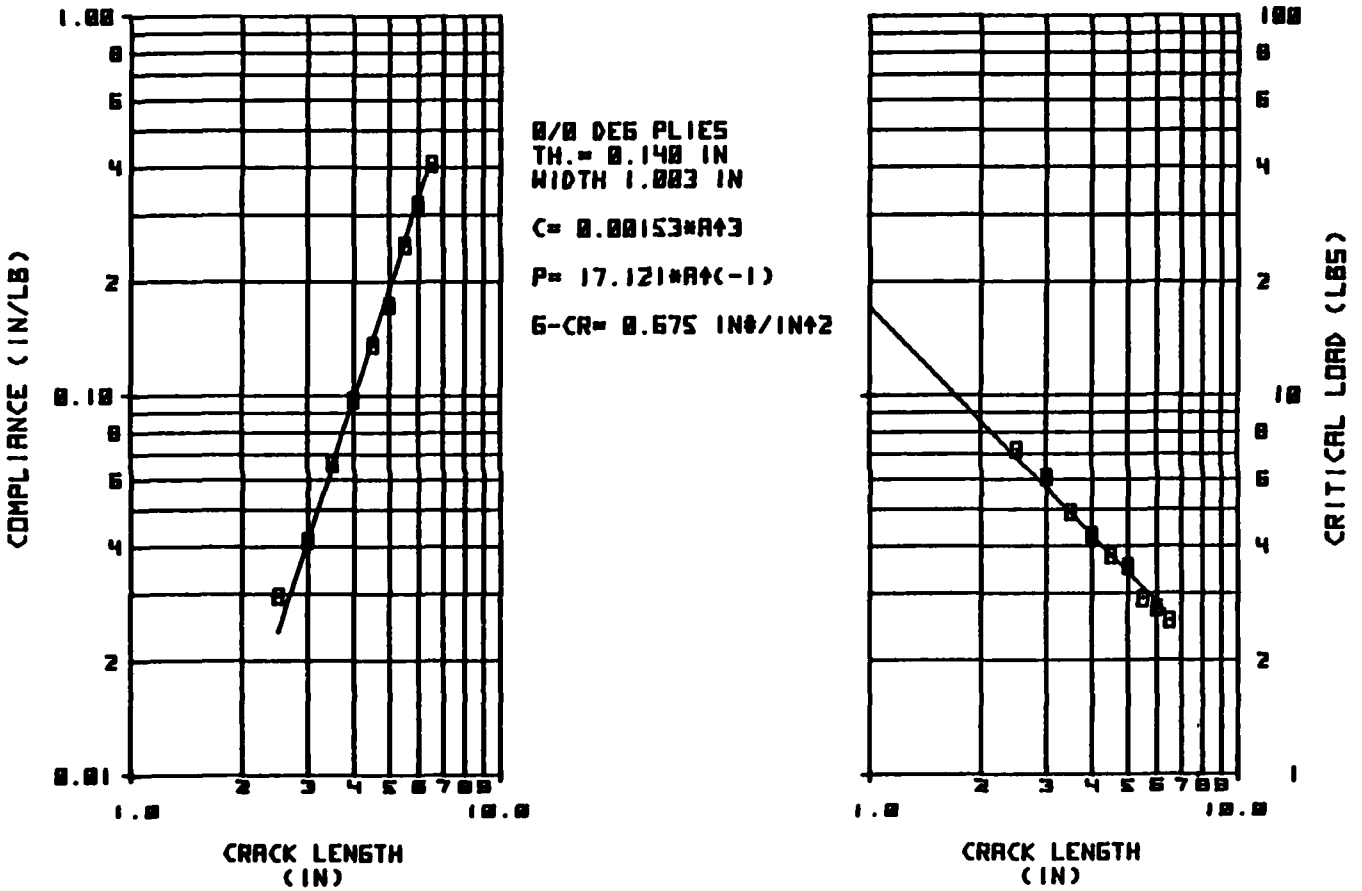

Figure B-18 Test P1CWS of Specimen P1-1-3

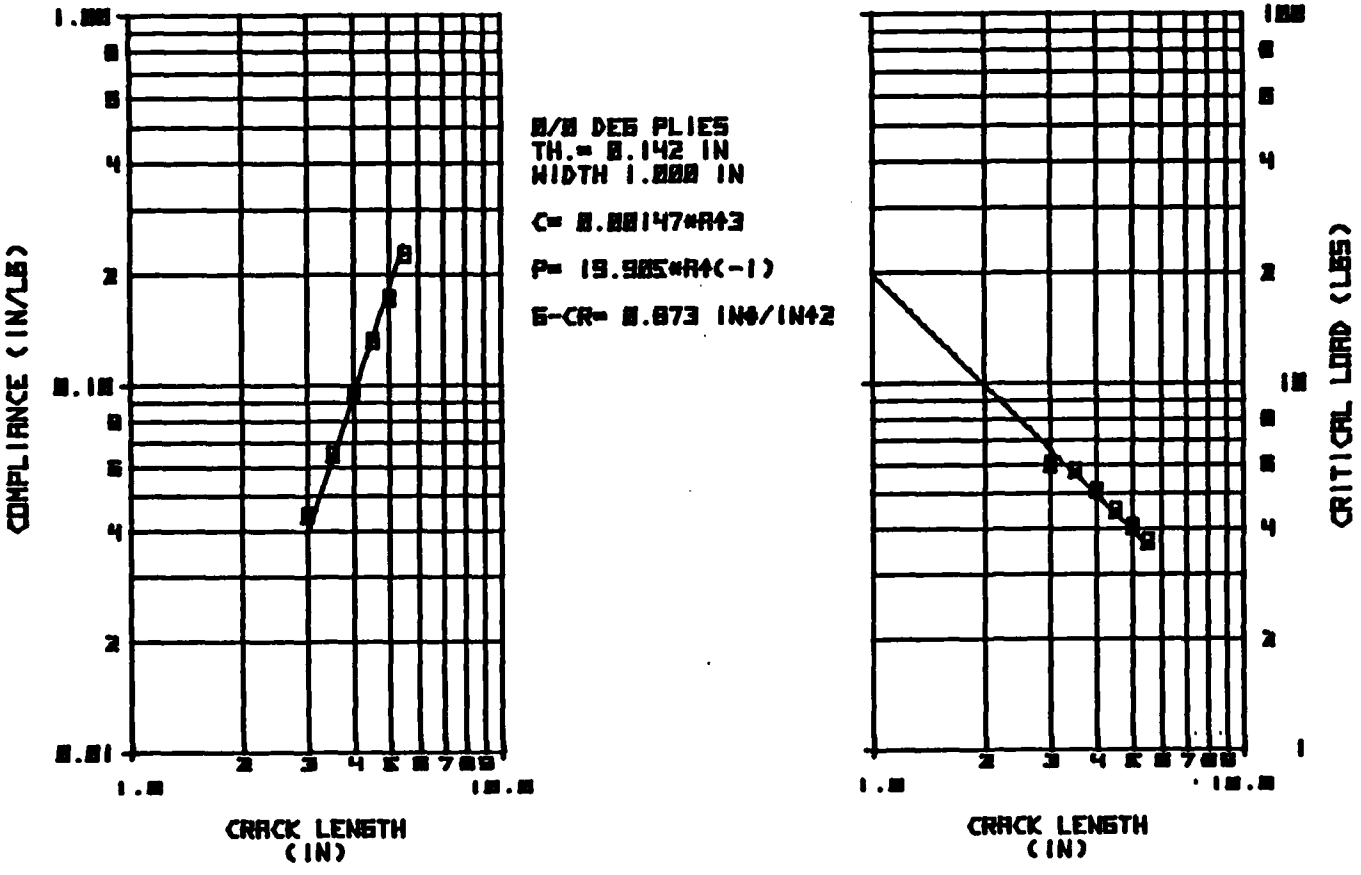

Figure B-19 Test P1RDS of Specimen P1-4-2

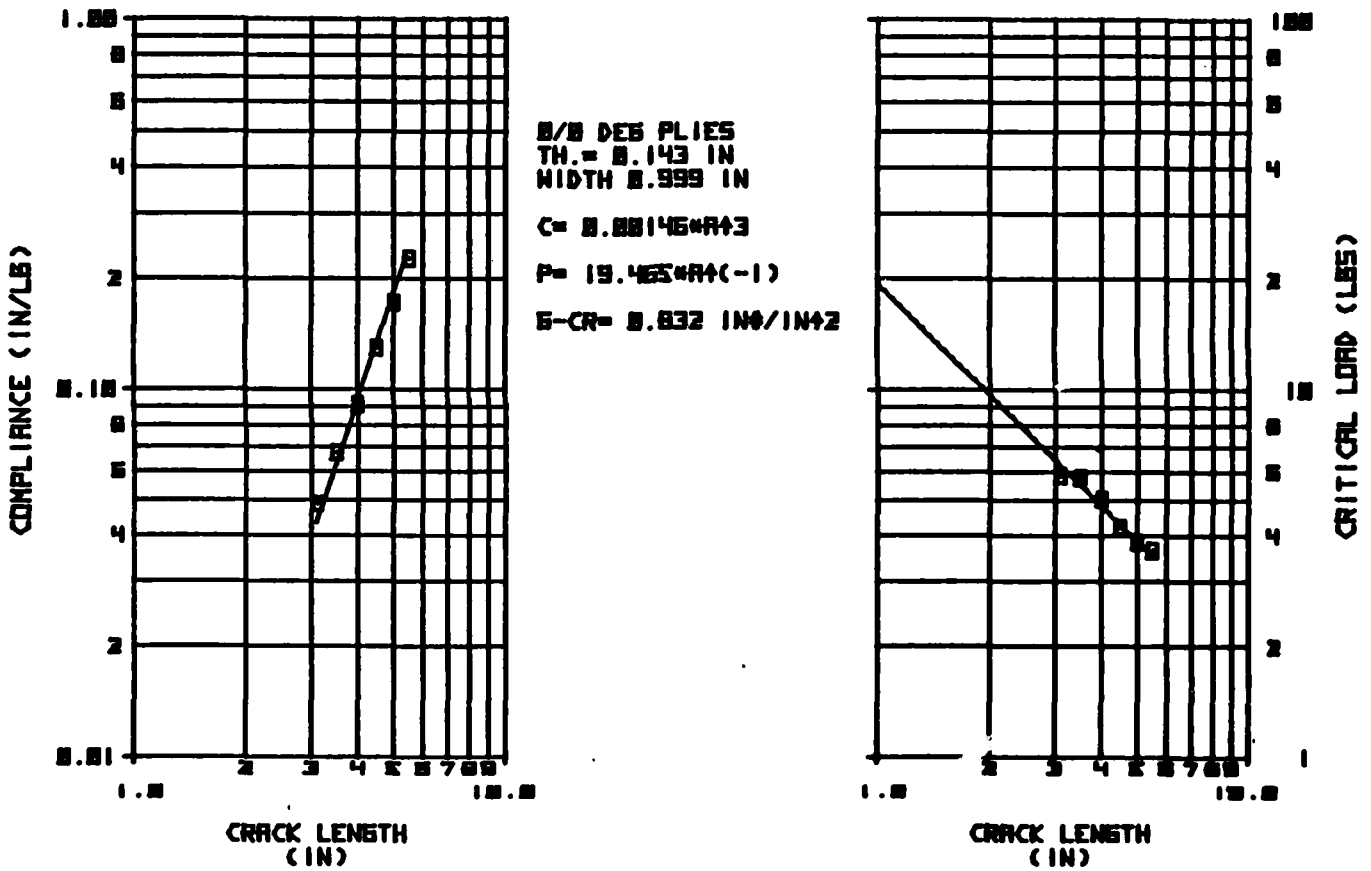

Figure B-20 Test PIRDS of Specimen P1-4-9

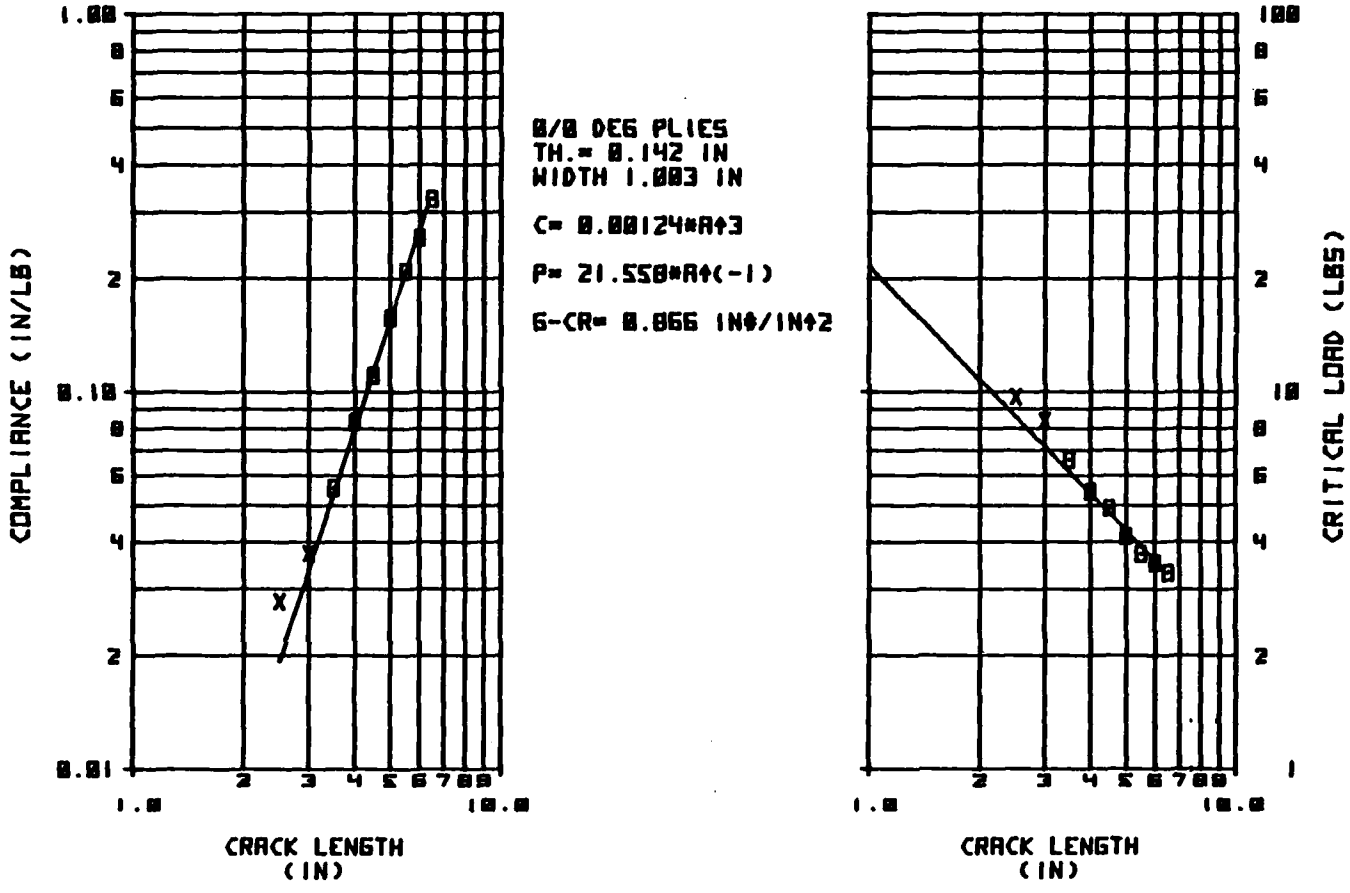

Figure B-21 Test P1RWS of Specimen P1-1-2

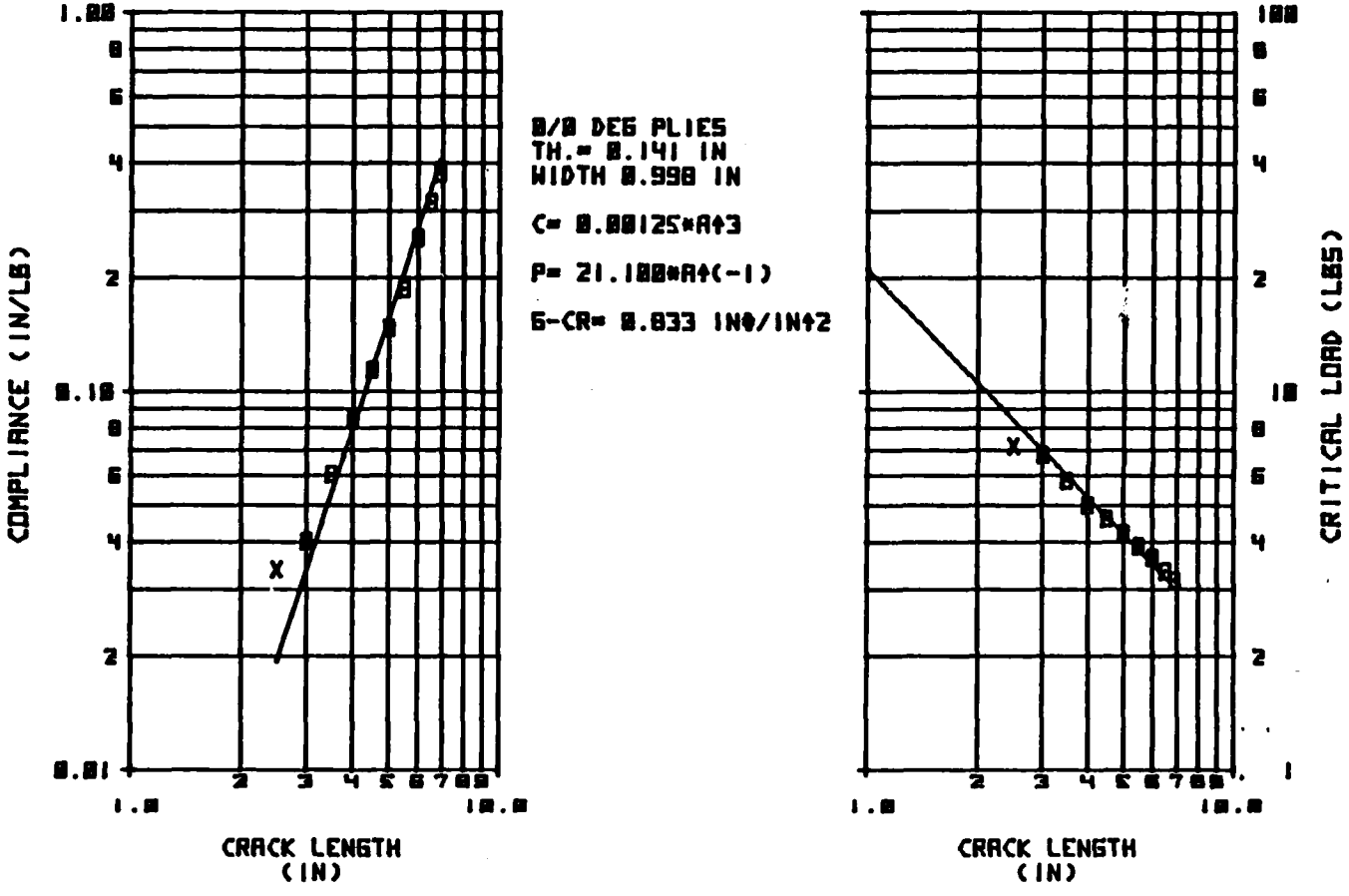

Figure B-22 Test P1EDS of Specimen P1-3-5

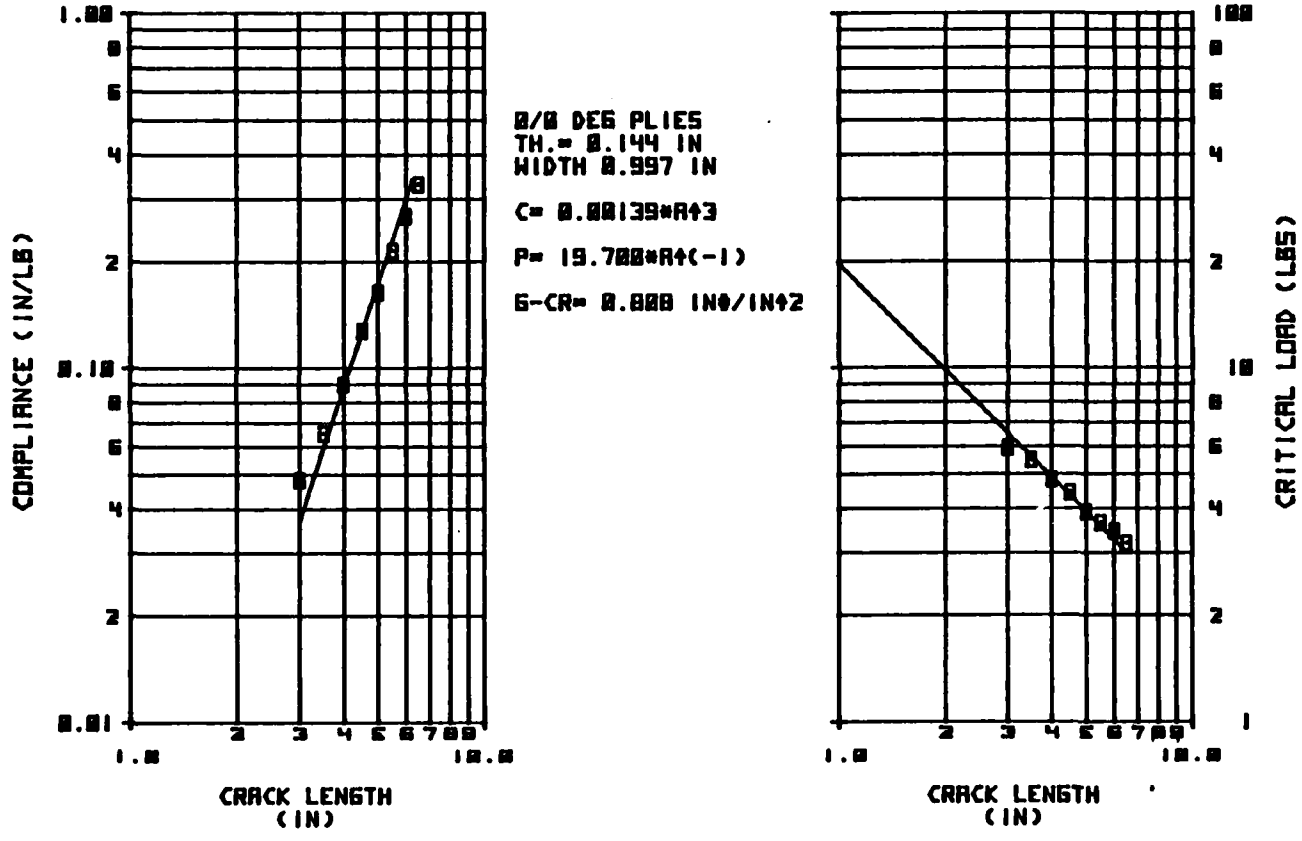

Figure B-23 Test P1EDS of Specimen P1-2-10

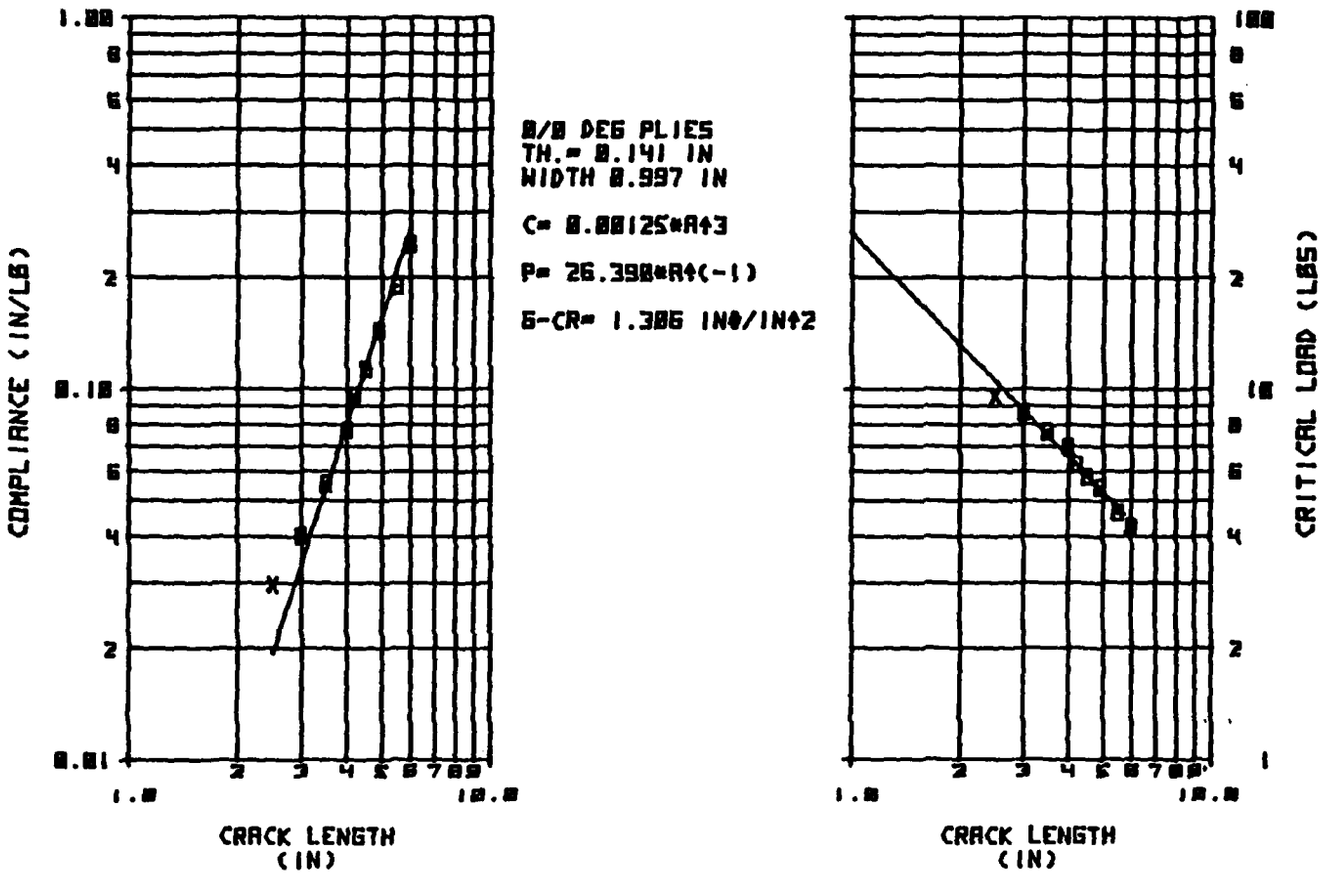

Figure B-24 Test P1PDS of Specimen P1-3-8

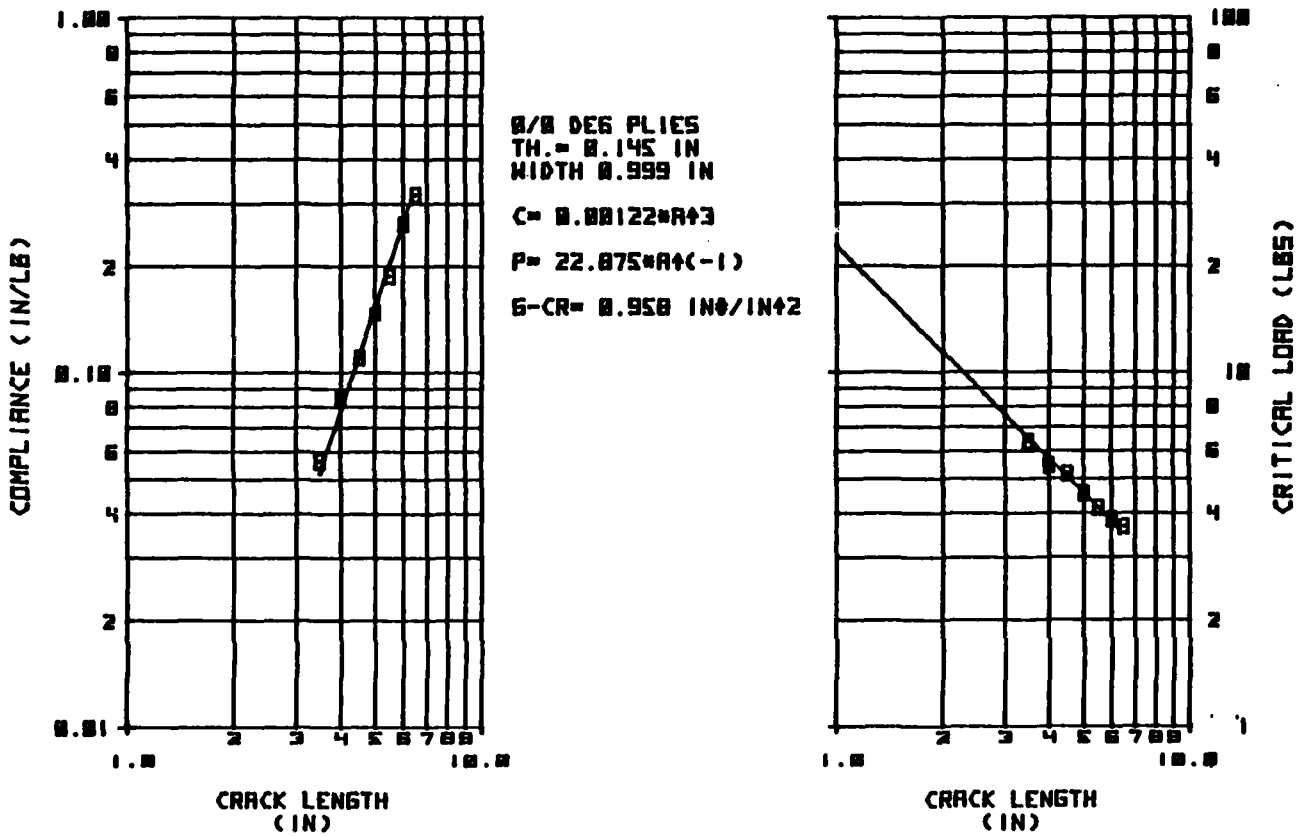

Figure B-25 Test P1PDS of Specimen P1-2-3

APPENDIX C

MODE I FATIGUE TESTING

Constant-amplitude (R = 0.1) fatigue tests were performed at a cyclic rate of 0.5 Hz in the same custom displacement-controlled test frames used for static testing. The applied load was measured by a spring-displacement device and was servo-controlled by position feedback. A Hewlett-Packard 3050B Data Acquisition System was programmed to automatically perform compliance measurements, compare them to the compliance/crack-length relationship developed in static tests, and calculate the instantaneous crack length. A procedure was developed to begin cycling at G values near the critical value to obtain cracking rates in the range of 10^{-4} to 10^{-3} in./cycle. As the crack extended, the G corresponding to the fixed displacement diminished, allowing slower cracking rates to be obtained. Cycle counts were selected to give accurately measurable crack growth increments of about 0.02 to 0.05 in.

The Hewlett-Packard data system used to control the fatigue tests was also employed to organize the data for presentation. After a prescribed number of cycles at a given maximum displacement, the incremental growth was divided by the cycle increment to give da/dN. These data, as well as absolute crack length, maximum load, and total cycle count, were stored on tape cassettes for subsequent plotting. These plots are shown on the following pages for both the epoxy and the bismaleimide material systems.

C.1 Epoxy Mode I Fatigue Data

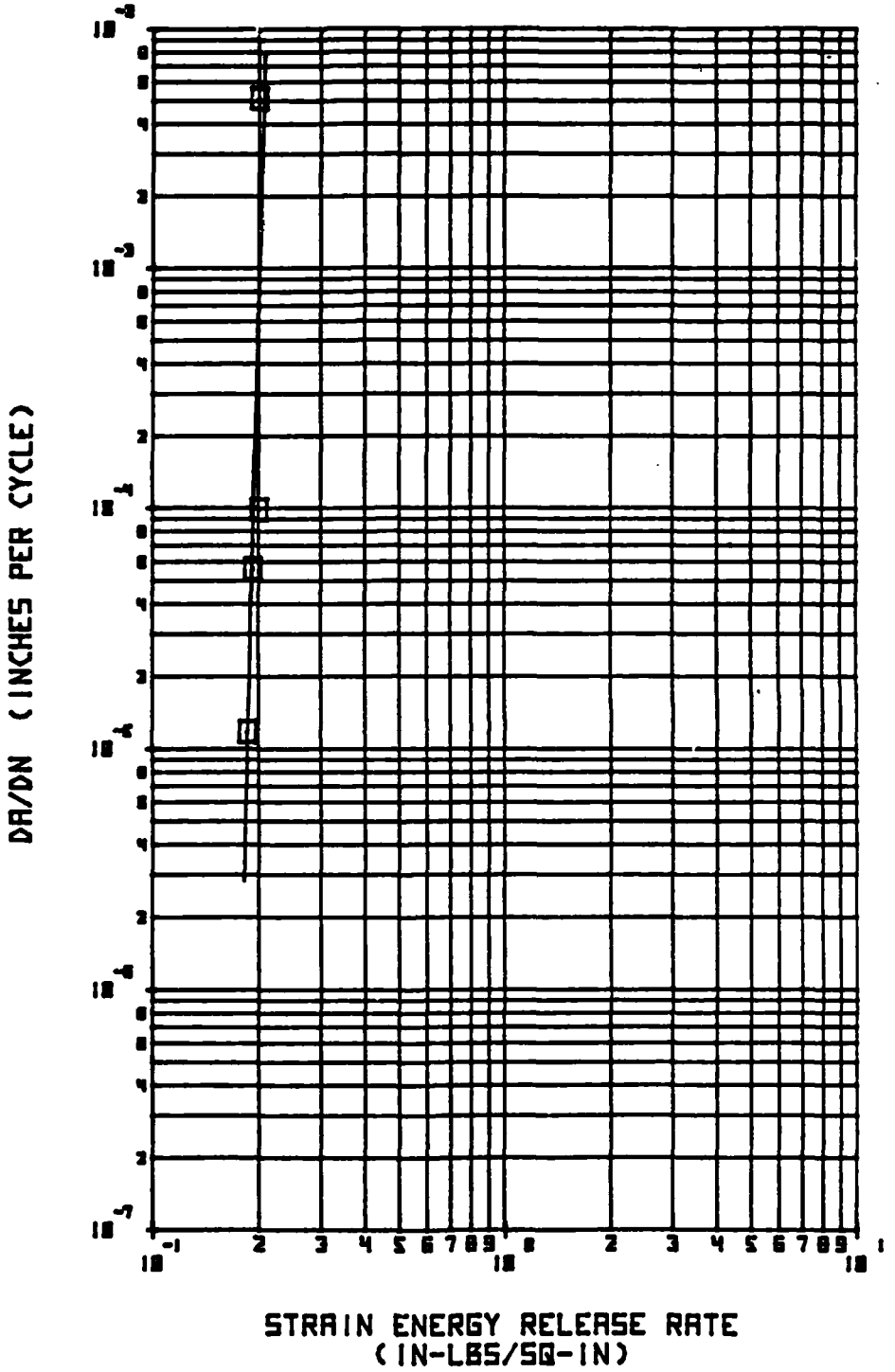

Figure C-1 Test E1CDF of Specimen E1-4-6

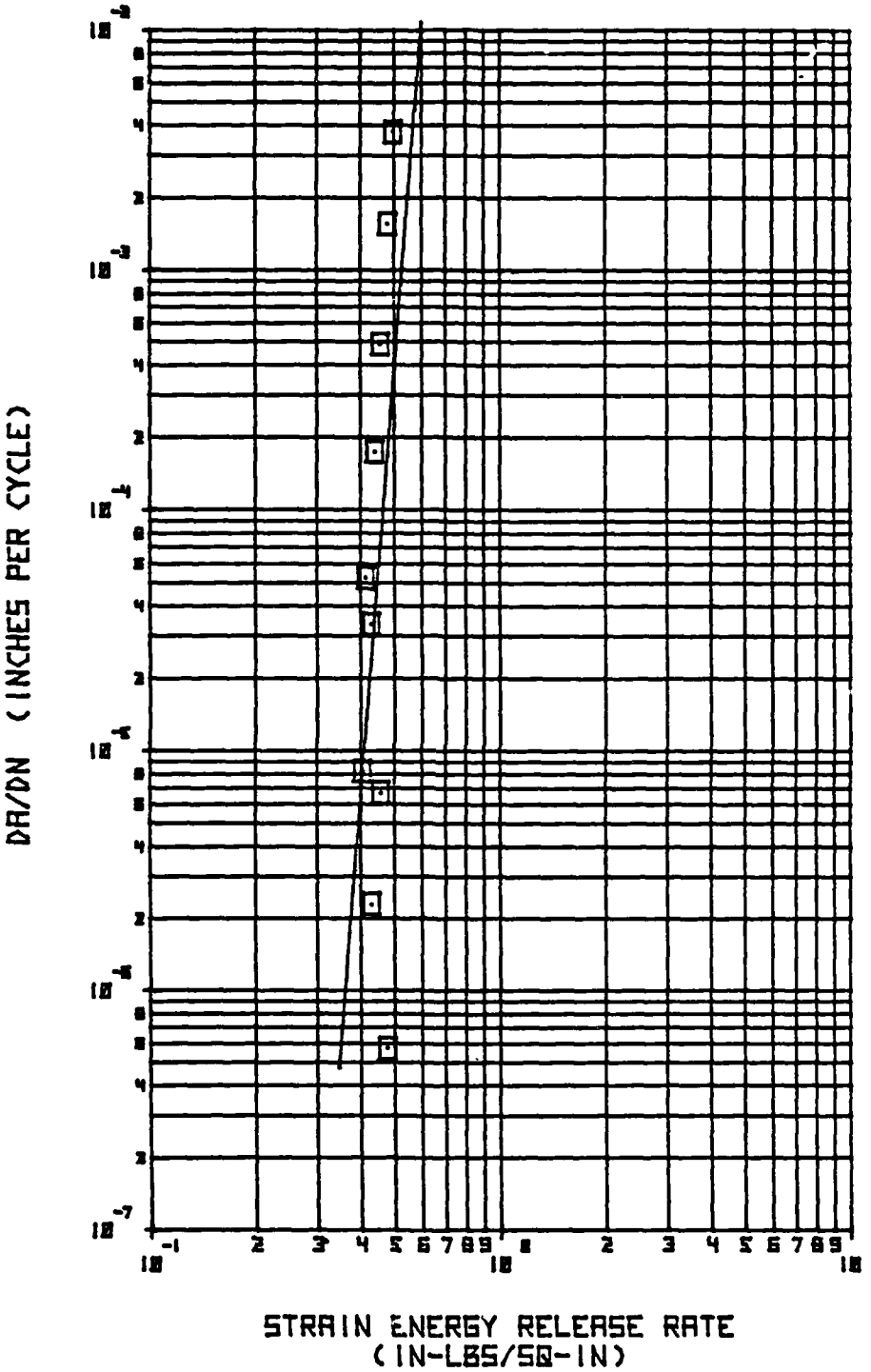

Figure C-2 Test E1CDF of Specimen E1-1-4

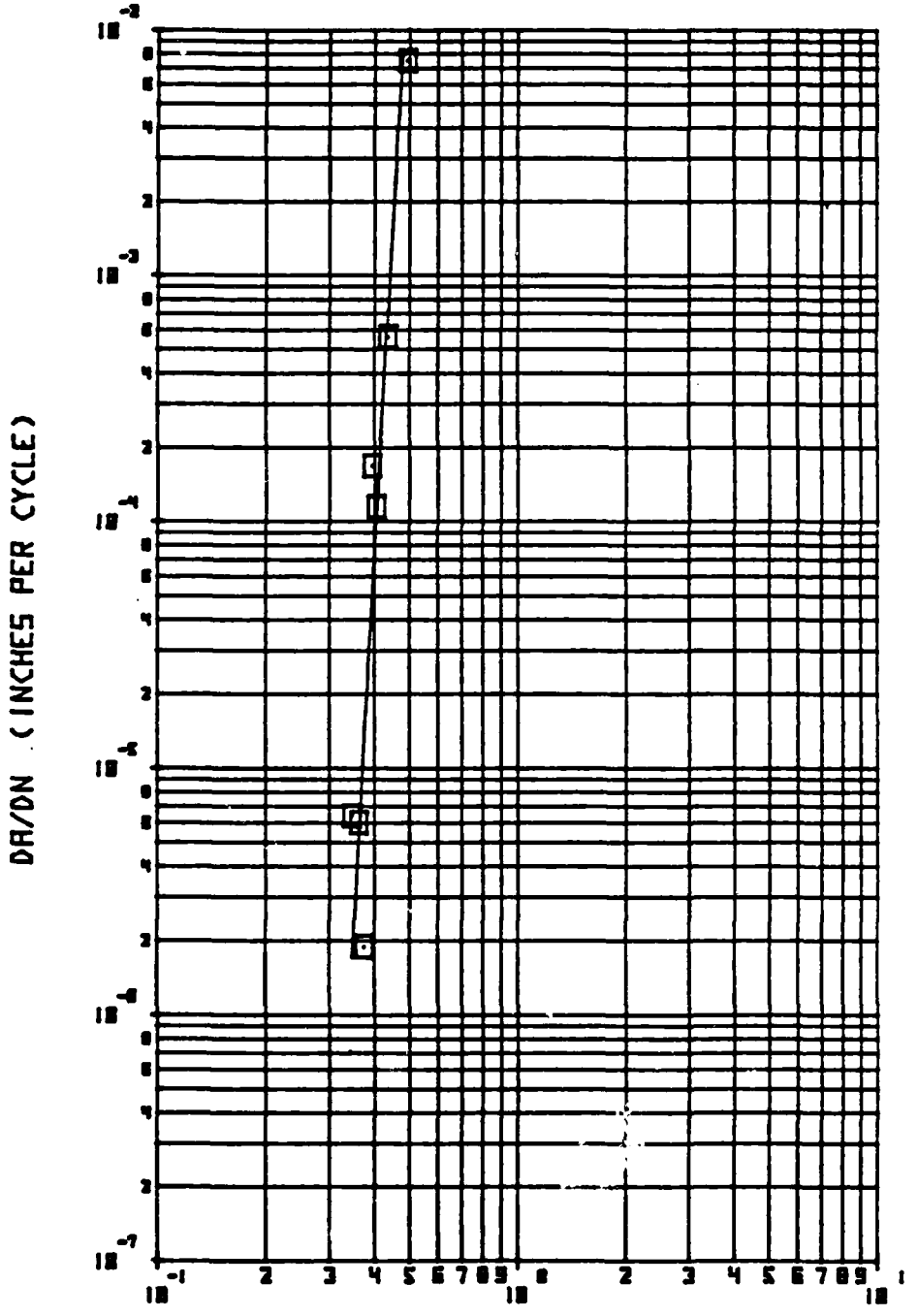

Figure C-3 Test E1CWF of Specimen E1-5-7

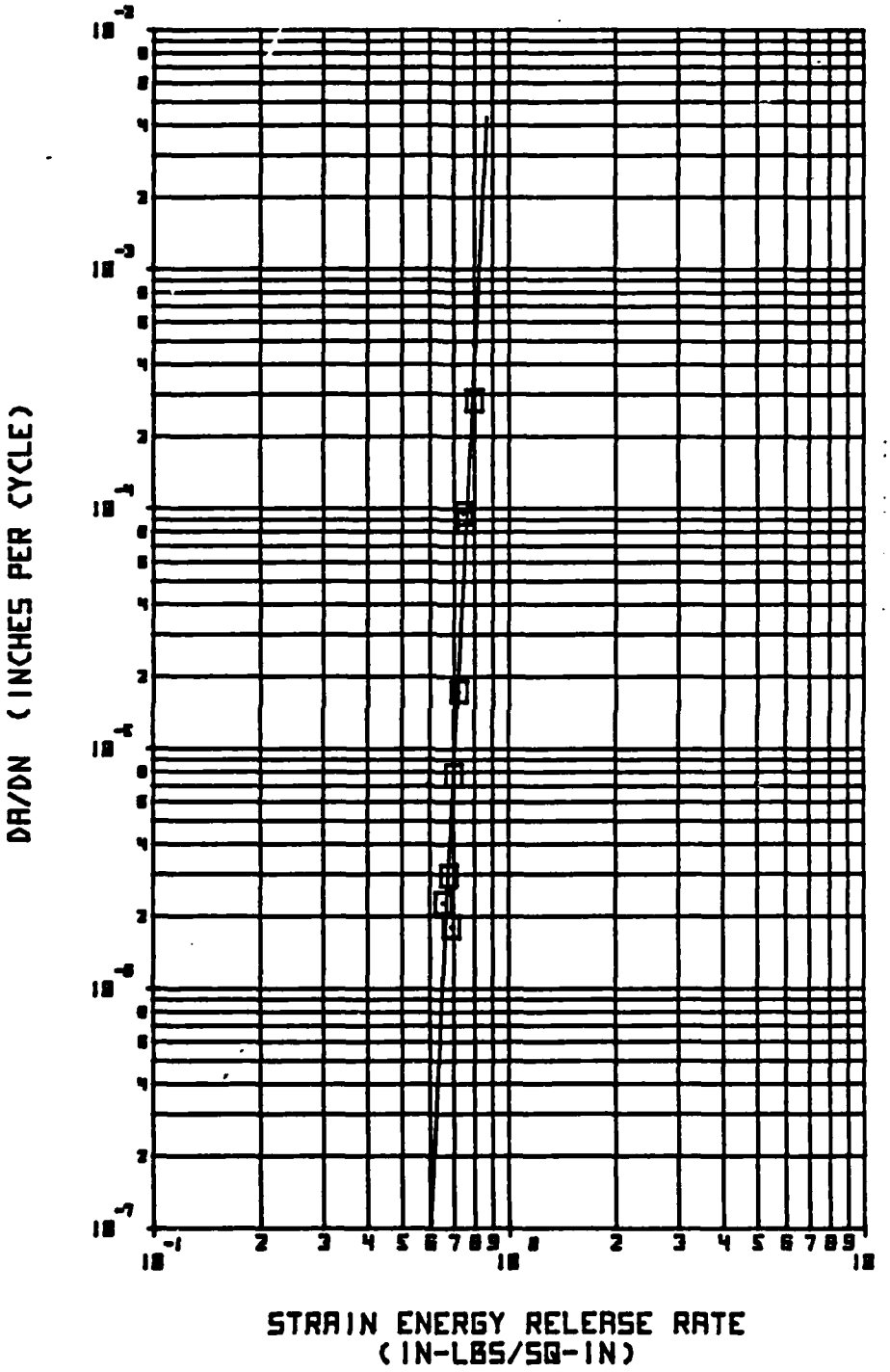

Figure C-4 Test E1RDF of Specimen E1-4-4

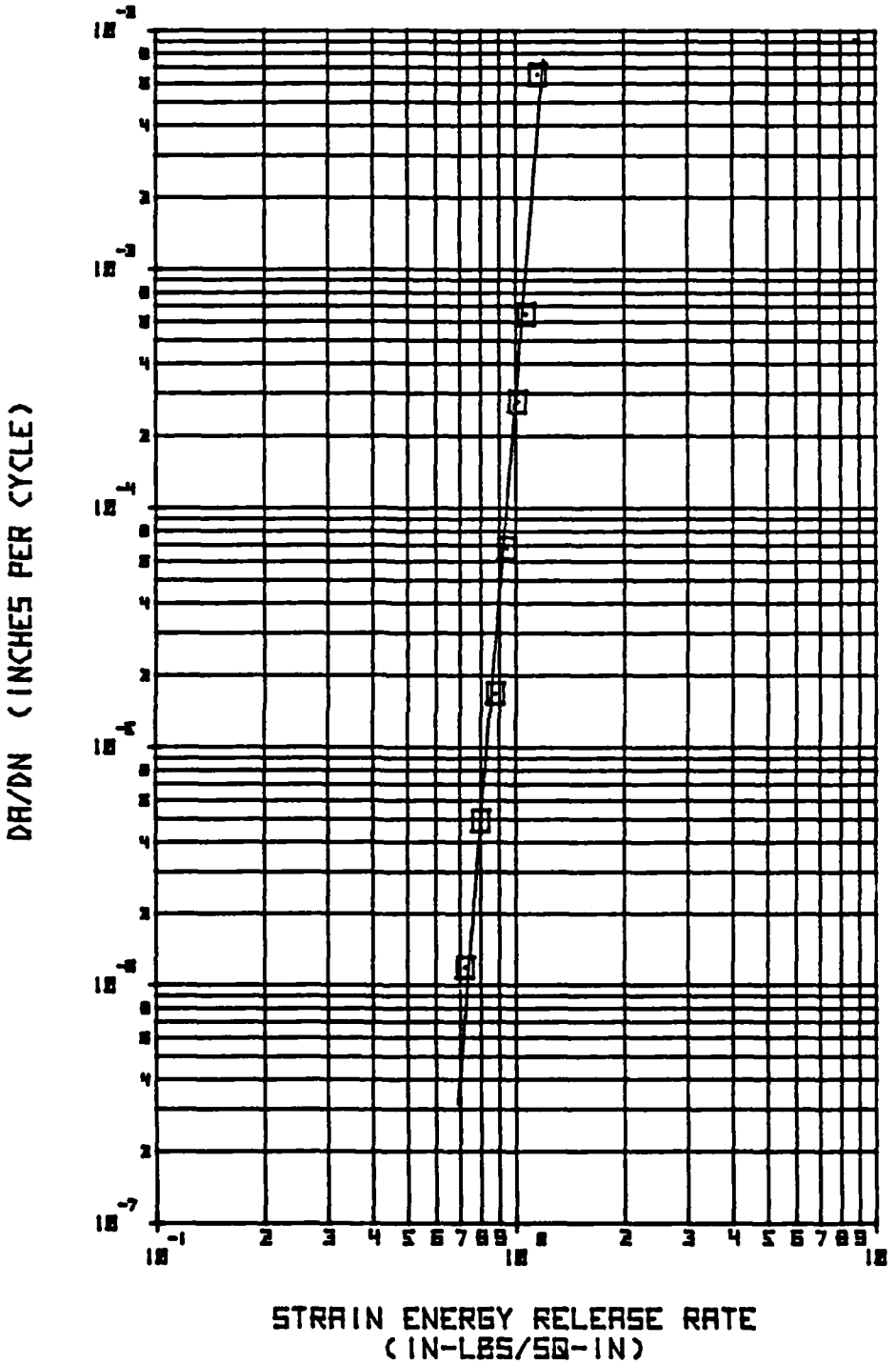

Figure C-5 Test E1RWF of Specimen E1-5-2

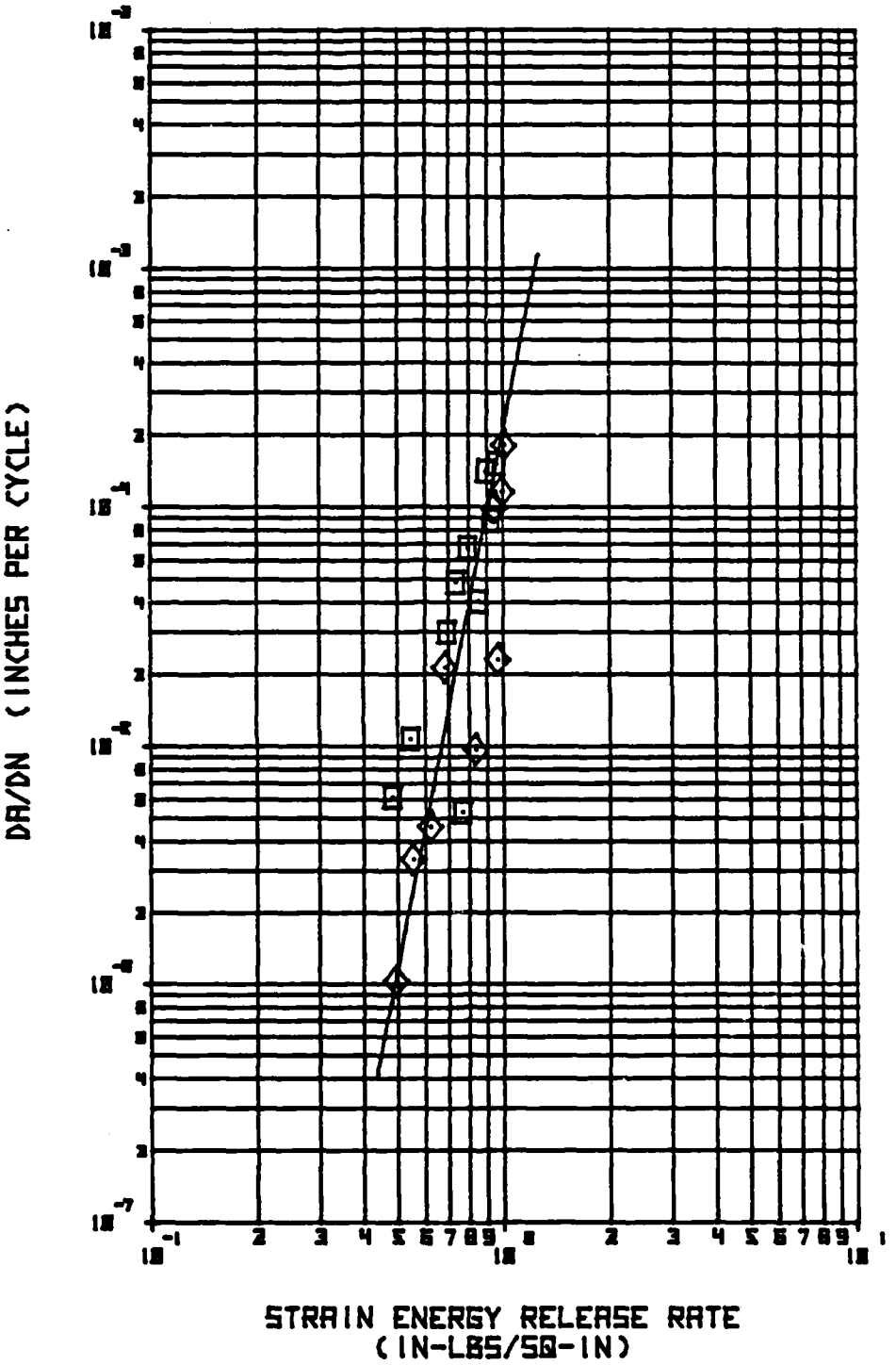

Figure C-6 Test E1RWF of Specimen E1-5-4

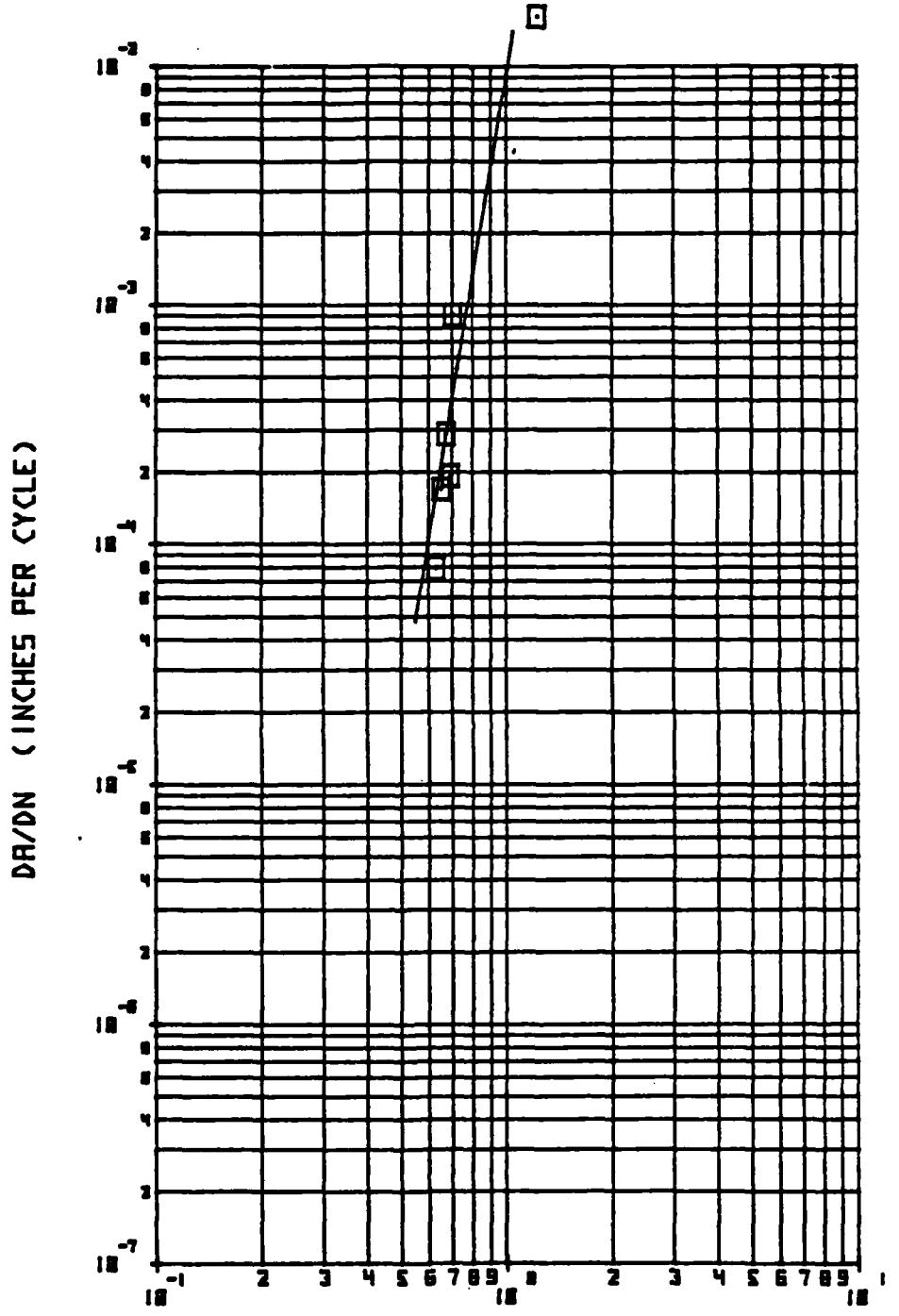

Figure C-7 Test E1EDF of Specimen E1-2-1

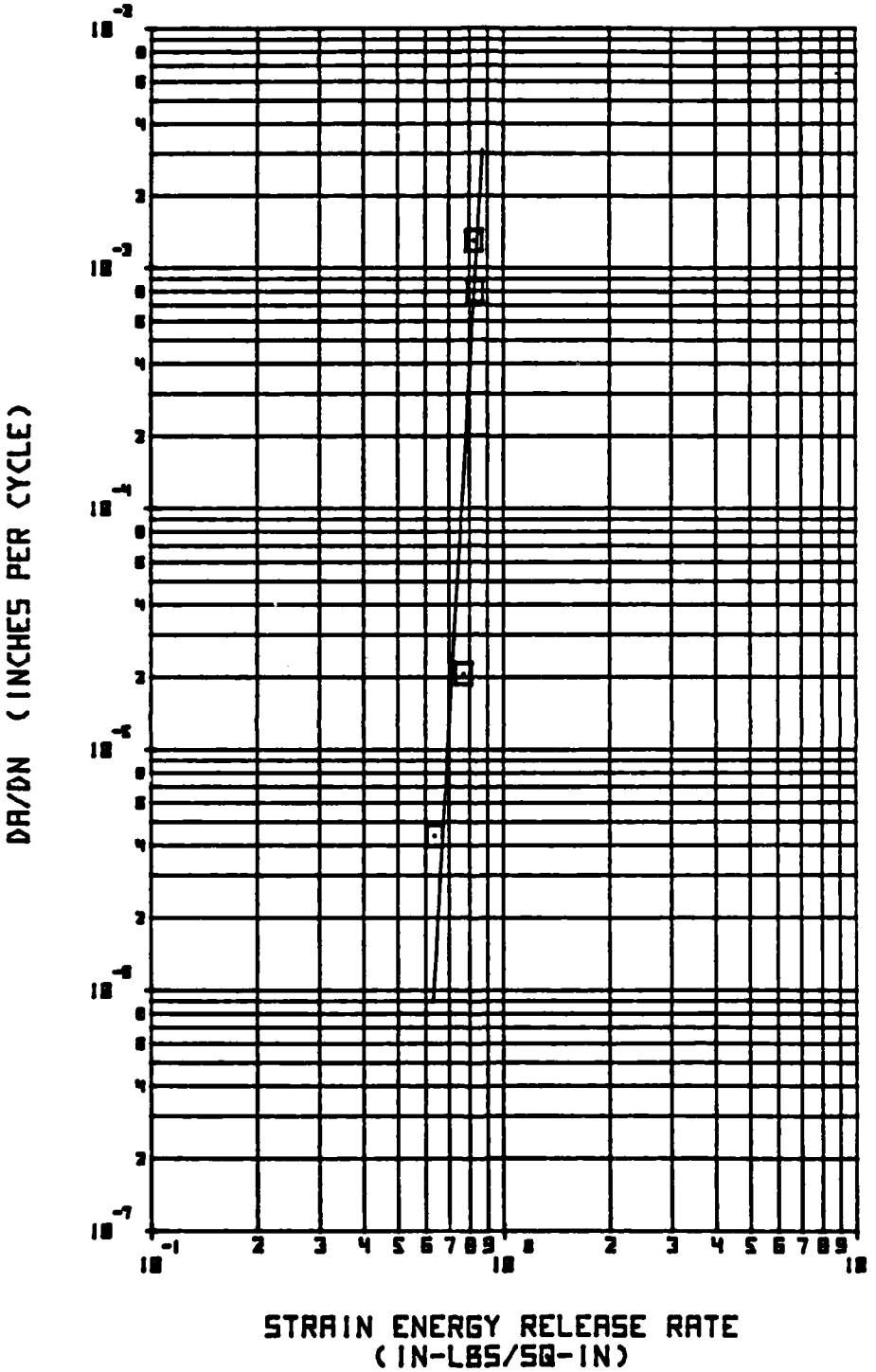

Figure C-8 Test E1EDF of Specimen E1-2-6

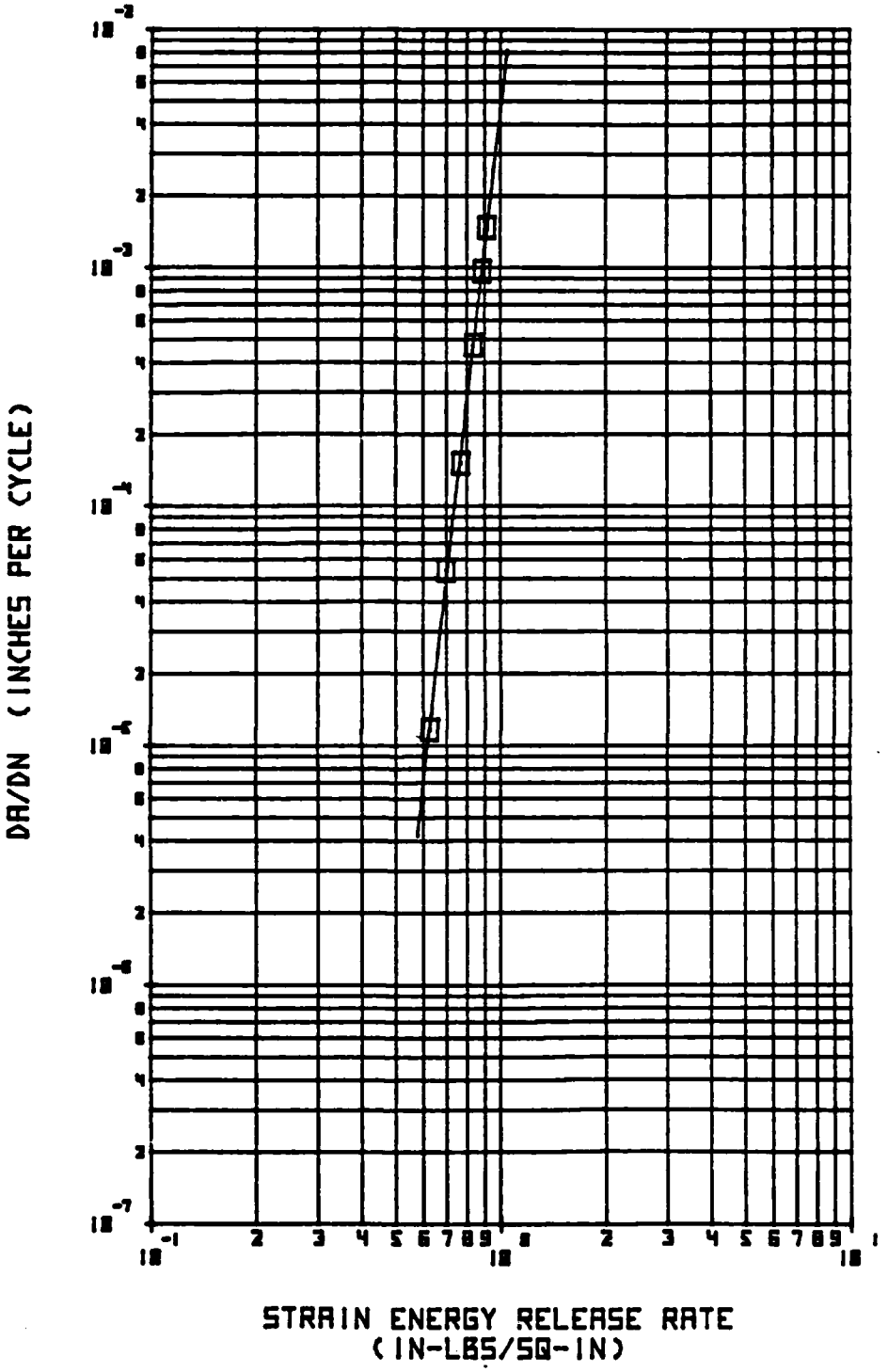

Figure C-9 Test E1PDF of Specimen E1-2-1

C.2 Bismaleimide Mode I Fatigue Data

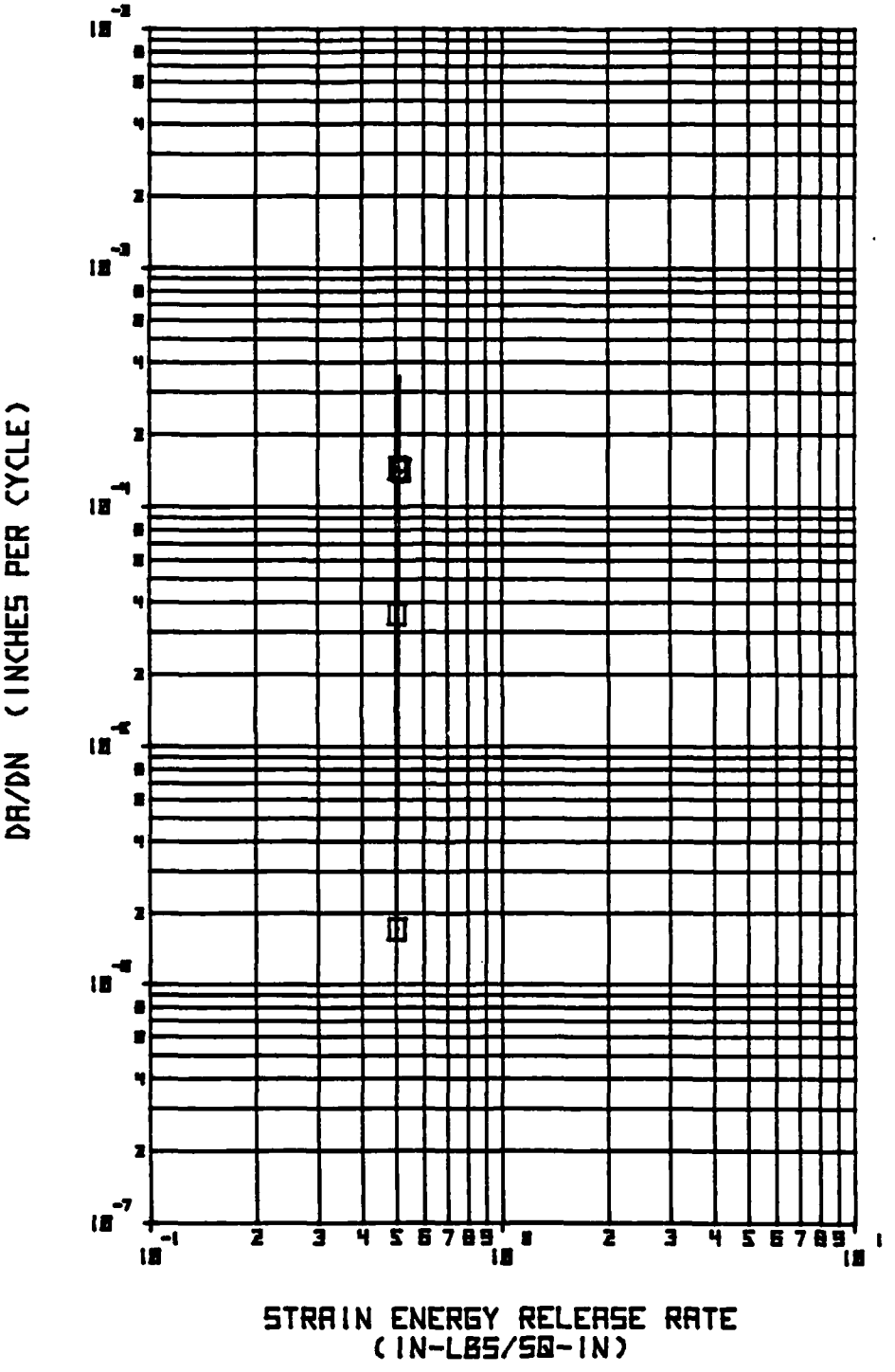

Figure C-10 Test P1CDF of Specimen P1-5-2

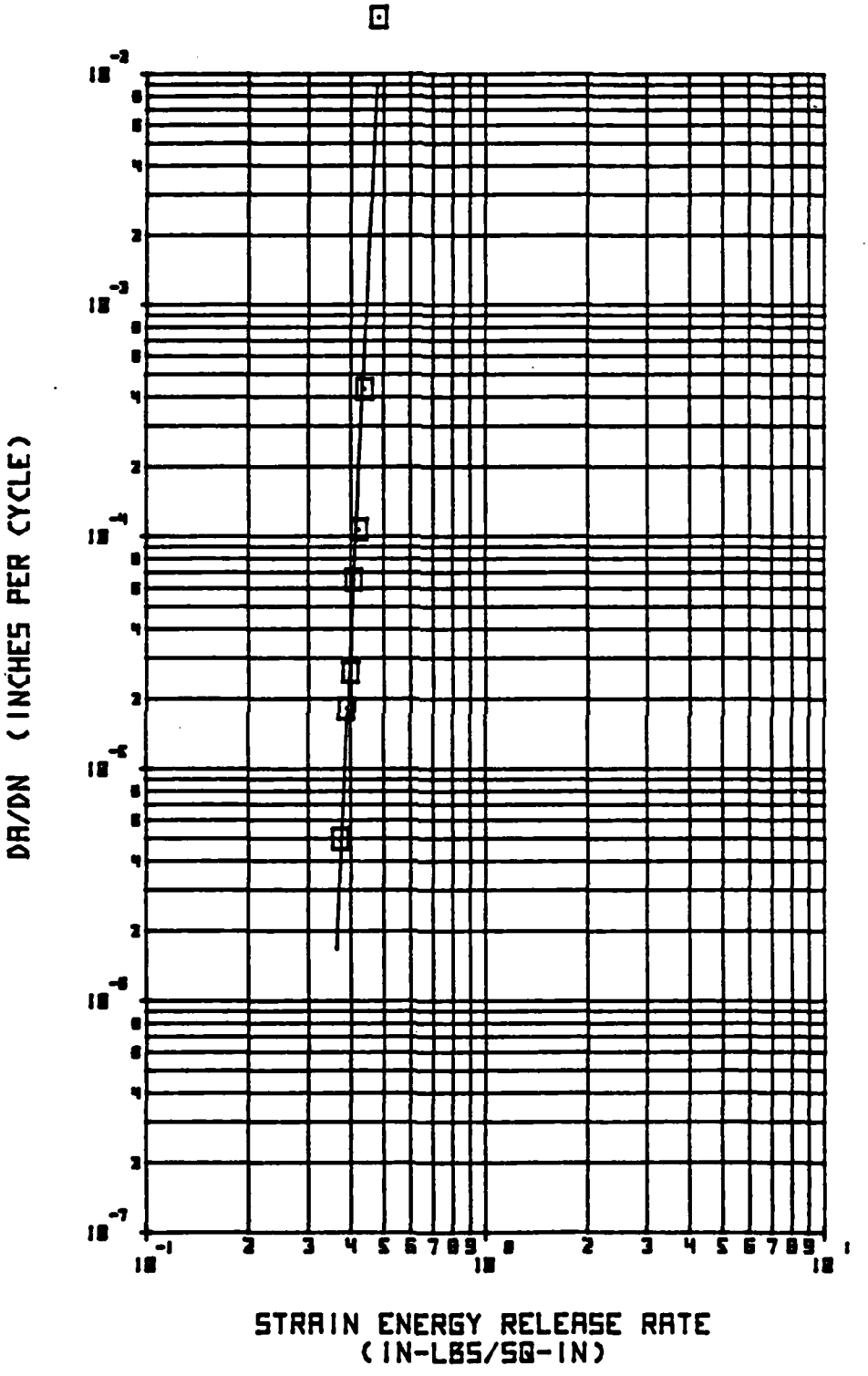

Figure C-11 Test P1CWF of Specimen P1-1-8

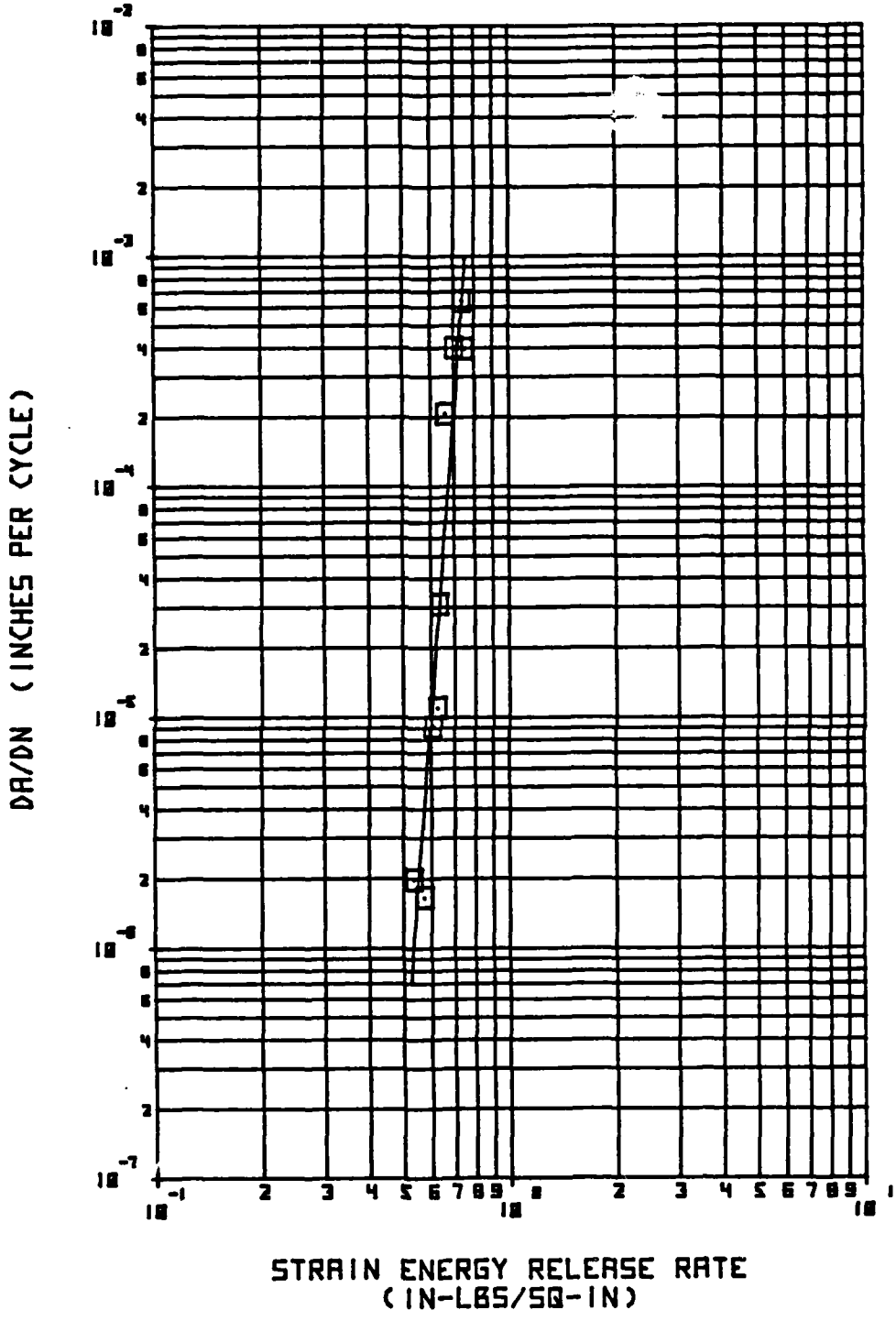

Figure C-12 Test P1RDF of Specimen P1-4-4

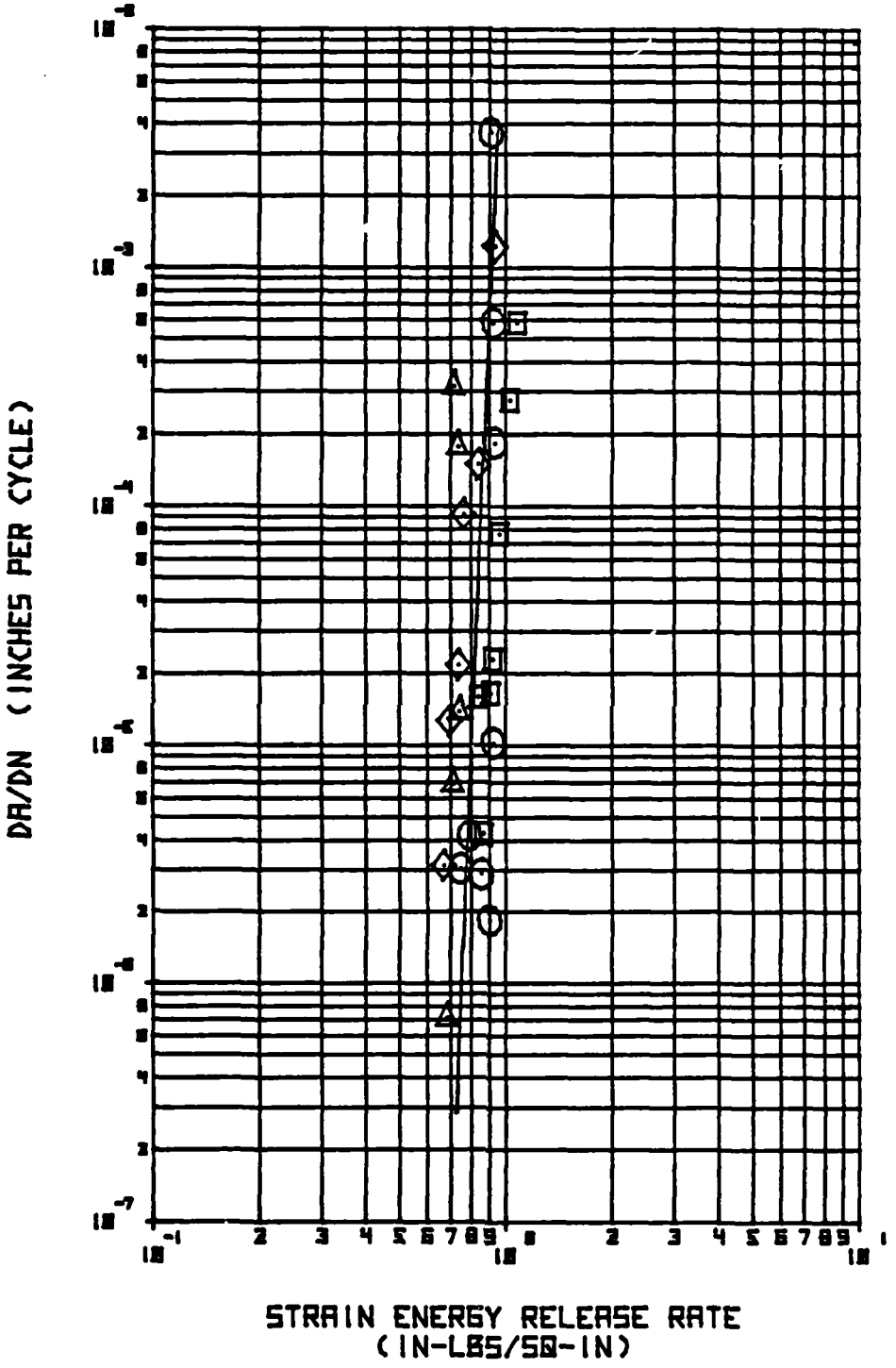

Figure C-13 Test P1RDF of Specimen P1-4-7

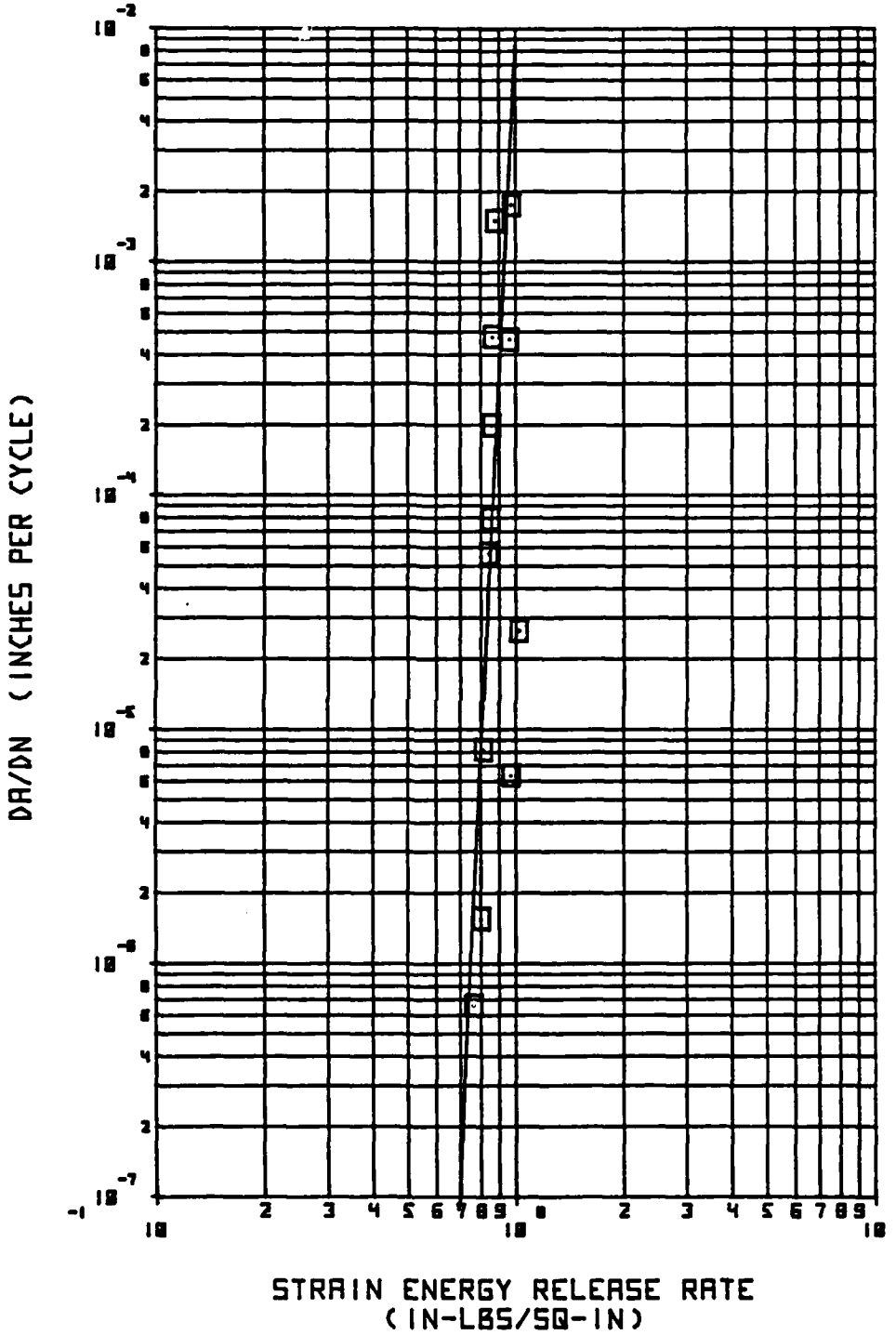

Figure C-14 Test P1RDF of Specimen P1-5-4

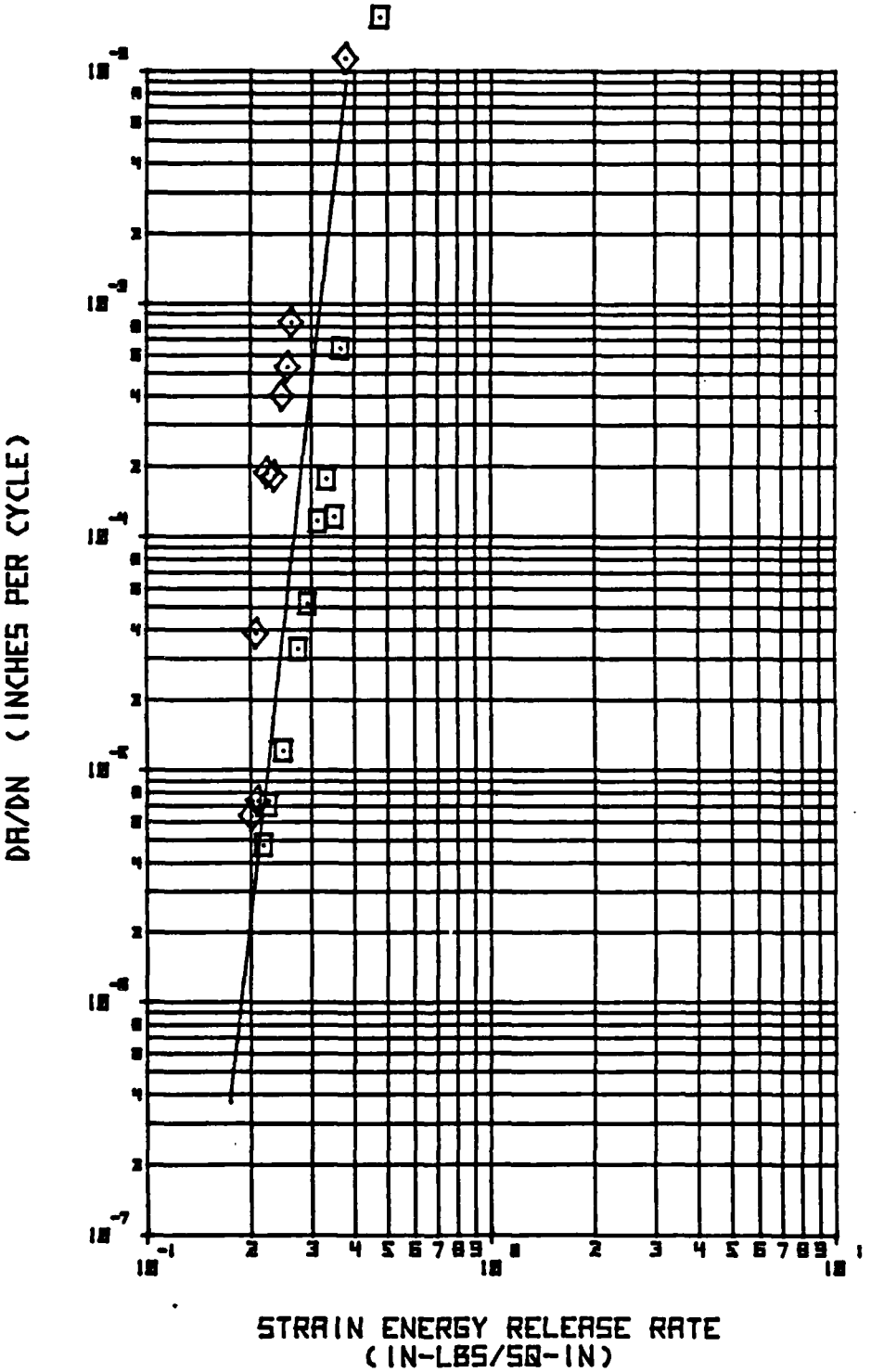

Figure C-15 Test P1RWF of Specimen P1-1-1

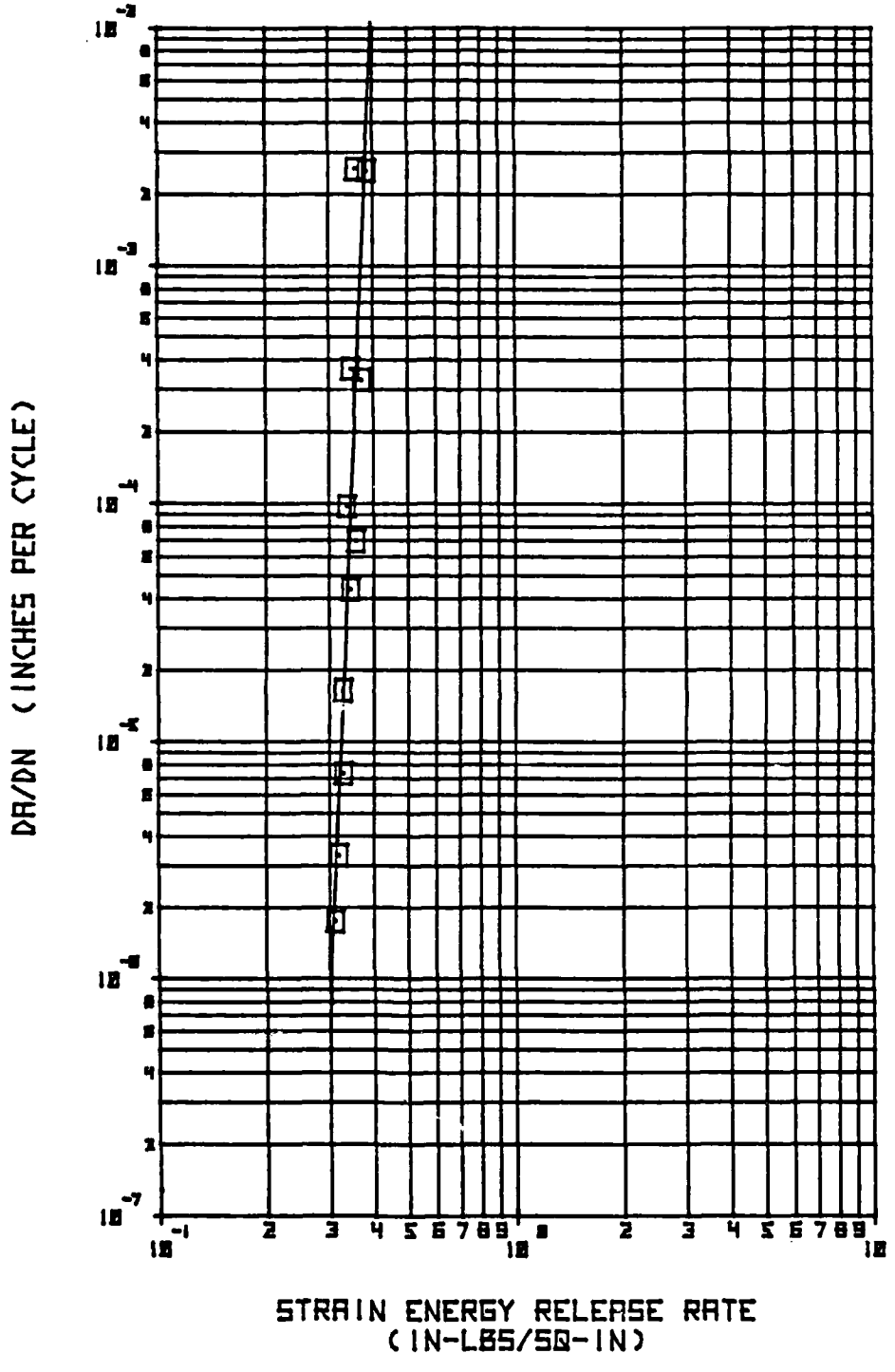

Figure C-16 Test P1RWF of Specimen P1-1-9

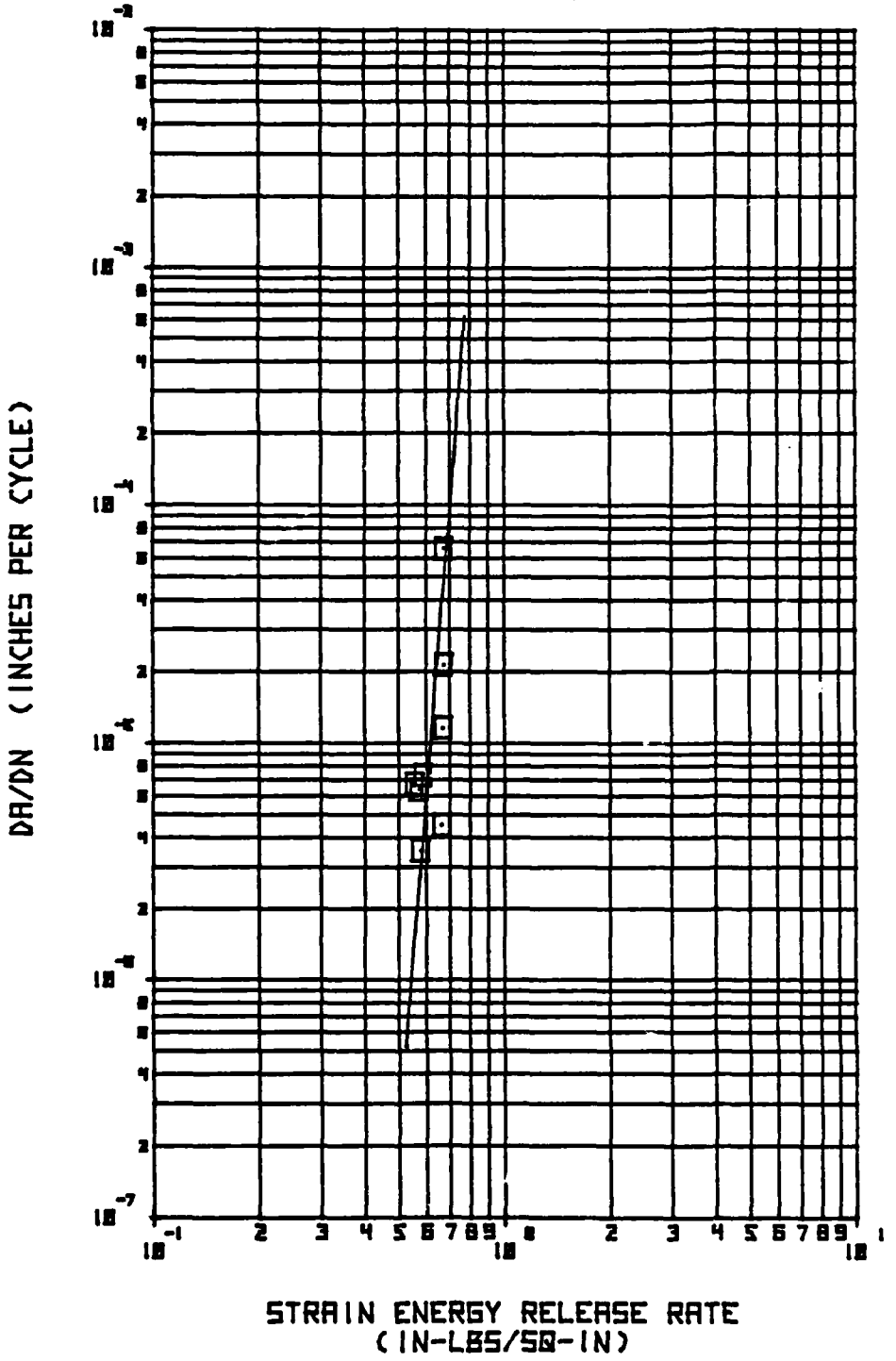

Figure C-17 Test P1EDF of Specimen P1-5-7

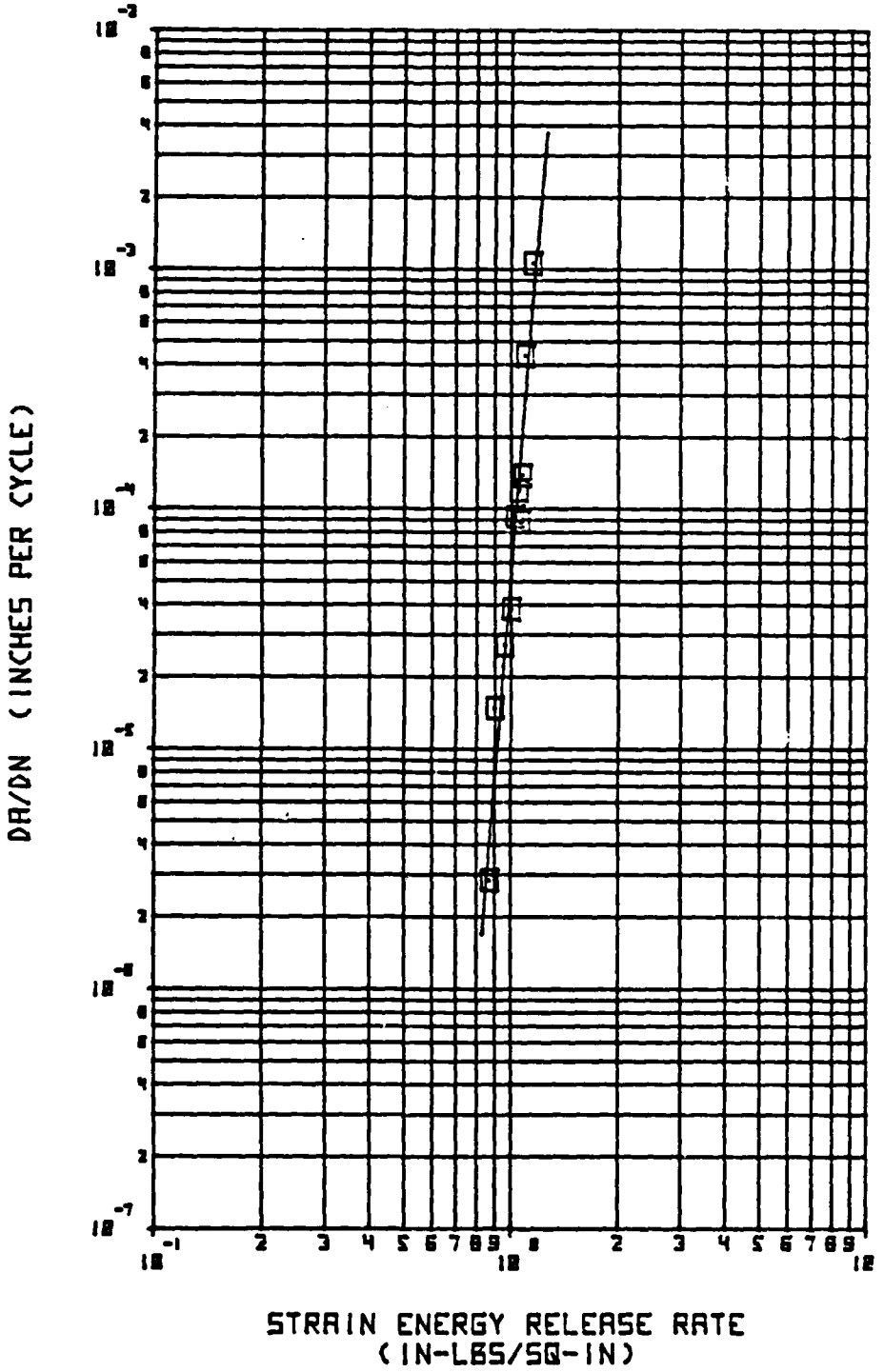

Figure C-18 Test P1PDF of Specimen P1-2-4

APPENDIX D

MODE II STATIC TESTING

The static tests of the Mode II coupon were performed in custom load-controlled fixtures (Figure D-1) commanded by a Varian computer and teletype interface. The specimens were tightly clamped between serrated grips to prevent spurious results due to slippage in the grip areas.

Curves of axial load versus axial displacement were obtained on an x-y plotter as a function of crack length. Load was measured from a load-cell strain-gage bridge; displacement was measured from a Linear Variable Differential Transformer mounted on the ram and crack length was visually measured from adjacent scales and X20 microscopes.

This section contains a sample data reduction for the Mode II static tests including a finite element analysis of the cracked lap shear (CLS) specimen. Also, all of the static test data for both the epoxy and the bismaleimide material systems are included.

D.1 Equations for the Mode II Specimen

Some insight into the analysis of the Mode II CLS specimen is obtained through a strength of materials approach illustrated in Figure D-2. Here, the axial deflection of the coupon is given as:

$$\delta = P(L-d)/wt_1E + Pa/wt_2E, \tag{D1}$$

and the compliance is

$$C = \delta/P = (L-a)/wt_1E + a/wt_2E. \tag{D2}$$

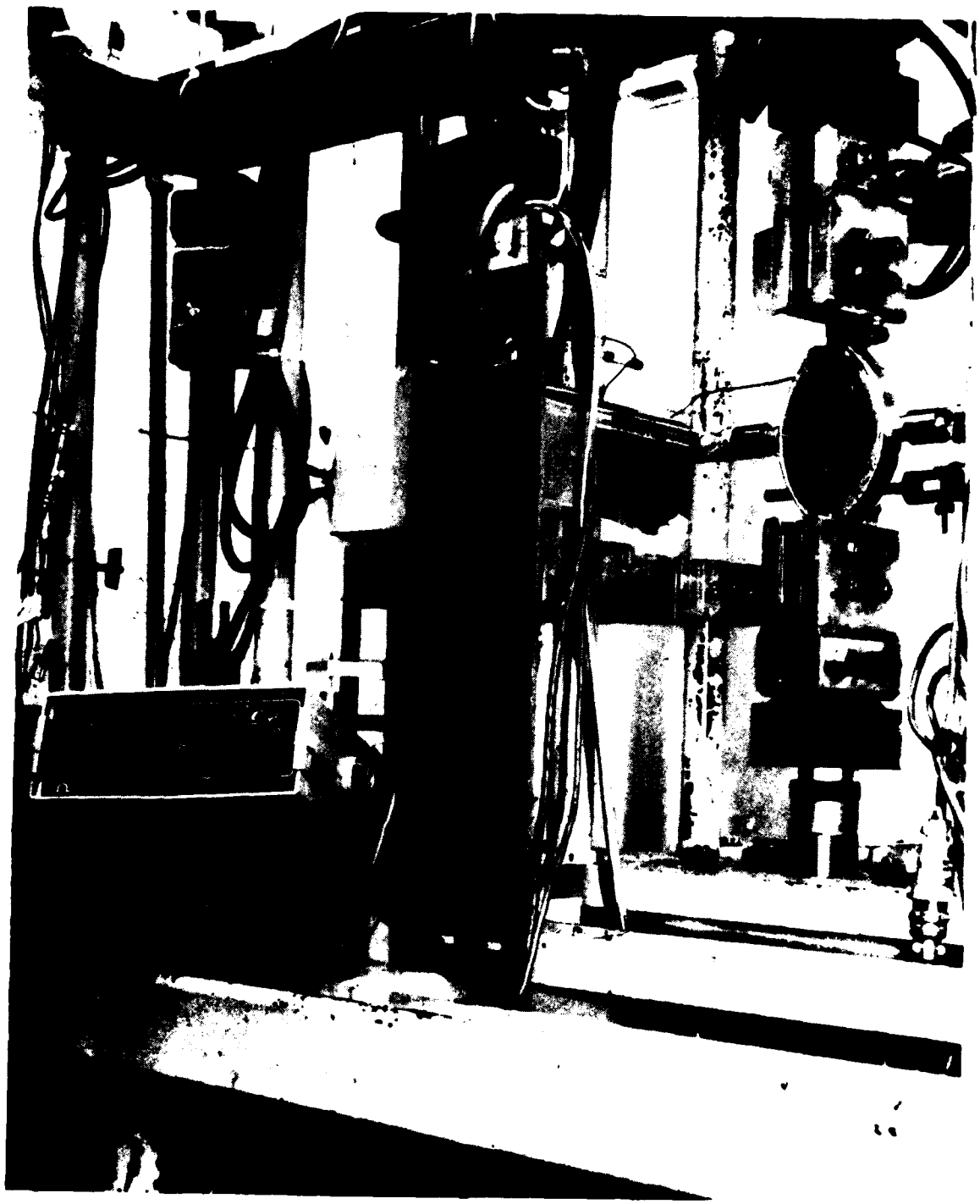

Figure D-1 Custom Load Frame for Mode II Static and Fatigue Fracture Testing

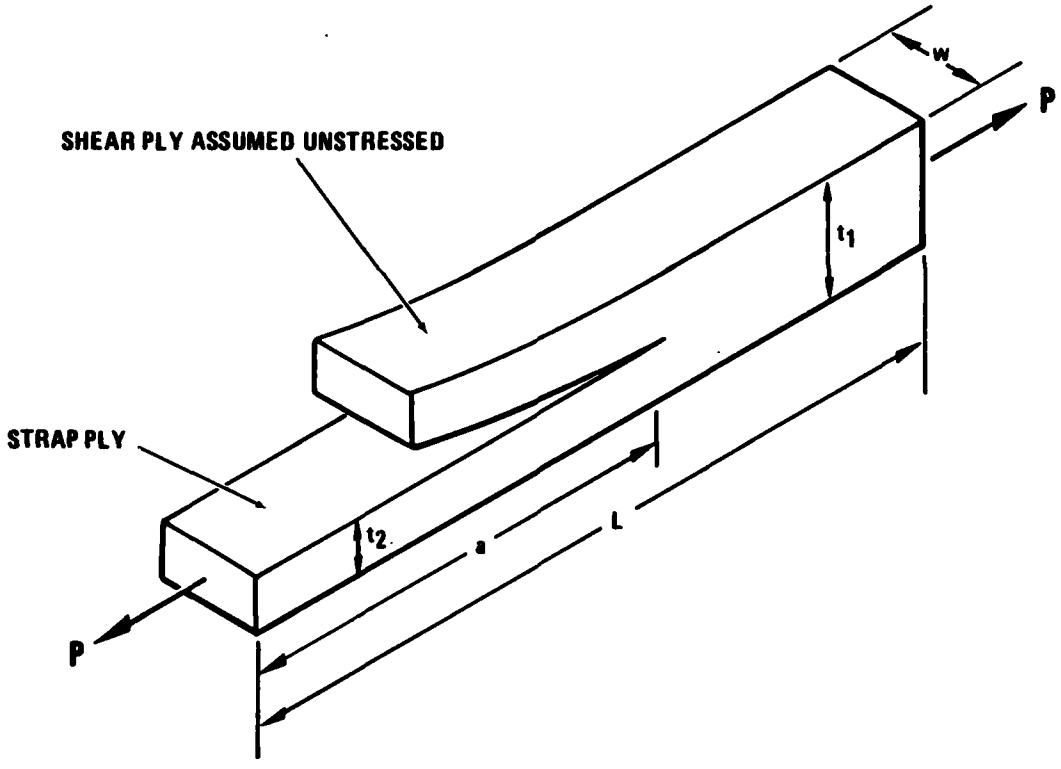

Figure D-2 Strength of Materials Model of CLS Specimen

Algebraic rearranging of Equation D2 yields

$$C = \delta/P = L/wEt_1 + a(t_1 - t_2)/wEt_1t_2. \quad \text{(D3)}$$

Thus, from the strength of materials approach, the compliance is found to be a linear function of crack length.

However, a linear finite element analysis of the CLS specimen proved unsatisfactory because the predicted displacements transverse to the load direction were too large to satisfy the assumptions of small displacement theory. Thus, the finite element analysis was repeated allowing for geometric non-linearity. This analysis was performed using the 3-D, 8-node brick element "CHEXA" and the "DMAP4" solver of the NASTRAN program. A typical mesh for this analysis is shown in Figure D-3.

The finite element analysis was performed for five crack lengths of a = 2, 3, 4, 5 and 6 inches. A linear regression analysis fitting the calculated compliance-crack length relation at a load of P = 1300 lbs. yielded

$$C = (1.125 \times 10^{-5})a + 1.484 \times 10^{-6} \text{ in/lb}, \quad \text{(D4)}$$

with a correlation coefficient of $r^2 = 0.9999$. Thus, the compliance may be taken as a linear function of the crack length.

The finite element analysis also has the capacity to determine the Mode I and Mode II components of the strain-energy release rate by using the modified crack closure method (Reference 5). Referring to Figure D-4, a single solution gives the crack tip force vector $\mathbf{F}_A$ at node A (equivalent to those at A') due to elements 1 and 2, and the

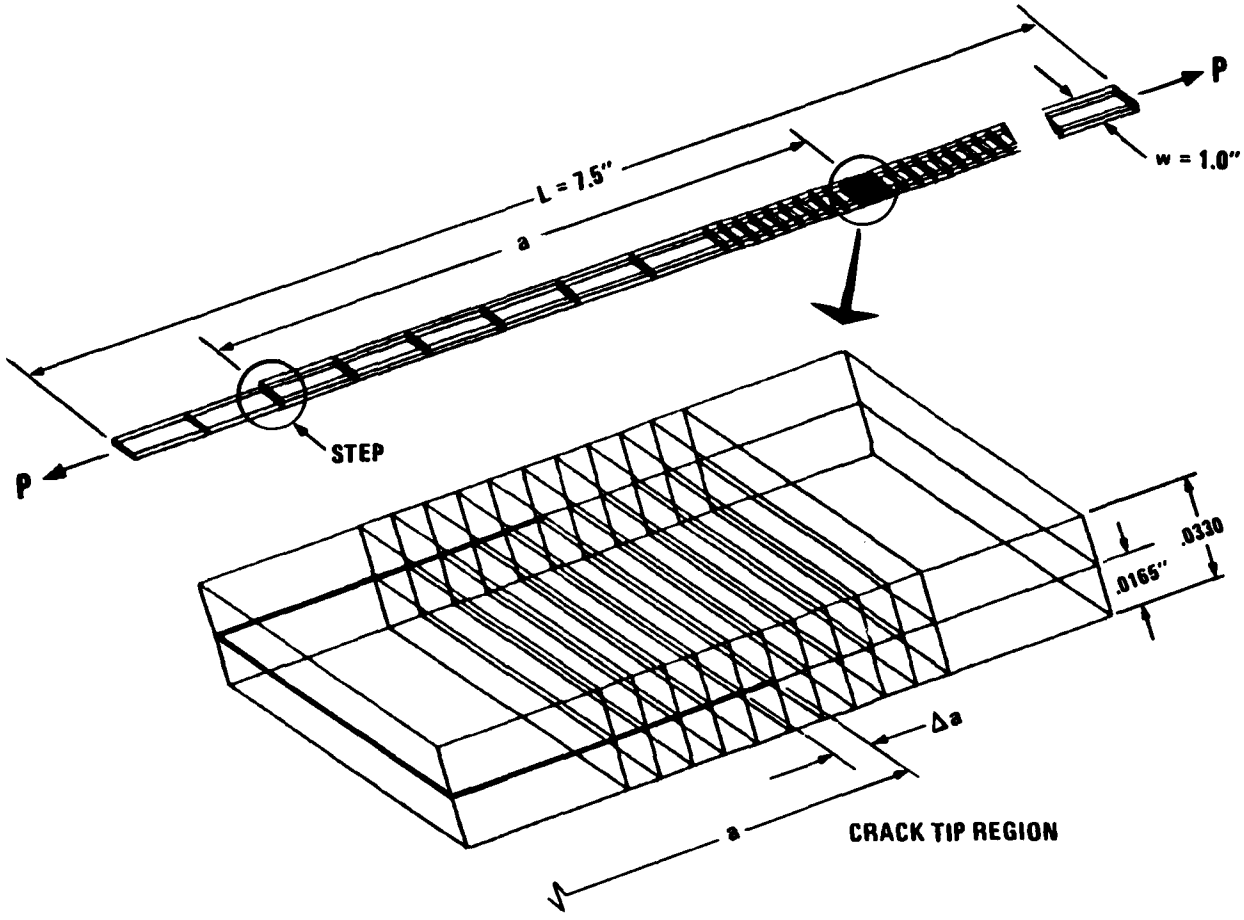

Figure D-3 Finite Element Model of CLS Specimen

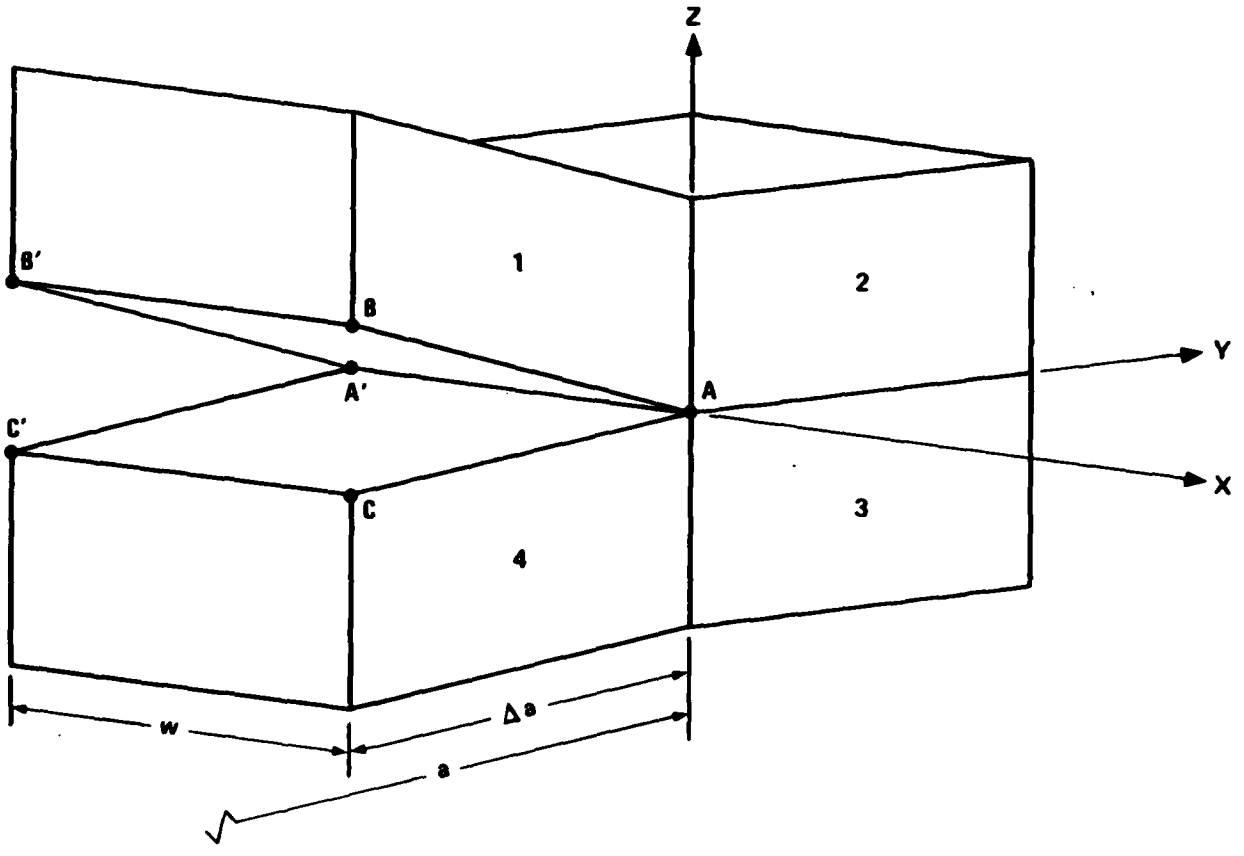

Figure D-4 Finite Element Mesh in Crack Tip Region Illustrating Modified Crack Closure Technique

deflection vectors of nodes B and C (equivalent to nodes B' and C'), denoted D_B and D_C. The components of the energy release rate for the crack of length a are then given as

$$G_I = F_{AZ} (D_{BZ} - D_{CZ})/2 \ \Delta aw \tag{D5}$$

and

$$G_{II} = F_{AY} (D_{BY} - D_{CY})/2 \ \Delta aw \tag{D6}$$

where the subscripts Y and Z indicate the components of the forces and displacements in the Y and Z directions.

The results of the analysis for crack lengths of a = 2, 3, 4, 5 and 6 inches indicate that $G_I = 0.2798$ in-lb./in^2 and $G_{II} = 0.9212$ in-lb./in^2, and they are constants over the range of the analysis, as shown in Figure D-5. These calculations indicate that the energy release rate consists of 76.5% Mode II and 23.5% Mode I for the current CLS specimen. Since the energy release rate is independent of the crack length, the critical load to cause crack growth is also independent of the crack length.

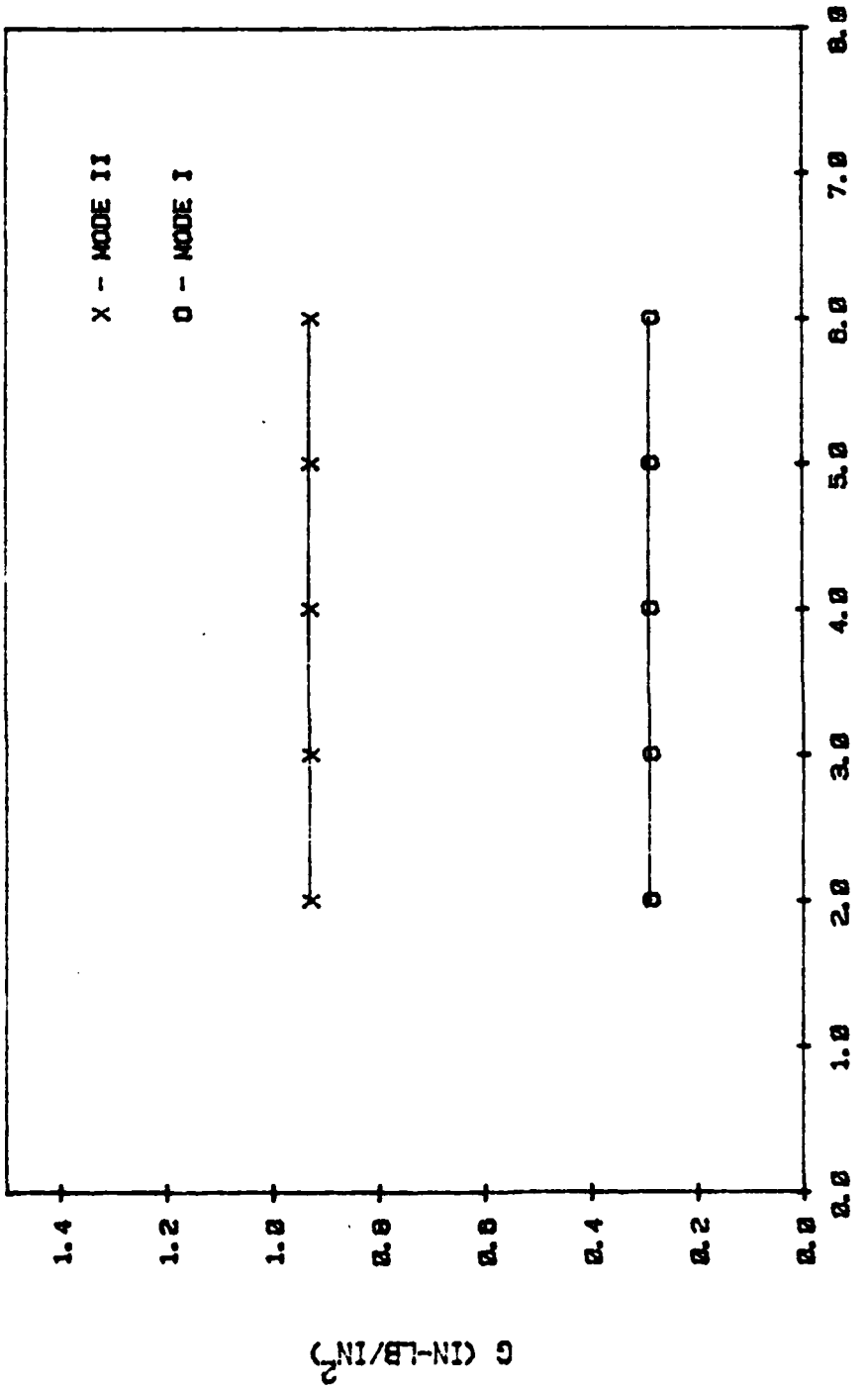

Figure D-5 Plot of Strain Energy Release Rate Versus Crack Length for CLS Specimen

D.2 Sample Data Reduction

A typical set of axial load - deflection curves for the CLS specimen are shown in Figure D-6. The coupons were loaded slowly until crack growth was visually observed (using a 20X optical lens), and then unloaded. The crack length on each edge of the coupon was then visually observed and the average was recorded along with the critical load, P_c. This process was repeated until the crack propagated beyond six inches.

The test data were then transferred to an HP9830 desktop computer. There the compliance for each crack length was calculated as

$$C = \delta/P_c - C_{sys} \tag{D7}$$

where C_{sys} is the compliance of the test frame and load cell. The compliance versus crack length data were then fitted by a least squares regression to a linear function, and the value of the critical energy release rate, G_c, was determined by

$$G_c = (P_c^2/2w)(dC/da) \tag{D8}$$

Finally, these data were plotted as illustrated by Figure D-7.

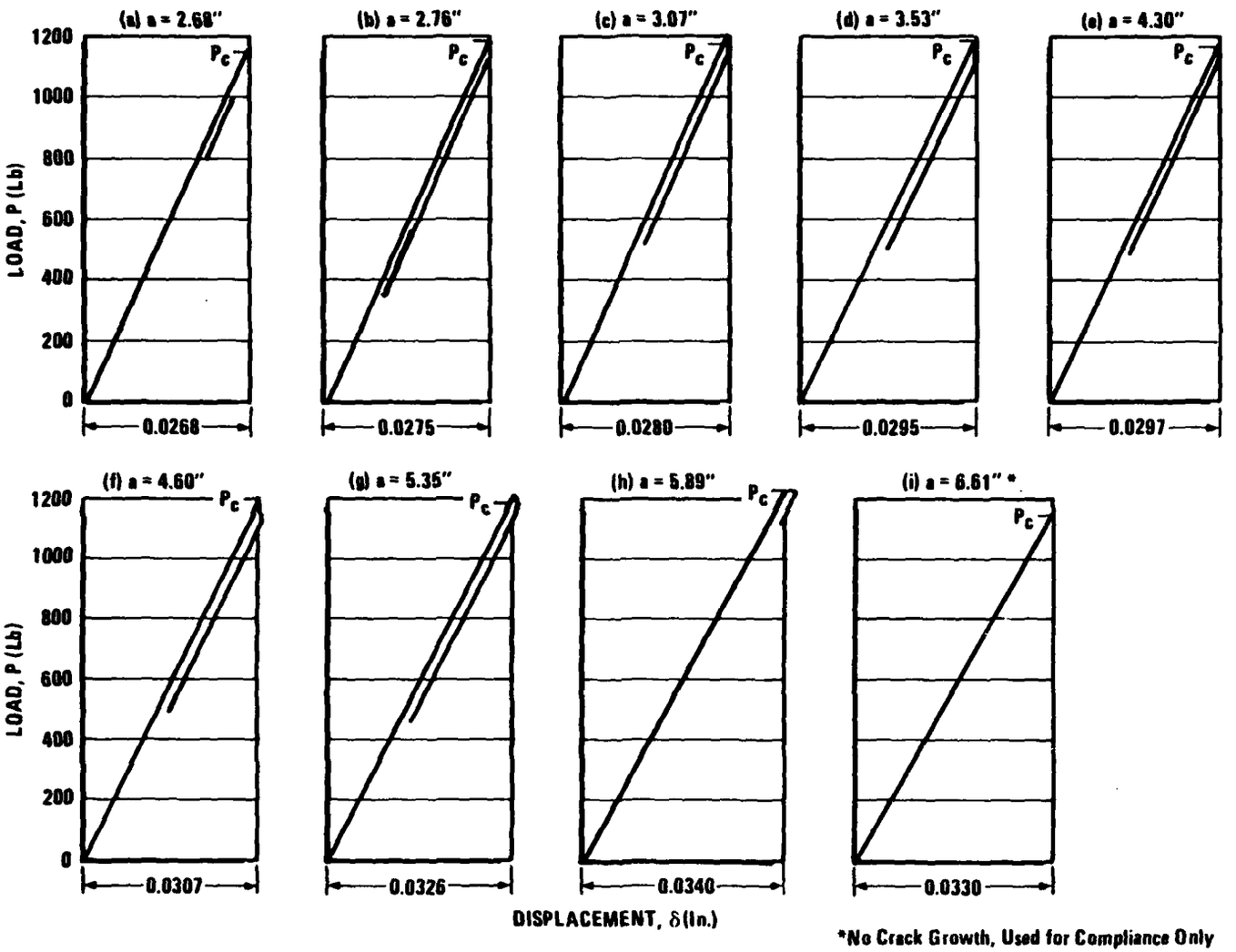

Figure D-6 Sample Load-Deflection Curves for a Mode II Static Test

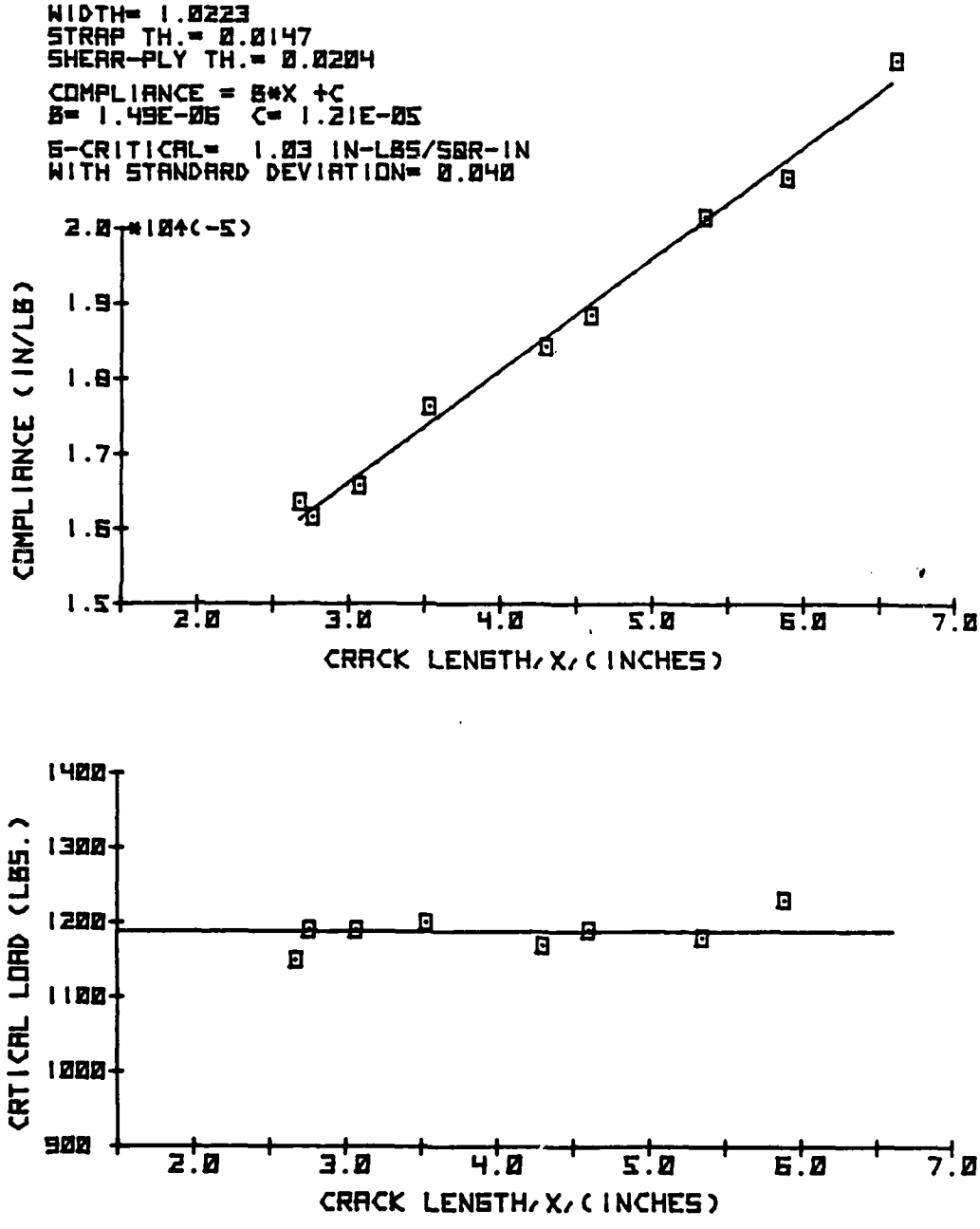

Figure D-7 Sample Computer Plots for Mode II Static Delamination Test

D.3 Epoxy Mode II Static Data

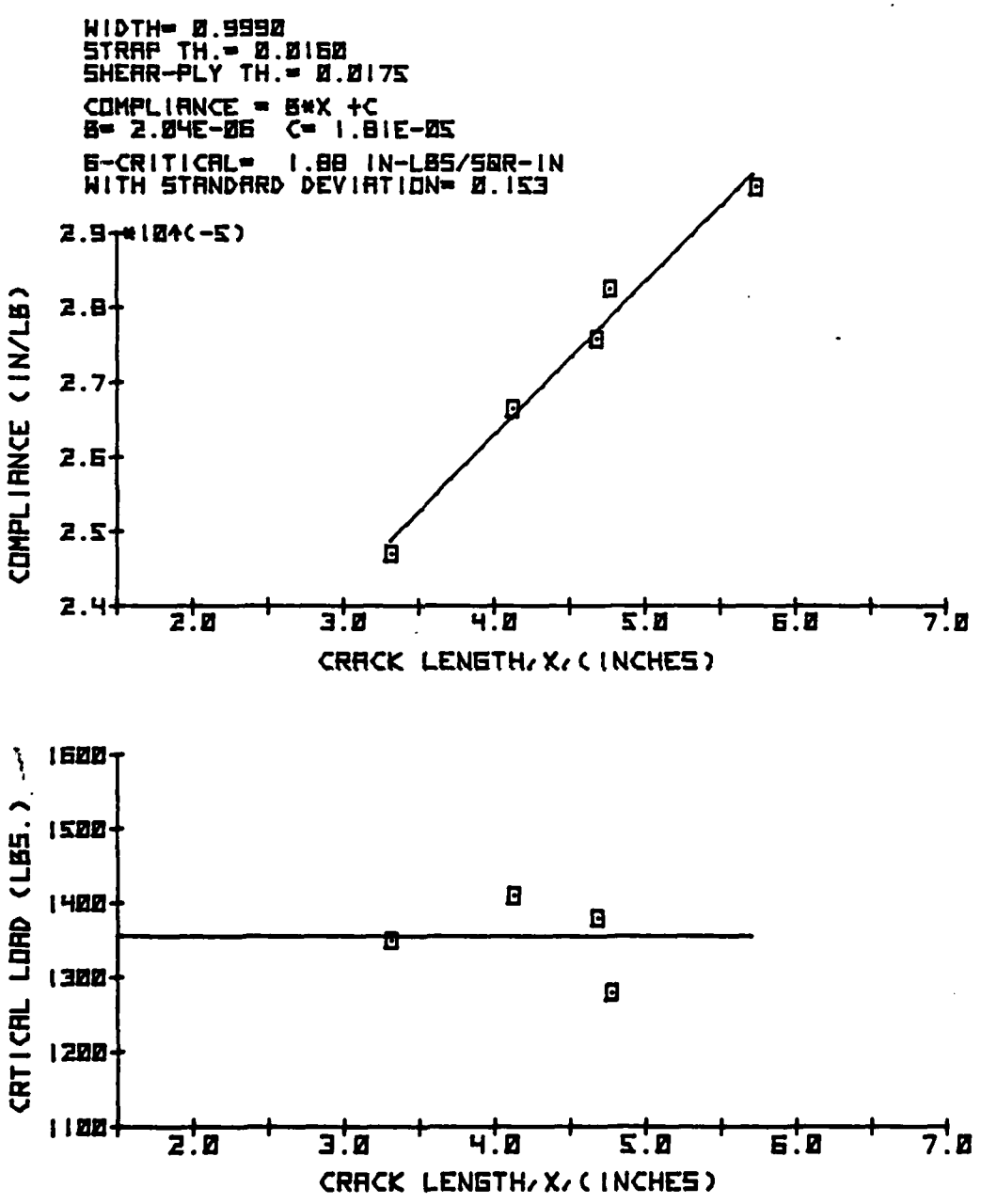

Figure D-8 Test E2CDS of Specimen E2-3-5

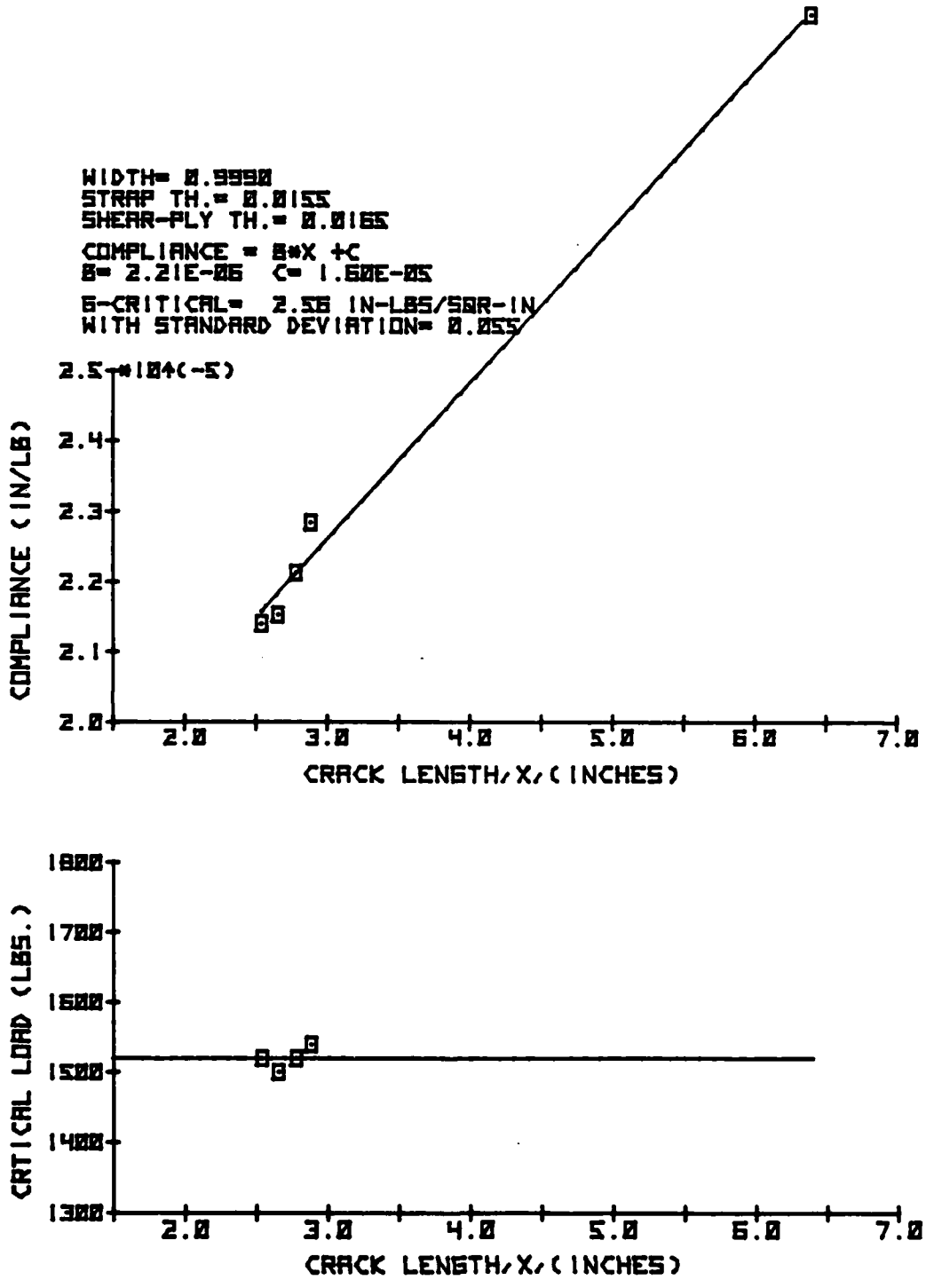

Figure D-9 Test E2CDS of Specimen E2-4-7

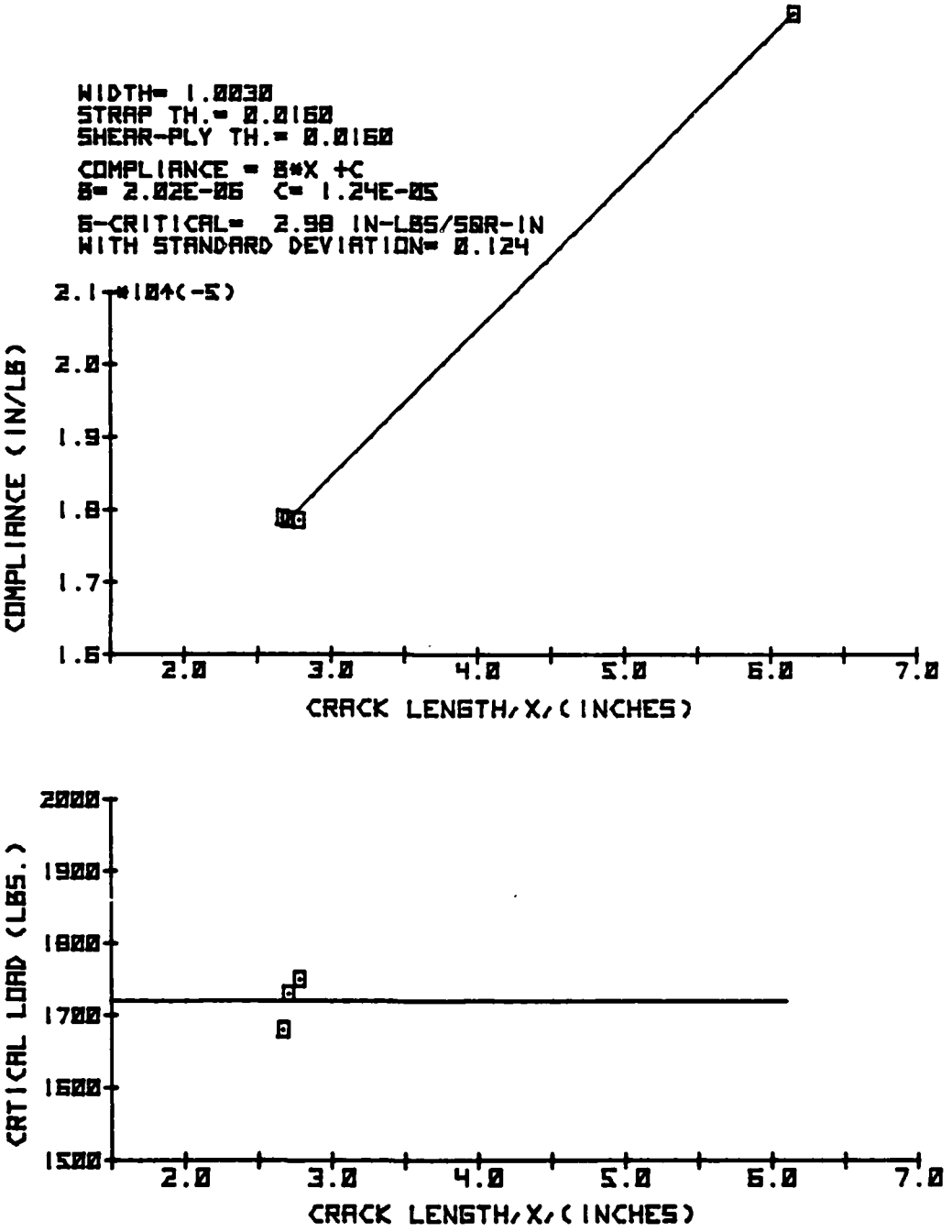

Figure D-10 Test E2CWS of Specimen E2-1-8

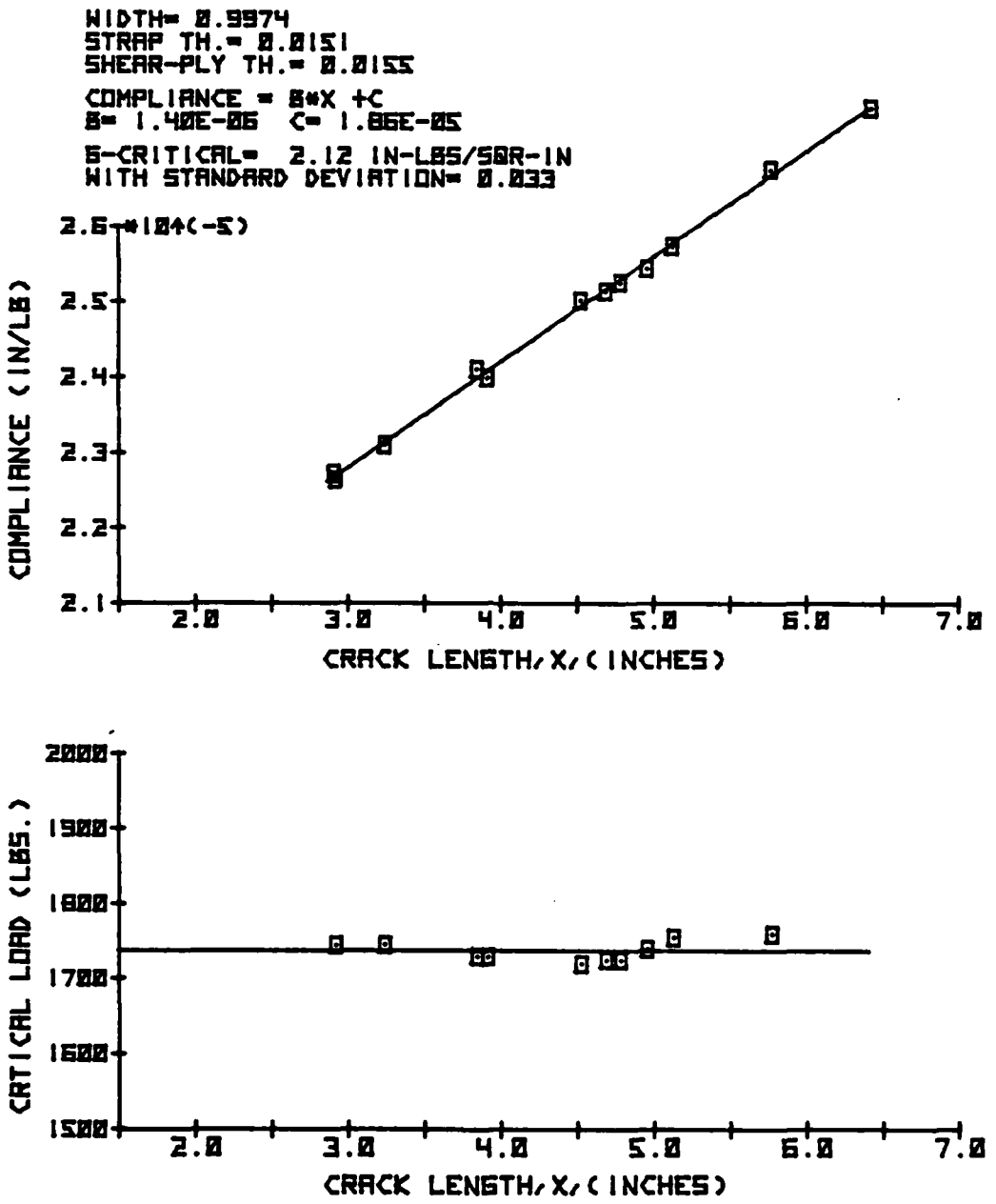

Figure D-11 Test E2RDS of Specimen E2-2-5

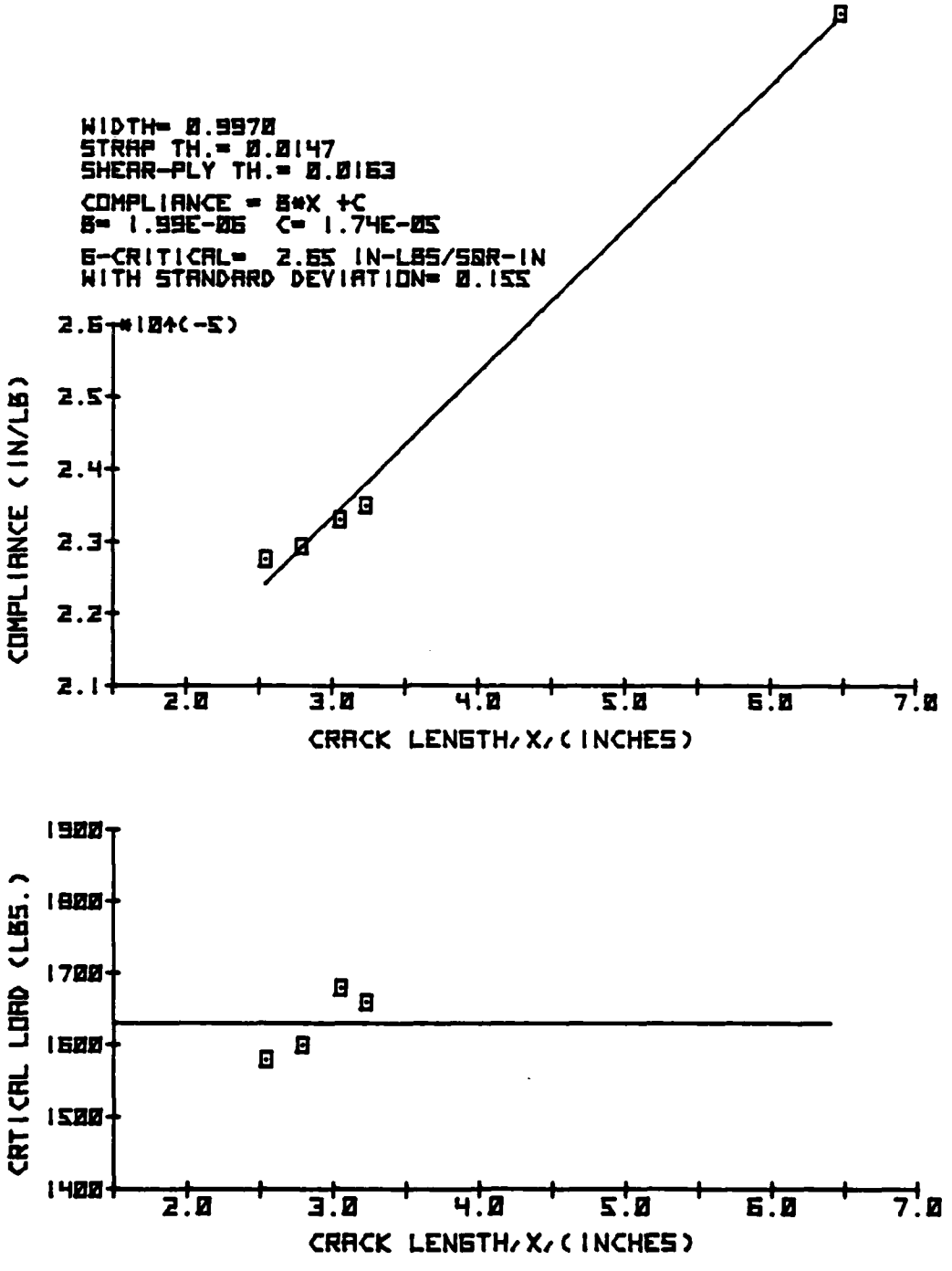

Figure D-12 Test E2RDS of Specimen E2-2-6

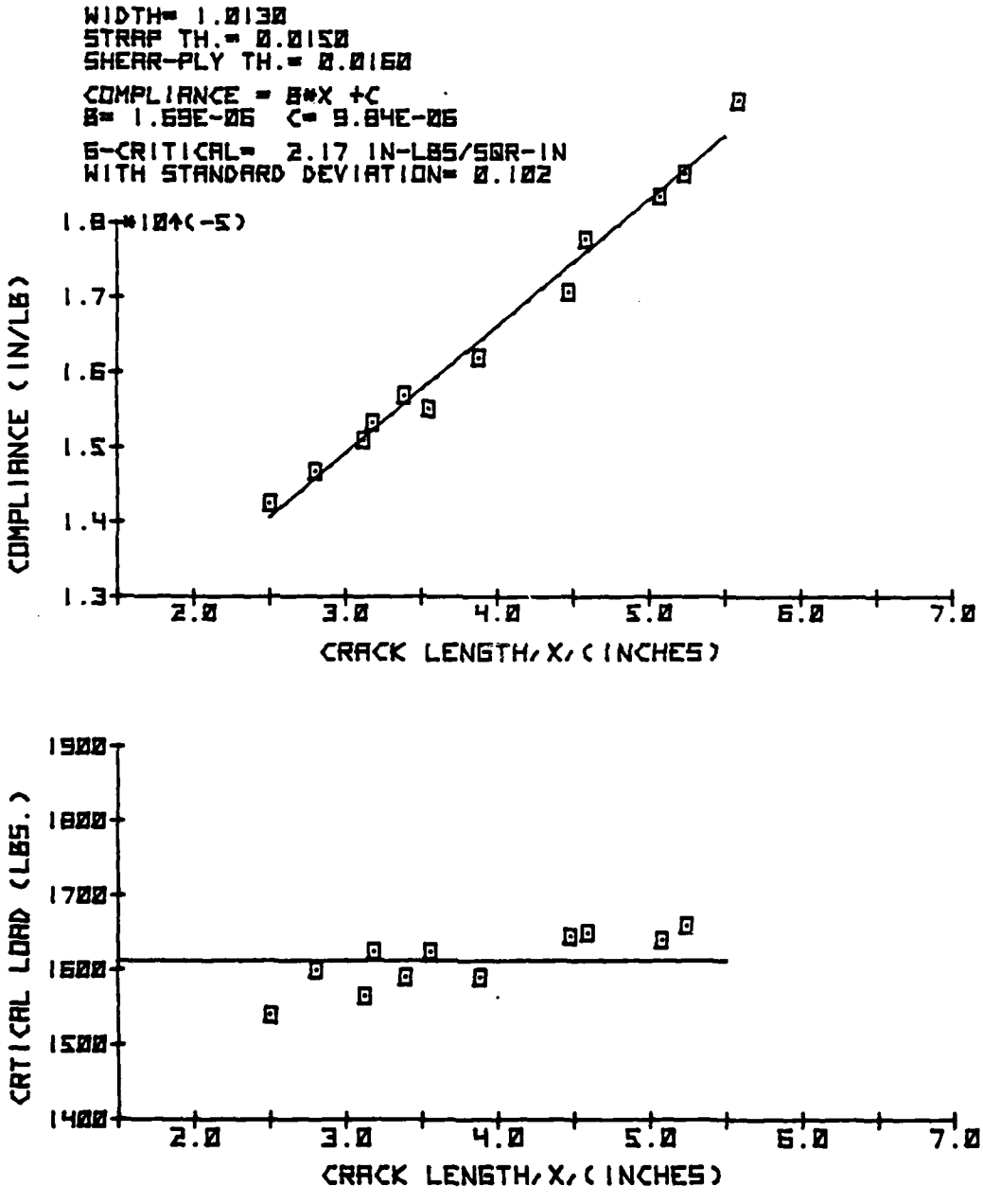

Figure D-13 Test E2RWS of Specimen E2-1-1

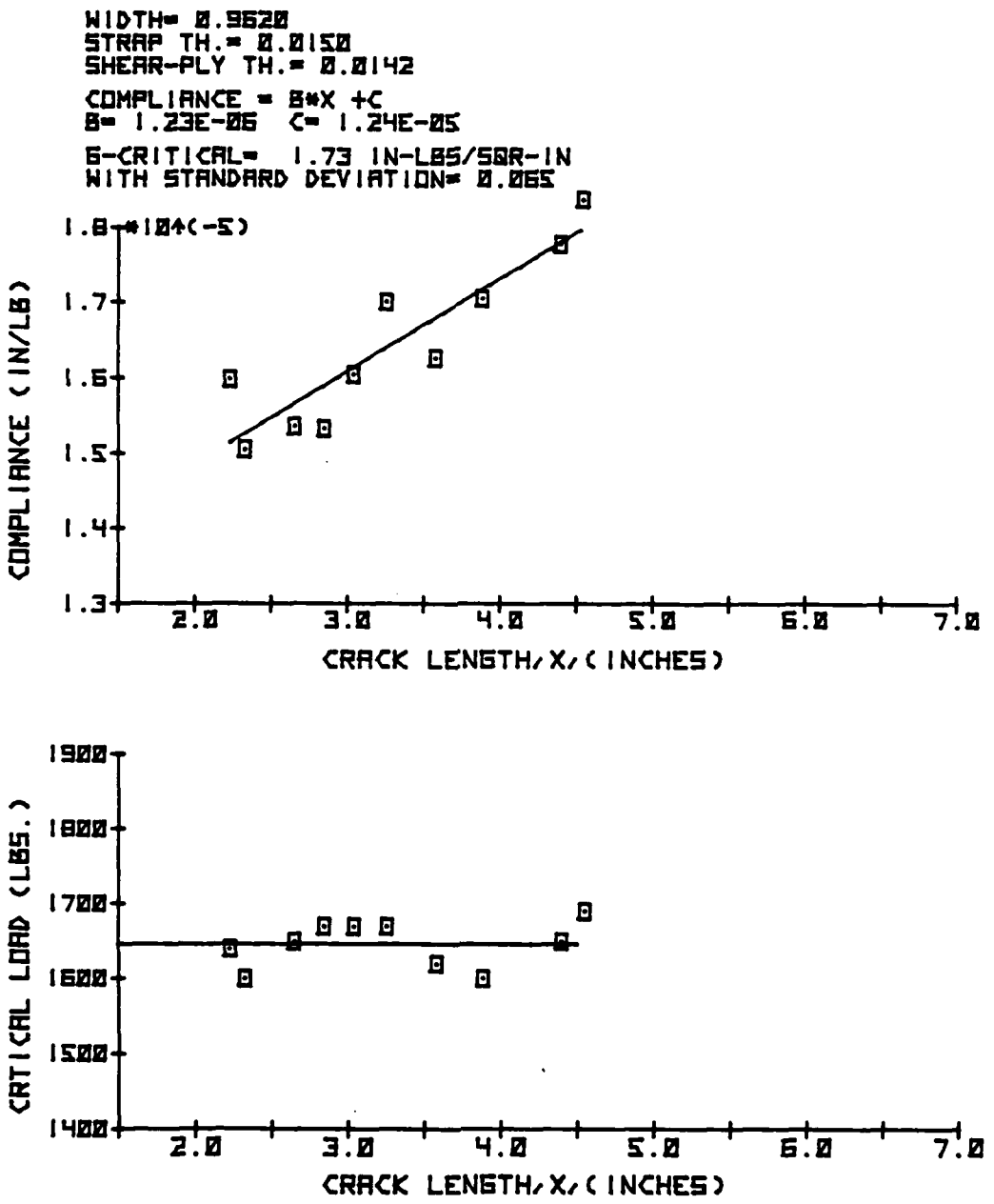

Figure D-14 Test E2EDS of Specimen E2-5-10

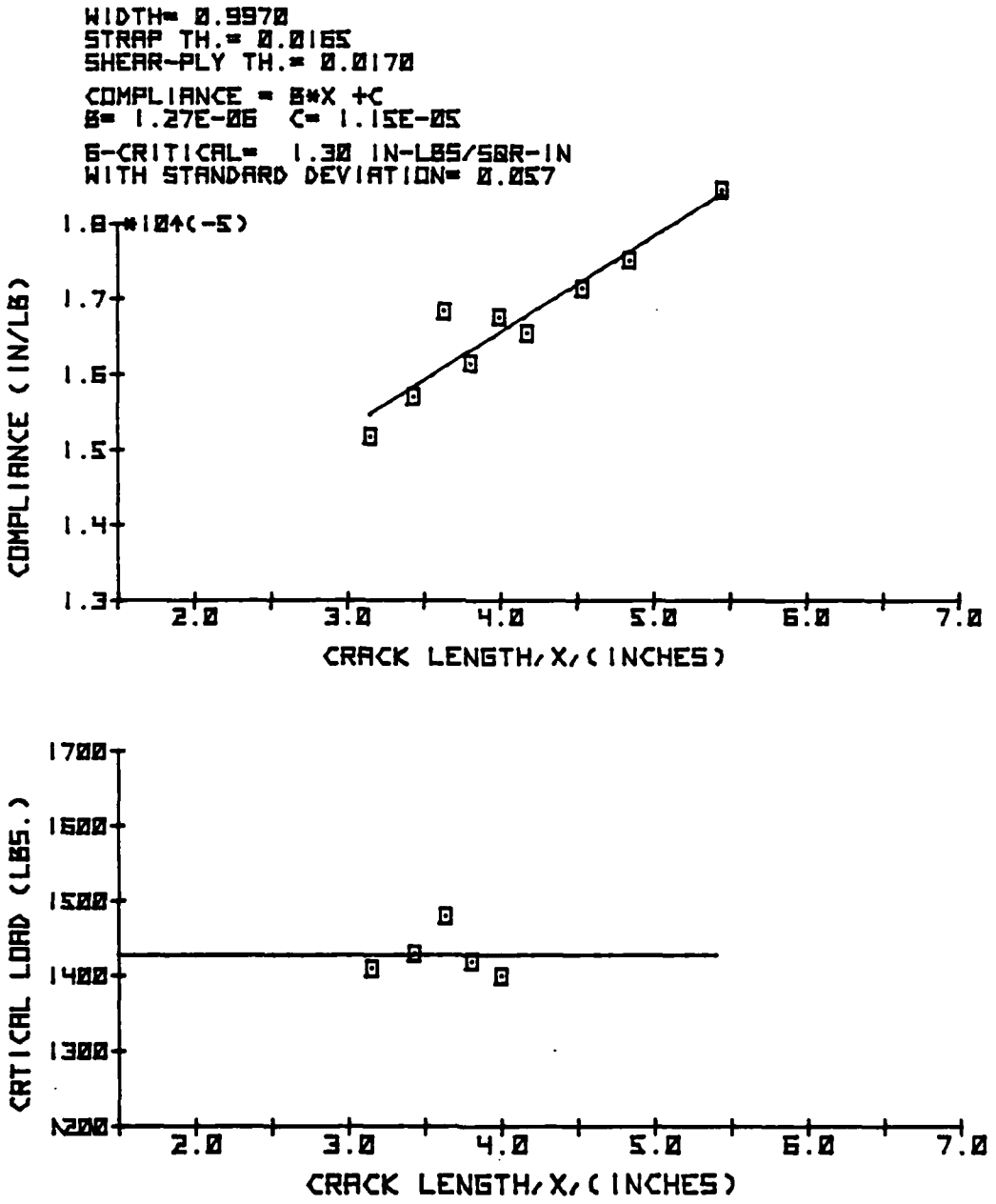

Figure D-15 Test E2PDS of Specimen E2-4-9

D.4 Bismaleimide Mode II Static Data

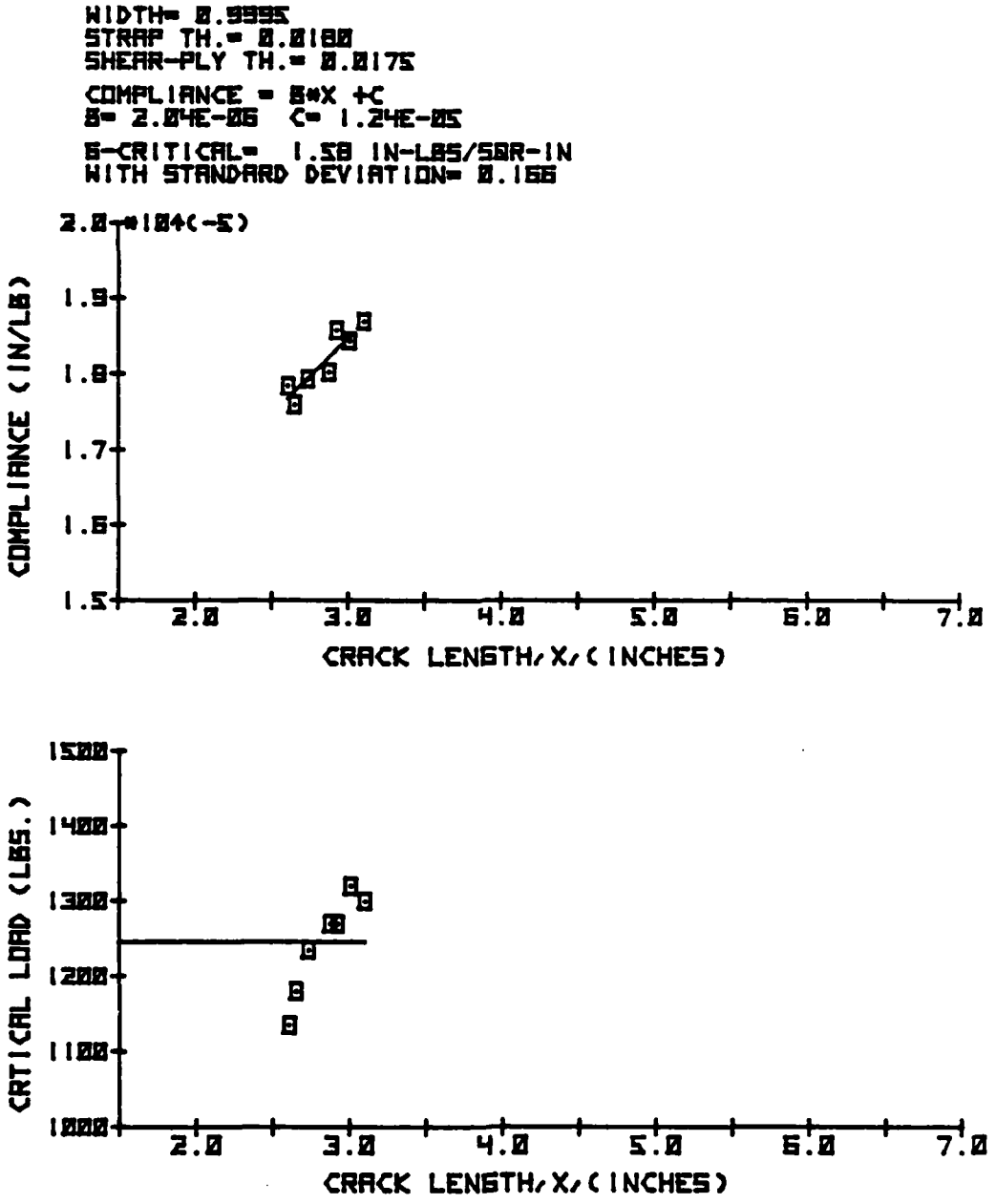

Figure D-16 Test P2CDS of Specimen P2-1-6

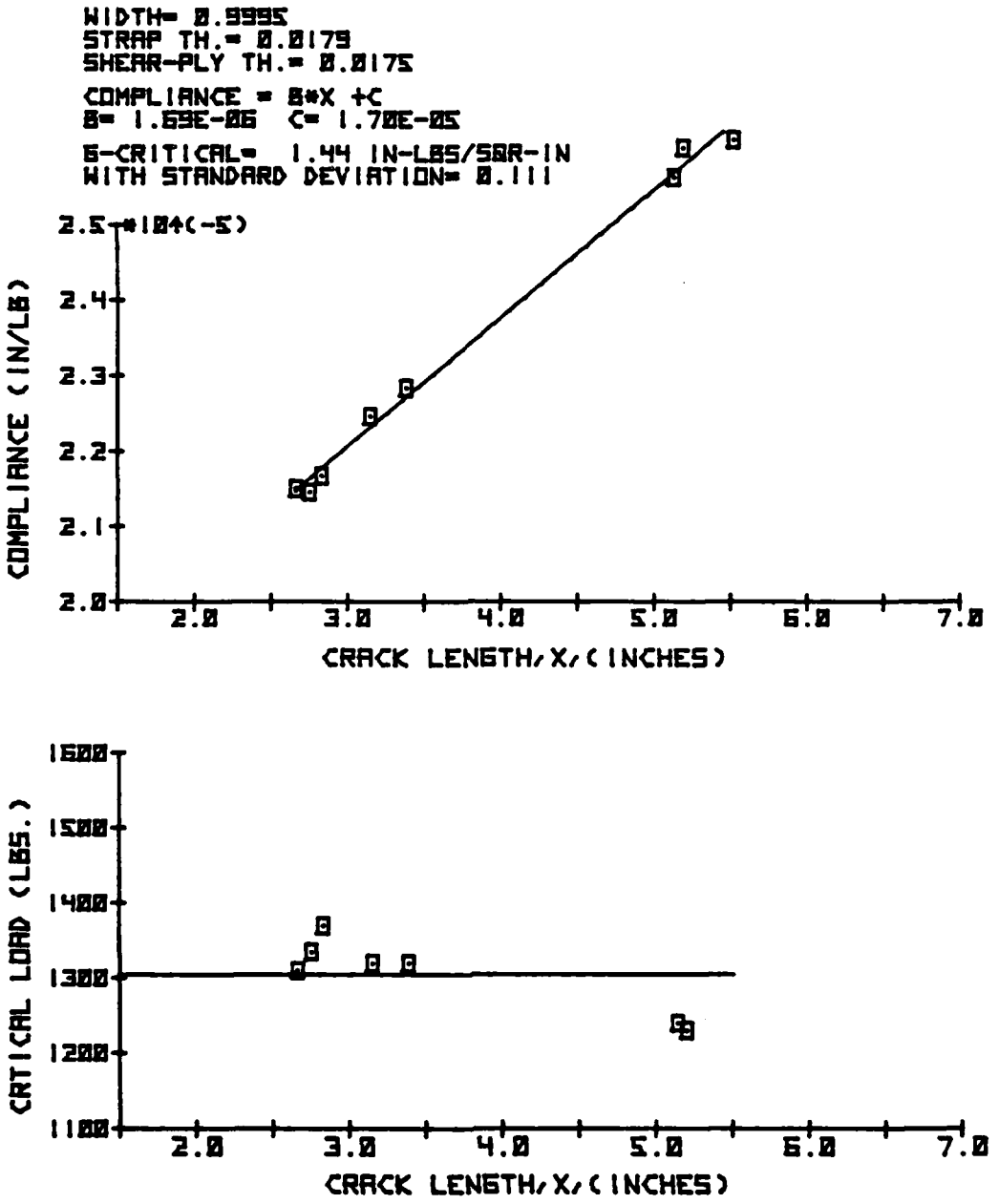

Figure D-17 Test P2CDS of Specimen P2-1-8

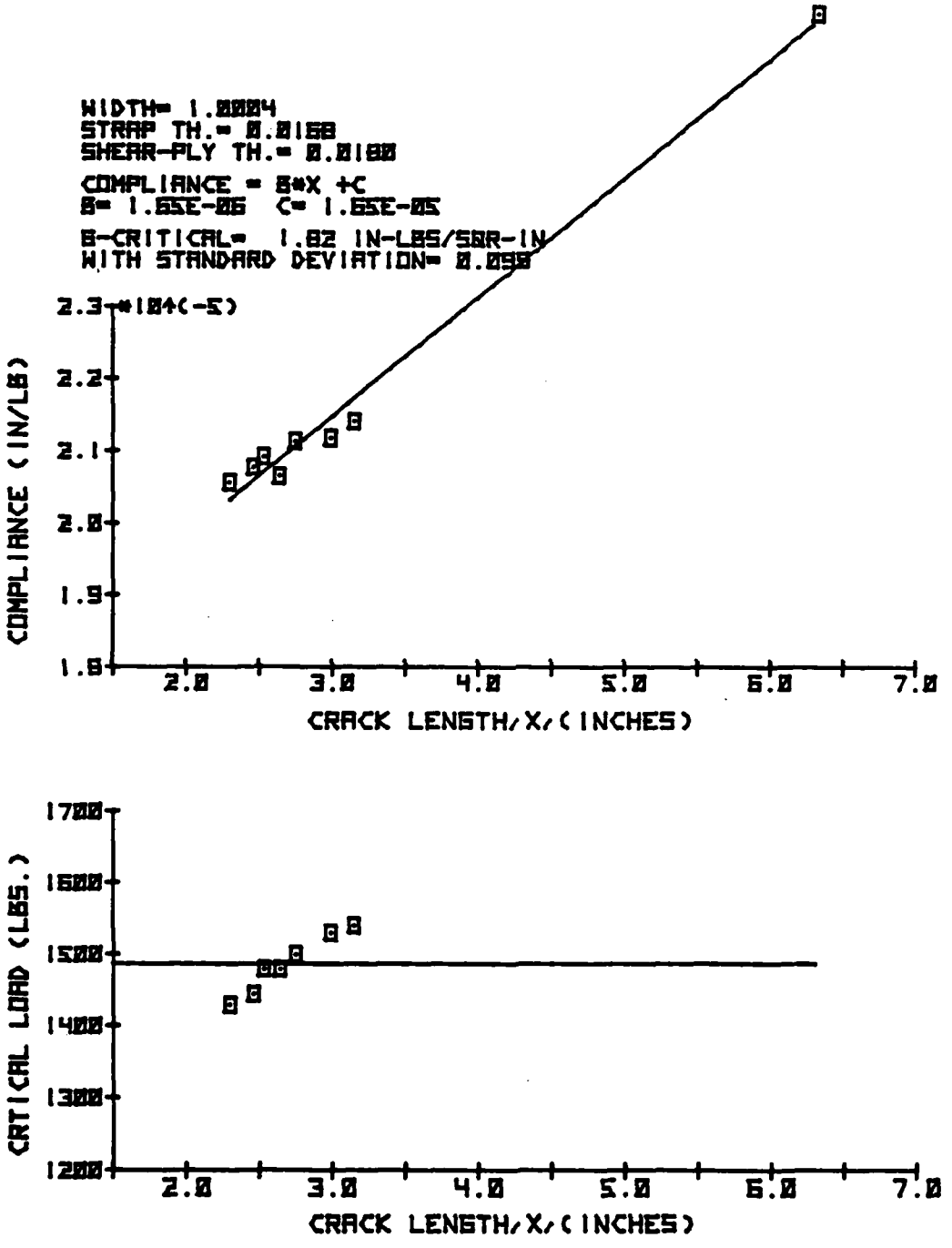

Figure D-18 Test P2CWS of Specimen P2-5-3

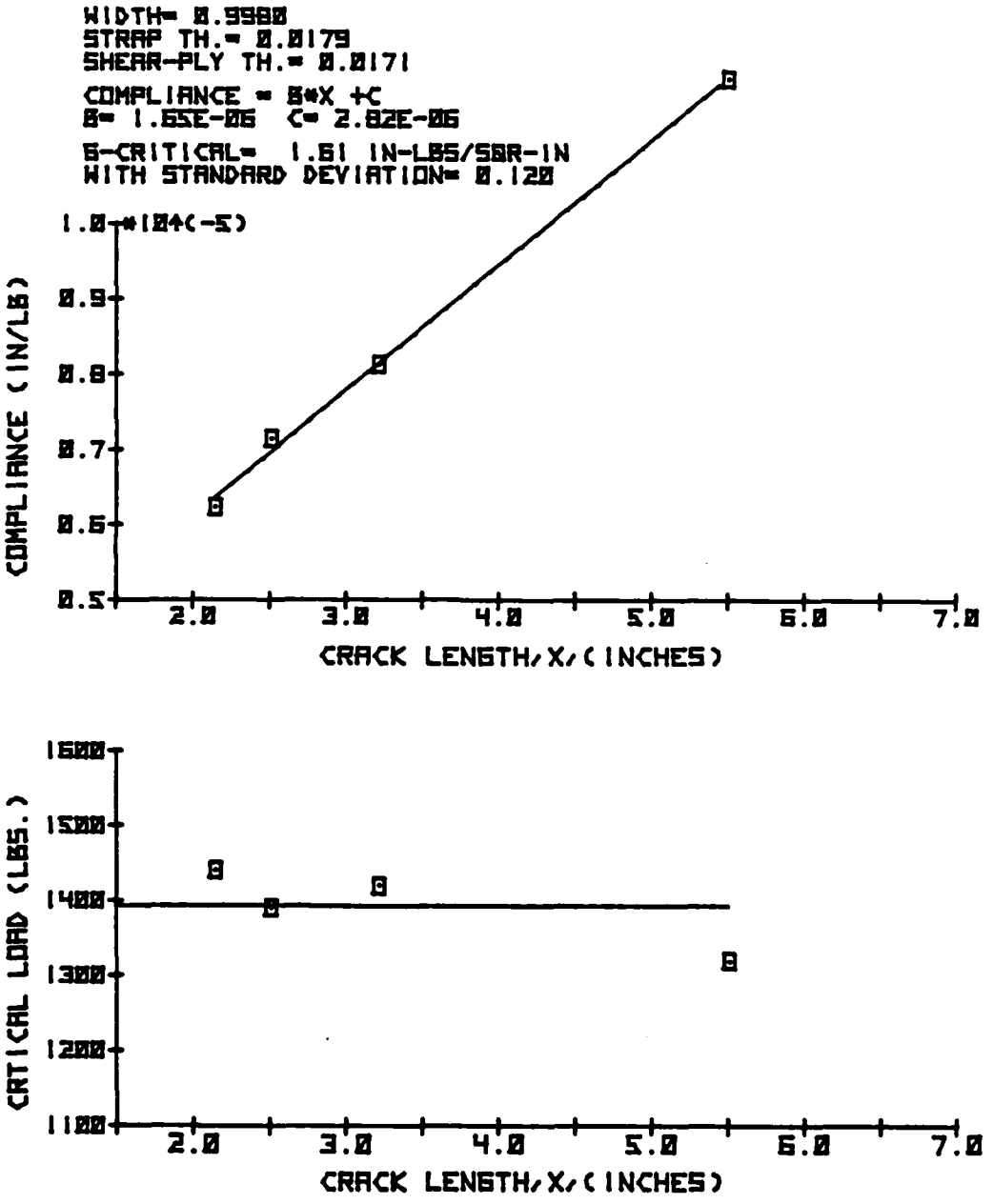

Figure D-19 Test P2RDS of Specimen P2-1-1

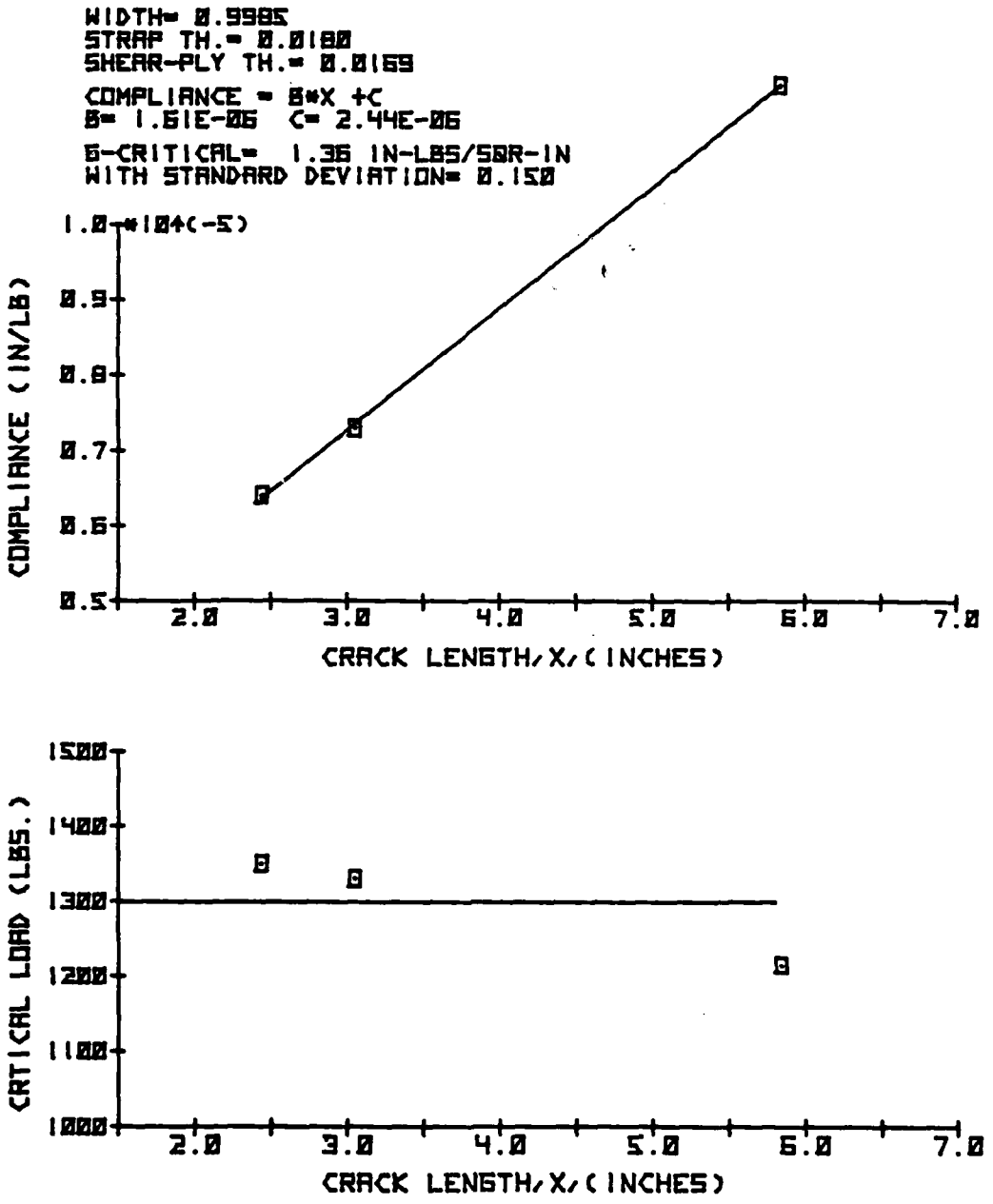

Figure D-20 Test P2RDS of Specimen P2-1-2

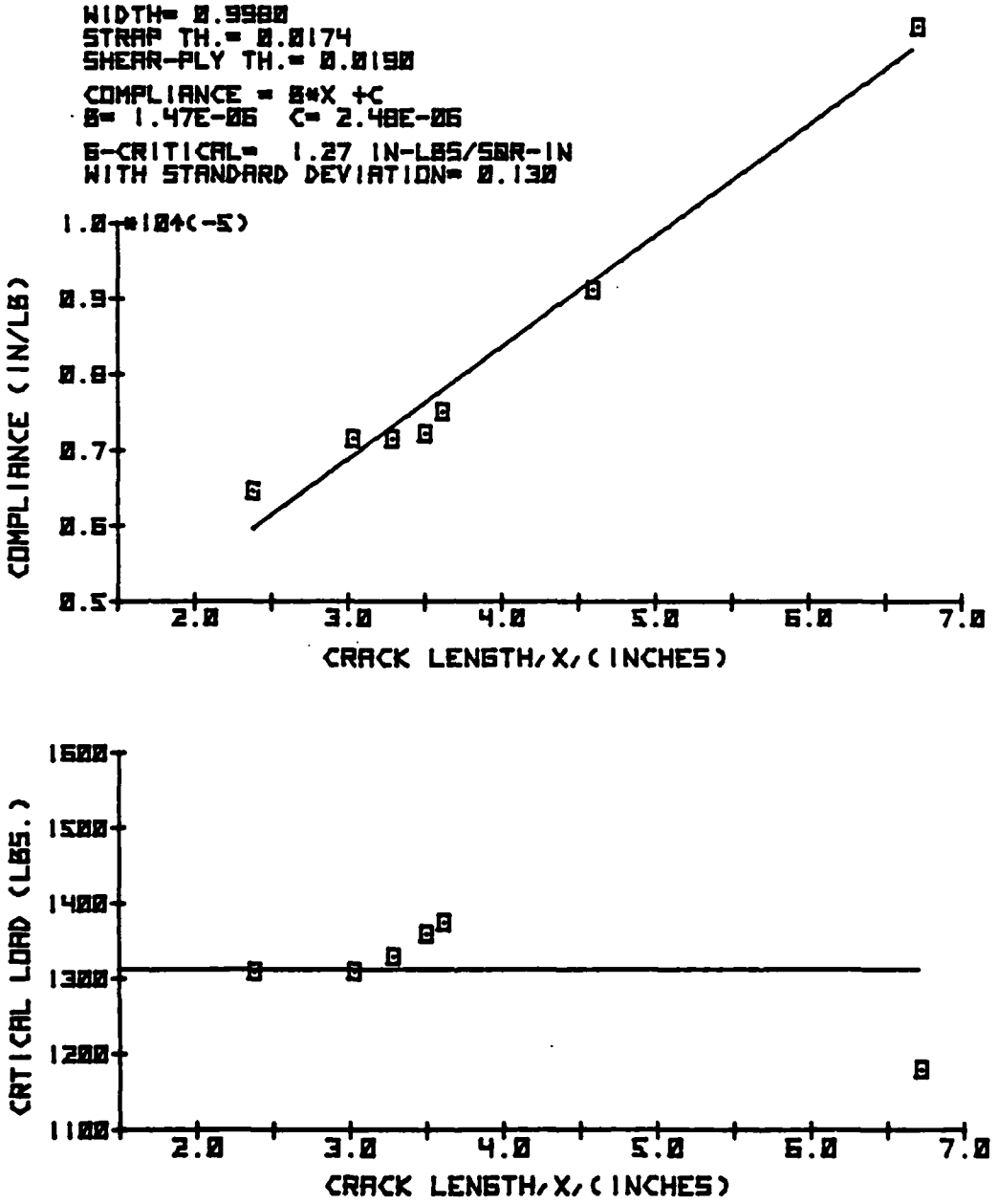

Figure D-21 Test P2RDS of Specimen P2-2-5

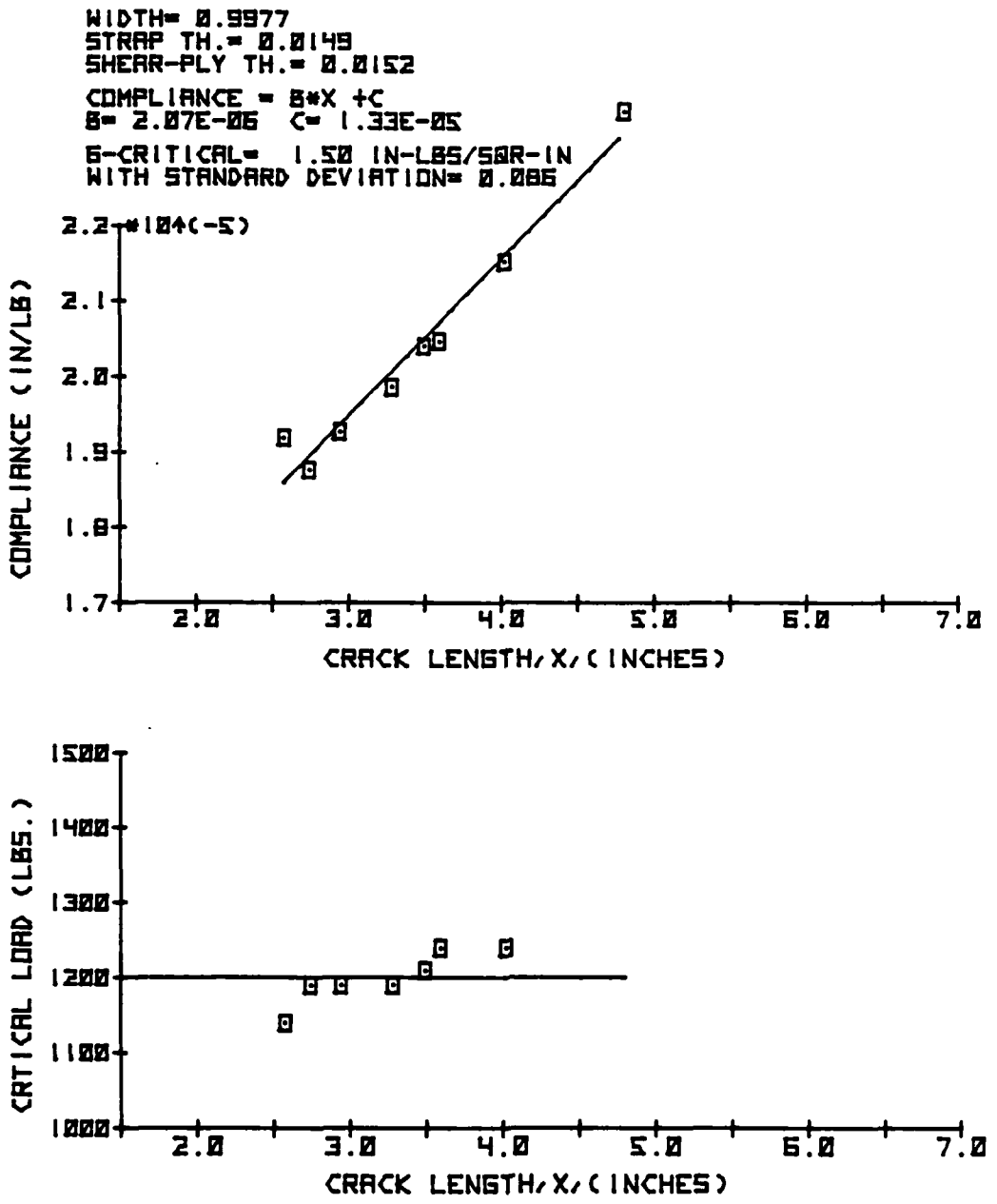

Figure D-22 Test P2RDS of Specimen P2-6-1

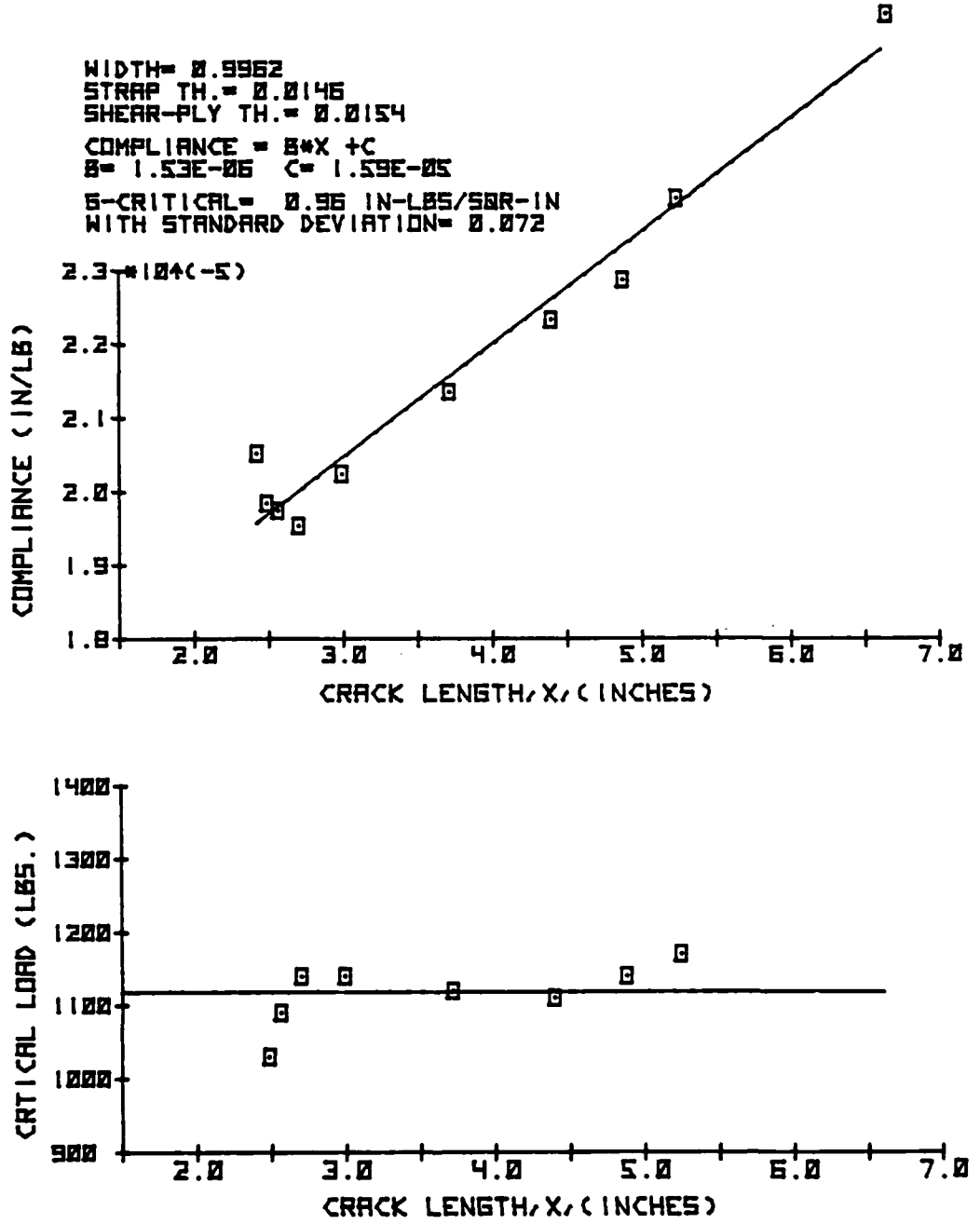

Figure D-23 Test P2RDS of Specimen P2-7-1

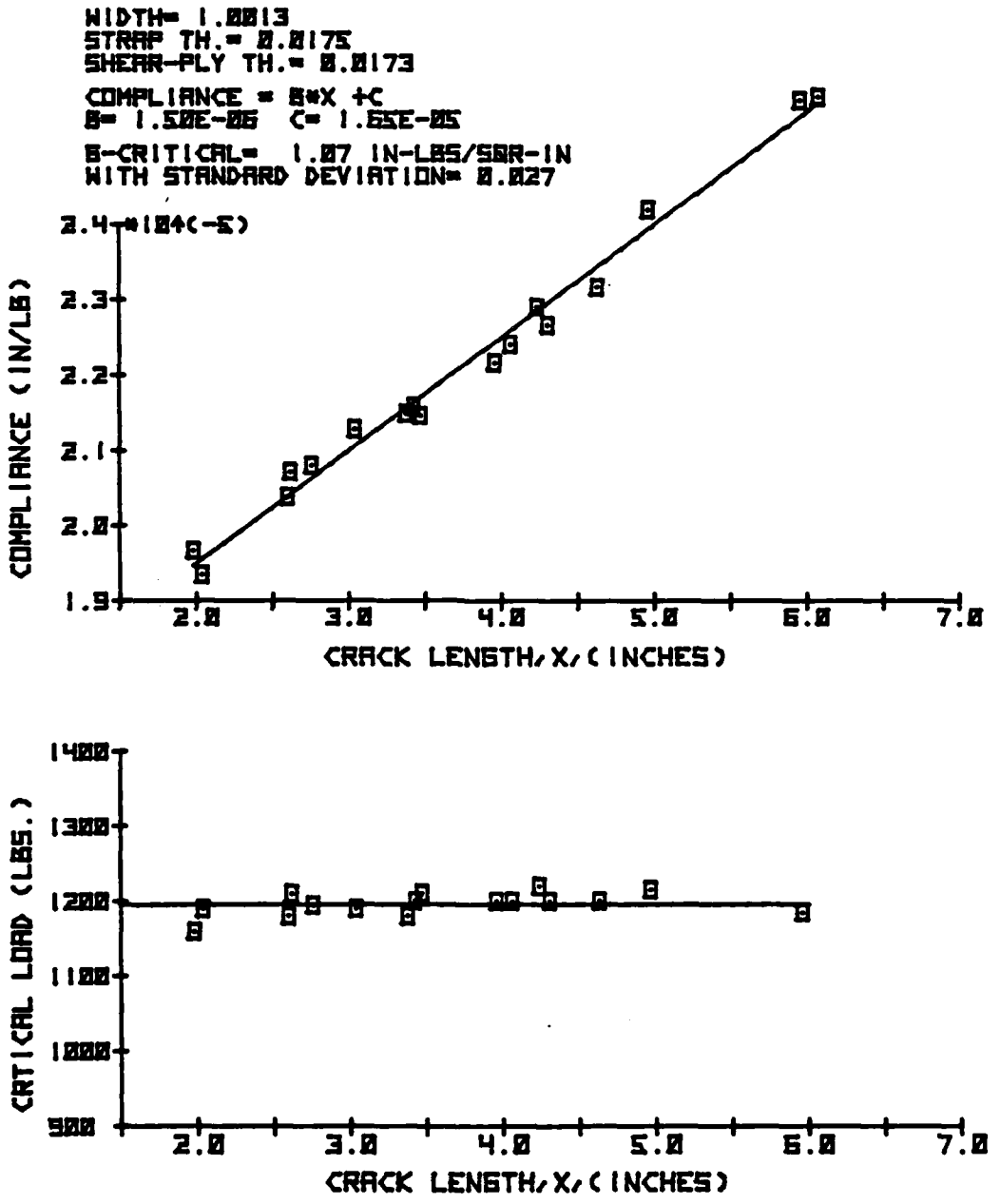

Figure D-24 Test P2RWS of Specimen P2-5-2

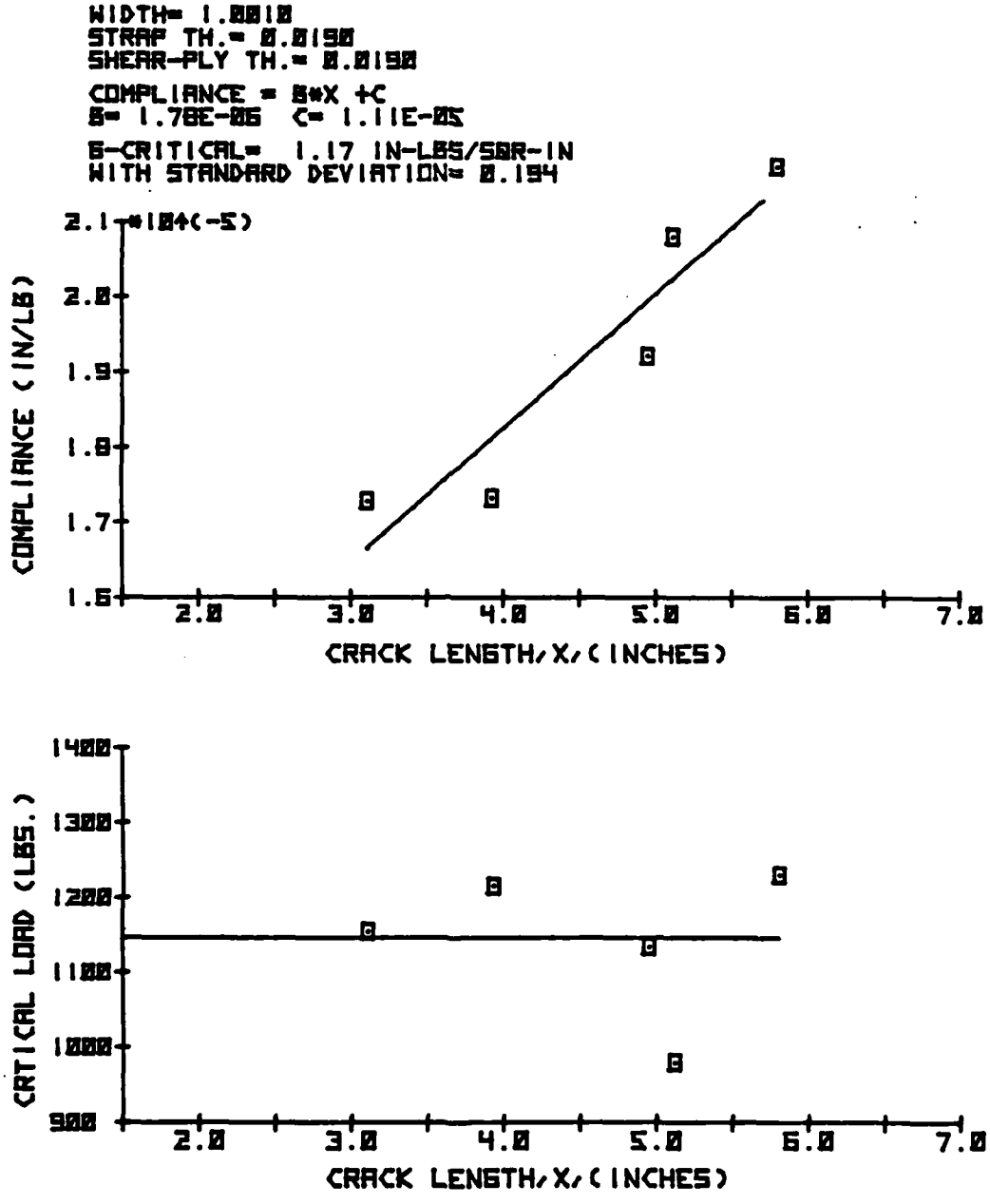

Figure D-25 Test P2RWS of Specimen P2-5-5

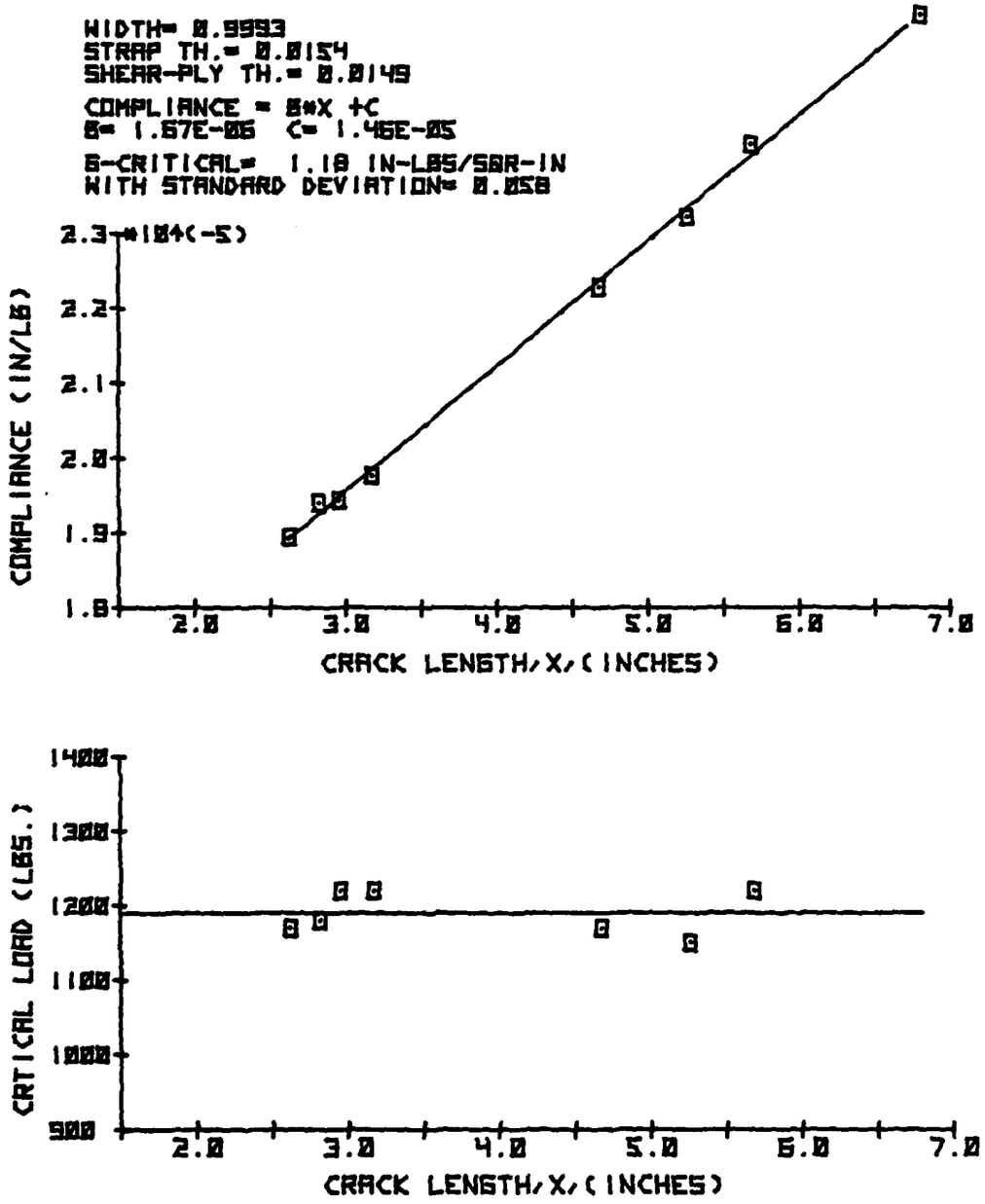

Figure D-26 Test P2RWS of Specimen P2-6-2

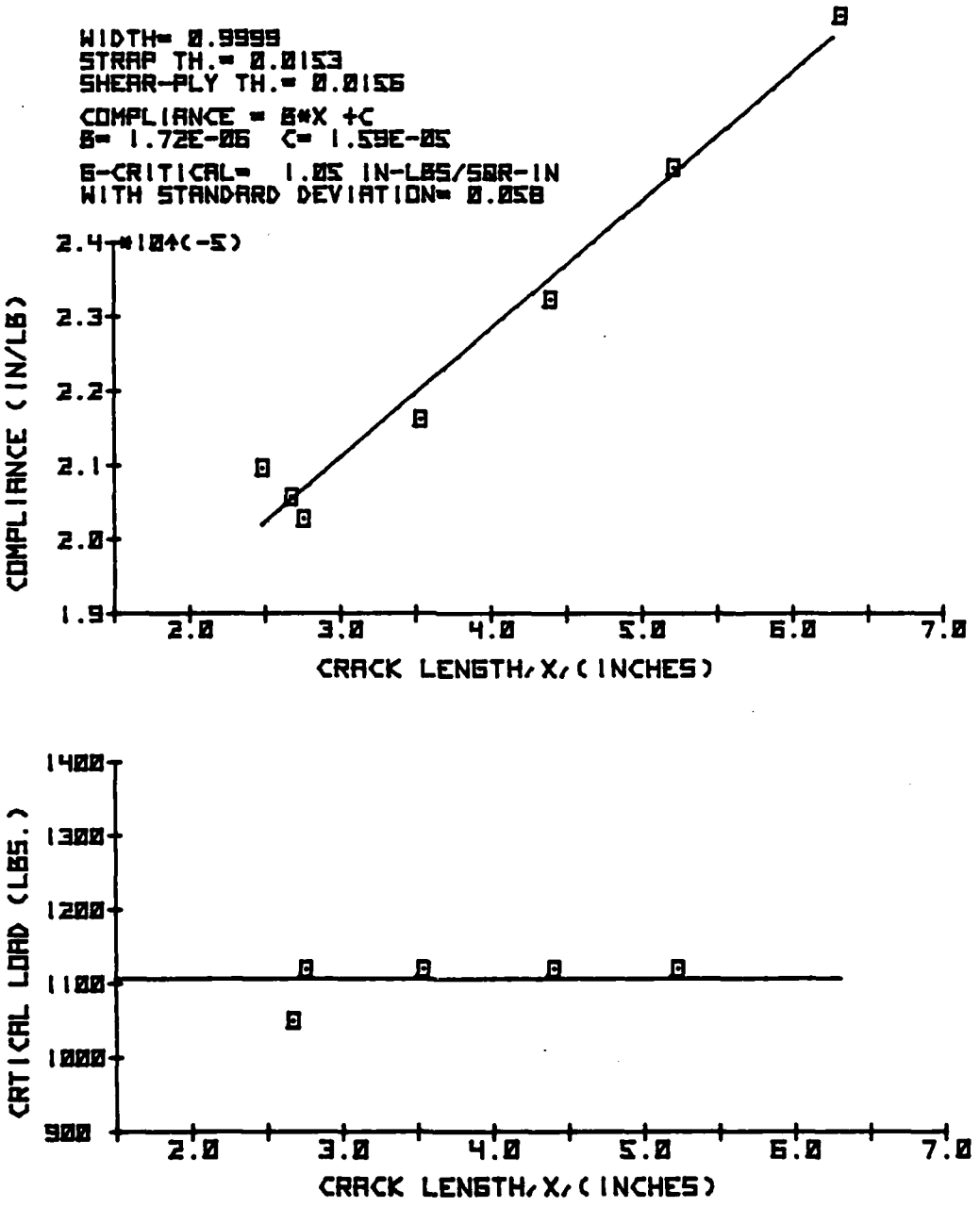

Figure D-27 Test P2RWS of Specimen P2-7-2

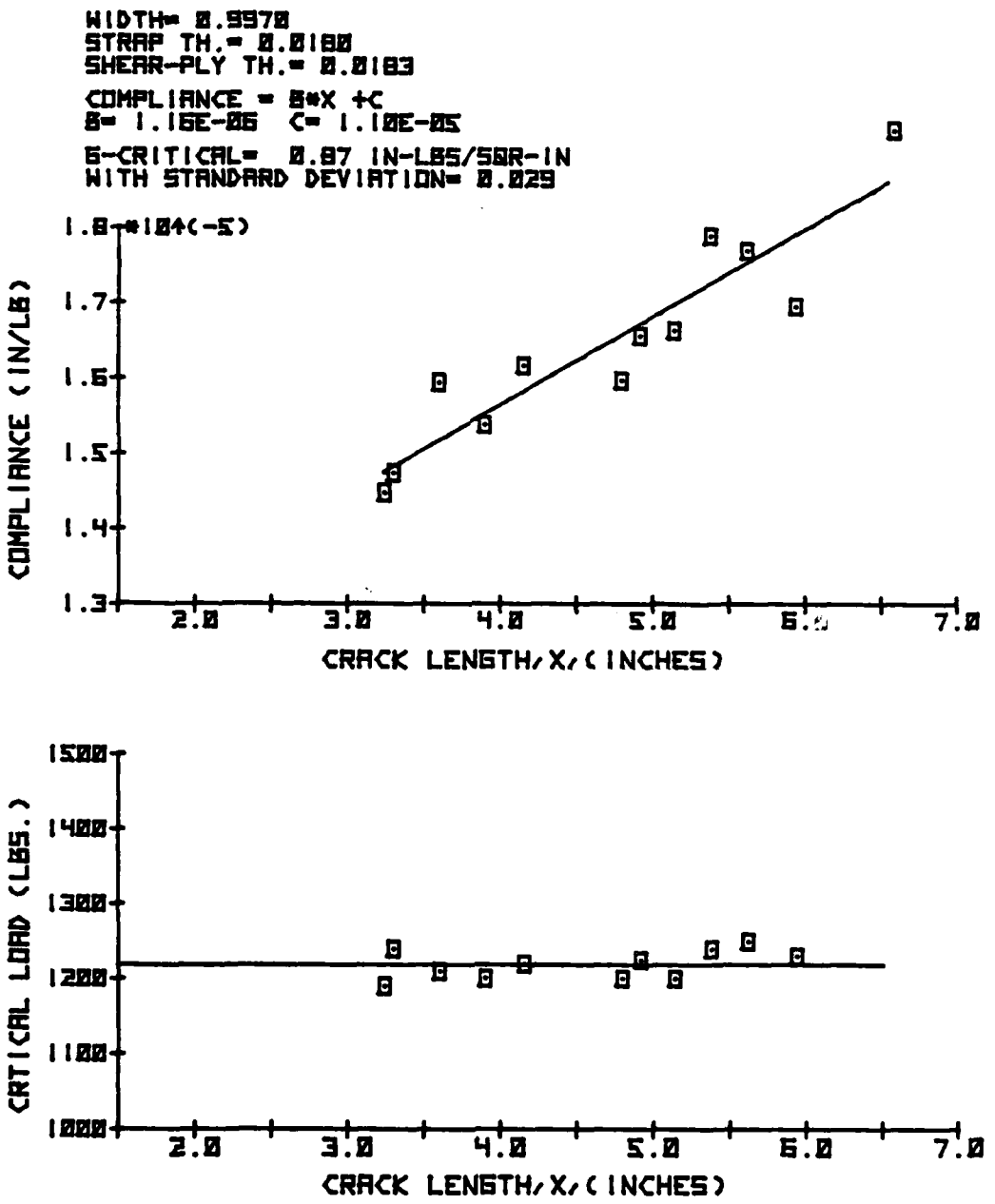

Figure D-28 Test P2EDS of Specimen P2-2-2

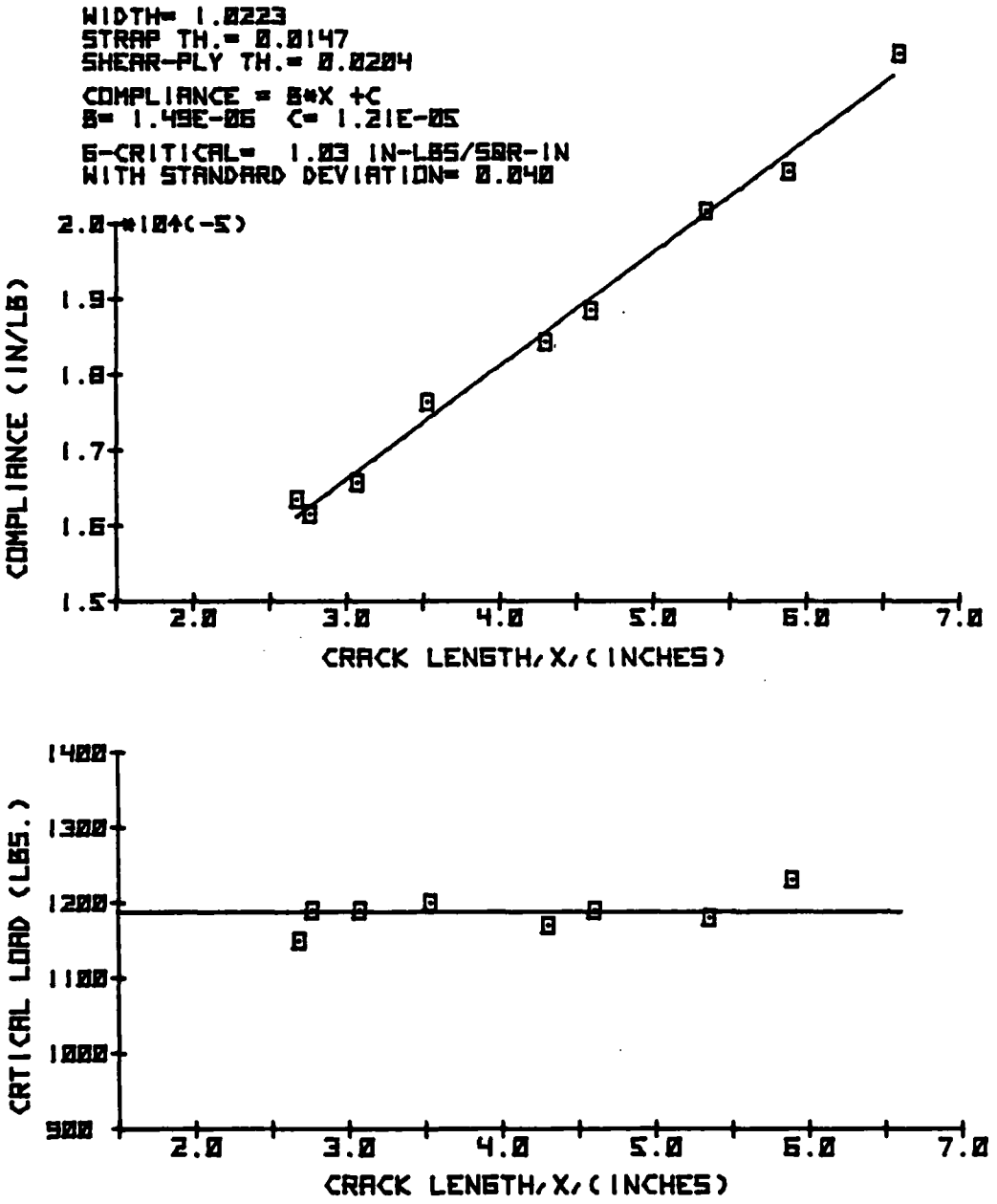

Figure D-29 Test P2EDS of Specimen P2-2-9

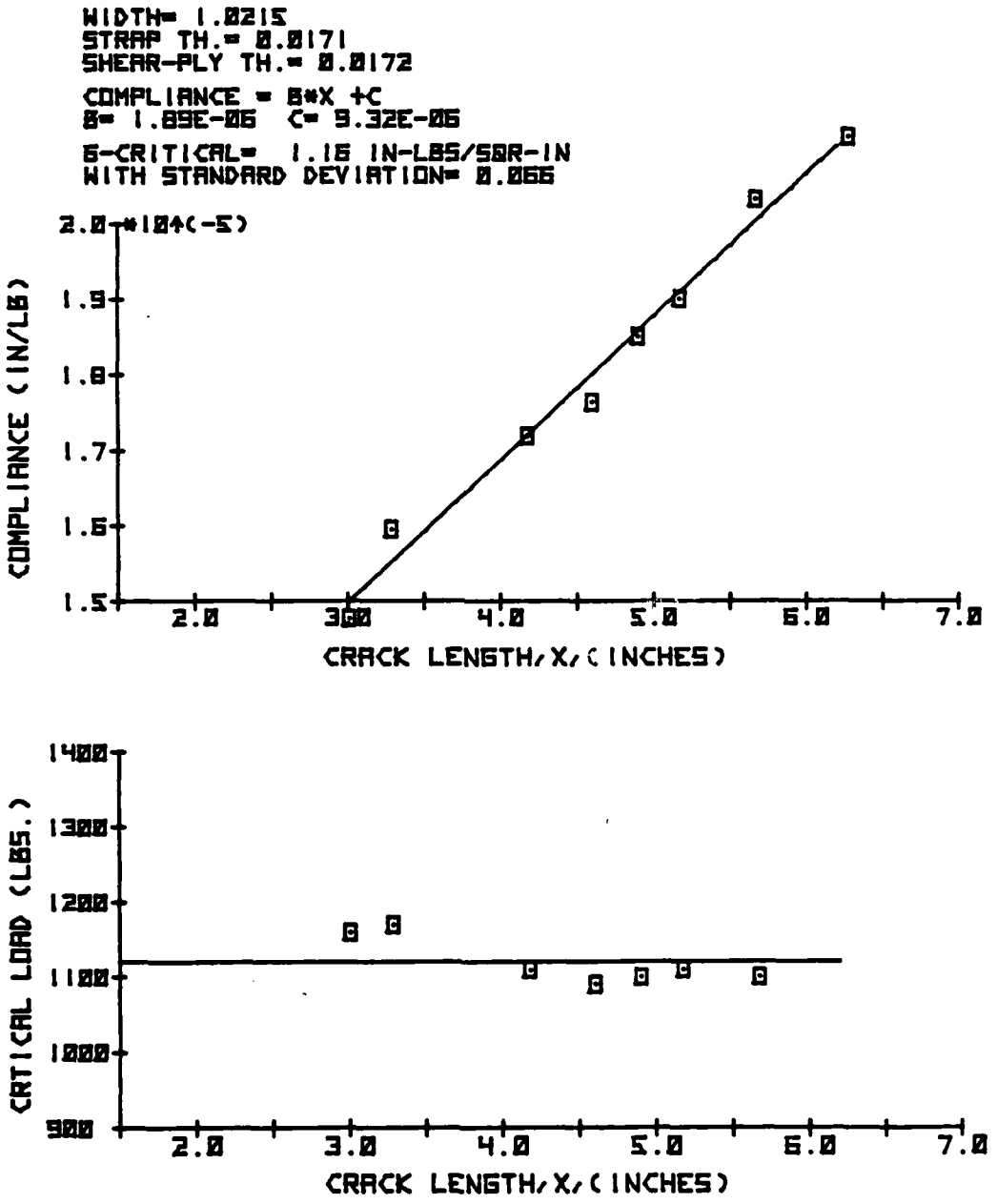

Figure D-30 Test P2PDS of Specimen P2-2-7

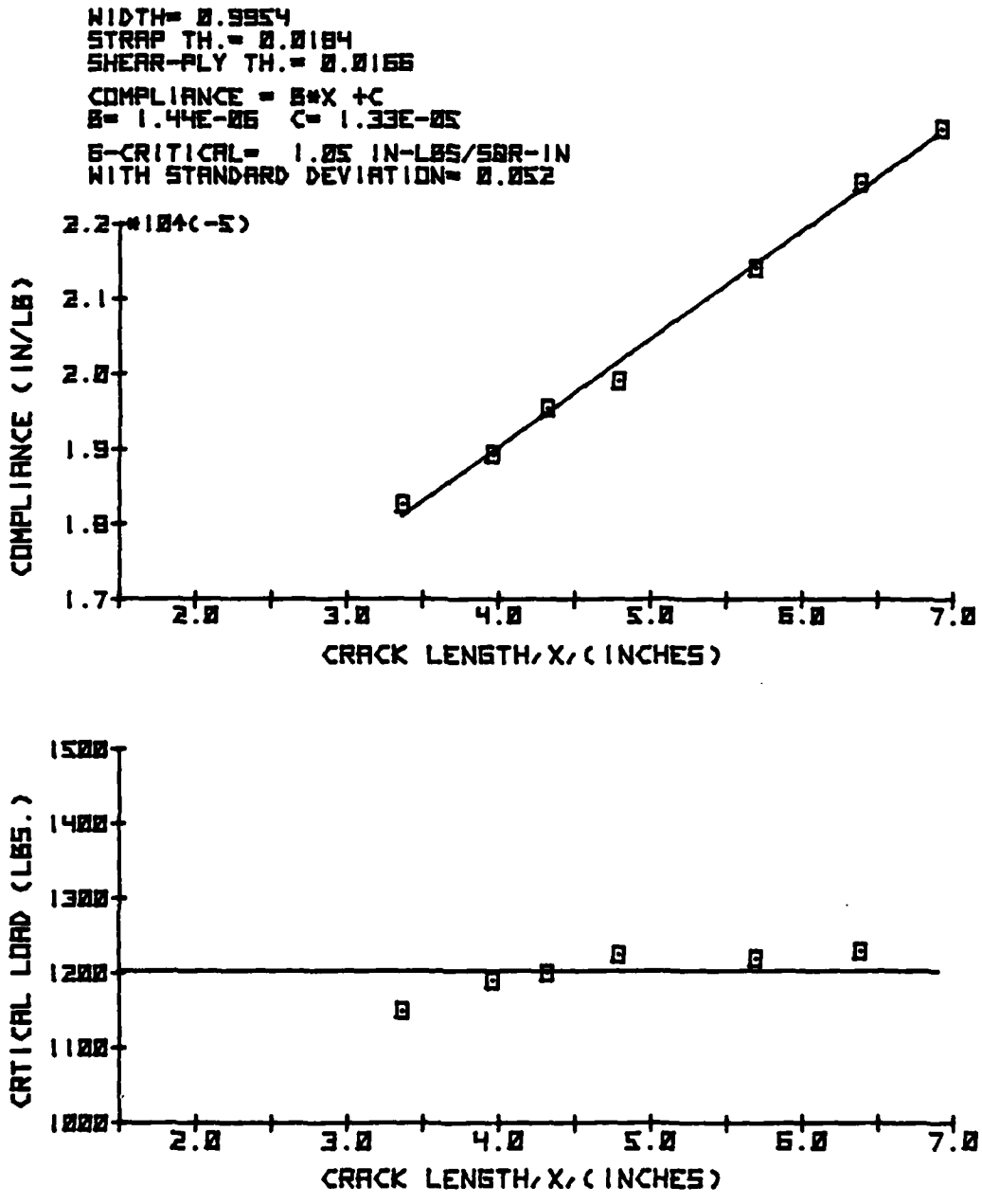

Figure D-31 Test P2PDS of Specimen P2-2-6

APPENDIX E

MODE II FATIGUE TESTING

The Mode II fatigue tests were performed in the test frame used for the Mode II static testing. The test procedure was identical to the Mode I fatigue testing procedure except that the crack length measurements were made visually using an X20 microscope. The Mode II fatigue data for the epoxy and bismaleimide material systems is contained in the remainder of this section.

E.1 Epoxy Mode II Fatigue Data

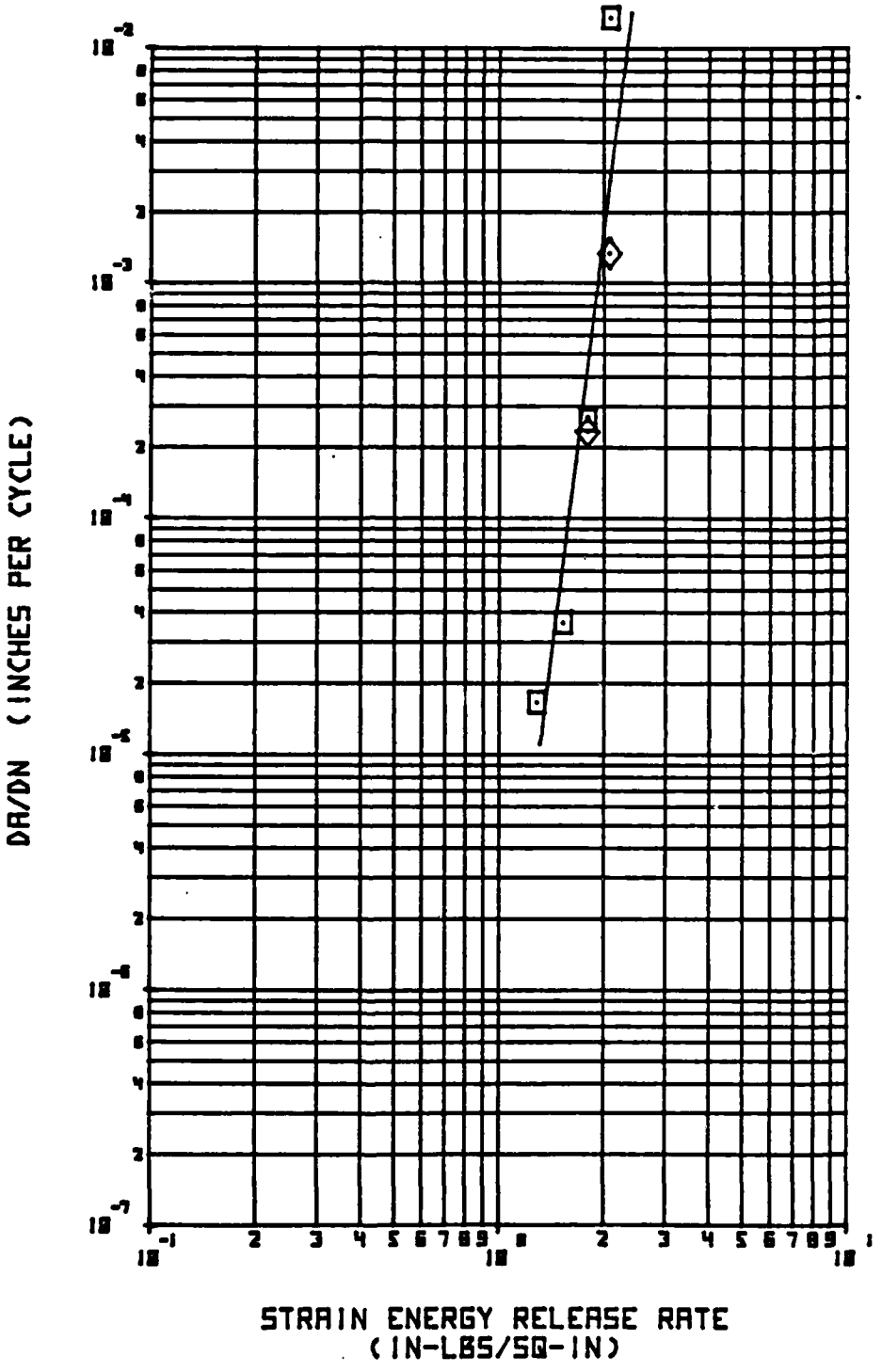

Figure E-1 Test E2CDF of Specimens E2-4-1 (◇) and E2-4-3 (⊡)

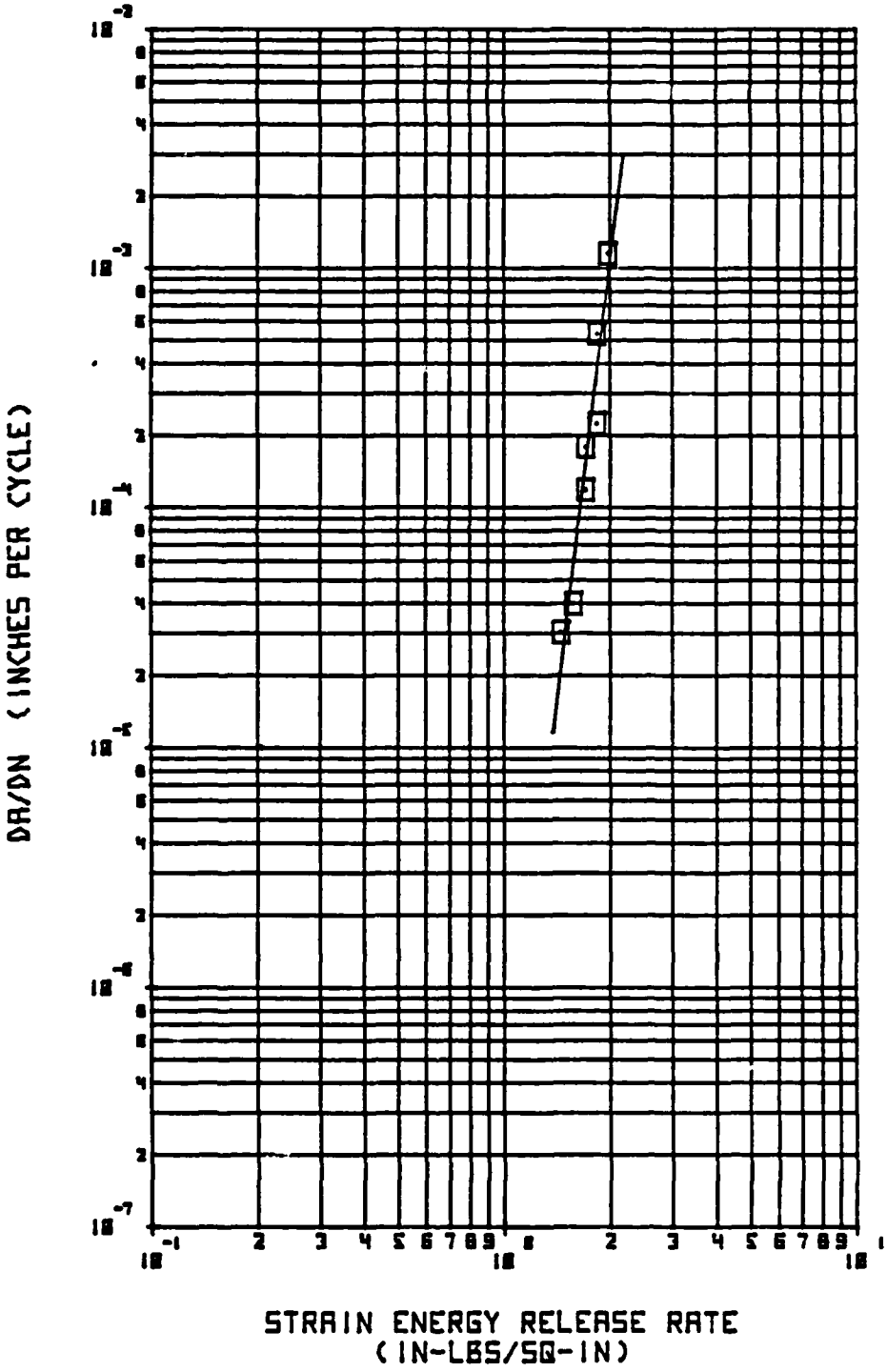

Figure E-2 Test E2CWF of Specimen E2-1-3

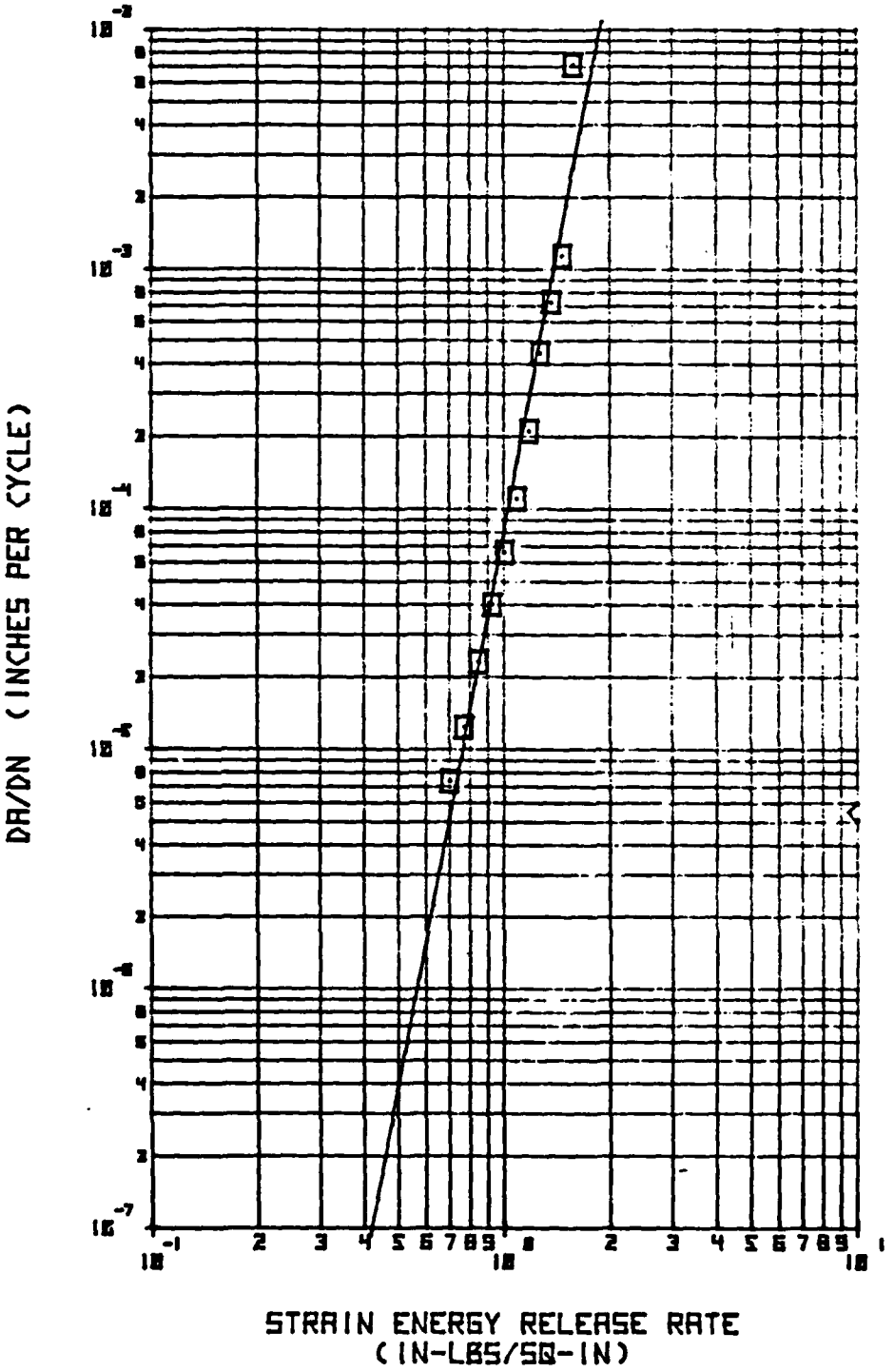

Figure E-3 Test E2RDF of Specimen E2-2-7

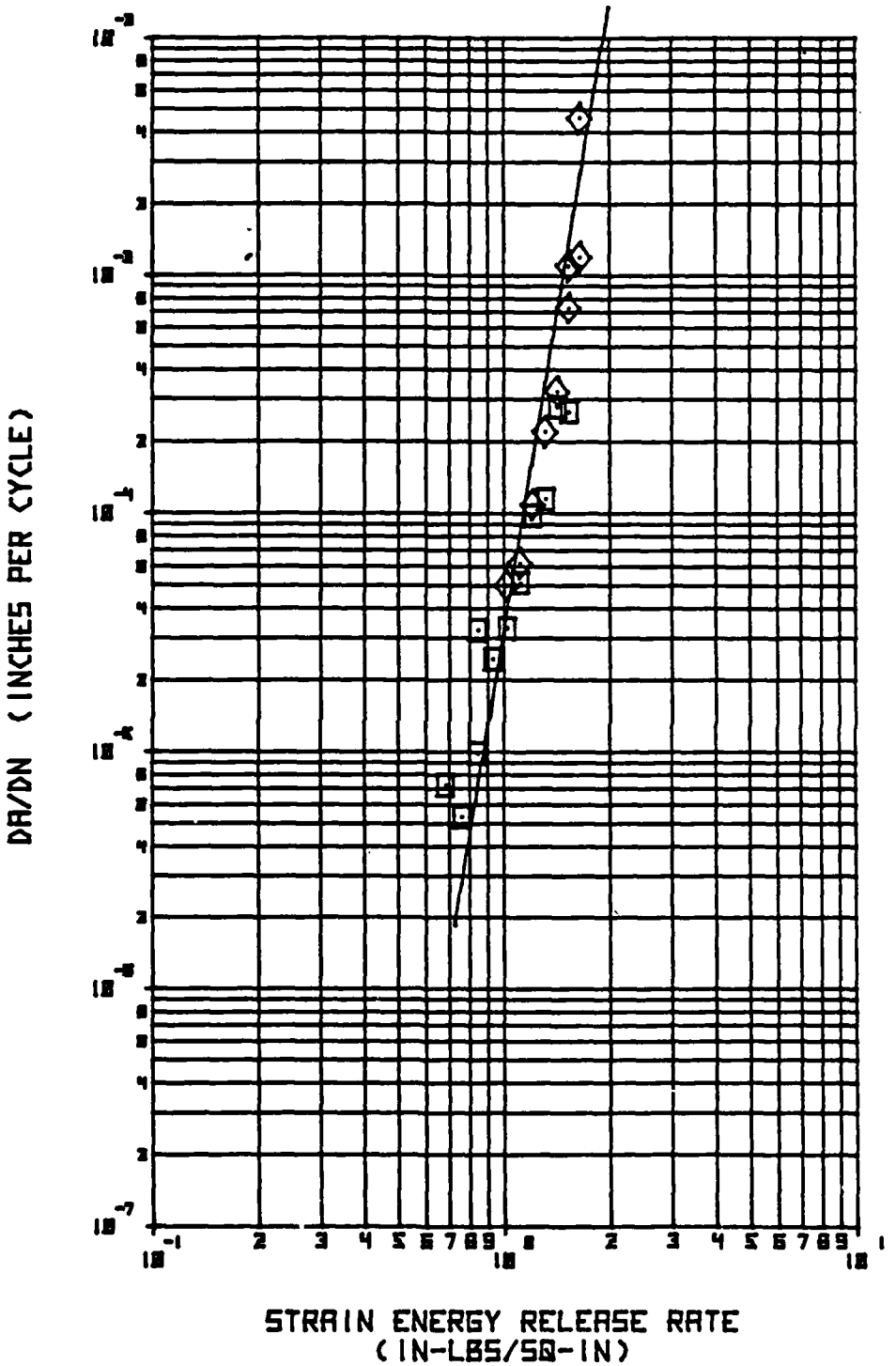

Figure E-4 Test E2RWF of Specimens E2-1-2 (◇) and E2-1-5 (⊡)

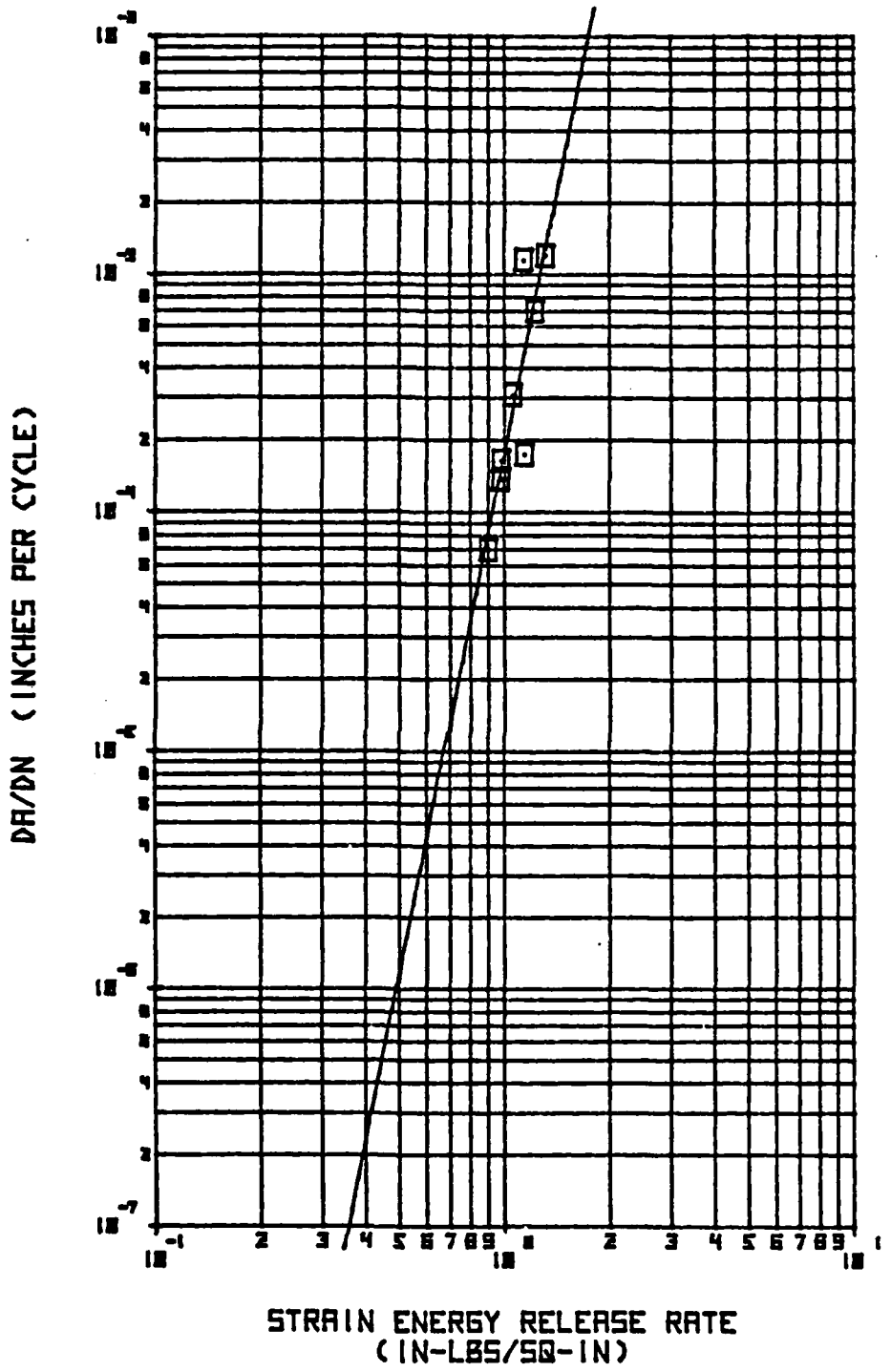

Figure E-5 Test E2EDF of Specimen E2-4-8

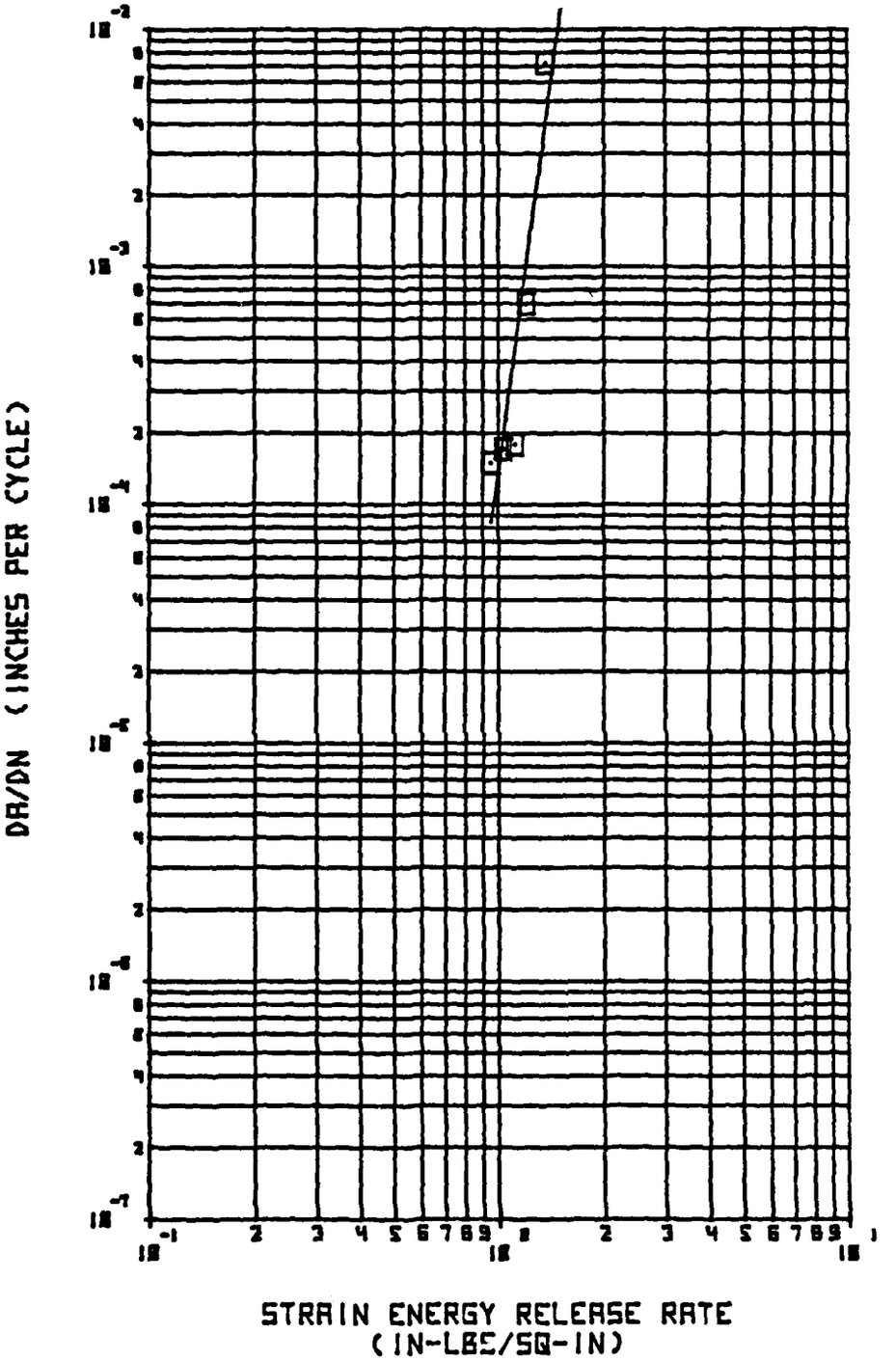

Figure E-6 Test E2PDF of Specimen E2-5-7

E.2 Bismaleimide Mode II Fatigue Data

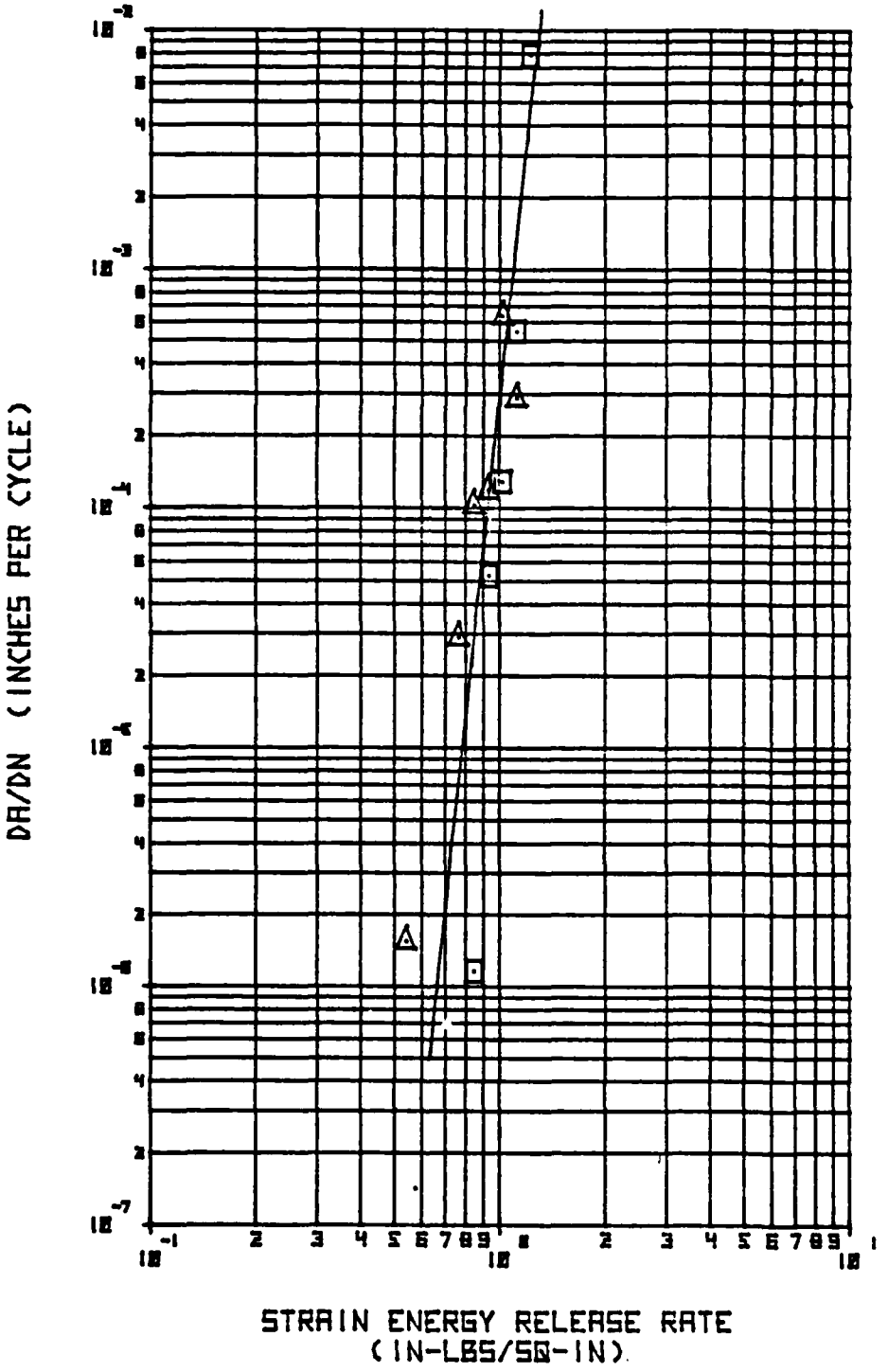

Figure E-7 Test P2CDF of Specimens P2-3-3 (△) and P2-3-1 (□)

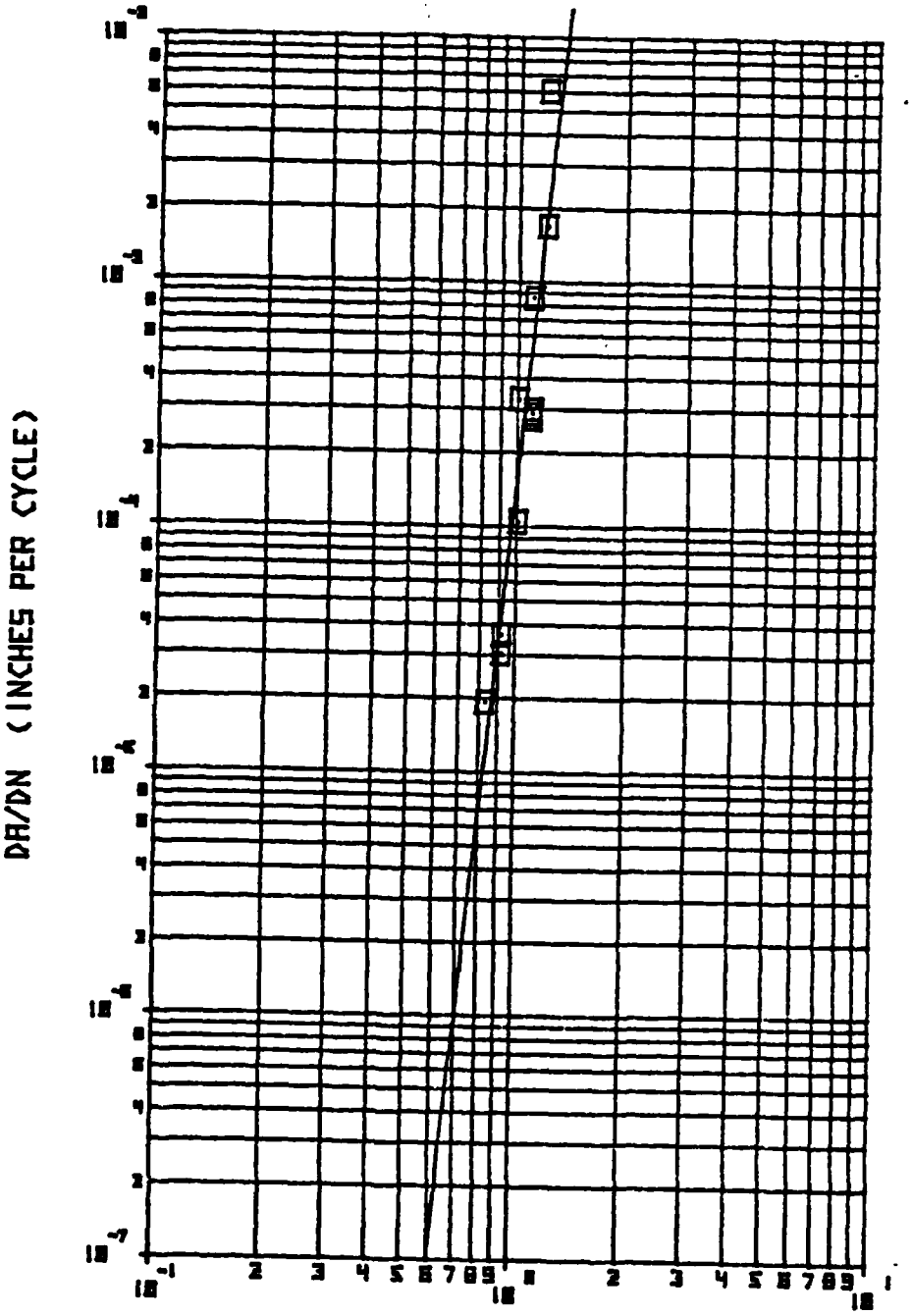

Figure E-8 Test P2CWF of Specimen P2-5-1

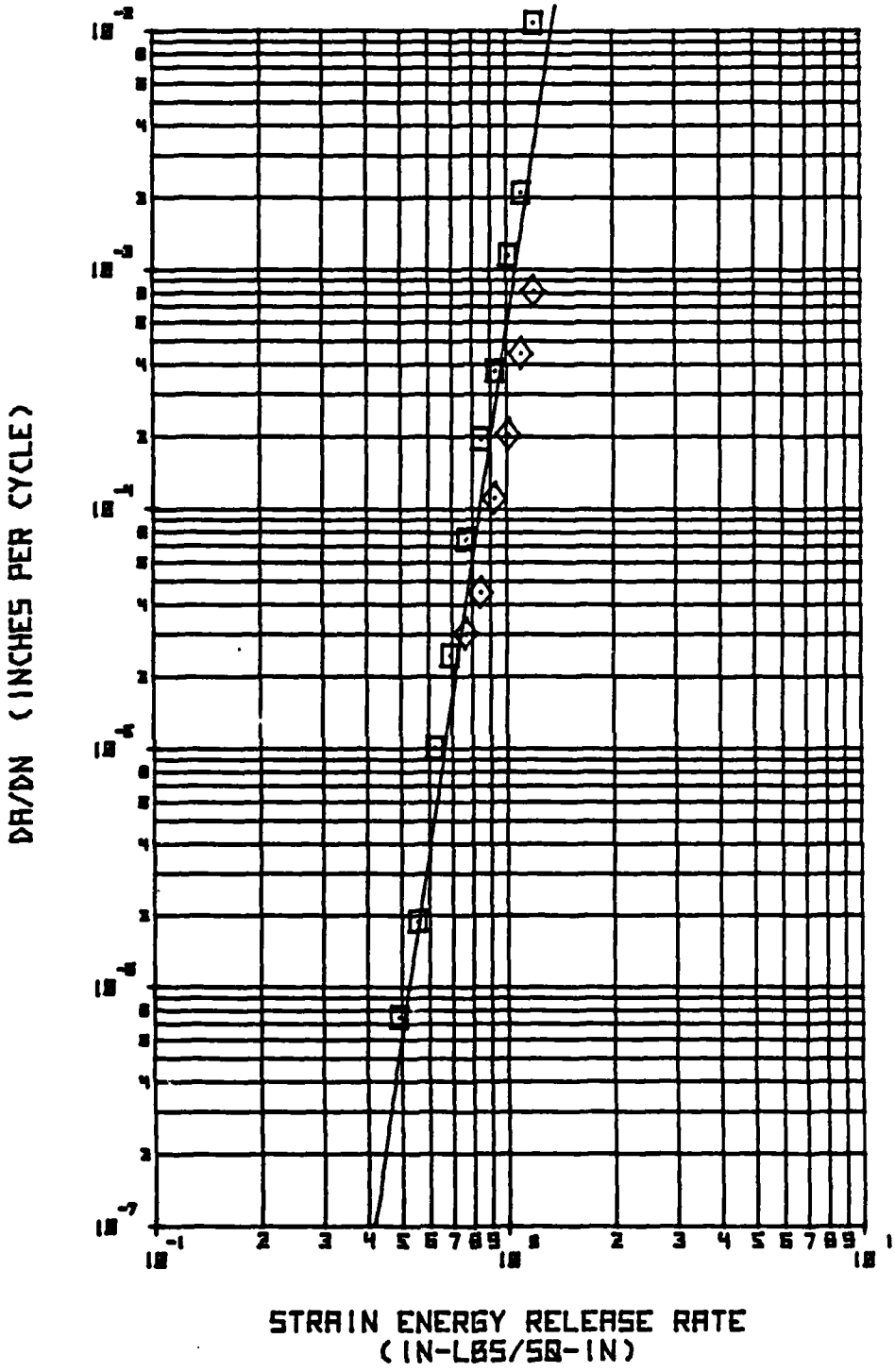

Figure E-9 Test P2RDF of Specimens P2-1-10 (◇) and P2-1-3 (□)

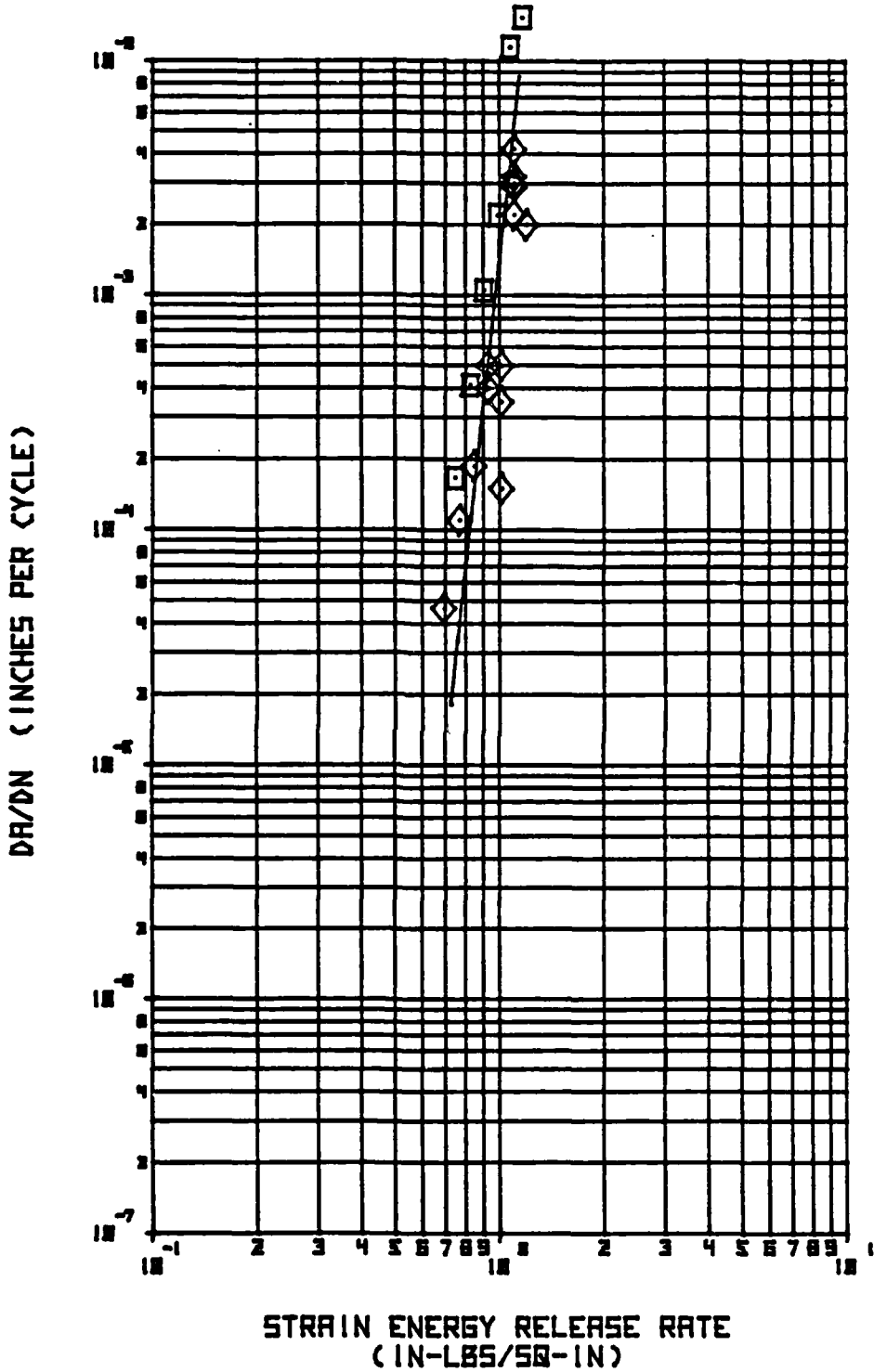

Figure E-10 Test P2RW7 of Specimens P2-5-7 (⊡) and P2-5-8 (◈)

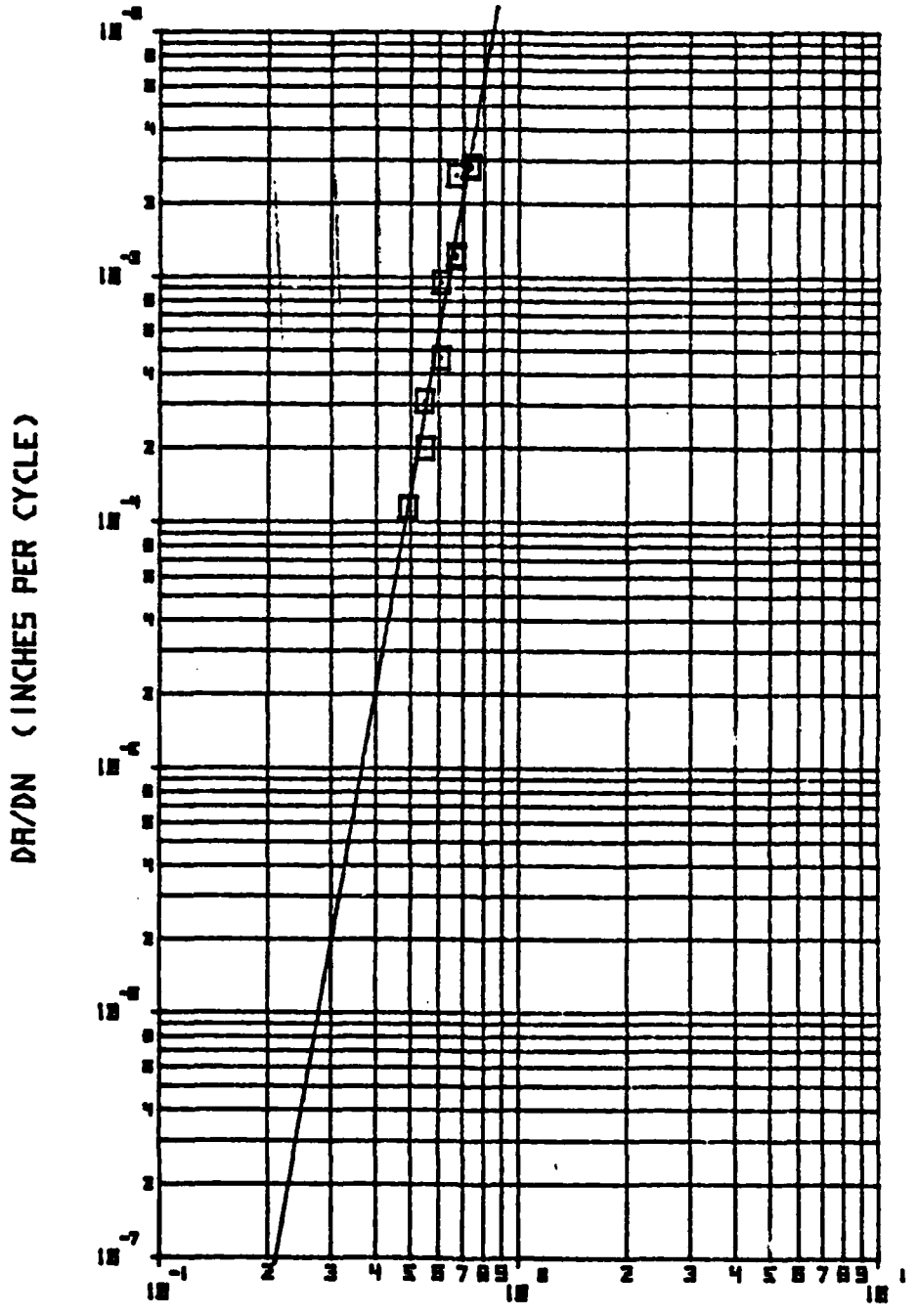

Figure E-11 Test P2EDF of Specimen P2-3-7

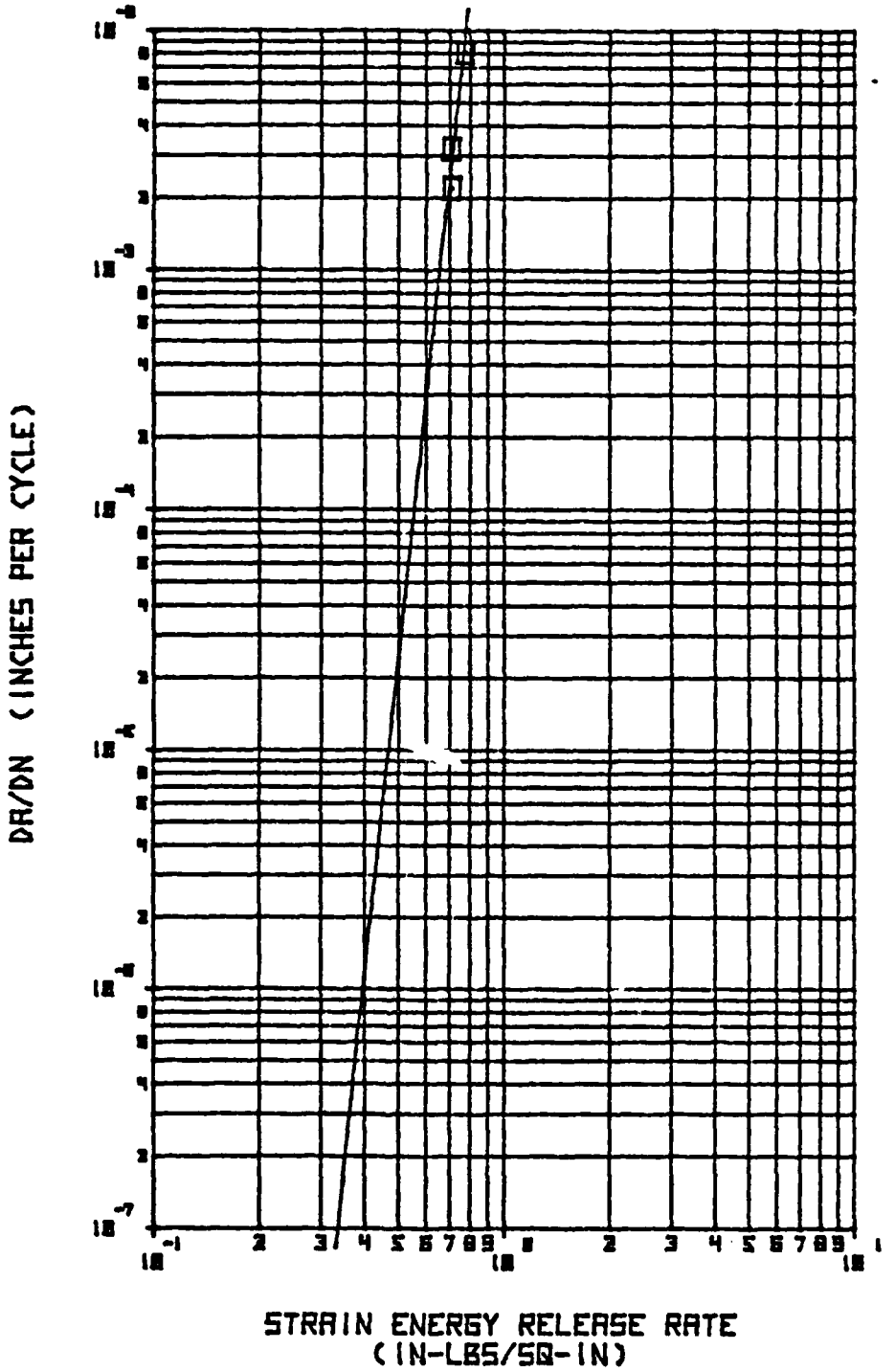

Figure E-12 Test P2EDF of Specimen P2-3-8

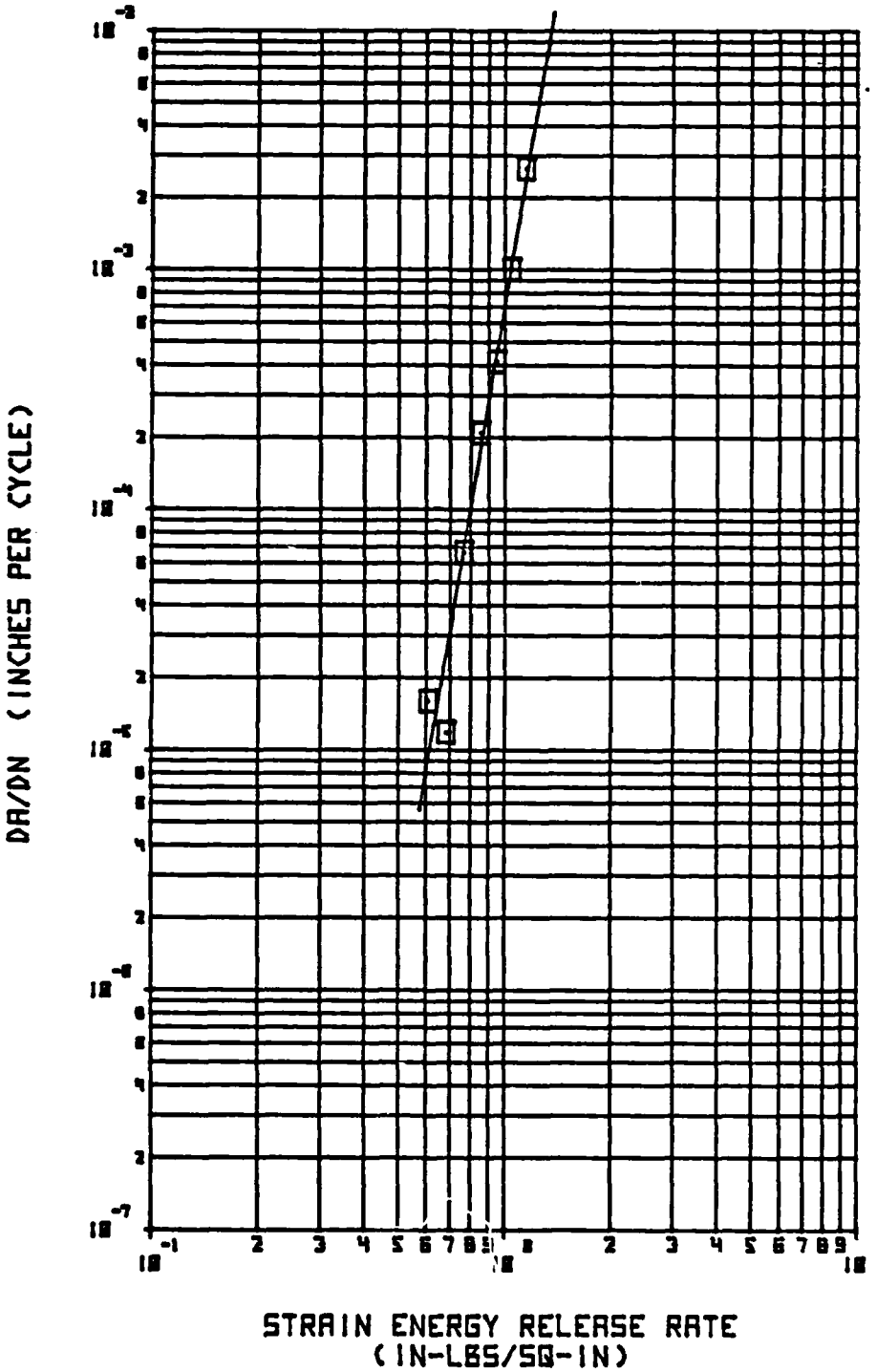

Figure E-13 Test P2PDF of Specimen P2-2-1

APPENDIX F

PHOTOMICROGRAPHS

The following pages contain photomicrographs of each of the cured panels used in the present study.

AD-A112 474 GENERAL DYNAMICS CORP FORT WORTH TX FORT WORTH DIV F/G 11/4
A COMPARISON OF THE DELAMINATION AND ENVIRONMENTAL RESISTANCE O--ETC(U)
SEP 81 D J WILKINS N00019-80-C-0415
UNCLASSIFIED NAV-GD-0037 NL

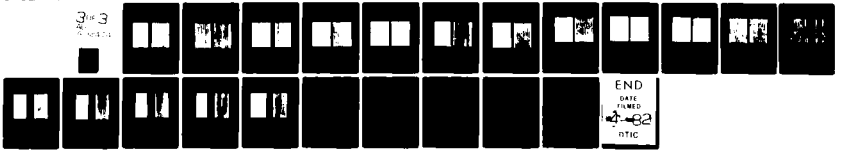

END
DATE FILMED
4-82
DTIC

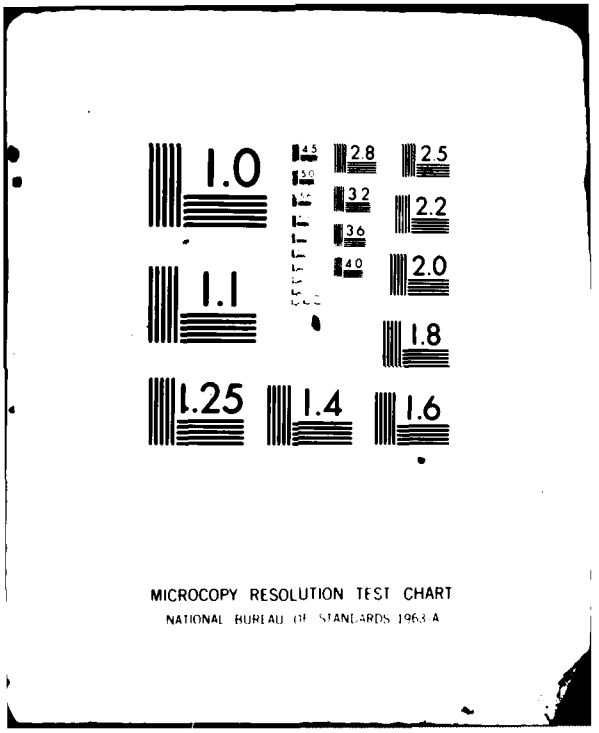

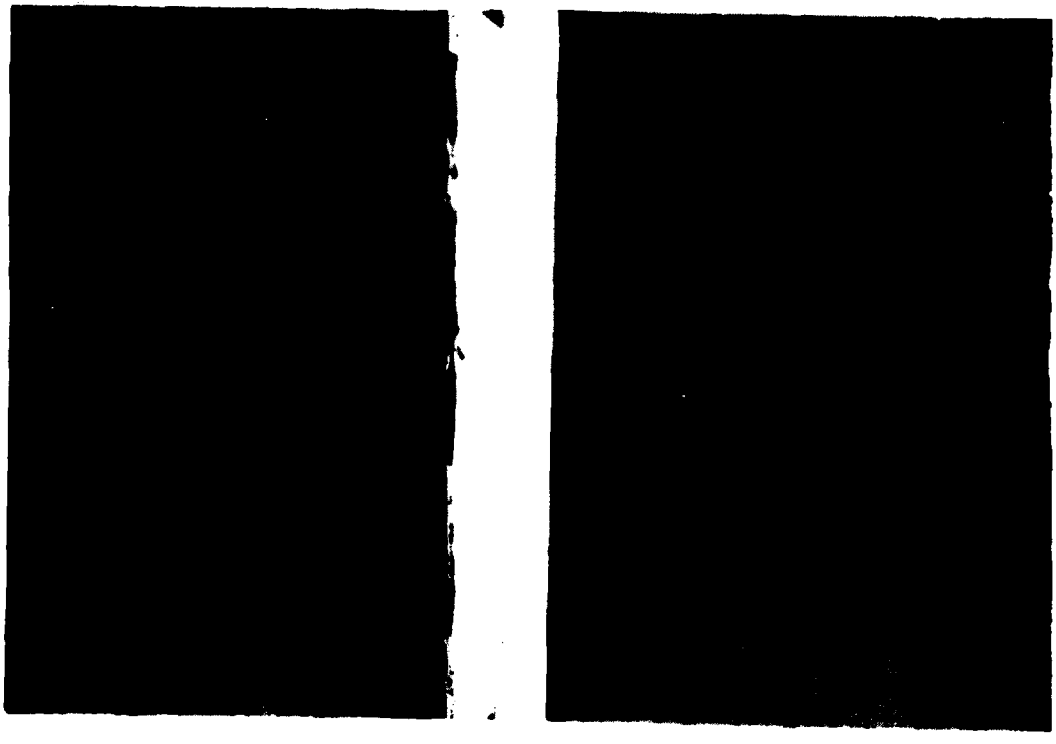

Figure F-1 Photomicrographs of Glass Transition Panels

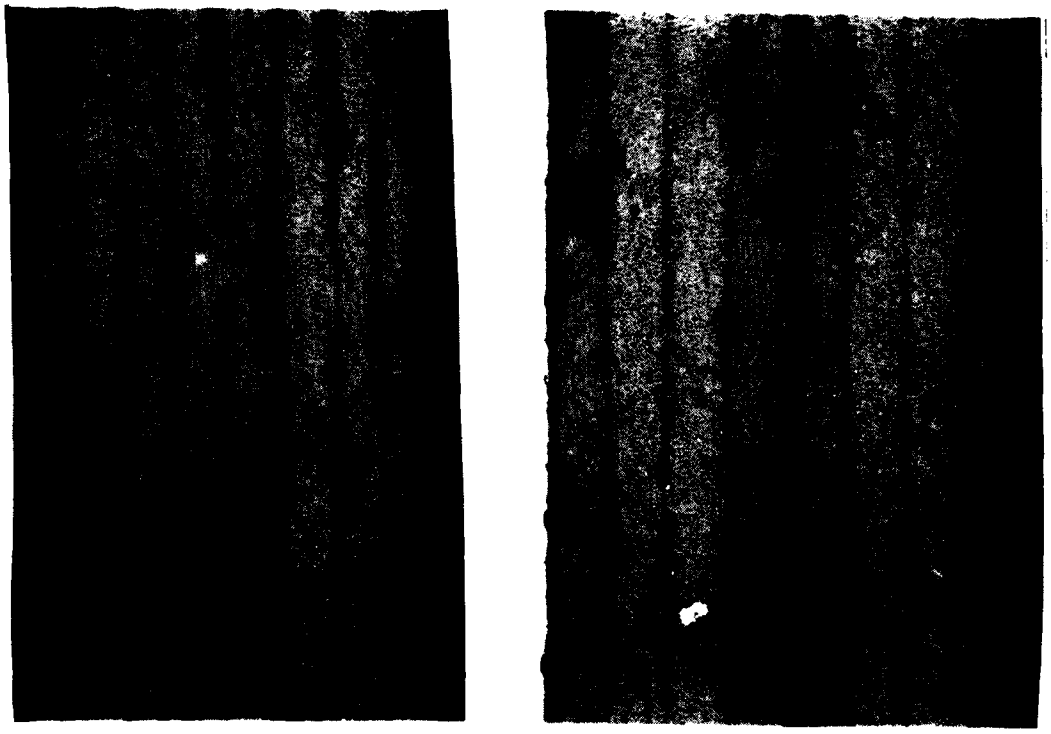

0.01 IN

AS1/3501-6

T300-6K/V378A

Figure F-2 Photomicrographs of Thermal Spike Panels

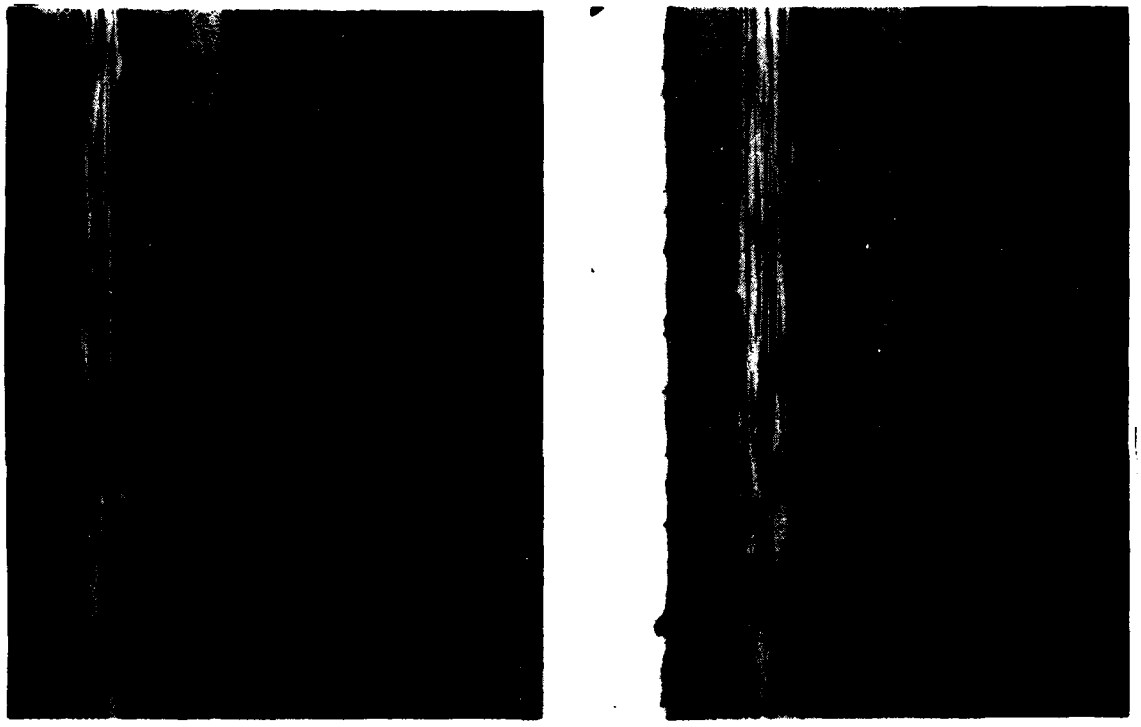

Figure F-3 Photomicrographs of Miniwich Panels

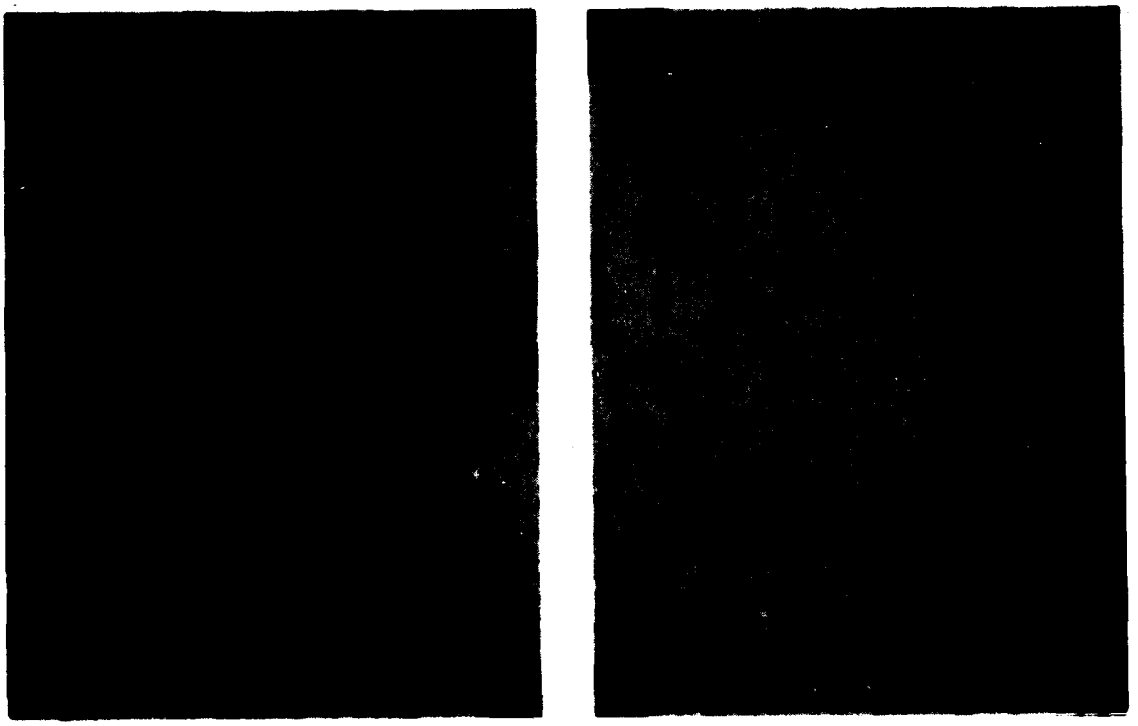

Figure F-4 Photomicrographs of #1 Flex Panels

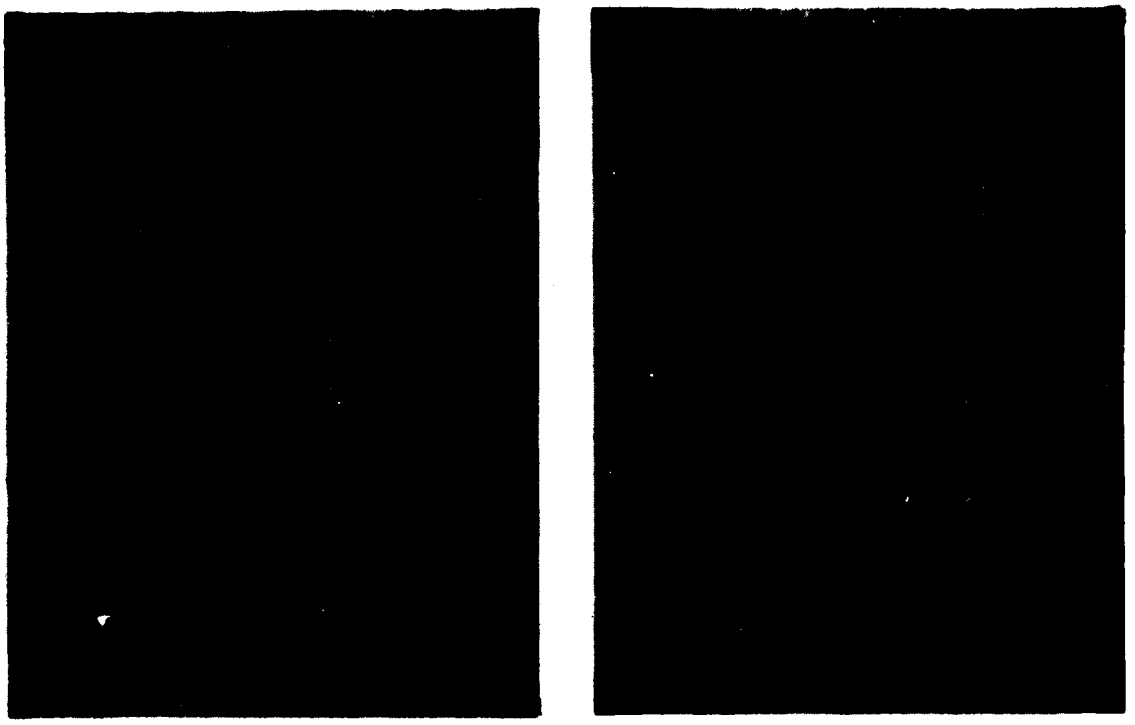

Figure F-5 Photomicrographs of #2 Flex Panels

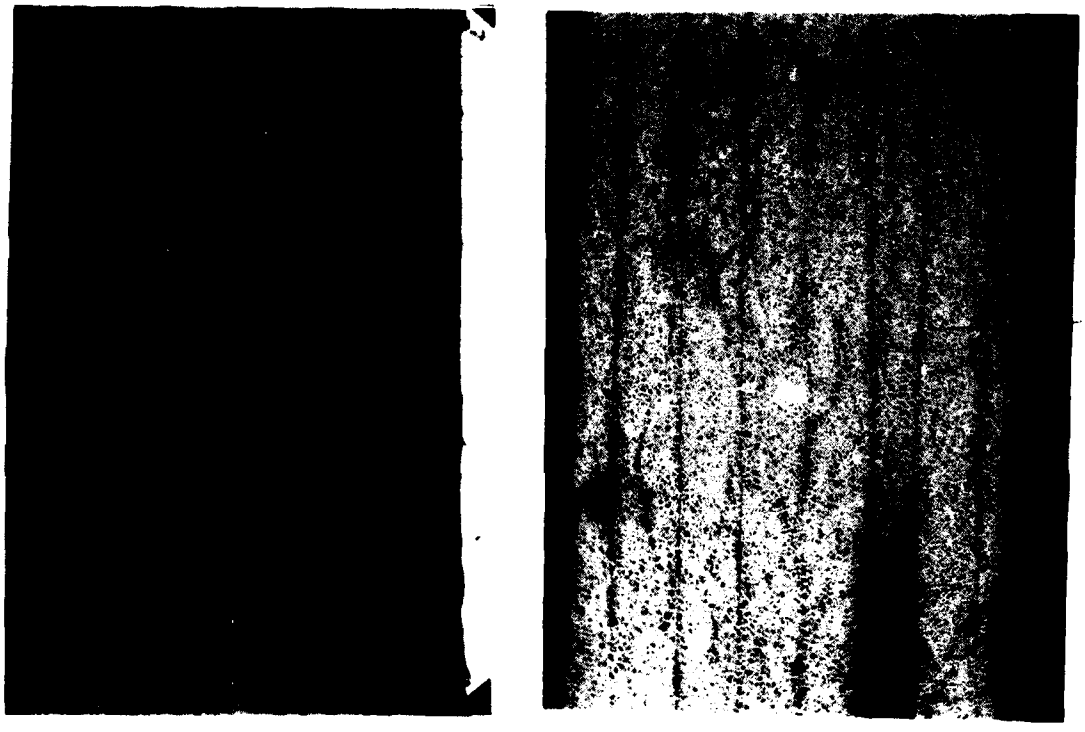

0.01 IN

AS1/3501-6

T300-6K/V378A

Figure F-6 Photomicrographs of #1 ±45 Panels

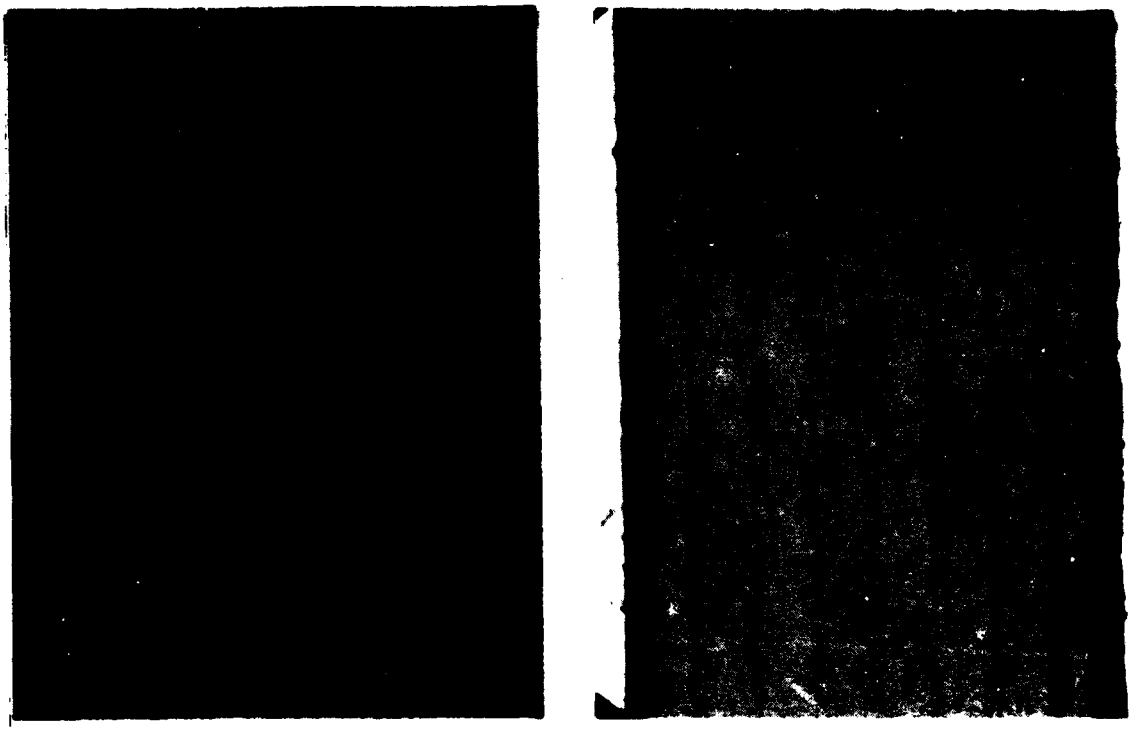

0.01 IN

AS1/3501-6 T300-6K/V378A

Figure F-7 Photomicrographs of #2 ±45 Panels

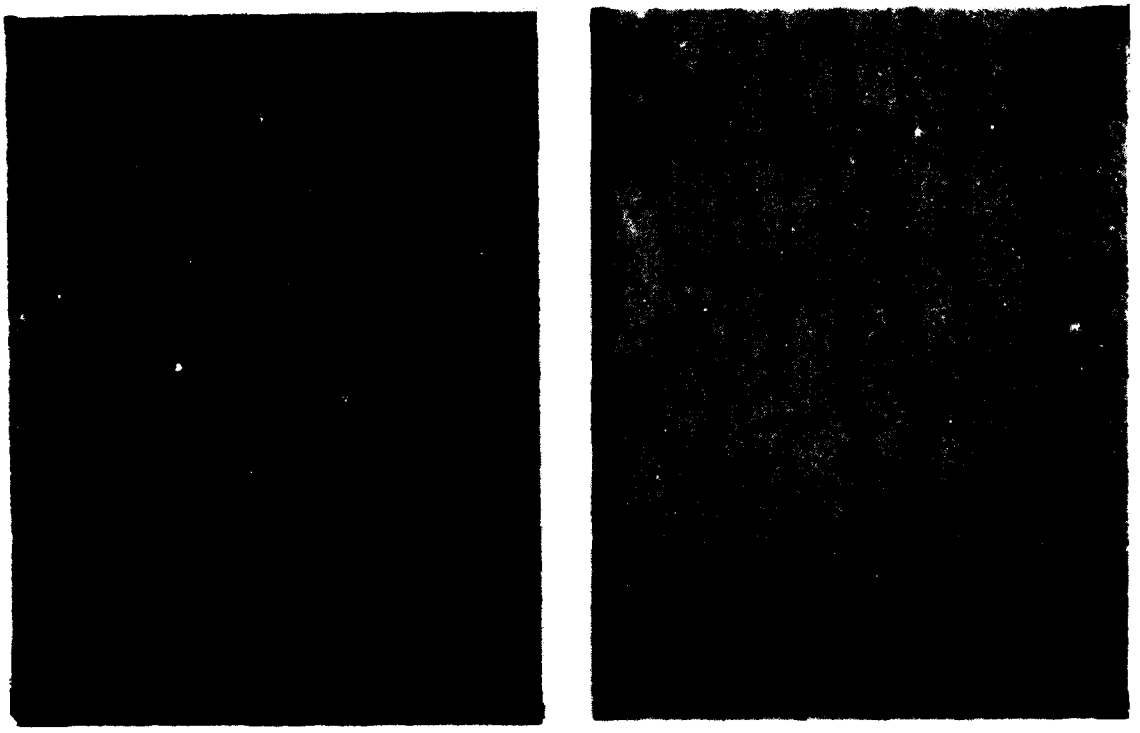

0.01 IN

AS1/3501-6 T300-6K/V378A

Figure F-8 Photomicrographs of #1 Mode I Panels

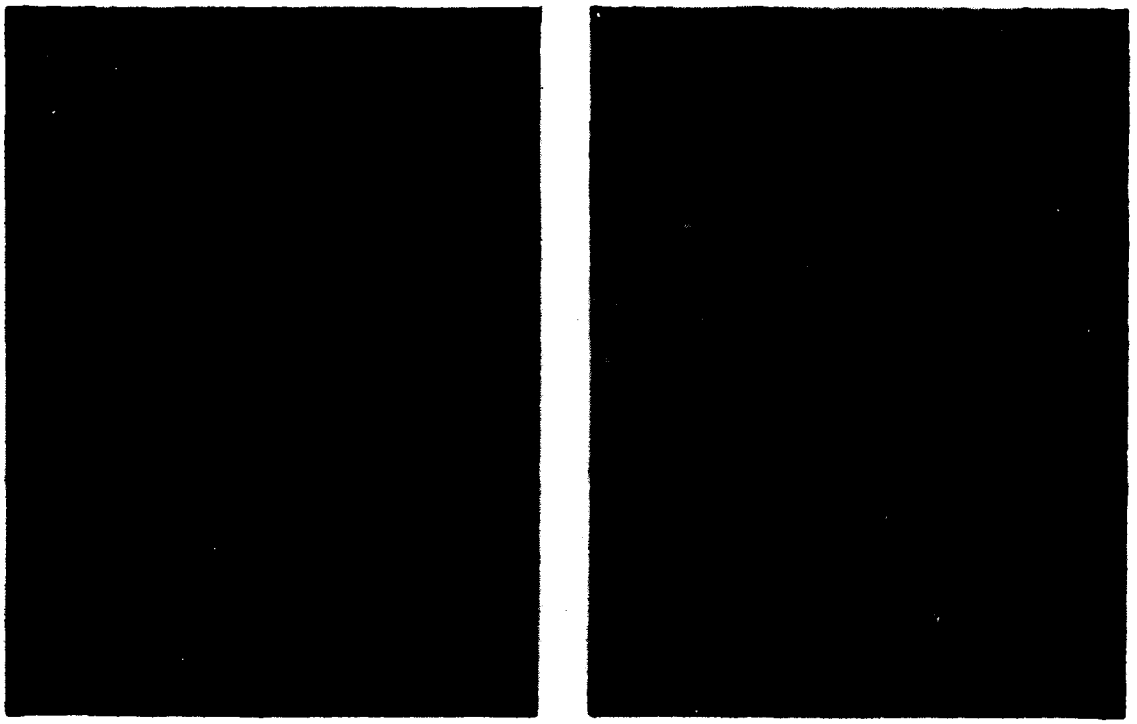

0.01 IN

AS1/3501-6 T300-6K/V378A

Figure F-9 Photomicrographs of #2 Mode I Panels

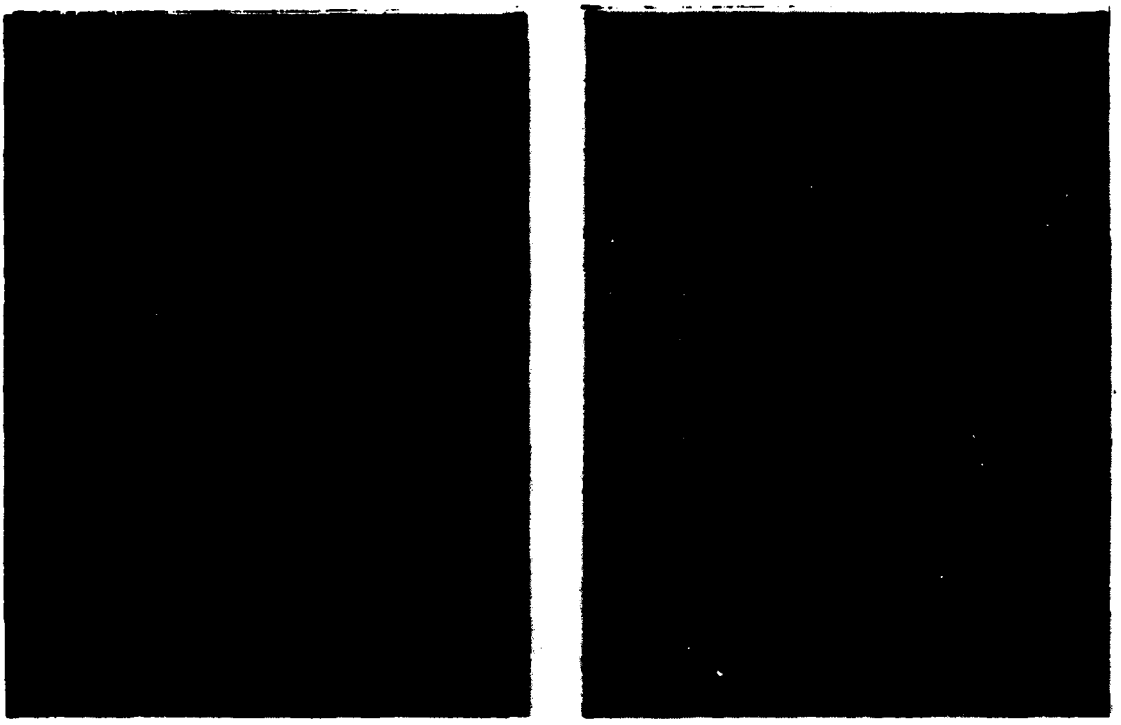

0.01 IN

AS1/3501-6

T300-6K/V378A

Figure F-10 Photomicrographs of #3 Mode I Panels

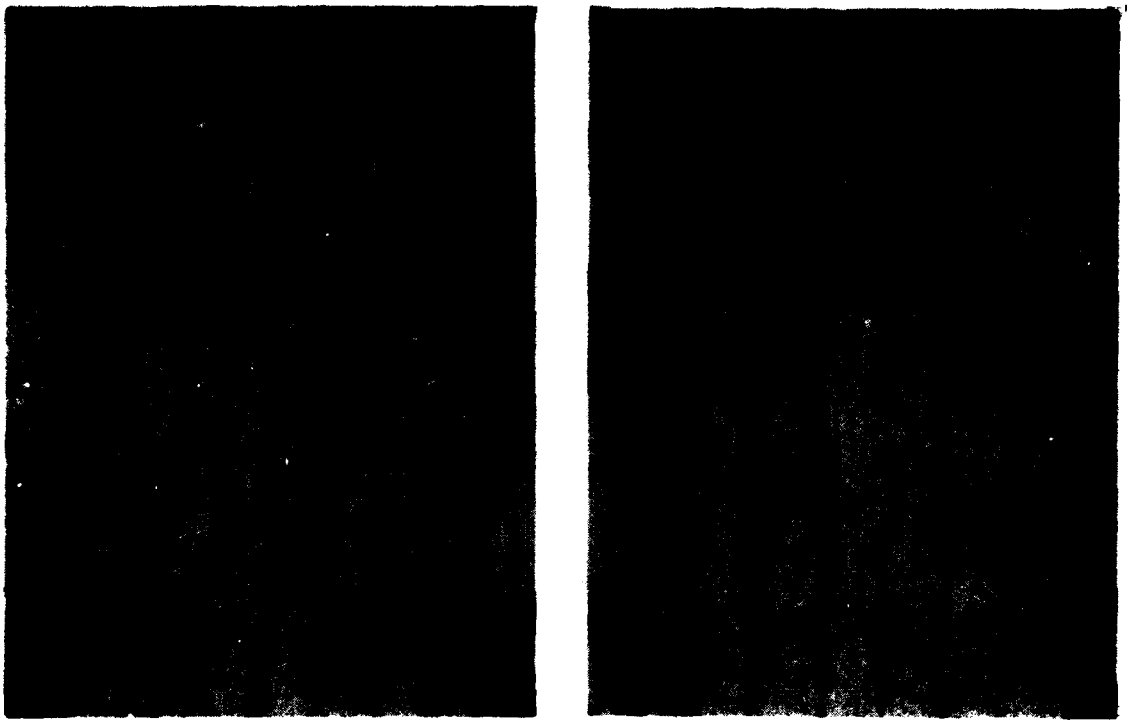

0.01 IN

AS1/3501-6

T300-6K/V378A

Figure F-11 Photomicrographs of #4 Mode I Panels

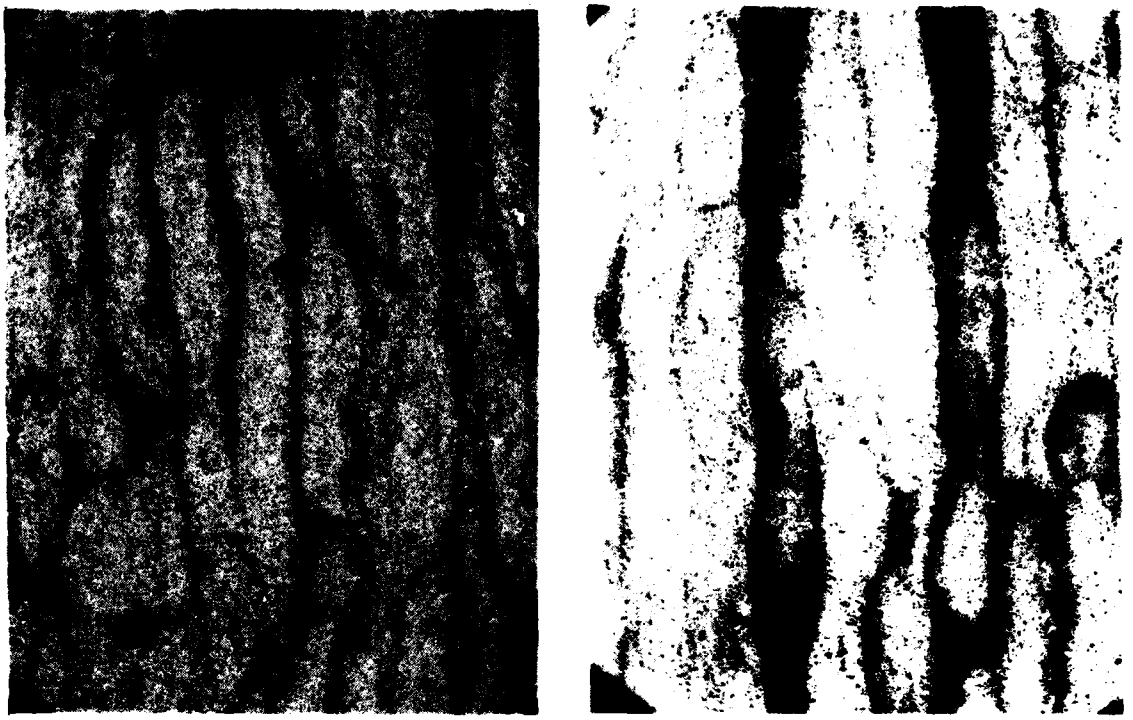

0.01 IN

AS1/3501-6

T300-6K/V378A

Figure F-12 Photomicrographs of #5 Mode I Panels

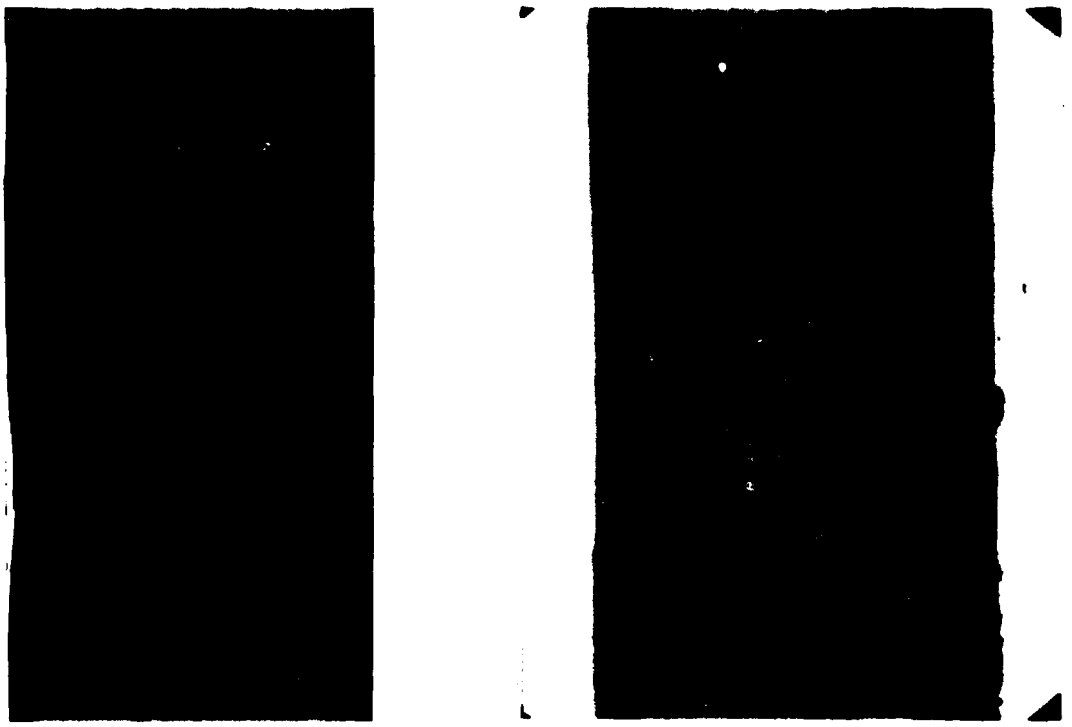

0.01 IN

AS1/3501-6

T300-6K/V378A

Figure F-13 Photomicrographs of #1 Mode II Panels

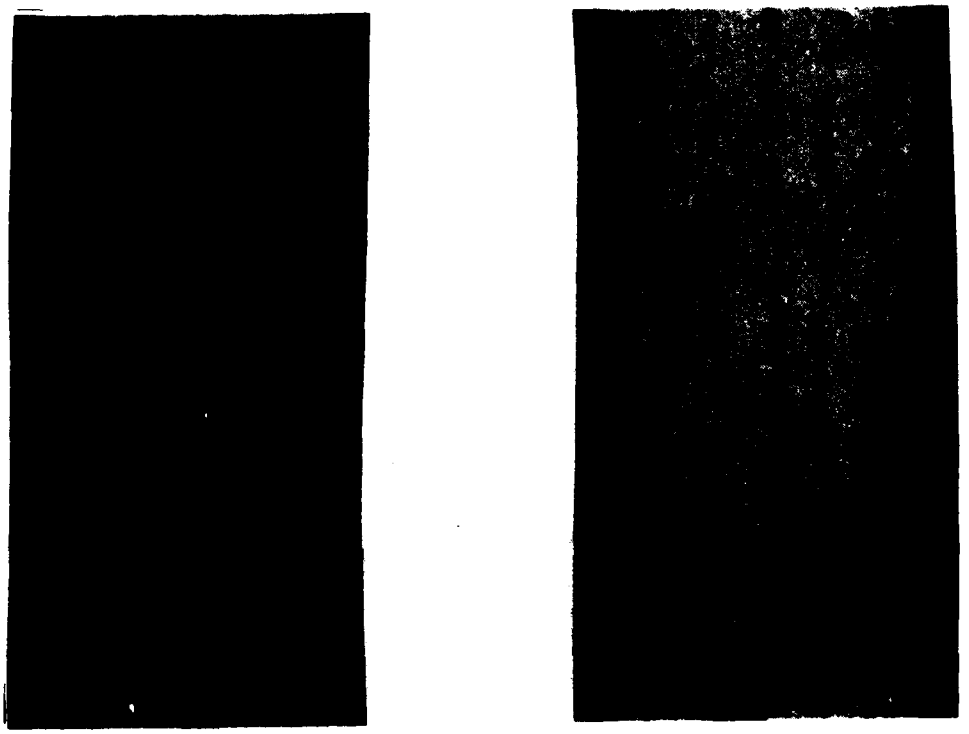

0.01 IN

AS1/3501-6

T300-6K/V378A

Figure F-14 Photomicrographs of #2 Mode II Panels

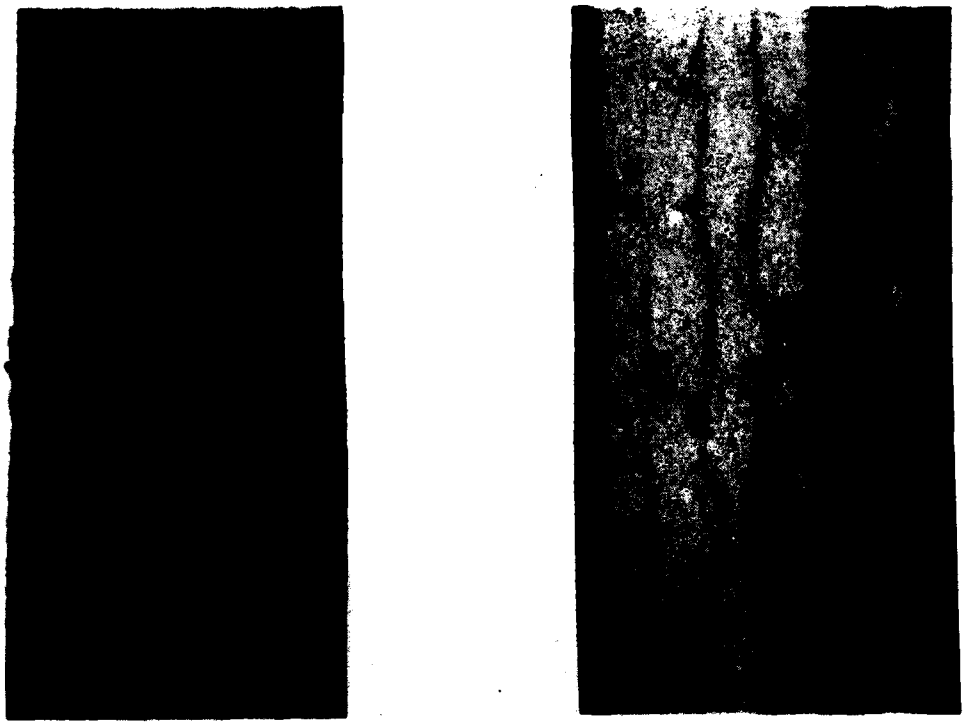

0.01 IN

AS1/3501-6

T300-6K/V378A

Figure F-15 Photomicrographs of #3 Mode II Panels

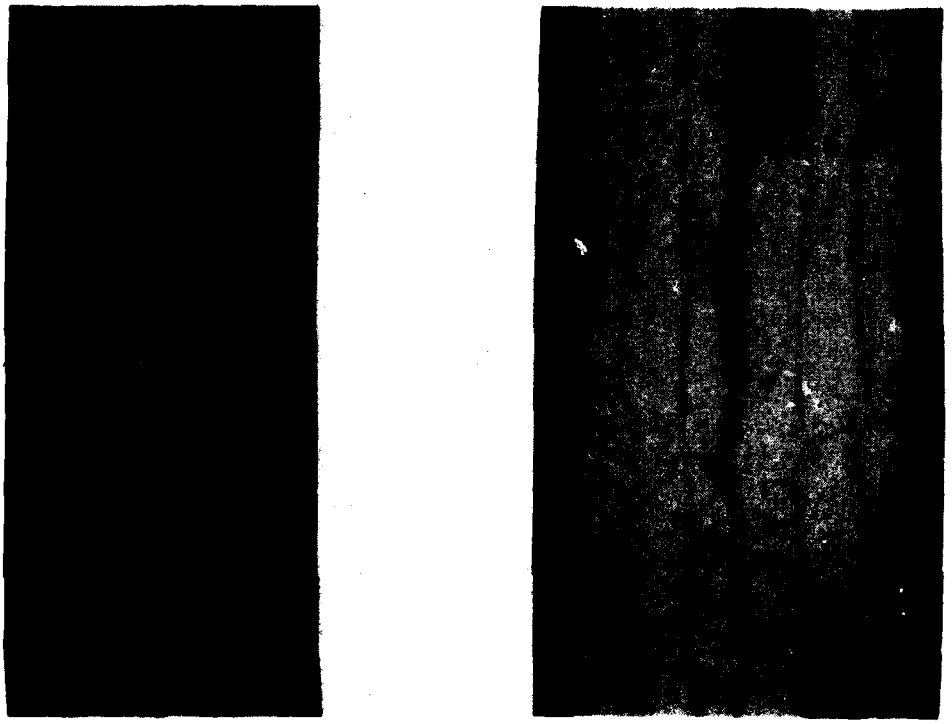

Figure F-16 Photomicrographs of #4 Mode II Panels

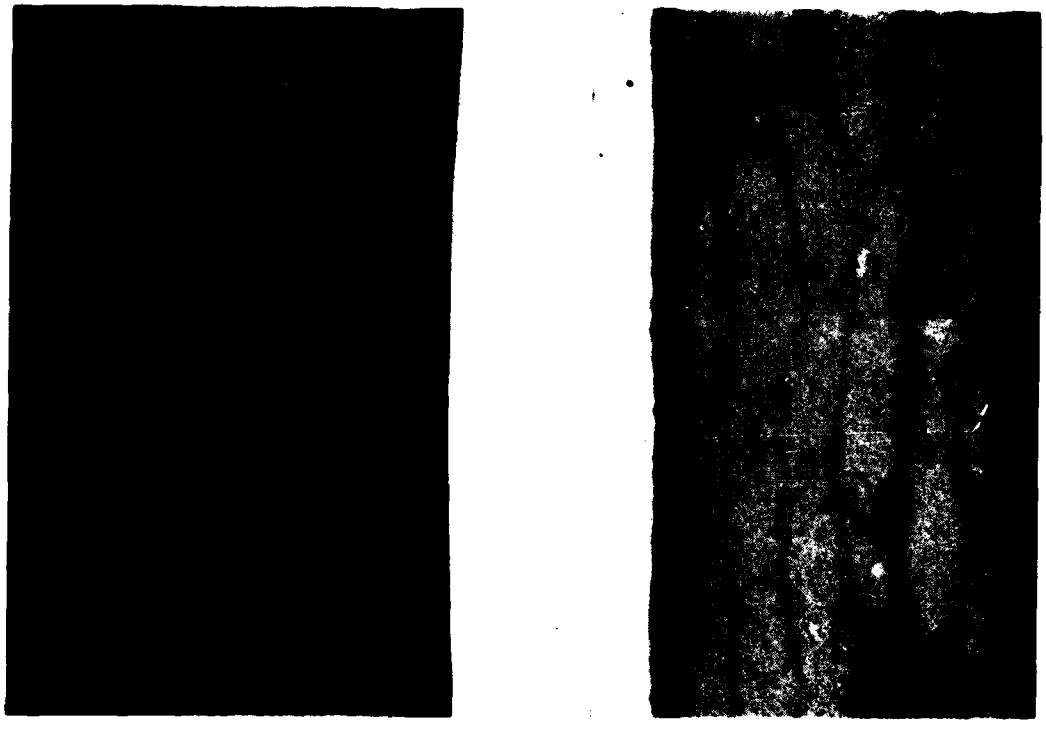

0.01 IN

AS1/3501-6

T300-6K/V378A

Figure F-17 Photomicrographs of #5 Mode II Panels

DISTRIBUTION LIST

	No. of Copies
Naval Air Systems Command Washington, D.C. 20361 14 for AIR-00D4, 3 for AIR-320B, 3 for AIR-5304 and 3 for AIR-5302	23
Naval Air Development Center Warminster, PA. 18974 ATTN: Code 6043, Mr. P. Kozel Code 6043, Dr. S. L. Huang Code 6043, Mr. T. Hess Code 6043, Mr. L. Gause Code 6052, Dr. J. DeLuccia	5
Naval Sea Systems Command Washington, D.C. 20362 ATTN: Code 05R15, Dr. H. Vanderveldt Code 062R4, Mr. M. Kinna Code 03R24, Mr. J. Gagorik Code 05E3, Mr. T. White	4
Office of Naval Research Arlington, VA. 22217 ATTN: Code 474, Dr. N. Perrone Code 471, Dr. B. McDonald	3
Naval Ship R&D Center Bethesda, MD. 20034 ATTN: Code 173.2, Mr. W. P. Couch	1
Naval Ship R&D Center Annapolis, MD 21401 Attn: Mr. J. Gudas	1
Naval Surface Weapons Center White Oak, MD. 20910 ATTN: Mr. J. Augl	1

Naval Research Laboratory 2
Washington, D.C. 20375
ATTN: Dr. I. Wolock, Code 6383
Dr. G. Yoder, Code 6384

Wright Aero Labs AFFDL 3
Wright Patterson AF Base, Ohio 45433
ATTN: Mr. C. D. Wallace/FIBCA
Dr. G. P. Sendeckyj/FIBE
Mr. W. Goesch/FIB

Wright Aero Labs, AFML 2
Wright Patterson AF Base, Ohio 45433
ATTN: Mr. T. G. Reinhart, Jr./MBC
Mr. F. D. Cherry/MLB

Air Force Office of Scientific Research 2
Bldg. 410 Bolling AFB
Washington, DC 20332
ATTN: Dr. A. Amos
Dr. M. Salkind

Defense Advanced Research Project Agency 1
1400 Wilson Boulevard
Arlington, VA 22209
ATTN: Dr. E. C. VanReuth

NASA 3
Langley Research Center, Hampton, VA. 23365
ATTN: Dr. J. Davidson
Dr. J. Starnes
Dr. G. L. Roderick

Army Air Mobility R&D Laboratory 1
Fort Eustis, VA. 23604
ATTN: Mr. H. Reddick

Army Materials & Mechanics Research Center 2
Watertown, MA. 02172
ATTN: Dr. E. Lenoe
Mr. D. Oplinger

Army Mobility R&D Lab., Ames Research Center 1
Moffett Field, CA. 94035
ATTN: Dr. Raymond Foye

Army Research Office
Research Triange Park, N.C. 27709
ATTN: Dr. F. Schmiedeshoff

1

Materials Science Corporation
Merion Towle House
Blue Bell, PA. 19422
ATTN: Dr. W. Rosen

1

McDonnell Douglas Corporation
McDonnell Aircraft Company
P. O. Box 516
St. Louis, MO 63166
ATTN: Mr. K. Stenberg
Mr. R. Riley
Mr. R. Garrett
Dr. D. Ames
Dr. C. Whitsett

5

Northrop Corporation
3901 W. Broadway
Hawthorne, CA. 90250
ATTN: Dr. N. Bhatia
Mr. L. Jeans
Dr. M. Ratwani

3

General Dynamics/CONVAIR Division
P. O. Box 80847
San Diego, CA. 92138
ATTN: Mr. W. Scheck

1

General Dynamics
Aerospace Division
P. O. Box 748
Fort Worth, TX 76101
ATTN: Dr. D. J. Wilkins
Dr. S. D. Manning

2

Lockheed Missiles & Space Co.
Sunnyvale, CA 94088
ATTN: Mr. H. Marshall

1

Vought Corp
Advanced Technology Center
Dallas, Texas 75266
ATTN: Dr. J. Renton
Mr. E. Donahu
Dr. D. H. Peterson

3

Grumman Aerospace Corpation
Bethpage, New York 11714
ATTN: Mr. R. Hadcock
Mr. S. Dastin
Mr. W. Grant

3

Sikorsky Aircraft
Stratford, CT. 06602
ATTN: Mr. M. J. Rich

1

Bell Helicopter
P. O. Box 482
Fort Worth, TX 76101
ATTN: Mr. J. McGuigan

1

Hughes Helicopters
Centinela and Teale St.
Culver City, CA. 90230
ATTN: Mr. G. Rock

1

Boeing Vertol Co.
Philadelphia, PA. 19142
ATTN: Mr. R. Peck

1

Kaman Aerospace Corporation
Old Windsor Road
Bloomfield, CT. 06002
ATTN: Mr. J. Schauble

1

Rockwell International Corp./Science Center
P. O. Box 1085
1049 Camino Dos Rios
Thousand Oaks, CA. 91360
ATTN: Dr. Neil Paton
Ms. R. Richards

2

Pratt & Whitney Aircraft 1
Division of United Aircraft Corp.
Florida Research & Development Center
P. O. Box 2691
West Palm Beach, FL 33402
ATTN: Mr. John Miller

The Franklin Institute Research Laboratories 1
Twentieth & Parkway
Philadelphia, PA. 19103
ATTN: Technical Director

National Bureau of Standards 1
Gaithersburg, MD. 20760
ATTN: Dr. Donald Hunston

Hercules Incorporated 1
Aerospace Division
Magna, Utah 84044
ATTN: Dr. Willard Bascom

University of Tulsa 1
Dept. of Mechanical Engineering
Tulsa, Oklahoma 74104
ATTN: Prof. E. F. Rybicki

Virginia Polytechnic Institute & State University 1
Dept. of Engineering Mechanics
Blacksburg, VA. 24060
ATTN: Prof. K. Reifsnider

University of Illinois 1
Dept. of Mechanical Engineering
Urbana, IL. 61801
ATTN: Prof. S. S. Wang

Drexel University 1
Dept. of Mechanical Engineering
Philadelphia, PA. 19104
ATTN: Prof. A. Wang

Rockwell International/NAAD 1
P. O. Box 1259
Columbus, OH. 43216
ATTN: Mr. F. Kaufman

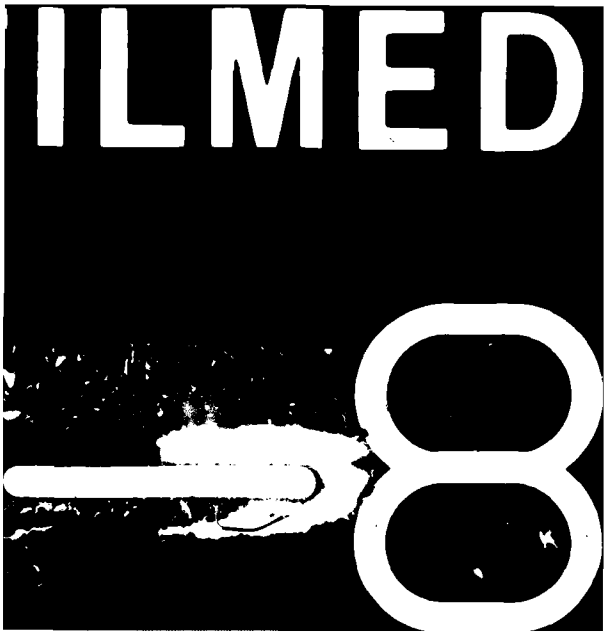
ILMED
8